STUDY OF RADIO-NUCLIDES DECAYING BY ORBITAL ELECTRON CAPTURE

by

J. Robert S. Drouin

A thesis submitted to the Faculty of Graduate
Studies and Research in partial fulfilment of
the requirements for the degree of
Doctor of Philosophy.

From the Radiochemistry Laboratory under the
supervision of Professor L. Yaffe.

McGill University
Montreal, Canada.

March 1961.

ACKNOWLEDGEMENTS

The author would like to express his grateful appreciation to:

Professor L. Yaffe for his kind suggestions.

His wife, Andrée, for her continued help and understanding.

The National Research Council of Canada, for financial assistance in the form of a Bursary held in 1956-57, and Studentships held in 1957-58, 1958-59, and 1959-60.

ABSTRACT

A windowless 2π-proportional counter which can be used as a detector and a spectrometer for the study of radiations was constructed and calibrated. The instrument can be operated at various pressures. One of the applications was to determine the disintegration rate of nuclides $(Z<50)$ decaying by orbital capture. Various factors, such as the resolving power for X-ray energies up to 20 kev and dependence of the gas multiplication factor "A" for different counter geometries (anode to cathode ratio) and counter gases (nature and pressure) were investigated. Experimental results were then compared with theoretical calculations. Fourteen radio-nuclides were studied. The half-life of Ca^{41} was re-determined and found to be $(7.5 \pm 1.1) \times 10^{4}$ years. The beta spectrum of H^3 was also re-investigated. K-fluorescence yields of argon and iron were experimentally evaluated each by a different method. Measurements of the capture probabilities and of the branching ratio of internal bremsstrahlung photons to K-capture events of Fe^{55} were determined.

TABLE OF CONTENTS

Page

B. PREPARATION OF RADIONUCLIDES

C. COUNTING APPARATUS

D. GAS MULTIPLICATION FACTOR "A"

Page

E. PULSE STATISTICAL FLUCTUATION

F. DISINTEGRATION RATE DETERMINATION

G. SPECTROMETRIC APPLICATIONS

H. MISCELLANEOUS RESULTS

LIST OF FIGURES

Page

LIST OF TABLES

A. INTRODUCTION

1) PREFACE

In the field of nuclear science, the radioactive species encountered will decay by alpha emission, by beta emission or by capture of one of the orbital electrons. Sometimes, the nucleus resulting after decay will be left in a metastable state and will lose its excitation energy by emitting a multipole radiation. If the excited state has a measurable half-life ($> 10^{-11}$ sec.), the nuclear metastable state is called a nuclear isomer.

Nuclear chemists and technologists are greatly concerned with measurements of these radiations. In radiochemistry laboratories, for instance, many problems often require the absolute determination of disintegration rates of many radioelements. In the past years, many scientists and engineers have spent a great deal of time and effort in developing accurate instruments for measuring and detecting nuclear and atomic radiations. This effort was increased with the advent of nuclear reactors and charged-particle accelerators. The methods of measurement became as varied as the properties of the radiations of the artificially-produced radionuclides.

The alpha particle emission rate can now be measured with an accuracy reaching 0.1 per cent. One of these methods, which is now widely used, suggests a flow proportional counter with a geometrical efficiency of 2π-steradians. A recent publication by Curtis et al. (1) used this method to study alpha absorption. Another technique, which was developed by Robinson (2) uses a phosphor coupled with a phototube. A third method applied at the National Bureau of Standards by Mann (3) employs a sensitive twin cup Peltier-effect microcalorimeter.

For beta emitters having a maximum energy greater than about 0.3 mev, the best and most widely used method of standardization is that of 4π-beta measurements. The application of this method was first suggested in 1944 by Simpson (4) who used a counter which appeared to have somewhat appreciably less than a 4π geometry. The first such counter to attain to what is now regarded as essentially a 4π geometry was designed by Schutzmeister-Meyer and described by Haxel and Houtermans in 1948 (5). These counters have since been carried to a high standard of working efficiency, for example by Pate and Yaffe (6), (7), (8), (9), and (10). If sufficient care is taken to ensure that all absorption corrections are accurately applied, these counters can indeed be used with beta emitters of lower maximum energy.

In some cases, gas counting techniques applied to low energy beta emitters are very useful for precision work. Depending on the investigators that have used gas counters, two general philosophies prevail: one which advocates the use of a long counter tube having negligible or calculable end corrections (11) and one which promotes the simultaneous use of a compensated set of counters, thus enabling end corrections to be made (12). Workers of both predilections have also performed experiments with counters of varying radii, with a view to determining the magnitude of the wall correction.

The method of beta-gamma or gamma-gamma coincidence measurements for beta emitters that have one or more gamma rays in coincidence is sometimes a powerful standardization aid. When very little precaution was taken to prevent self-absorption of the beta particles, Gunnink et al. (13) have found that in most cases, the counting efficiency varied approximately exponentially with the energy. Recently, Campion (14) has described a 4π beta-gamma system whose performance suggests that accuracies of the order of 0.1 per cent (15) are now feasible.

The remaining group of radionuclides, which sometimes requires absolute knowledge of the disintegration rate, involves nuclides decaying by capture of an orbital electron. This need is often stimulated by problems met in Nuclear Physics and in Nuclear Chemistry. Examples of these are the determination of fluxes by the activation method (16), the determination of the excitation functions of absolute yields of nuclear reactions, the investigations of distribution of mass and charge among the product of spallation, and also, the search for decay constants of long-lived radioisotopes (17). Frequently, in the field of medicine, the absolute determination of the disintegration rates of some particular nuclides decaying by electron capture is important in the preparation of standard doses for diagnostic or therapeutic uses.

Moreover, from the absolute study of such nuclides, accurate experimental data permit the measurement of transition capture probabilities, branching and internal bremsstrahlung ratios and fluorescence yields. These measurements are very powerful aids to the theoretical physicists in the elucidation of the structure of matter.

On the other hand, if these radionuclides are used only as tracers in various fields such as chemistry, agriculture and industry, the experiment can be designed so that no knowledge of the disintegration rate is required. For example, in most tracer experiments, only relative disintegration rates need generally to be known accurately when the samples are to be measured under similar exactly reproducible conditions.

Nuclides decaying by electron capture are usually the result of charged-particle irradiations of a stable element by accelerators such as electrostatic generators, accelerating tubes, linear accelerators, cyclotrons, synchrocyclotrons, betatrons, or synchrotons. These irradiations normally lead to the formation of a new nucleus where the proton to neutron ratio is greater than that required for stability. In turn, the proton in excess will decay by one or two different modes, namely positron emission and/or capture of one of the orbital electrons.

The two transformations can be represented as a nuclear transition from a proton state to a neutron state with accompanying neutrino (ν) emission in the following schematic picture:

$$p \longrightarrow n + \beta^{+} + \nu \qquad \ldots\ldots\ldots (1)$$

$$p + e^{-}_{K,L,M\ldots} \longrightarrow n + \nu \qquad \ldots\ldots\ldots (2)$$

The first transformation can be determined either by measuring the positrons themselves using one of the accurate methods previously proposed for the standardization of beta emitters or by measuring the radiation due to the annihilation of the positron. Accurate methods of measurements of the latter suggest the following applications: (a) high pressure ionization chamber (18), (19), (b) large NaI(Tl) crystal having a high efficiency well established (20), or (c) gamma-gamma coincidence measurement of the annihilation radiation.

The second transformation can be described by the following energy diagram which will be further elaborated in the section of this thesis treating the theoretical aspect of nuclides decaying by electron capture. A parent nucleus with atomic number (Z+1) captures one of its own orbital electrons and emits a neutrino transforming itself to the nucleus with atomic number (Z).

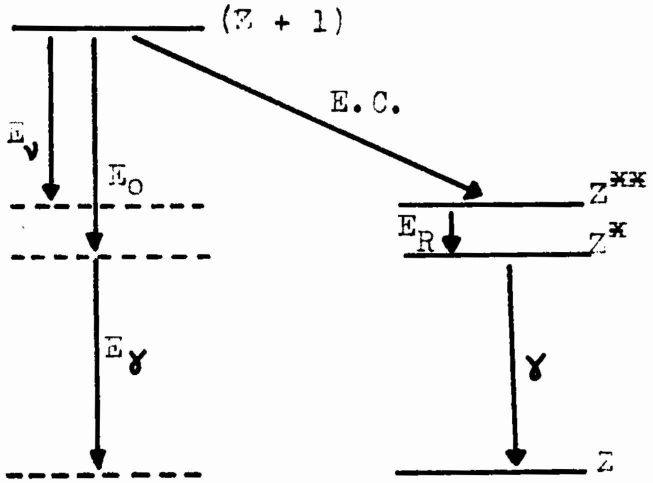

Subsequent de-excitation by gamma-ray emission may occur with energy E_γ. Thus, the total energy for the transition equals $(E_o + E_\gamma)$, where E_γ may be zero. Furthermore, $E_o = (E_\nu + E_R)$ where E_ν is the energy available for the neutrino and E_R is the energy of the radiation characteristic of an atomic shell re-arrangement i.e., a characteristic X-ray or an Auger electron.

In a small fraction of the cases, a photon called internal bremsstrahlung may result from the sudden change of the nuclear charge. In this case, the photons will have an energy which will be shared with the energy of the neutrino, (E_ν). The energy distribution will then give rise to a continuous spectrum where the upper limit will be equal to the energy available for the transition.

As explained earlier, one often needs to know the absolute rate of disintegration of such nuclides. Various methods have been tried with varying degrees of success (18), (20), (21), (22), (23), (24), (25), (26), and (27).

Since most nuclides of interest which decay by electron capture lie in the low atomic number (Z) region of the periodic table, the energy of the X-ray following K capture is low. For example, when the nucleus of Fe^{55} captures a K electron and changes to Mn^{55}, the energy of the X-ray emitted by the manganese atom when the K vacancy is filled is only 5.9 kev. The probability of L capture further complicates the picture. This probability will depend on the atomic number and the energy available for the transition. Also, one has to consider the fluorescence yield which represents the probability of the X-ray actually "escaping" from the atom when a radiationless transition occurs. The process of radiationless re-organization of an atom ionized in an inner shell is usually known as the Auger effect, and the ejected electrons are known as Auger electrons (28). This is an alternative mode of photoelectric emission and the yield becomes very important for elements of low atomic number, ($Z < 40$), (29). The energy of the Auger electrons is slightly less than that of the characteristic X-rays, and therefore very difficult to use for direct assay.

A good approach to the problem of the standardization of nuclides decaying by electron capture would be the absolute measurement of the emission rate of the characteristic X-rays. This thesis will describe experiments aimed at improving the accuracy of such measurements with the help of a windowless 2π proportional counter which can be used at elevated pressures. According to criteria that will be enunciated later, this counter can be satisfactorily operated as a detector and a spectrometer.

Some of the nuclides were prepared locally in the McGill proton synchrocyclotron and were separated almost "carrier-free" from their target. To verify the purity of the separated radioelements, their half-lives were determined.

In the following sections of this general introduction, we shall briefly give a theoretical and descriptive picture of these nuclides and study the fundamental properties of proportional counters. Various methods of determining disintegration rates will be discussed, whereafter our method will be described. The correction factors which had to be used will also be discussed.

2) THEORY OF NUCLIDES DECAYING BY ORBITAL CAPTURE.

Until 1933, two kinds of radioactive transformations were known: alpha radioactivity where an element (A,Z) decayed to form the element (A-4,Z-2) after emission of an helium nucleus, and beta radioactivity where an element (A,Z+1) gave the neighbouring isobar (Z) after emission of a negatron; Z and A are respectively the atomic number and the mass number. The first radioelements prepared artifically were discovered by Joliot and Curie in 1934 (30) and these, namely p^{30} and N^{13}, supplied two examples of another mode of transformation: element (A,Z) giving (A,Z-1) after emission of a positron.

At that time, no theory could explain such atomic transformations. However, some knowledge about the structure of nuclear matter came soon after the positive evidence of the existence of the neutron inside the nucleus. Two months after the discovery of the neutron by Chadwick in 1932 (31), Heisenberg (32) considered the interaction of "Platzwechsel" between the neutrons and the protons inside the nucleus. This was followed by Fermi in 1934 (33) who treated the problem of beta decay based on the neutrino hypothesis suggested by Pauli. The theory considers the interaction between a neutron and a proton leading to the emission or the absorption of an electron-neutrino pair.

Unfortunately, the interaction energy calculated with such assumptions is much too small to account for the binding energies of neutrons and protons (34), and (35). To remove this defect, Yukawa (36) has hypothesized the creation of a massive quantum accompanying these nuclear transitions. During the transitions of a heavy particle from a neutron state to a proton state, there is not always an emission of light particles, i.e., a neutrino and an electron, but the energy liberated by the transition is taken up sometimes by another heavy particle, which in turn will be transformed from a proton state into a neutron state. Such intervention does not alter essentially Fermi's theory which is based on the hypothesis of direct coupling of a heavy particle and a light particle. It only accounts for larger interaction energies between the nucleons.

Yukawa and Sakata have calculated in 1935 (37), (38), the possibility of an isobar (Z) changing into (Z-1) by absorbing one of the orbital electrons in the K state on the basis of their knowledge concerning the interaction between elementary particles and utilizing the suggestion that it will be very rare that two isobars with consecutive atomic number happen to be both stable. Independently, Møller (39) and Bethe and Bacher (40) have also shown the theoretical possibility of such a radioactive transformation. In 1942, Marshak (41) considered the possibility of a nucleus capturing an orbital electron in an L state and special attention was paid to the energy and degree of forbiddenness of such transitions.

Within the framework of Fermi's theory, the most complete calculations on the probability of electron capture have been published (37), (38), (39), (40), (41), (42), (43), (44), (45), (46), (47), (48), (49), (50), and (51). The usual theory is based on the description of the Coulomb shells by means of individual states for the electrons. For different order of forbiddenness, one calculates the probabilities of capture of a s, p_1, p_2 ....-electron separately. The capture of an electron in an n-state is always accompanied with the emission of a neutrino having the energy E_ν which is the available energy, (E_o-E_n), for the transition. E_o, as before, is the energy difference between the initial and the final atom and E_n is the total energy of the captured electron, the difference between its rest mass energy and its binding energy in the shell.

The allowed transitions are those in which the total angular momentum change ΔJ and the change of parity (+,-) between the initial and the final nucleus lead to the most favoured transition probabilities. According to the type of interaction selected between the nucleons and the field of leptons, (electron-neutrino), one essentially characterizes two types of allowed transitions:

$\Delta J = 0$; no parity change: Fermi interaction.

$\Delta J = 0, \pm 1$; no parity change: Gamow-Teller interaction.

However, in the formulae giving the total probability of disintegration by electron capture, the terms which depend on the nature of the chosen interaction factor and the unknown wave functions of the nucleus in its initial and final state can be replaced by terms which will only depend on the transition energy E_o and electron wave functions of the shells. This would enable us to carry on a discussion of the capture probabilities without introducing the following inherent nuclear concepts: (a) the coupling term, G, related to the universal Fermi constant, g, which depends upon the selected interaction between the field of nucleons and leptons, and (b) the square of the element of nuclear matrix, $|M|^2$, which depends on the wave functions of the nucleons and the selected interaction factor.

For an allowed transition, $s(j = 1/2, \ell = 0)$ or $p_1(j = 1/2, \ell = 1)$-electrons have an appreciable capture probability. For an s-electron, it is proportional to

$$(E_o - E_n)^2 . g^2_{ns}(R),$$

and for a p_1-electron, it is proportional to

$$(E_o - E_n)^2 . f^2_{np}(R).$$

The factors for proportionality are of nuclear origin and are essentially the same in both cases. The terms $g^2_{ns}(R)$ and $f^2_{np}(R)$ are bound to wave function components of s and p_1-electrons in the nuclear field at a distance R from its centre.

The total disintegration probability of electron capture during an allowed transition will be equal to the summation of the capture probabilities for different s and p_1-electrons. Hence, it is proportional to

$$(E_0 - E_K)^2 . n_K . g_K^2(R) + (E_0 - E_L)^2 . \left(n_{L_1} . g_{L_1}^2(R) + n_{L_{11}} . f_{L_{11}}^2(R)\right)$$

$$+ (E_0 - E_M)^2 . \left(n_{M_1} . g_{M_1}^2(R) + n_{M_{11}} . g_{M_{11}}^2(R)\right) + \dots \quad \dots\dots\dots \quad (3)$$

where n_K, n_{L_1}, $n_{L_{11}}$ ..... are the number of electron K($n = 1$, $j = 1/2$, $\ell = 0$), L_1 ($n = 2$, $j = 1/2$, $\ell = 0$), L_{11} ($n = 2$, $j = 1/2$, $\ell = 1$) .... appearing in the atom. With respect to L_1, the L_{11}-electron capture is less probable in an allowed transition. One can use the following expression for $f_{L_{11}}^2(R)$,

$$f_{L_{11}}^2(R) = \frac{3}{16} . \alpha^2 . Z_L^2 . g_{L_1}^2(R), \quad \dots\dots\dots\dots \quad (4)$$

where α is the usual fine structure constant and Z_L is the effective Z corrected for screening effect.

The study of electron wave functions in the neighbourhood of the nucleus has drawn solutions proposed by Marshak (41), Hartree, (52), and Reitz (53). Their results were compared by Benoist (45). Hartree's non relativistic function for atomic number up to 25 and Reitz's relativistic wave function for atomic number greater than 25 seemed to be the most consistent. Rose and Jackson (54), have also calculated electron densities $g^2_{L_1}(R)/g^2_K(R)$ at the limit of the nucleus as a function of the atomic number and their results are reported in Fig. 1.

According to the theoretical Eq. (3) for the total probability of disintegration by electron capture, the ratio P_{L_1}/P_K, that is, the L to K capture probability, for an allowed transition will be:

$$\frac{P_{L_1}}{P_K} = \left(\frac{E_o - E_L}{E_o - E_K}\right)^2 \cdot \left(\frac{g^2_{L_1}(R) + f^2_{L_{11}}(R)}{g^2_K(R)}\right) \quad \ldots\ldots. (5)$$

In general, E_L and E_K are experimentally known with precision. A table of the K and L X-ray emission and critical absorption energies for all the elements was published by Fine and Hendee in 1955 (55).

If E_o is known, the experimental value of P_L/P_K will supply a direct test of the validity of the curves shown in Fig. 1. The small correction due to $f^2_{L_{11}}(R)$ can be evaluated according to the Eq. (4).

When there is a competition between electron capture and positron emission for the same nuclide, E_o is given by the upper limit of the positron spectrum. Consequently, E_o will be

Figure 1

Electron Densities Calculated at the Limit of the Nucleus

when using

(1) Reitz Relativistic Wave Function with Thomas-Fermi Field plus Exchange.

(2) Hartree Self-consistent Field Wave Function.

From, Rose, M.E. and Jackson, J.L., Phys. Rev., 76, 1540 (1949).

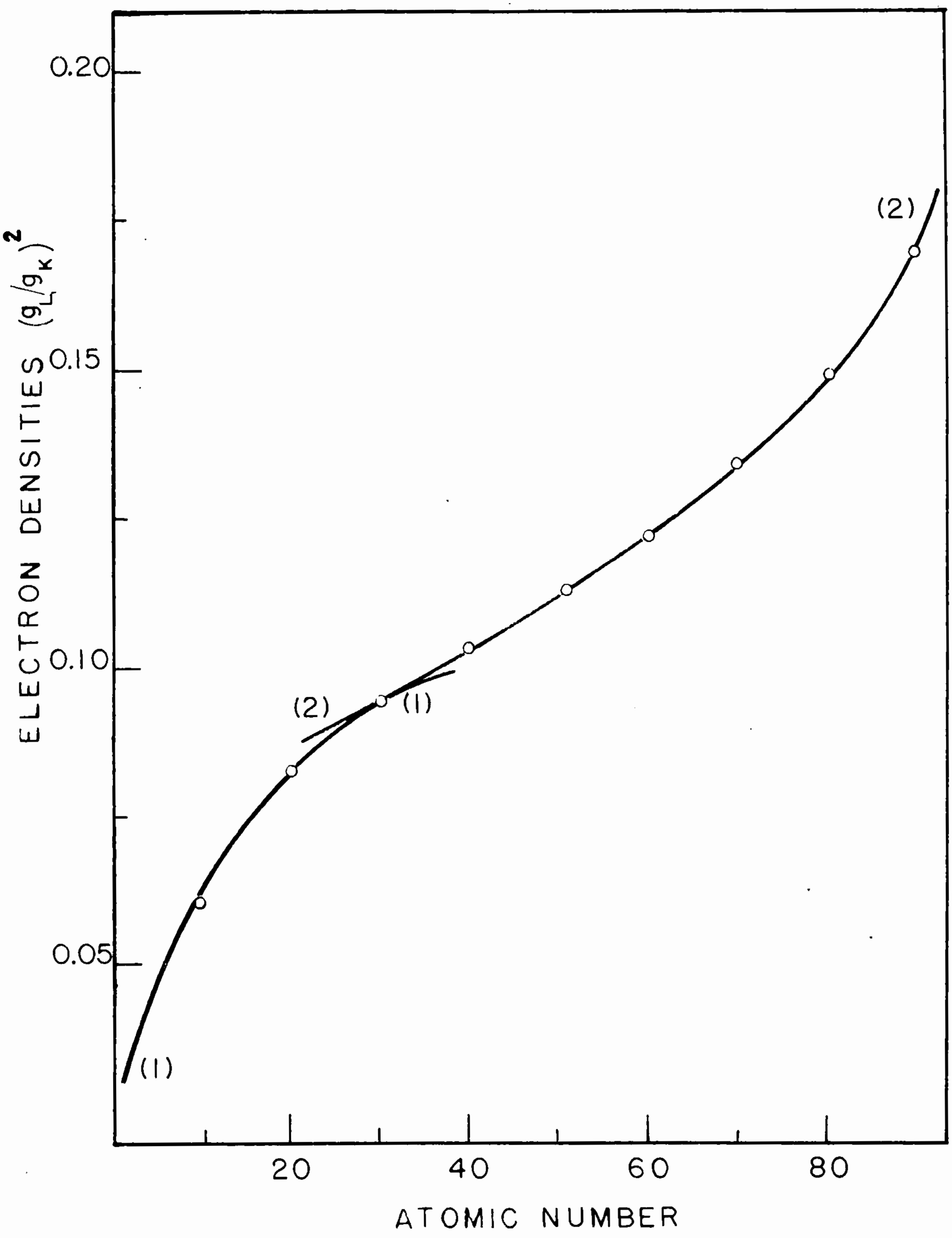
ELECTRON DENSITIES $(g_L/g_K)^2$
0.20
0.15
0.10
0.05
20
40
60
80
ATOMIC NUMBER
(1)
(2)
(1)
(2)

greater than one and the ratio $\left(\frac{E_o - E_L}{E_o - E_K}\right)^2$ between 1.2 and 1 for $Z = 90$. For $Z < 90$, the ratio will tend towards one. In such a case, for an allowed transition, the ratio P_L/P_K is in the order of $g^2_{L_1}/g^2_K$, that is, it will increase slowly from about 0.02 to 0.20 from low to high atomic number Z. The ratio P_L/P_K, in this case, is relatively small and L capture is experimentally difficult.

If positron emission is energetically impossible, E_o becomes smaller than one, where $\left(\frac{E_o - E_L}{E_o - E_K}\right)^2$ is greater than one and increases rapidly when E_o tends towards $+E_K$. L capture will be relatively more important but new experimental difficulties arise especially for low atomic number Z where the lifetime of the nuclide increases with decreasing E_o and the L characteristic X-rays are very low in energy.

In contrast to allowed transitions and according to the nature of the selected interaction factors between the nucleons and the field of leptons, forbidden transitions do not only lead to different selection rules, but different expressions in the terms where the electron wave functions intervene. Moreover, in some cases, for a particular ΔJ and for a given change of parity (+,-) the theory does not permit the factorization of the nuclear factors before the electron wave functions (41). Furthermore, in the study of the relative probabilities of K and L capture, an estimation of the nuclear factors will be required.

In the framework of the actual theory, experimental and theoretical results for forbidden transitions are not compatible for many cases. For this reason, the above theoretical description must be confined to allowed transitions only.

However, advanced theoretical predictions for nuclides decaying by electron capture were published in 1958 by Brysk and Rose (51). They discussed transition probabilities and branching ratios for K shell and the L subshells for allowed through second-forbidden captures. Also, the figures supply the values of the bound electron radial wave functions with corrections for the finite size of the nucleus, the effect of screening and take into account the variation in the electron wave functions over the nuclear volume.

3) DESCRIPTION OF NUCLIDES DECAYING BY ORBITAL CAPTURE

(a) Fermi Energy Diagram.

In calculating the energy available for an electron capture, it is not possible to use atomic masses M_a instead of nuclear masses M_n without due caution. For instance, the considerations of the binding energies of the electrons must be brought in to make the discussion more complete (56). The decay can be written symbolically as:

$$\begin{array}{ll} (Z+1) + e^-_{K,L,M...} \longrightarrow (Z)^* + \text{neutrino} & \\ \qquad\qquad\qquad\qquad\qquad\quad \downarrow & \qquad ..... (6) \\ \qquad\qquad\qquad\qquad\qquad\quad (Z) + \text{radiations} & \end{array}$$

When the nucleus captures an electron, a neutrino leaves the atom simultaneously and carries with it the available energy E_ν which is necessary for the transition. Thereafter, a subsequent radiation is emitted following the rearrangement. Let E_R denotes its energy and B_{Z+1} and B_Z the total electron binding energies of the two isobars and m_e the mass of the electron. Then, we have:

$$E_\nu = M_n(Z+1)c^2 + m_e c^2 - M_n(Z)c^2 - E_R - (B_{Z+1} - B_Z) \quad ...... (7)$$

Obviously, the difference between B_{Z+1} and B_Z would not appear if one uses exact atomic masses. Thus, the available energy for the transition would be reduced to:

$$E_\nu = M_a(Z+1)c^2 - M_a(Z)c^2 - E_R \qquad .... (8)$$

Electron-capture transitions can be clearly displayed on an energy diagram shown in Fig. 2. This picture is originally due to Fermi (57) when he attempted to give a

<u>Figure 2</u>

Descriptive Fermi Energy Diagram for Beta Decay.

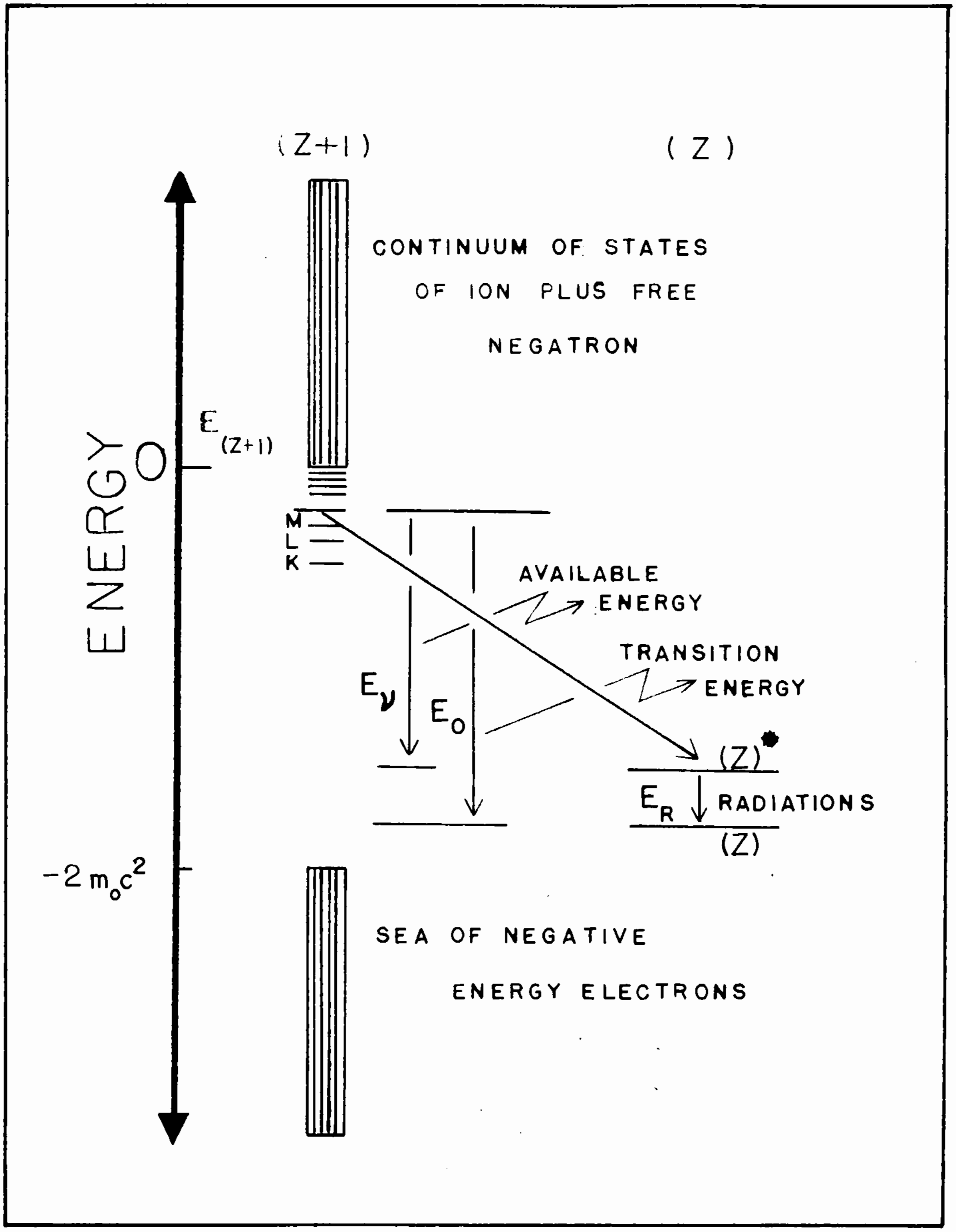
(Z+1)
(Z)
CONTINUUM OF STATES OF ION PLUS FREE NEGATRON
ENERGY
0
$E_{(Z+1)}$
M
L
K
AVAILABLE ENERGY
TRANSITION ENERGY
E_ν
E_0
$(Z)^*$
E_R
RADIATIONS
(Z)
$-2m_0c^2$
SEA OF NEGATIVE ENERGY ELECTRONS

descriptive image of beta decay. E_o is the total energy of the transition $(E_\gamma + E_R)$ where E_R is the energy of the radiations emitted during the atomic re-arrangement. The zero of the scale is taken so (Z+1) plus the free electron at rest have total energy zero. The total energy of the neutral atom (Z+1) is therefore equal to the negative value of the first ionization potential of the atom.

Suppose E_Z lies below $E_{(Z+1)}$ but is greater than $-2mc^2$, the transition $(Z) \longrightarrow (Z+1)$ is impossible because the Pauli exclusion principle operates. However, the transition $(Z+1) \longrightarrow (Z)$ will be possible if the available energy allows the nucleus (Z+1) to absorb an electron from those of the discrete levels. Usually, the K shell supplies the electron, but L, M,.... capture is also possible. The new atom (Z) is produced in an excited atomic state $(Z)^*$ corresponding to K, L, M,... shell vacancy.

If the level $(Z)^*$ corresponding to K-shell vacancy is above $E_{(Z+1)}$ but $(Z)^*$ for L excitation is below, then only L, M,... capture can occur. In addition, there are two cases where electron capture is impossible. The first one is when $(Z)^*$ for minimum excitation, (valence electron vacancy), is above $E_{(Z+1)}$ and the second case is if the level of (Z) is below the level at which an electron can be created into a discrete state of atom (Z). The latter case is unlikely since the discrete energy levels occupy only a small energy range compared to the actual energy differences between isobars.

The competition between electron capture and positron emission will happen when the available energy will be less than zero by $-2mc^2$ or more. In such a case, the nucleus will capture an orbital electron or/and will take an electron from the sea of electrons in negative energy states, thus creating a positron which will be emitted.

(b) Atomic Re-arrangement.

The hole created in the inner shell is filled by an electron coming from an outer shell where the binding energy is weaker. The liberated energy of the process is equal to the difference between the electron binding energy in its initial state and final state. This energy will appear in form of an electromagnetic radiation or will be used to eject another electron of lower binding energy. The former case is currently called characteristic X-ray emission while the latter is the emission of Auger electrons.

(I) Characteristic X-ray Emission.

Barkla and Saddler,(58),were the first to study characteristic X-rays by classifying them into different types, namely K and L, and according to measurement of their absorption coefficient. Soon after the discovery of X-ray diffraction in 1912, Moseley (59) was able to use an X-ray spectrometer to study the characteristic wavelengths. For one series, the most intense were called K_α lines and the less intense, K_β lines. Various L lines were also designated by Greek letter subscripts. The respective intensity of different lines K_α and K_β of K X-radiations does not vary sensibly with the atomic number (2:1). Meyer (60) has found some experimental results for 24 elements and agreement between observation and theory for these is excellent.

Beside the intensity rules, selection rules derived from theoretical considerations in optical spectra also apply in X-ray spectrometry. The relative probabilities of transitions between the various level are predicted by wave mechanics. For various quantum numbers, n(principal number), ℓ(subshell number) and j(spin number), the selection rules for the allowed transitions are:

$$\Delta n = \text{any integer greater than zero}$$

$$\Delta \ell = -1 \text{ or } +1$$

$$\Delta j = -1,\ 0 \text{ or } +1$$

Regarding higher energy levels, the various transition probabilities are sketched in Fig. 3.

Figure 3

Transition Probabilities in the Higher Energy Levels.

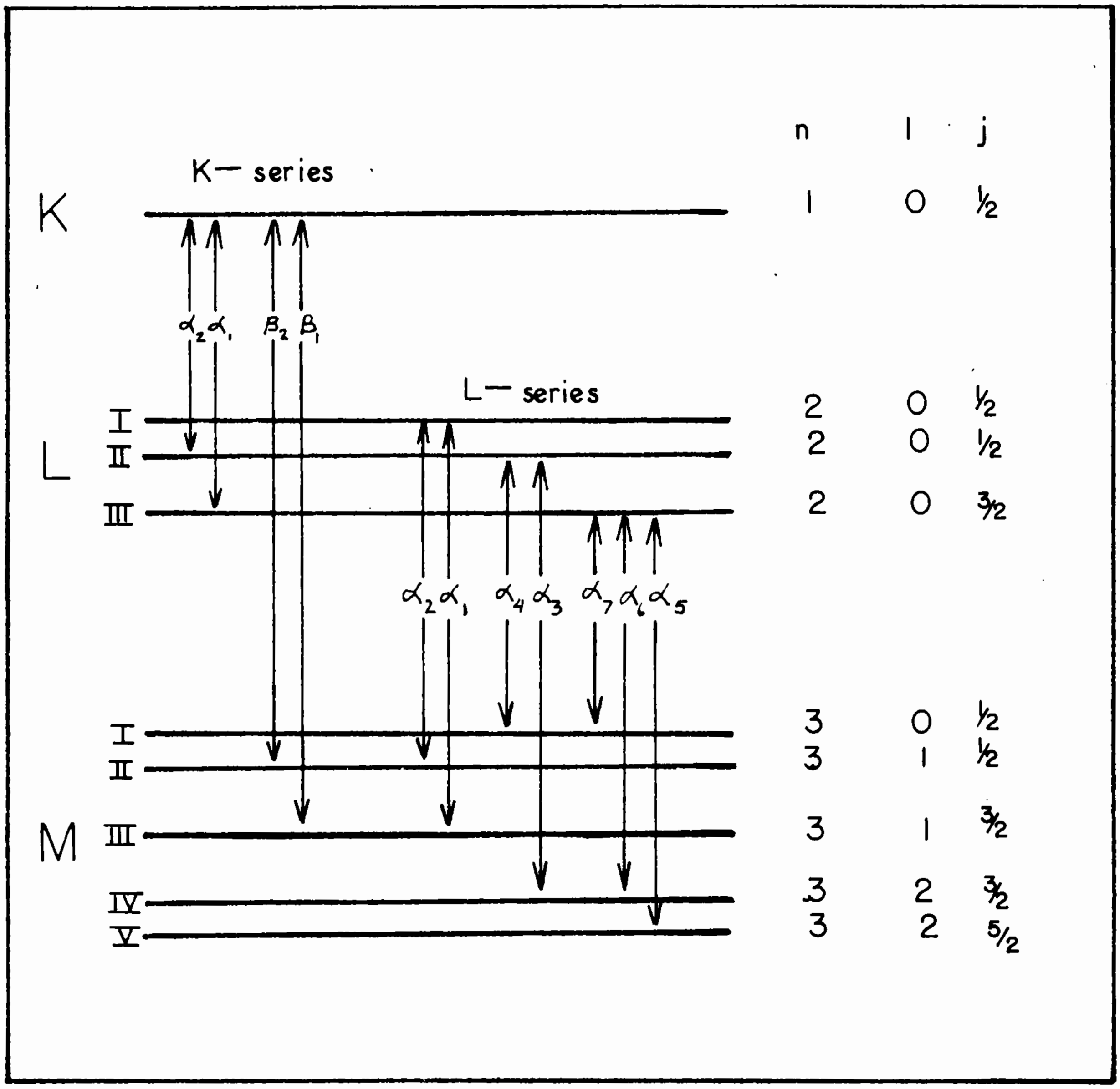

TYPICAL REARRANGEMENT IN THE

HIGHER ENERGY LEVELS

(II) Auger Electron Emission.

Auger electrons were discovered by Auger in 1925 (30). They are emitted with discrete energy from any lower shells except the K shell. It is an alternative mode of characteristic X-ray emission. According to Burhop's theoretical calculations (61), it is immaterial whether the phenomenon is regarded as an internal conversion of the characteristic X-rays or the result of a direct interaction between the two electrons.

Many possibilities are expected, namely K→LL, K→LX, or K→LY, where X and Y represent shells of lower order than L. The importance of group K→LX increases with the atomic number and groups K→LL and K→LX are far from the most important (62).

A similar effect to that of Auger was discovered by Coster and Krönig in 1935 (63). In fact, they have found that for atomic numbers $Z < 50$ and $Z > 75$, the energy difference between L_1 and L_{11} or L_{111} levels was higher than the binding energy of the M and N-electrons. Consequently, M-electrons could be ejected after a L-subshell transition, that is $L_1 \rightarrow L_{11}$, or $L_1 \rightarrow L_{111}$, and this effect bears the name of the discoverers.

The results of K X-rays emitted relative to K capture events (K-fluorescence yield) have been collected by Broyles et al. (29). The values are fairly scattered and for low atomic numbers, the error is at least of the order of 10 percent. However, within the deviation of the experimental points, theoretical non-relativistic calculations worked out by Burhop (61) and by Pincherle (64) and relativistic calculations by Massey and Burhop (65) agree fairly well. The work of Broyles et al. (29) is reported in Appendix 1 and these reported data will be very useful in the application of the final equation for the determination of disintegration rate of nuclides decaying by electron capture.

In a recent publication, Robinson and Fink (66) have reported a private communication of Roos in which the best measurements on K-fluorescence yields are given. They write that for atomic numbers greater than 26 and smaller than 50, the measurements delineate the steeply rising portion of the K-fluorescence yield (W_K) versus atomic number (Z) and the errors are said to be of the order of 2 to 3 percent.

A pictorial atomic re-arrangement is described in Fig. 4 for a K or an L capture. Each time the intensity of the process is considered and there is no distinction between an L process having origin in different subshell L_1, L_{11}, or L_{111}.

(c) Internal Bremsstrahlung

Another type of radiation that appears when a nucleus captures an orbital electron and falls to a stable state is an

Figure 4

Re-arrangement after a K or L-electron Capture.

Terminology:

X = number of K-capture event.

Y = number of L-capture event.

k = K_α to K_β ratio.

k' = L-ionization after K-Auger electron emission.

W_K = K-fluorescence yield.

W_L = L-fluorescence yield.

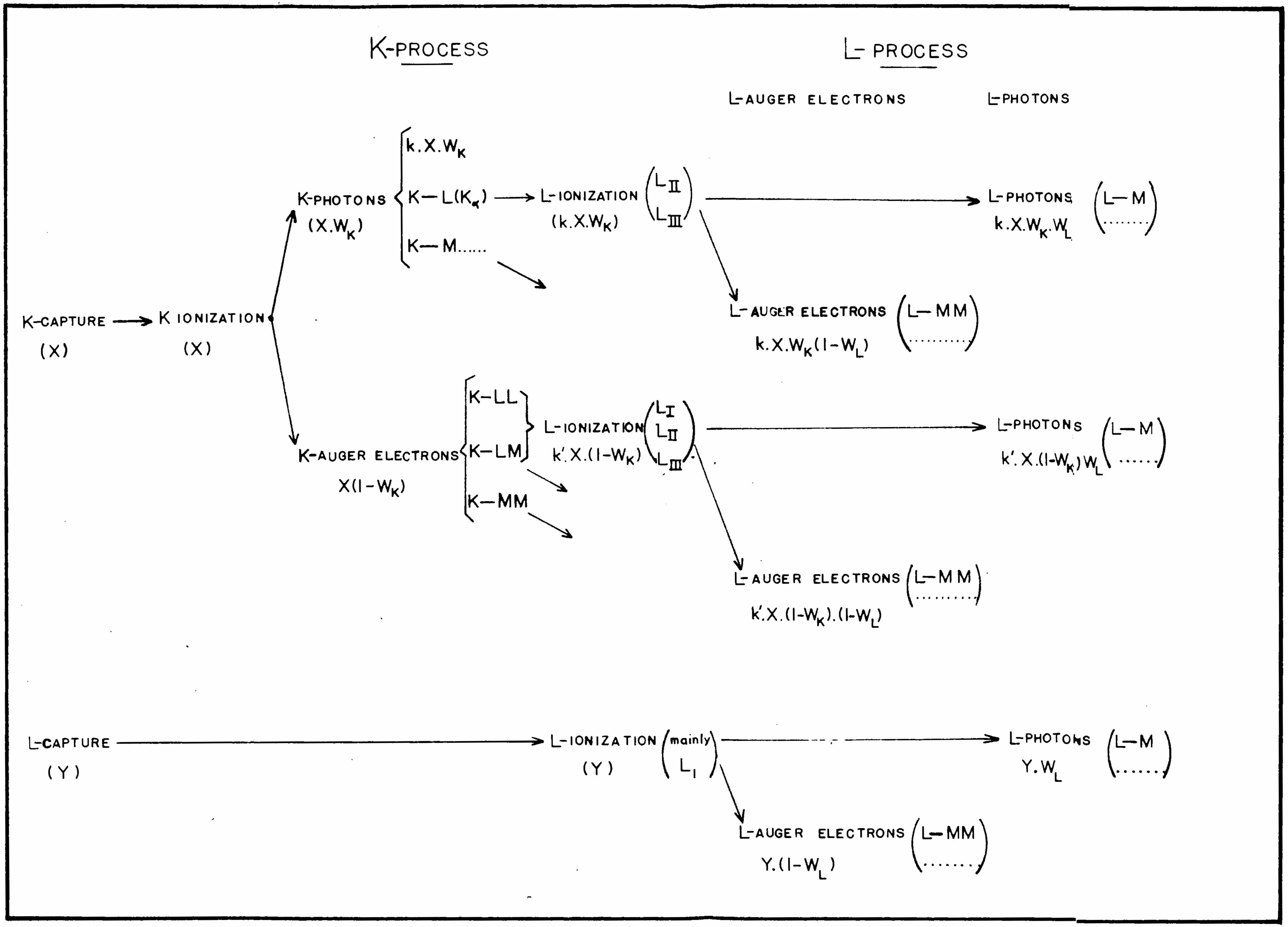
K-PROCESS
L- PROCESS
L-AUGER ELECTRONS
L-PHOTONS
K-CAPTURE (X)
K IONIZATION (X)
K-PHOTONS ($X.W_K$)
$k.X.W_K$
K—L(K_α)
K—M......
L-IONIZATION ($k.X.W_K$)
L_{II} L_{III}
L-PHOTONS $k.X.W_K.W_L$
(L—M ....)
L-AUGER ELECTRONS $k.X.W_K(1-W_L)$
(L—MM ....)
K-AUGER ELECTRONS $X(1-W_K)$
K-LL
K-LM
K—MM
L-IONIZATION $k'.X.(1-W_K)$
L_I L_{II} L_{III}
L-PHOTONS $k'.X.(1-W_K)W_L$
(L—M ......)
L-AUGER ELECTRONS $k'.X.(1-W_K).(1-W_L)$
(L—MM ....)
L-CAPTURE (Y)
L-IONIZATION (Y)
(mainly L_I)
L-PHOTONS $Y.W_L$
(L—M ....)
L-AUGER ELECTRONS $Y.(1-W_L)$
(L—MM ....)

internal bremsstrahlung photon. The origin of this radiation is due to a sudden change of charge when the nucleus captures an electron, and its energy is shared with the neutrino. This primary radiation is in coincidence with the secondary radiations, namely the characteristic X-rays or the Auger electrons. The intensity and energy depend on the atomic number and the energy available for the transition.

This process was first investigated theoretically by Morrison and Shiff in 1940 (67). Allowed transitions for 1s-electrons were the only ones considered. Later, Glauber and Martin (68), (69), (70), and (71) made a more detailed study of this phenomenon when they considered 2s and $2p_{\frac{1}{2}}$-electrons. In the low energy part of the continuum, a major contribution due to $2p_{\frac{1}{2}}$-electrons was theoretically predicted. This prediction was experimentally confirmed by Madansky and Rasetti in 1954 (72). Further theoretical and experimental details will be given in the part of this thesis dealing with miscellaneous results.

4) FIRST EXPERIMENTAL EVIDENCE OF DECAY BY ORBITAL CAPTURE NUCLIDES

Three years after the theoretical calculations on the probability of nuclides decaying by capture of one of the orbital electrons, Jacobsen (73) in Copenhagen attempted in vain to detect the characteristic X-rays resulting from the disintegration of Sc^{43}. The detector that he used was a Wilson cloud chamber. A few months later, in California, Alvarez (74) successfully showed the absorption of the X-rays of titanium when thin aluminium foils were interposed between a source of radioactive vanadium and a proportional counter filled with argon gas at one atmosphere.

The first L-electron capture was experimentally confirmed, in 1948, by Kirkwood et al. (75) in Chalk River. The ionization chamber was operated in the proportional region and A^{37} was studied.

5) DISINTEGRATION RATE DETERMINATION

(a) Nature of the Radiations.

One may attempt to measure the disintegration rate of nuclides decaying by electron capture in three ways: (1) absolute measurement of the internal bremsstrahlung photons; (2) absolute measurement of the Auger electrons; (3) absolute measurement of the characteristic X-rays.

An elegant proposal for the first method was suggested by Rasmussen in 1955 (25). The method is based on coincidence measurements of the internal bremsstrahlung photons and the characteristic X-rays. The method would be applicable for exceptionally pure radionuclides and especially those in which 100 percent of the transitions go to the ground state of the daughter nucleus. Recent theoretical calculations by Glauber and Martin (71) and experimental results by Hayward (76) have demonstrated the impracticability of the method for low energy transitions and radionuclides of high atomic number where the apportioning of the photons due to internal bremsstrahlung and the characteristic X-rays becomes very difficult. Also, the background interference and the low probability (~0.001 percent) of such emission per capture event do not militate in favour of such a method of standardization.

The second method, the absolute measurement of Auger electrons, is also not very suitable on account of the experimental difficulties encountered in preparing the source in such a manner that there will be no self-absorption or backscattering of the Auger electrons. According to the K-fluorescence yield reported in Appendix I, elements with atomic number smaller than about 35 have a high probability of Auger electron emission and the energy of these Auger electrons is only few kev.

A most profitable approach to the problem would then be through the third method, namely the absolute measurement of the characteristic X-rays, irrespective of whether photons of high energies are emitted in coincidence or not. In the next few paragraphs, we shall briefly study the interaction of these X-rays with matter.

(b) Interaction of X-rays with Matter.

In sharp contrast to the relation between energy and range which characterizes the absorption of a heavy charged particle, a beam of X-rays exhibits a characteristic exponential absorption in matter. The reason is as follows. In the process of absorption or scattering which removes X-ray photons from the incident beam, each photon is eliminated individually in a single event. If we denote by σ the total cross-section per atom for either the scattering or the absorption of a photon of the original energy, the beam intensity, I_x, at the distance t centimeter within the absorber will have the following form:

$$I_x = I_o e^{-N\sigma t} = I_o e^{-\mu t} \qquad \ldots\ldots\ (9)$$

where I_o is the incident intensity, N is the number of atoms of the absorber per centimeter cube, and $\mu = N\sigma$ $(\text{cm.})^{-1}$, the linear absorption coefficient of the impinging radiation.

Apart from resonance effects at special frequencies which correspond to atomic or nuclear transitions, there are three main processes, all smooth continuous functions of the photon energy contributing to the total cross-section σ.

These are: (1) photoelectric absorption (77), (78), and (79); (2) Compton scattering (80); and (3) pair production of a positron-electron in the field of the atom (81). For the range of X-ray energies which concerns us (up to 25 kev) and according to the results of White (82) reported in Appendix II, processes (2) and (3) have a negligible cross-section when argon is the gas undergoing ionization.

In the photoelectric process, all the energy ($h\nu$) of the incident photon is transferred to a bound electron which is emitted from the atom with a kinetic energy $T=(h\nu - I)$, where I is the ionization potential of the particular shell in which the electron is originally found. The effect for a given shell in the atom is largest at photon energies close to the ionization potential for the shell and falls off rapidly with increasing photon energy, (see Appendix II). In 1930, Bethe (83) published a theory of the energy lost by a fast electron undergoing inelastic collisions with atomic electrons. The average energy expended in forming one ion-pair is larger than the ionization potential I, since many of the collisions lead to excitation of the gas without ionization. In the case where those collisions lead to ionization, fast secondary electrons may in turn lead to secondary ionization and various forms of ionization will be measured in terms of the primary or total specific ionization respectively.

(c) Basic Methods of Measurement.

The measurement of disintegration rates depends on the detection and the assessment, by various methods, of radiations emitted by a source. The methods most successfully used may be divided into two groups, namely the energy emission and the radiation measurement.

(1) Energy Emission Methods.

The energy methods can be subdivided into three: calorimetric, loss of charge by the source and ionization current measurements. The applicability of these methods was thoroughly detailed by Pate in his Ph.D. thesis (84). A major reason which does not permit us to use such methods is due to the low specific ionization of X-rays.

(2) Radiation Measurement Methods.

The most direct approach is by the measurement of the radiations leaving the source. Hence, individual disintegrations are detected and specificity may also be measured since the nature of the radiation and its energy are characteristic of the nuclear transition. With the advent of refined techniques in chemical separations (85) and in source preparations (86) the method is unquestionably the best. Moreover, the availability of standard electronic equipment militate in favour of this method.

Two main types of radiation detectors, namely scintillation and ionization, have been employed. Attempts were made to use solid (87) and liquid scintillators (88), and (89), for the detection of the soft characteristic X-rays but no successful measurements were reported on account of some intrinsic instrumental factors. The main ones are:

(1) high voltage applied on the photomultiplier tube which lead to the distortion of the pulses and the arising of low level spurious noise.

(2) high amplifier gain (20 to 40 x 10^3) applied on the photomultiplier tube.

(3) poor energy resolution of the detector (70 to 80 percent for energies in the range of 6 kev).

(4) an escape peak probability of about 40 percent for energies above K binding energy of the detector and having a mediocre geometrical efficiency ($< 2\pi$).

(5) finally, chances of incomplete photon absorption if thin scintillators are used.

Gas scintillation techniques using rare gases of high atomic humber have shown almost complete intensitivity to electromagnetic radiations (90), and no one has yet attempted to standardize nuclides decaying by electron capture in this manner. This leaves ionization methods and in the next paragraphs, we shall investigate the properties of various counting chambers.

Counting Chambers.

The modes of operation of ionization chambers, proportional counters, and Geiger-Müller counters constitute a voluminous literature (91), (92), (93), (94), (95), and (96). The first publication goes back to 1908 when Rutherford and Geiger (97) wrote on the detection of single alpha particles passing through a gas. Much work was done from 1908 onwards, but little progress is the understanding of the mechanisms of operations has been made.

The basic circuit of a gas-discharge counter is diagramatically described below and was used by Geiger and Müller in 1928 (98).

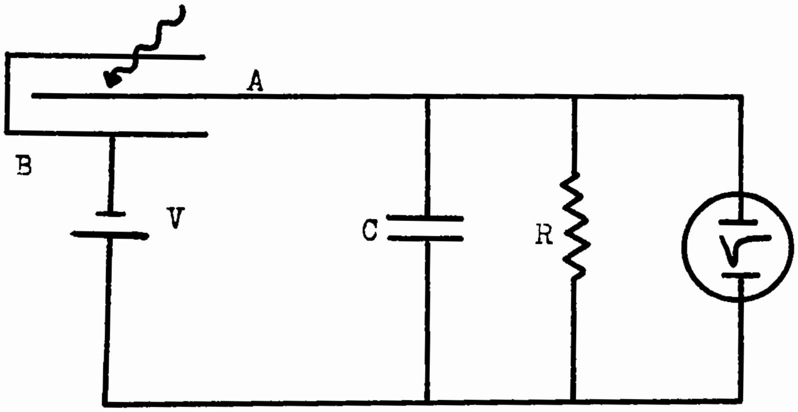

It consists of an anode A and a cathode B. The field between is energized by the application of a potential difference supplied by a voltage set V. The passage of an ionizing radiation will cause a momentary discharge in the counter triggered off by primary electrons and amplified by secondary electron collision processes inside the counter. After the discharge has caused a momentary voltage pulse to appear on the wire, the whole system returns to its quiescent state, in readiness for the next discharge. To prevent counter break down into a steady glow discharge, high input resistance R matched with a low capacitance C would lead to a circuit time constant of the order of 10^{-2} second. Neher and Harper (99) have developed a quenching circuit in which the recovery of the system would be controlled by an RC time constant of a grid circuit and may be made of the order of 10^{-4} sec. Another solution to remedy the very long resolving time constants of early Geiger-Müller counters was proposed by Rossi (100) in which two or more counters are used in coincidence. Many aspects of counter work including Rossi coincidence counting were revolutionized by the appearance of a series of papers by Trost in 1937 (101), (102), and (103). He noted that the addition of small amounts of complex polyatomic organic vapors to the more usual simple gas such as argon, radically altered the type of gaseous discharge taking place and very low values of R, still enabled the chamber to produce a pulse. The discharge appeared to be quenched inside the counter and not, primarily, by circuit action. A voluminous literature on the mechanism of this quenching action exists.

Counter Characteristics.

A complex relationship exists between the voltage applied to a discharge counter and the current passing through it. The counter characteristics operated within the basic circuit previously described are explained in Fig. 5. The collected charge (pulse size) is plotted against the anode voltage for two different initial ionizing events. The ionization is initiated by an alpha particle and a beta particle, each producing different number of ion-pairs in the primary ionizing event.

These curves can be divided into four main regions. In region I, there is a competition between the loss of ion-pairs by recombination and the removal of charge by collection on the electrodes. With increasing field the drift velocity of the ions increases; therefore the time available for recombination decreases and the fraction of the charge which is collected becomes larger. In region II, the recombination loss is negligible and the charge collected is equal to the number of electrons formed in the primary ionization. This

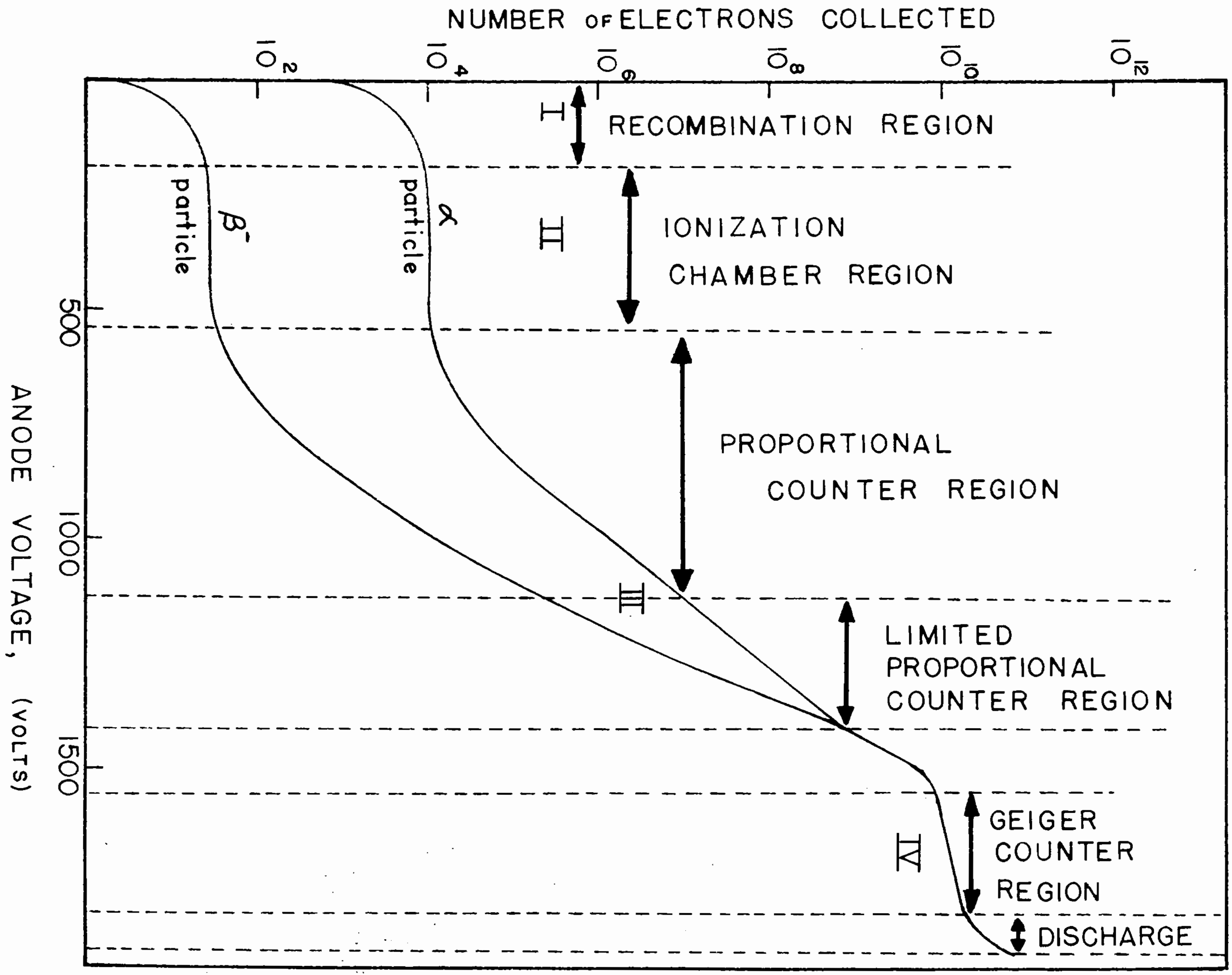
NUMBER OF ELECTRONS COLLECTED
10²
10⁴
10⁶
10⁸
10¹⁰
10¹²
ANODE VOLTAGE, (VOLTS)
500
1000
1500
β⁻ particle
α particle
I
RECOMBINATION REGION
II
IONIZATION CHAMBER REGION
PROPORTIONAL COUNTER REGION
III
LIMITED PROPORTIONAL COUNTER REGION
IV
GEIGER COUNTER REGION
DISCHARGE

region is referred to as the saturation region or the ionization chamber region. Rose and Ramsay (104), in particular, have successfully studied the upper limit of this region. As the voltage is raised further, we reach region III, in which the collected charge is increased by a gas multiplication factor "A" through the phenomenon of the familiar Townsend avalanche. The electrons which are released in the primary ionization are accelerated sufficiently to produce additional ionizations and thus add to the collected charge. At the onset of region III, the gas multiplication "A" for a given applied voltage is independent of the amount of the initial ionization, thus preserving the proportionality of pulse sizes. This strict proportionality breaks down with increase in applied voltage where the upper limit of region III, until at the pulse size becomes independent of the amount of the initial ionization. This region in which gas multiplication is employed while, at the same time, some dependence of the collected charge on the initial ionization remains, is known commonly as the proportional region and its upper limit is designated as the region of limited proportionality.

On the basis of a discharge mechanism in which the gas multiplication factor "A" is due to an electron avalanche, theoretical and experimental investigations of the onset of region III were made by Rose and Korff (105). Their calculations relied on the fact that the factor could be expressed in terms of the first Townsend coefficient α as:

$$A = e^{\int_{x_1}^{x_2} \alpha dx} \qquad \text{........ (9)}$$

This equation assumes a coaxial cylinder geometry in which the mechanism of the pulse formation is examined electrostatically. The lower limit x_1 and the upper limit x_2 may be set equal to r_1, the wire radius and to r_c, the critical radius where the electric field become high enough to initiate the avalache. At the threshold, r_c equals the wire radius r_1, and never becomes much greater. From this crude remark based on involved calculations made on the "mean free path for ionization", we may assume an approximately linear dependence on the voltage. Hence, we may relate the radius r_c where the threshold voltage V_P initiates the multiplication to the operating voltage, V_o, applied to the chamber by the following relation:

$$\frac{r_c}{r_1} = \frac{V_o}{V_P} . \qquad \text{........ (10)}$$

At this point, Rose and Korff have given a new treatment to the problem, assuming an ionization cross-section linear with energy above the threshold. The addition of the assumption that the electron-energy spectrum shows a monotonic decrease at the ionization potential leads to an effection α , the reciprocal of the mean free path for ionization or the first Townsend coefficient, of the form:

$$\alpha = \left(\frac{a.N.c.V}{r} \right)^{\frac{1}{2}} . \qquad \ldots\ldots\ldots \; (11)$$

Hence, combining this with Eq. (10) and using the definition of "A" from Eq. (9), we obtain:

$$A = e^{2(a.N.c.r_1.V_o)^{\frac{1}{2}}} . \left[\left(\frac{V_o}{V_P} \right)^{\frac{1}{2}} - 1 \right] \ldots\ldots \; (12)$$

which defines the gas multiplication factor "A" in terms of experimentally measurable quantities, namely the rate of increase of cross-section ionization, a, of the counter gas, the pressure, N, of the counter gas, a constant, c, which is the capacity per unit length, the anode wire radius, r_1, the operating voltage, V_o, across the chamber and finally, the threshold voltage, V_P, at which the avalanche starts. Further discussions of Eq. (12) will take place in part D of this thesis which will deal with the experimental verification of Rose and Korff's theoretical equation.

Within the region IV, true proportionality is not obtained, hence the charge collected is independent of the amount of the ionization initiating it. An important criterion we can make here is this: purely from pulse size measurements, no information as to the nature of the primary particle can be obtained. The gas multiplication increases the charge to a value that is limited by the characteristics of the chamber and the external circuit. This region is known as the Geiger region. In general, in regions II and III, the ionization is localized and confined to the neighbourhood of the path of the triggering electron or electrons the discharge spreads to some extent in region III; and all pulse sizes are equal due to spreading of the discharge to the ends of the counter at each count in region IV.

In this thesis, we will use a counter operated in region III, namely the proportional region where, for a constant voltage across the chamber, the pulse sizes will be proportional to the number of ions formed in the initial ionizing event. From this qualitative property, and when they are matched with electronics which permits the differentiation into various pulse heights, such counters are also called spectrometers.

The curves of Fig. 5 are not to be confused with the high anode voltage characteristics of a chamber, which is the relationship between the counting rate observed and the polarization voltage, with a given number of particles entering the chamber per unit interval. Fig. 6(a) displays the shape of such curves, called plateaux. They are the regions in which

Figure 6

General Characteristics of Proportional Counters

(a) Voltage-plateau for two different particles of different energies.

(b) Bias discrimination properties for two different particles of different energies.

(c) Differentiation of the count rate with respect to the energy of the respective particles versus bias discriminator.

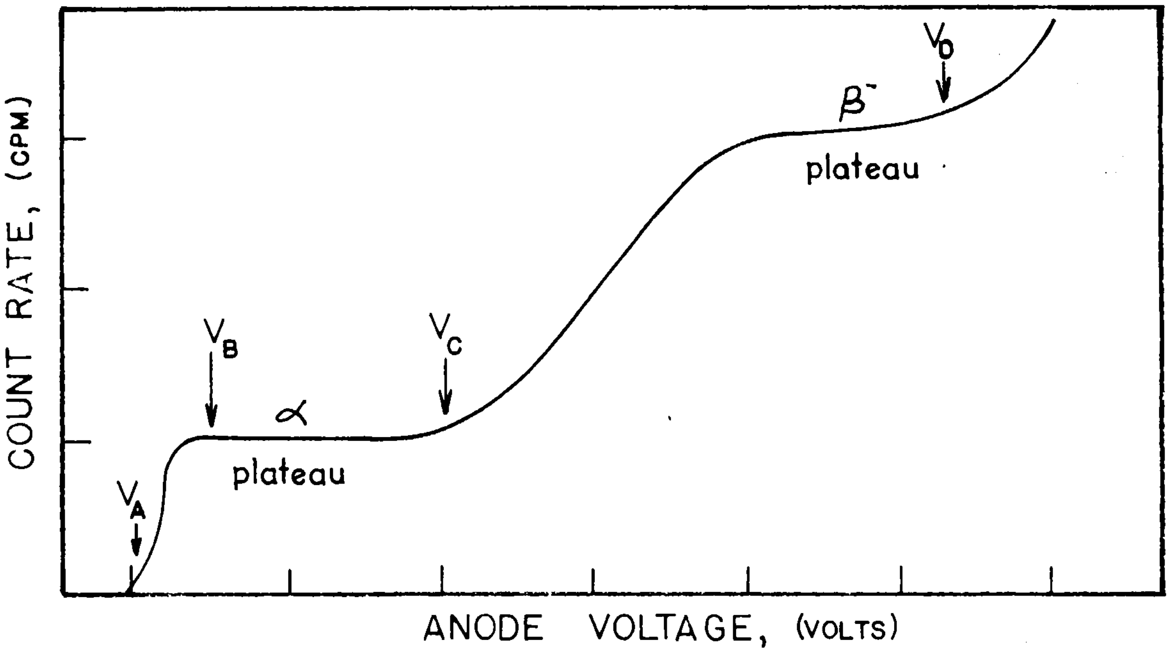
COUNT RATE, (CPM)
ANODE VOLTAGE, (VOLTS)
V_A
V_B
α
plateau
V_C
β^-
plateau
V_D

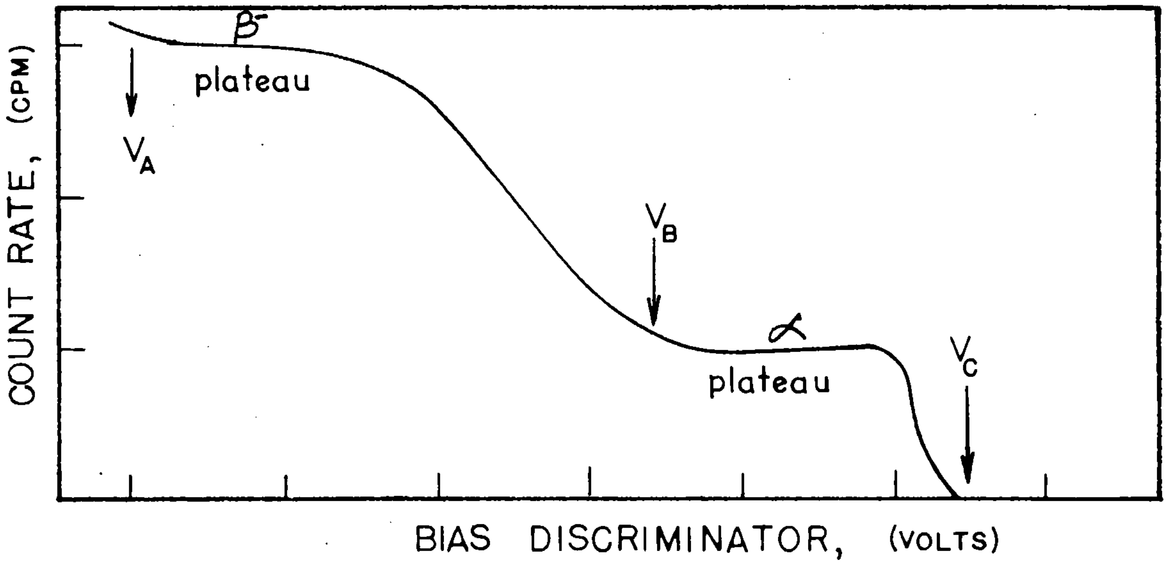
COUNT RATE, (CPM)
BIAS DISCRIMINATOR, (VOLTS)
β^-
plateau
V_A
V_B
α
plateau
V_C

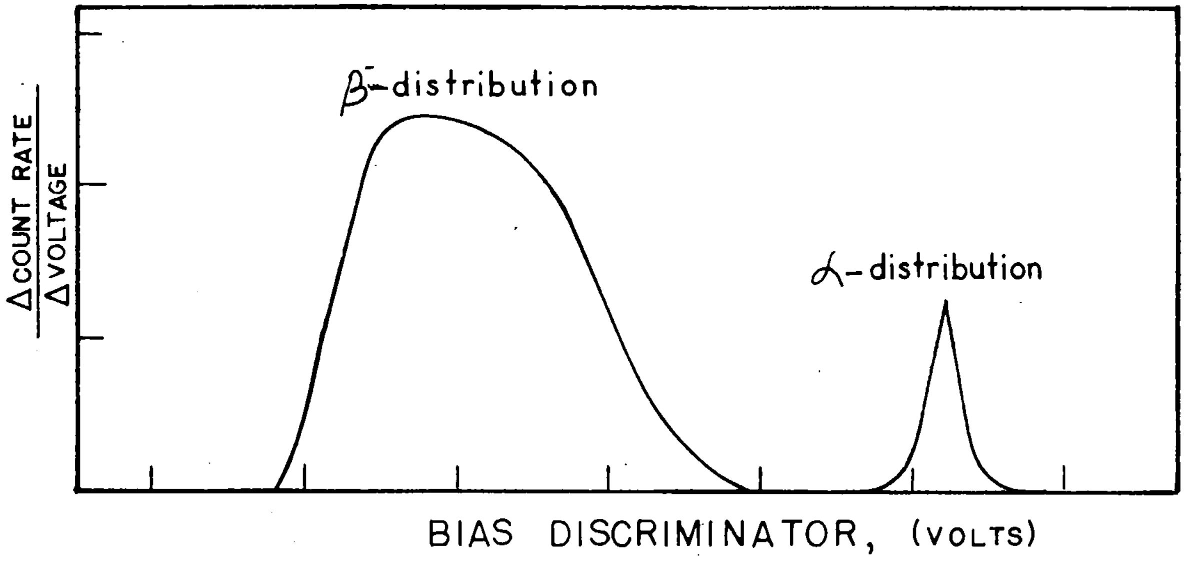
$\frac{\Delta \text{COUNT RATE}}{\Delta \text{VOLTAGE}}$
BIAS DISCRIMINATOR, (VOLTS)
β^--distribution
α-distribution

the measurements are performed and are partly a function of the counter gas (nature and pressure), the anode to cathode ratio, and the electronic circuit coupled with the counter. Here, the counter is operated in the proportional region and the radiations are monoenergetic alpha particles and also beta particles which have an energy distribution. The starting voltage V_A for the alpha plateau represents the conditions for which the most energetic alpha particles dissipate their entire energy in the counter and the gas multiplication factor is just sufficient to allow the pulses to trigger the recorder or pass over the discrimination line. As the voltage is increased further, V_B, the region is reached where all the alpha particles produce pulses which pass the discriminator line; this condition leads to the alpha plateau. As the applied voltage is increased above V_C, the count rate starts to rise again. This occurs when the gas multiplication becomes sufficiently great that some beta particles are counted. After a transition region, a beta plateau is obtained.

Another characteristic often given in the literature for counters of various type is the discriminator bias. Such a characteristic curve is represented in Fig. 6(b). For example, if one takes a fixed polarization anode voltage with the gas multiplication high enough so all the pulses will pass over the minimum discrimination line, then at low bias discrimination,

V_A, all the pulses will trigger the recorder. As the voltage is increased, a bias-plateau due to all beta and alpha particles will be screened out until V_B is reached for another bias-plateau only due to pulses from alpha particles. At higher bias voltages such as V_C, the rate falls due to the fact that some pulses from the ionizing events fail to register. In Fig. 6(c) the differentiation of the integral count rate with respect to bias voltages is plotted against the bias voltages. One can then obtain the relative distribution of the two different particles on an energy scale.

Counting chambers operated in the ionization chamber region and in the proportional region enable us to evaluate, in principle at least, the number of radiations emitted by a source in two different ways. Although they are the same in origin, one can measure the integral counting rate on a scaler or measure the counting rate beneath the area of the photopeak after a pulse height analysis.

The proportional counters have numerous advantages over the ion-chamber counters. The most important are the following.

(1) Smaller chances of recombination after primary ionization.

(2) Easier discrimination between noise levels and primary ionization levels.

(3) A gas multiplication factor which serves to amplify the pulses and which is constant at any definite voltage.

(4) Linearity of the gas multiplication factor with the variation of the polarization voltage.

(5) Requirement of standard electronic equipment having moderate gain amplification (about 5,000).

Proportional counters also have some marked advantages over the Geiger-Müller counters. The main ones are the following.

(1) A reasonable resolving time ~ 0.5 μsec. compare to ~ 400 μsec. for the Geiger-Müller counters. The resolving time of a Geiger-Müller counter also varies with counting rates while that of a proportional counter does not.

(2) The counter gas pressures can be varied over a wide range and the use of flow systems is very suitable.

(3) The use of a smaller anode voltage to create a field across the chamber.

(4) Less chances of gas discharge, especially corona-discharges.

(5) Spectrometric properties which allow the discrimination between charged and uncharged radiations.

(6) The proportional counter can tolerate the presence of some "contaminative" gases such as air, organic molecules, etc., which is intimately mixed with the counter gas, whereby such

"contaminative" gases would alter the flatness of the Geiger-Müller plateau sensibly.

(7) The fact that the background counting rate decreases with decreasing anode voltage, while the sample counting rate does not is also a subtle advantage that proportional counting offers over Geiger-Müller counting. This advantage has a marked effect for samples where the radiations have specific ionization which is high.

From the above advantages, the use of a proportional counter in an attempt to solve the problem of disintegration rate determinations of nuclides decaying by electron capture is presumably the most convenient. Now, we shall proceed to discuss various methods of such absolute disintegration rate measurement which have employed radiation detectors.

(i) Coincidence.

The coincidence methods of absolute standardization of nuclides are applicable whenever a radioisotope with a simple decay scheme emits simultaneous radiations (within a time which is short compared with the electronic resolving time) (106). In 1954, Putman and Allen (24) proposed three different coincidence methods of standardizing nuclides which decay by electron capture. In the first method, they suggested the measurement of the characteristic X-rays in coincidence with the gamma rays using counters external to the source for both measurements. The second method is the measurement of the characteristic X-rays plus the Auger electrons with a 4π Geiger-Müller or proportional counter which is in coincidence with the gamma rays measured with an external gamma counter. The third possible method would be the measurement of the characteristic X-rays in coincidence with the gamma rays using two scintillation counters.

Although the second method will establish the efficiency of the 4π counter for a particular source, the calibration cannot, unfortunately, be used for other sources of the same type because of self-absorption variations.

Methods one and three will consist in mounting a source in which the Auger electrons will be filtered out and thereafter be placed between an X-ray detector and a gamma-ray detector so that disintegration rates will be recorded by each. From the number of coincidences observed, the absolute disintegration rates may be estimated. If the overall efficiency of the X-ray detector is ε_X, that of the gamma-ray detector ε_γ and N_o is the number of disintegrations of the source in unit time, then, the counting rate, R_X, in the X-ray detector will be

$$R_X = \varepsilon_X . N_o, \qquad \text{.........} \ (13)$$

while in the gamma-ray detector,

$$R_\gamma = \varepsilon_\gamma . N_o. \qquad \text{........} \ (14)$$

The coincidence rate of counting is $R_{X-\gamma} = \varepsilon_X \cdot \varepsilon_\gamma \cdot N_o$ since of $\varepsilon_X N_o$ counts recorded in the X-ray detector a fraction causes counts in the gamma-ray detector. Eliminating ε_X and ε_γ from these equations, we get,

$$N_o = \frac{R_X \cdot R_\gamma}{R_{X-\gamma}} , \qquad \text{........ (15)}$$

from which the disintegration rate may be deduced without knowledge of the counter efficiencies.

According to Putman (107), the eq. (15) for the disintegration rate N_o will hold if any two of the three following criteria are valid.

(1) Uniformity of the activity over the whole source area.

(2) Constant efficiency of the X-ray detector to X-γ radiations.

(3) Constant efficiency of the gamma-ray detector to gamma-radiations.

Although the theory of coincidence methods measurements is relatively simple, difficulties may arise in the following cases:

(1) nuclides exhibiting a branched scheme when gamma rays may accompany only a proportion of the characteristic X-rays or Auger electrons. It is assumed that for a branched decay scheme, the K/L ratio is equal in different branches, but the X-ray

detector has a different efficiency for K and L X-rays. Also, many nuclides decaying by electron capture have sometimes an alternative mode of decay, namely positron or negatron emission. In such cases, the coincidence counting technique is not applicable.

(2) nuclides in which internal conversion is important. This concerns, especially, nuclides emitting low energy de-excitation gamma rays. In such a case, if the low energy photon is internally converted in the K shell, this will lead to an additional characteristic X-ray. Also, the X-ray detector will invariably be sensitive to low energy photons which are not internally converted.

(3) incorrect compensation for dead time losses in the separate counters. This may be considerable since quite intense sources need to be used if coincidence counting rates are to be measured to good statistical precision.

(4) incorrect compensation for background effects. The natural background counting rate of the two detectors separately and in coincidence must be substracted from the relevant reading.

(5) incorrect compensation for random coincidences. Although the counting rates of the gamma and the X-ray detectors may not be directly related, a certain random coincidence rate is always observed. The random coincidence rate is $R_X.R_\gamma (t_X+t_\gamma)$ where R_X and R_γ are the observed activities and t_X and t_γ are the

resolving times of the two detector assemblies.

(6) the method is definitely not applicable to nuclides which decay directly by electron capture to ground state. At least, thirty-four such nuclides are known in the literature.

(7) the possibility that some error may arise in such coincidence method due to X-ray — gamma-ray or Auger electron — gamma-ray angular correlation. The X-ray — gamma-ray angular correlation in orbital electron capture has been theoretically investigated by Brysk and Rose (108). Their work suggests that, while angular correlations exist in general, selection rules enforce isotropy in most cases where nuclear information is available.

The coincidence method is easily and with good accuracy applicable only to nuclides which decay by a single capture event to an excited state (metastable state) of the product nucleus of very short half-life, ($<10^{-10}$ sec.). The nuclides satisfying this criterion form a very small proportion of those it is of interest to observe.

(ii) <u>Gas Counting</u>.

For standardization of low atomic number (Z) nuclides decaying by electron capture (<20), the radioactive material can sometimes be introduced into the counter itself in gaseous or vapor form (91). The gas must be suitable for operation in the region of ionization. For beta-ray measurements of this type, much is gained by having no self-absorption or source backscattering problems. On the other hand, in X-ray counting, self-absorption and backscattering are not major sources of error. Kirkwood, Pontecorvo, and Hanna (77) in 1948 were the first to use this technique with nuclides decaying by electron capture. They studied for the first time L capture of A^{37} and applied the properties of the proportional counter to calculate the L/K capture ratio. In the same field of research, Fink (109) has published extensively giving experimental data on L/K capture ratios. This method is incontestably the best for the relative study of capture ratios and for the detection of very low X-ray energies. However, no attempt was made to apply the method, in a general manner, to determine the disintegration rate of nuclides decaying by electron capture.

The following sources of error are inherent in the gas counting method and corrections for these must be applied.

(1) The sensitive volume. The sensitive volume of a gas counter is approximately that enclosed by the cathode if the centre wire passes right through it. In some designs, the sensitive volume is governed by the exposed length of the centre wire. The distorsion of the field at both ends (end effects) will invariably alter the disintegration rate. A loss of counts may also occur near the walls of the cathode corresponding to those

radiations which escape without producing ionization. This wall effect was investigated by Engelkemeir and Libby (11) in the case of beta particles. Concerning the dead volume at both ends, Mann and Parkinson (12) have proposed an elegant method of correction by use of a set of compensated gas counters. If this gas counting technique is applied to nuclides decaying by electron capture, the same factors of sensitive volume corrections can be applied even to a greater extent to X-rays.

(2) Cross-contamination, which is called "memory effect" by Bernstein and Ballentine (110). This contamination is due to the adsorption or exchange with the wall of the counter.

(3) Complete transmission of the X-rays through the counter gas which does not lead to backscattered fluorescence-excitation radiations.

(4) Quenching of the counter gas due to addition of the radioactive gas (111), and (112).

(iii) Defined Angle.

The radiations from a radioactive source are isotropic except to the extent that they are modified by absorption and scattering. In the low geometry counting methods, the conventional Geiger-Müller end-window counter represents a system amenable to absolute disintegration rate determinations. However, its application to the problem at hand necessitates a careful evaluation of the many correction factors which are necessary.

Burtt (113), and Zumwalt (114) have determined an expression relating the count rate, R, to the disintegration rate, N_o, of the source. The relation is,

$$R = N_o . G . f_W . f_A . f_B . f_H . f_S \qquad \text{........ (16)}$$

where G is the solid angle subtended by the counter at the source divided by 4π-steradians and the f's are the factors due to

W -- absorption of the radiations in the counter window and air between the source and the counter.

A -- scattering of radiations into the counter.

B -- backscattering of radiations from the source mount.

H -- scattering of radiations due to counter support and housing.

S -- absorption and scattering of radiations within the material of source itself.

In addition to the above, corrections need to be made for the counter background, the counter dead-time, the excitation-fluorescence radiations and the transmission of the X-rays through the chamber. It is clear that in view of the multitude of corrections that has to be supplied, it is difficult to obtain great accuracy with this method. With a counter of low geometrical efficiency ($< 2\pi$), namely an end-window-type proportional counter, Lyon and Reynolds (27) have applied this method in 1957. They attempted to standardize nuclides decaying by electron capture emitting X-rays in the range between 5 and 13 kev.

4π-steradian Counters.

In 1957, Allen (26) used a 4π-steradian cylindrical proportional counter which can be operated at elevated pressures. The source is sandwiched between aluminum foils thick enough to filter out the Auger electrons and is placed between the two halves of the detector. The observed count rate is plotted on a semi-logarithmic scale as a function of reciprocal pressure. Extrapolation to infinite pressure gives the total X-ray absorption inside the sensitive volume. The method is very ingenious since it gives an absolute measurement of the X-rays leaving the source. However, one difficulty which arises from the method is due to the geometrical arrangement of the anodes with respect to their respective halves. This leads to some restrictions concerning the energy resolution and energy linearity.

In the same year, Campion and Merritt (27) described a method similar to that of Allen. They employed an 8 in. diameter spherical 4π-steradian proportional counter. This counter can be operated at pressures high enough to get total absorption of the X-rays. Utilizing this method, samples of Fe^{55} were standardized.

For routine work in radiochemistry laboratories, the above two counters are not too versatile. Moreover, one often needs to standardize nuclides decaying by electron-capture having atomic number (Z) greater than 30. We have attempted to use a counter which has simultaneously the properties of a detector and a spectrometer. The electrodes are cylindrical and coaxial and the geometrical efficiency was found to be 2π-steradians.

6) 2π PROPORTIONAL COUNTER

(a) History

Since 1948, the proportional counter, as we now know it, has been developed rapidly. It is true that prior to this time it was widely appreciated that counters could be used at voltages such that the output pulses differed according to the nature of the ionizing particle passing into or through the vessel.

The first study of the proportional counter defined as an aid to analyze a spectrum of various radiations was made in the year of 1948. It was shown by Curran, Angus, and Cockroft (115) that the chamber could exhibit the complete spectrum of the beta rays of tritium, each beta particle emitted by the source giving rise to a pulse of amplitude proportional to the energy of the primary beta itself. The energy scale was fixed by means of the photoelectrons produced in the gas of the counter by virtue of the photoelectric absorption of standard characteristic X-rays. In the same year, Kirkwood, Pontecorvo, and Hanna (77) examined K and L capture phenomena in A^{37} using the same method.

These developments were highly significant for they demonstrated that in the new type of proportional counters, one had a device which was capable of detecting and analyzing in energy the whole range of the radiations, from those of minimum specific ionization to those of high specific ionization, i.e., fission fragments.

The application of the spectrometric properties of such counters to determining the rate of disintegration of nuclides decaying by electron capture goes back to 1950, when Friedlander et al. (22) studied Ni^{57}.

In recent years, different schools (22), (26), and (27) have used the same method with varying degrees of success. Using similar instrumentation with improved characteristics, we have attempted to increase the accuracy inherent in the method.

(b) Advantages of the Method.

The design is not original but the instrument has some properties which offer some advantages over all the others. The most important are the following.

(1) A source-to-counter geometry of 2π-steradians.

(2) A counter which can be used as a windowless detector.

(3) A counter having an additional thin window made of beryllium. This window will be very useful for external source measurements or for simultaneous energy calibration such in beta spectroscopy.

(4) The operation of the counter at low or high pressures.

(5) The use of the counter as a gas-flow counter.

(6) The radial displacement of the source with respect to the anode when a movable platform is used.

(7) Ability to change the anode wire readily. When high pressures or high atomic number counter gases are required the use of proper anode size enables one to use a lower voltage across the chamber.

(c) Correction Factors.

To determine a disintegration rate, one has to apply some correction factors to the observed counting rate. The relation between disintegration rate and the counting rate will be given by,

$$R = N_o.G.f_e.f_A.f_T.f_{W_K}.f_R \qquad \ldots\ldots\ldots (17)$$

where, R is the counting rate observed on the scaler or beneath the main photopeak, and N_o is the disintegration rate.

A foil of sufficient thickness is used to screen out any contribution due to the Auger electrons. The data, reported in Appendix III, give the thickness of aluminum or beryllium necessary for the screening of Auger electrons at various energies.

The correction factors are as follows:

(1) a factor G due to the source-to-counter geometry. This is equal to the solid angle subtended between the source and the counter divided by 4π-steradians.

(2) a factor f_e which will correct for the probability that a characteristic K X-ray of the counter gas will escape detection.

(3) a factor f_A correcting for lack of total absorption of the X-rays inside the sensitive volume. X-rays have a high probability of transmission through matter and therefore an average path length must be derived if one wants to correct for the X-rays passing through the vessel without ionizing the counter gas.

(4) a factor f_T correcting for the absorption of the X-rays inside the foil which screens the Auger electrons. In 1957, Campion and Merritt (27) derived an accurate equation which can be applied here.

(5) a factor f_{W_K} which is due to the total absorption of the K Auger electrons inside the filter. Data concerning the K-fluorescence yield are reported in Appendix I.

(6) finally, a factor f_R correcting for the contribution due to L-capture events (51), and (66).

The last two factors, of course, do not depend on the counter itself, but are inherent in the electron-capture process.

Other factors of correction, very small in nature, are (a) the failure of the counter to respond to every ionizing radiation, (b) the statistical fluctuations in the disintegration rate of the source, (c) the natural background which will be discussed in the second part of the experimental work and finally (d) any effects which cause an apparent decrease in the gas multiplication.

Since most of the radionuclides can be separated almost carrier-free, with the help of refined chemical techniques, the factor due to the self-absorption of the soft X-rays in the source itself does not concern us appreciably. In the next part of this work, we will apply one of these chemical techniques, namely ion-exchange reactions. Some results concerning the half-lives of the separated nuclides will also be given.

B. PREPARATION OF RADIONUCLIDES

1) INTRODUCTION

The investigation of the properties of a proportional counter to be used as a spectrometer necessitates examination of various calibration factors such as energy linearity and energy resolution. To perform these calibrations, emitters of monoenergetic radiations are required in order to produce pulses of known size.

In the early studies with proportional counters (116) the beam from an ordinary A.C.-operated X-ray generator was adjusted to operate at a small output intensity. This emitted soft radiations which were allowed to fall on a thin foil and the scattered radiation was detected in the counter at an angle to the beam direction. This radiation entering the tube consisted mainly of the fluorescence X-rays of the scattering element. However, the size of such an X-ray generator makes it cumbersome and the method is not ideal. Also, it may give rise to spurious pulses (due to electrical interference) and the calibration pulses are usually accompanied with an increase in the "background" of the counter.

Alternative sources of X-rays which are cheap, compact, easily transportable and simple to use have been made from (a) a thin foil bombarded with atomic or nuclear low energy photons,

(b) a thin foil bombarded with charged particles and (c) relatively long-lived radioactive species decaying by orbital electron capture.

The first method is presumably based on the photoelectric absorption of the photons in the inner shells of the scattering element. It was first applied by Insch (117) in an attempt to do an energy calibration on proportional counters. The fluorescence radiations were excited with the help of radioactive nuclides decaying by electron capture or decaying by low energy isomeric transitions. However, the technique suffered from the accompanying "background" due to the radioactive sources. Moreover, it required many sources to cover the range of X-rays needed for the investigation. This is due to the rapid variation in the absorption cross-section with the energy.

In the second method, the excitation is ascribable either to direct interaction between a charged particle and an atom or to the photoelectric absorption of bremsstrahlung photons emitted by a charged particle in the Coulomb field of the nucleus. Charged particles such as alpha rays or beta rays may be used.

Joliot and Curie (118) have deposited and volatilized an intense sourse of polonium on nickel, copper, and zirconium. The alpha rays from the polonium produced the characteristic X-rays of the element used as a source mount. However, there is a limit in the energy scale beyond which the X-rays cannot be produced by the nuclear alpha particles. Simple considerations of conservation of linear momentum and energy, taking account of the motion of the K-electrons, set this limit at an X-ray energy of about 14 kev. In fact, the most energetic X-rays that were obtained in this manner had an energy of about 12 kev (119). These came directly from the polonium source and are probably the L X-rays of either lead (Z=82) or polonium (Z=84).

With beta particles, Edwards and Pool (120) and later Siegbahn and Slatis (122) obtained characteristic X-rays when nuclear betas interacted with metallic radiators. However, no details of the dependence of the X-ray yield on the radiator thickness or atomic number and the maximum energy of the particles were available. In 1955, Reiffel (122) estimated the K X-ray yield versus the beta energy when the particles of a Sr^{90}-Y^{90} mixture were filtered through lucite and a radiator made of lead was used. More accurate results were obtained by Starfelt et al. (123) when measurements were made with beta particles of various energies. They showed how the yield and purity of the K-radiations varied with radiator material and thickness and with the beta spectrum.

In a recent publication, Cameron and Rhodes (124) encapsulated one millicurie of Kr^{85} in a small nickel tube and excited fluorescence radiation of various metallic foils. The energy of the characteristic X-rays obtained ranged from 5 to 24 kev.

These methods of producing X-rays when beta particles interact with a metallic radiator are very elegant, but bremsstrahlung photons leading to a continuous spectrum interfere with the main photopeak which is under inspection. Moreover, chemically pure radiators in the form of thin foils for particular elements are not always available. Hence, the number of calibration points in the range of energy of interest will be limited.

The application of the third method, namely the use of relatively long-lived radionuclides decaying by electron capture is for many reasons desirable. These could readily be produced in the McGill proton synchrocyclotron[*]. Then, the radionuclides could be directly used for calibrating the counter. Once the correction factors were established, disintegration rates could then be obtained. Also, the project of preparing some radionuclides decaying by electron capture was undertaken because of difficulties in obtaining nuclides of interest. This unavailability is probably due to the inherently high cost in producing relatively small quantities of long-lived species

---

[*] The author is indebted to Dr. H. Taniguchi for supervising the bombardments.

in large and costly charged-particle accelerators.

The series of radionuclides that we used for calibrations of the counter is summarized in Table I. Nine of them were prepared in this laboratory while five others were purchased. The energy of the characteristic X-rays to be studies ranged from 3 to 24 kev. The upper limit of 24 kev was chosen because our counting room is equipped with a 3 in. by 3 in. NaI(Tl) crystal which is calibrated for absolute measurements of X and gamma ray energies having a lower limit of about 25 kev.

As a guide in planning irradiations, cyclotron yield data reported, in 1952, by Martin and Breckson (125) were used. When available, chemically pure metallic foils were mounted directly on the probe. Otherwise, powdered targets were inserted into aluminium tubing. Thick targets were always used and the duration of the bombardments depended on the lifetime of the particular radioactive species.

To avoid absorption and energy degradation problems due to thick sources, attempts were made to achieve carrier-free separations from the targets. Then, the radioactive material would be mounted by one of the most common methods, namely the evaporation to dryness of the source after the mounting foil had been moistened with a hydrophilic agent. More refined source

TABLE I

Characteristics and Source of Supply of Nuclides

Nuclide	Half-life	Mode of Decay	Energy[**] kev	Source of Supply
Be^7	54 days	E.C. and γ	.052	McGill
Ca^{41}	10^5 years	E.C.	3.3	Chalk River
V^{48}	16 days	E.C., β^+ and γ	4.5	McGill
Cr^{51}	28 days	E.C., and γ	4.9	McGill
Mn^{54}	291 days	E.C., and γ	5.4	U.S.A.
Fe^{55}	3 years	E.C.	5.9	Chalk River
Co^{57}	270 days	E.C., and γ	6.4	U.S.A.
Zn^{65}	245 days	E.C., β^+ and γ	8.0	McGill
Se^{75}	125 days	E.C., and γ	10.5	McGill
Sr^{85}	64 days	E.C., and γ	13.3	McGill
Nb^{92}	10 days	E.C., and γ	15.7	McGill
Pd^{103}	17 days	E.C., and γ	20.2	McGill
Cd^{107}	6.7 hours	E.C., and γ	22.0	McGill
Sn^{113}	120 days	E.C., and γ	24.0	McGill

---

[*] U.S.A.: from Atomic Accessories Inc., Bellerose, 26, N.Y.

[**] Energy of Characteristic X-rays taken from Fine, S., and Hendee, C.F. Nucleonics <u>13</u>, 36, (1955).

preparation techniques were recently investigated and published by Blanchard, Khan and Birkhoff (86).

The foils for mounting the radioactive species were made of aluminium. The reason for this choice is the commercial availability, chemical resistivity, and the added advantage that no precautions are necessary to prevent charging of the source.

Various chemical procedures have been reported for radiochemical separations of many elements artifically produced (126), and (127). However, these separations involve the addition of stable isotopes of the same element as carrier, so that the chemical operation can be performed with minute quantities of the radioactive species sought. Since carrier-free radioelements are the desired products, these separations are unsuitable for our purposes. Chemical separation procedures for sub-microgram quantities of radioisotopes must be those which are practically mass independent such as ion-exchange (cation and anion) (88), paper electrophoresis or chromatography (128), solvent extraction (129), (130), vacuum thermal volatization (131), spontaneous or induced electrodeposition (31), co-precipitation ("scavenging") with non-isotopic carriers (132), and a few other particular methods.

The anion exchange technique was the one most generally used. This is due to the great versatility which the method offers (133). The radionuclides which were separated are summarized in Table II. For every separation, a standard column of 6 mm. inside diameter and 20 mm. total length was used. The bed, made of Dowex I (200 to 400 mesh), was 10 mm. long. As a check, the half-lives were followed with a 1 in. by 1 in. well-type NaI(Tl) counter and with the proportional counter described in this thesis. In the following pages, carrier-free separations procedures will be given and these are suitable for routine work.

2) CARRIER-FREE SEPARATIONS AND RESULTS

(a) Beryllium from Lithium.

The bombarded Li_2CO_3 target was dissolved in dilute HF. The Be^{++} ions were complexed as $(BeF_4)^{--}$ (134) while the Li^+ ions remained as cations (135). The solution was evaporated to dryness, redissolved in water and passed through the column which had been previously washed with water. All containers, including the ion exchange column were made of polythene. Fig. 7(a) shows the elution of the complexed $(BeF_4)^{--}$ with 0.5M HCl.

(b) Vanadium from Titanium.

For the separation of vanadium from the titanium target, a method originally due to Walter (136) was applied.

TABLE II

Carrier-free Separations

Target	Nuclide Separated	Time of Separation minutes
Li_2CO_3	Be^7	10
Ti	V^{48}	5
V	Cr^{51}	5
RbCl	Sr^{85}	15
Rh	Pd^{103}	120
Ag	Cd^{107}	5

Figure 7

(a) Elution of Beryllium

(b) Half-life Determination of Be^7: 53.5 days.

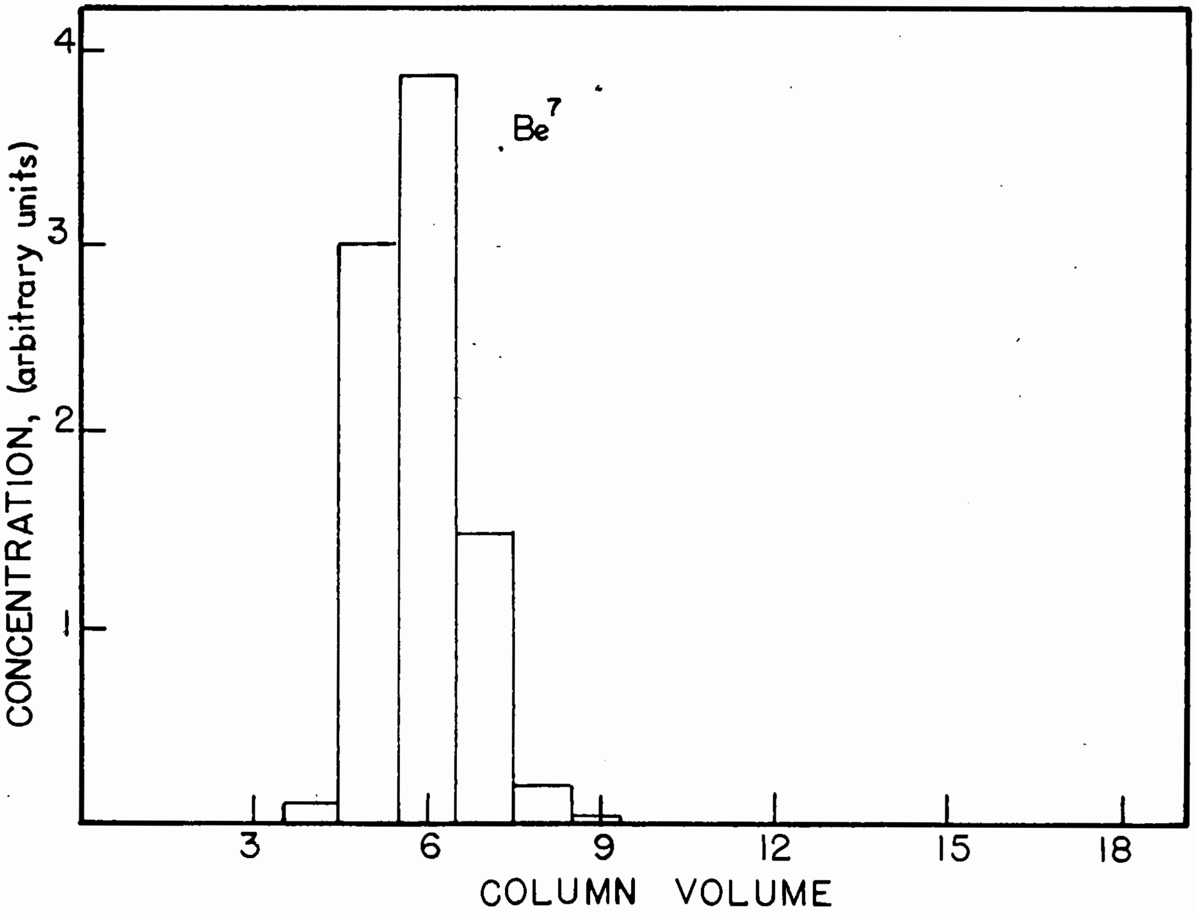
Be7
CONCENTRATION, (arbitrary units)
1
2
3
4
3
6
9
12
15
18
COLUMN VOLUME

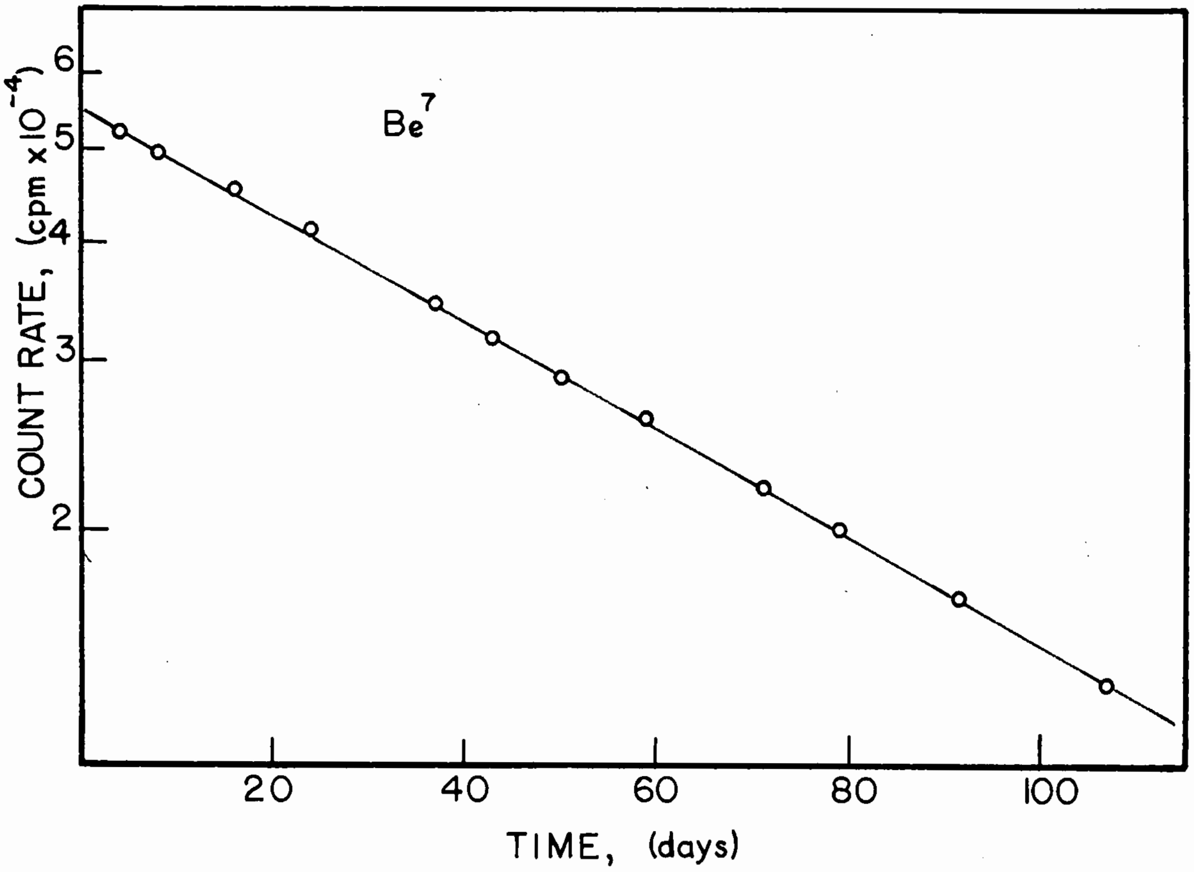
Be7
COUNT RATE, (cpm x 10-4)
2
3
4
5
6
20
40
60
80
100
TIME, (days)

The target was dissolved in a warm solution of 0.5M HCl. After dissolution, an equal volume of 0.1M $H_2C_2O_4$ was added and the solution was passed through the column which had been washed with the eluant (0.5M HCl + 0.1M $H_2C_2O_4$). As shown in Fig. 8 (a), the vanadium came out after the first few column volumes while the titanium could be eluted with 0.1M HCl.

(c) Chromium from Vanadium.

The radioactive vanadium foil was dissolved in hot "aqua regia", dried and redissolved in (0.1M HCl + 0.1M $H_2C_2O_4$). Then, the solution was passed through the column which had been washed with the eluant (0.1M HCl + 0.1M $H_2C_2O_4$) and a strong green band due to the complexed $(VCl_6)^{--}$ appeared at the top of the column. As shown in Fig. 9(a), the chromium came out at the very beginning while the vanadium could be eluted with a mixture of (0.5M HCl + 0.1M $H_2C_2O_4$).

(d) Strontium from Rubidium.

The bombarded RbCl target was dissolved in 0.1M disodium EDTA (ethylenediaminetetraacetic acid) hydrate solution buffered with NH_4OH to a pH of 9. The solution was then passed through the column and the rubidium came through while the strontium could be eluted with 1M HCl as shown in Fig. 10(a). Rb^{86} as a radioactive tracer was mixed with the target.

Figure 8

(a) Elutions of Vanadium and Titanium

(b) Half-life Determination of V^{48}: 16.5 days.

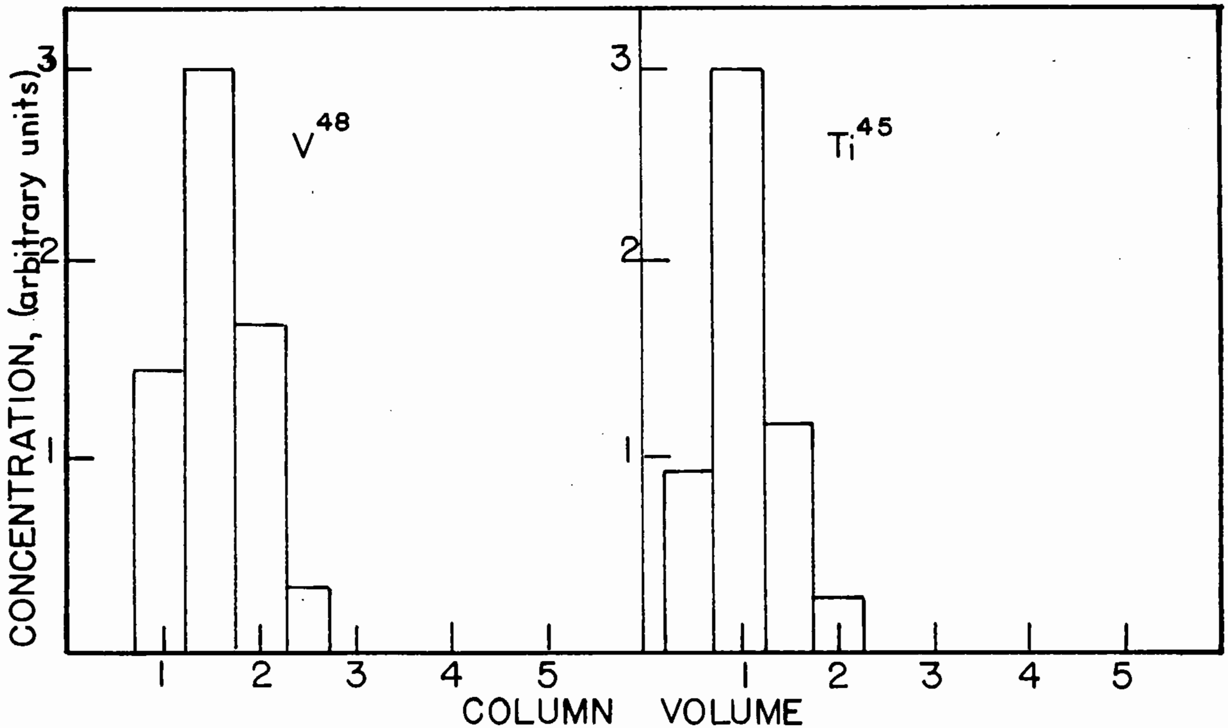
CONCENTRATION, (arbitrary units)
3
2
1
V⁴⁸
Ti⁴⁵
1
2
3
4
5
COLUMN VOLUME

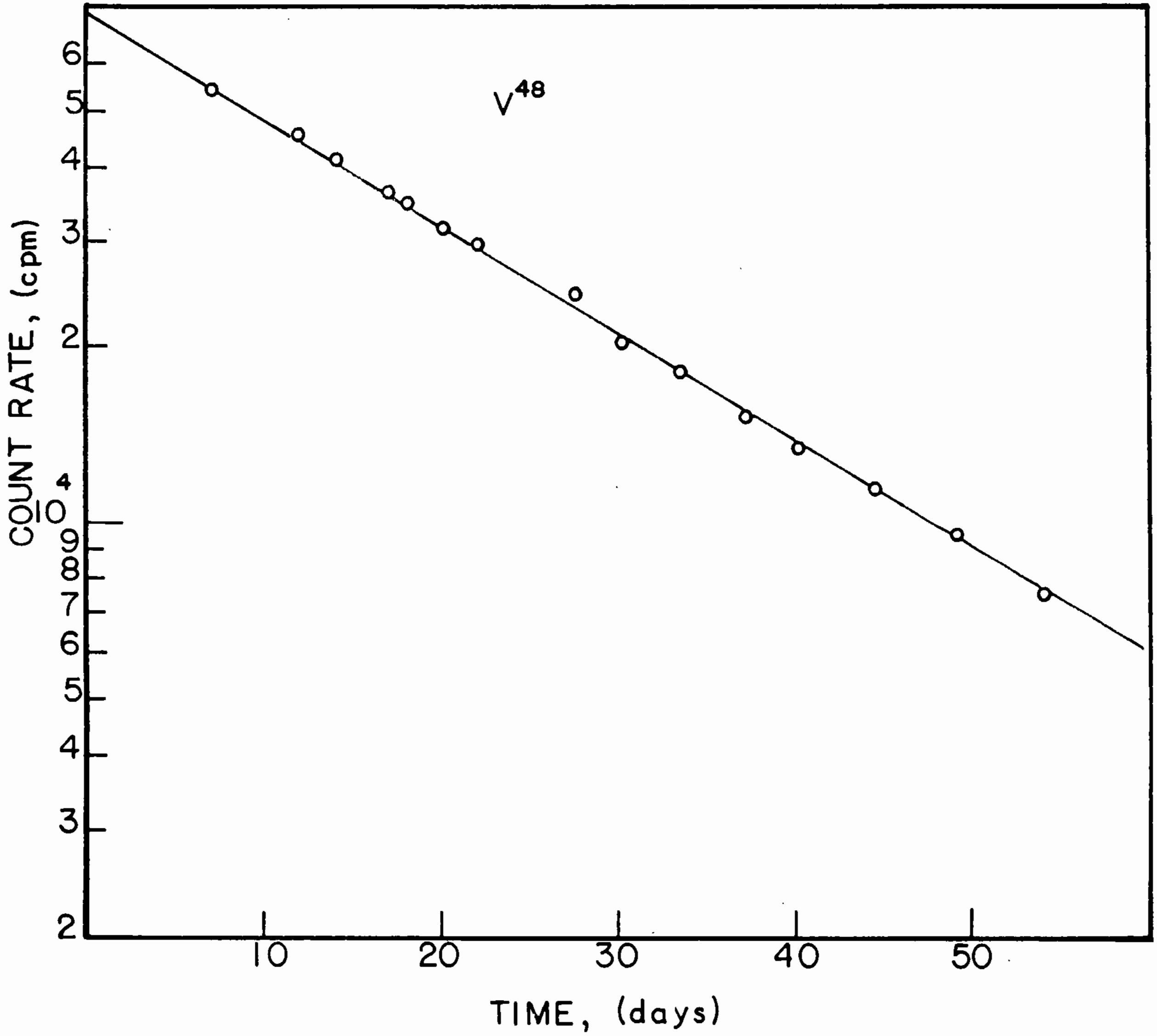
V⁴⁸
COUNT RATE, (cpm)
6
5
4
3
2
10⁴
9
8
7
6
5
4
3
2
10
20
30
40
50
TIME, (days)

<u>Figure 9</u>

(a) Elutions of Chromium and Vanadium

(b) Half-life Determination of Cr^{51} 27.7 days.

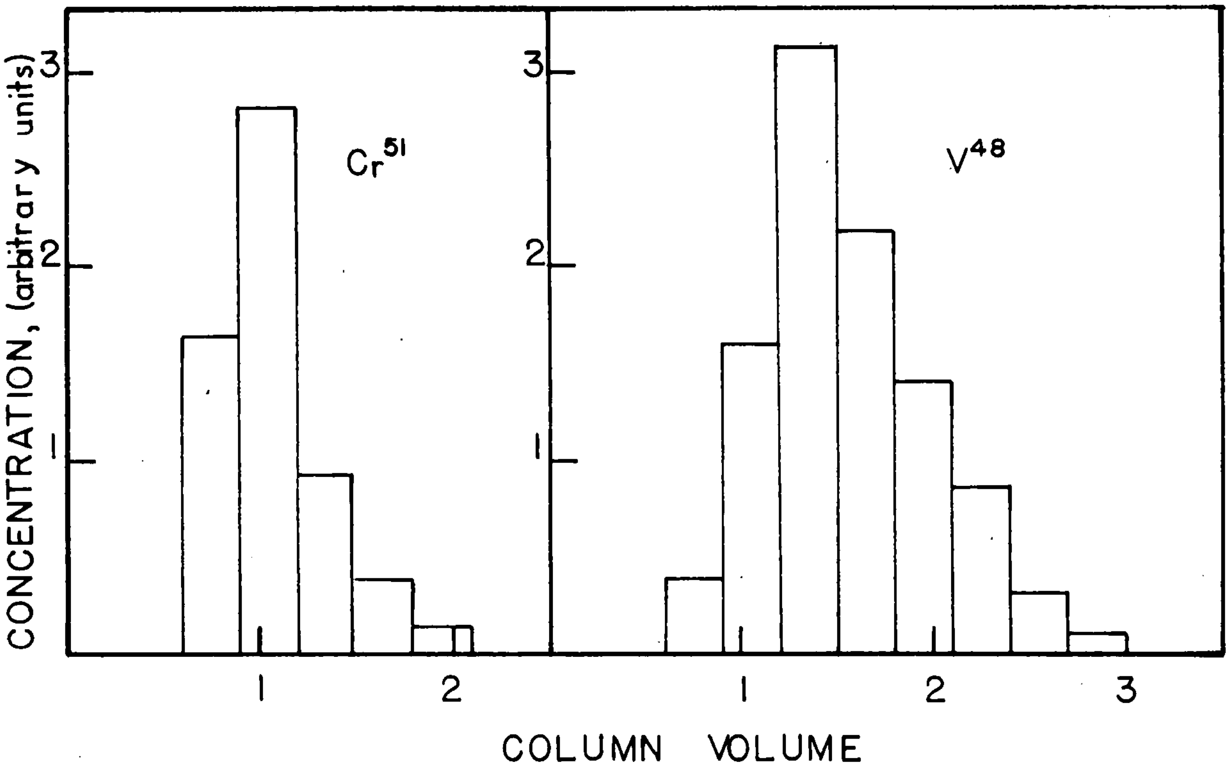
CONCENTRATION, (arbitrary units)
3
2
1
Cr^{51}
V^{48}
1
2
3
COLUMN VOLUME

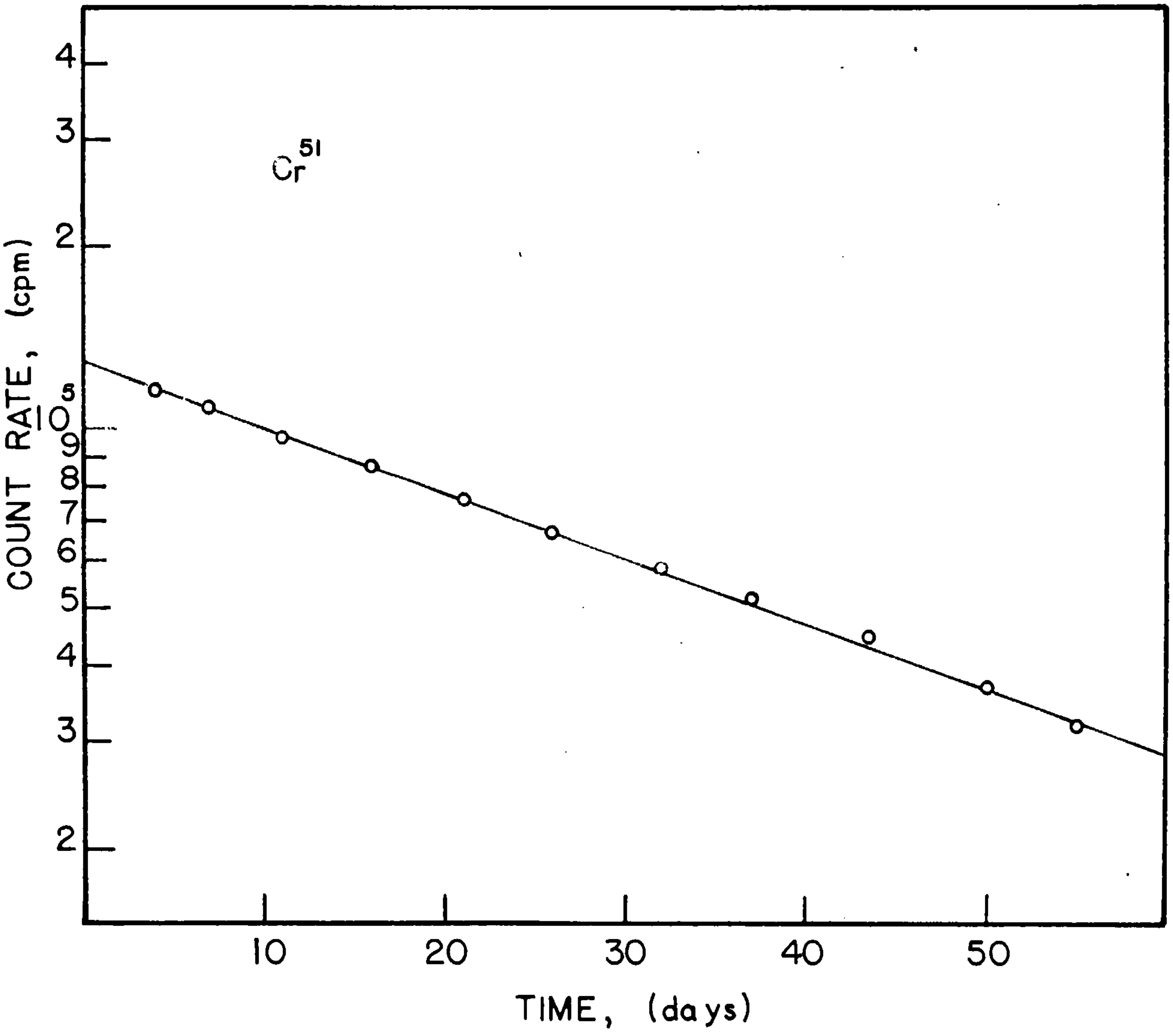
COUNT RATE, (cpm)
4
3
2
10^5
9
8
7
6
5
4
3
2
Cr^{51}
10
20
30
40
50
TIME, (days)

Figure 10

(a) Elutions of Rubidium and Strontium

(b) Half-life Determination of Sr^{85}: 65.0 days.

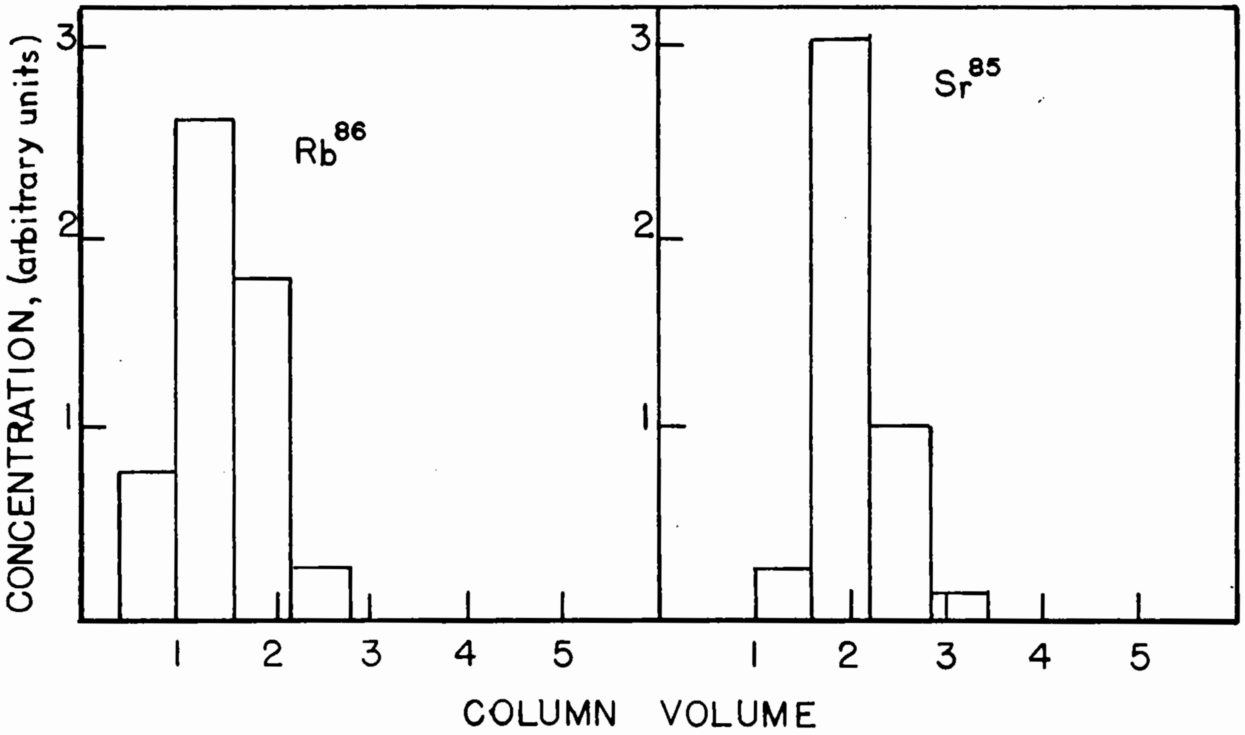
CONCENTRATION, (arbitrary units)
3
2
1
Rb^{86}
Sr^{85}
1
2
3
4
5
1
2
3
4
5
COLUMN VOLUME

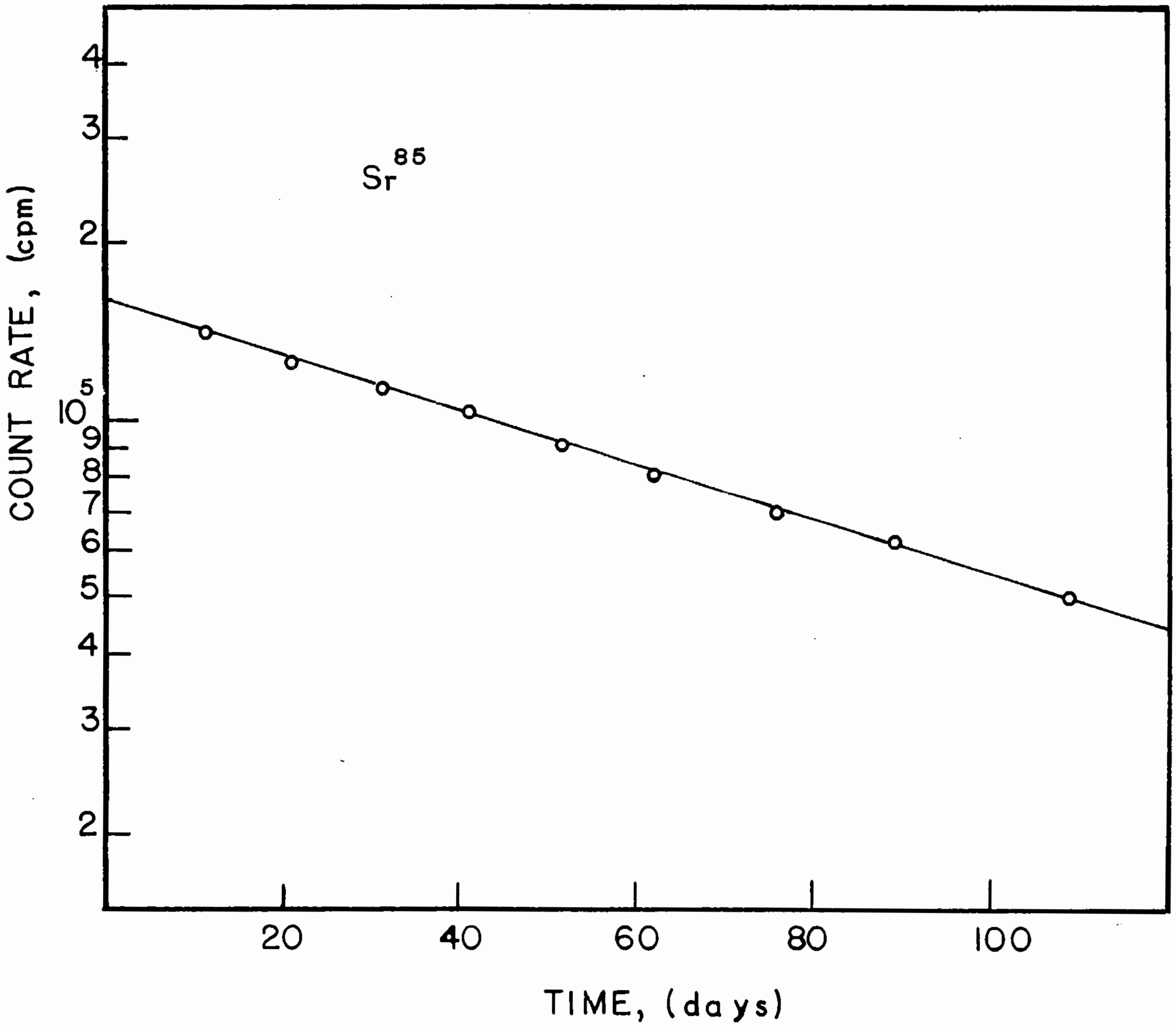
COUNT RATE, (cpm)
4
3
2
10^5
9
8
7
6
5
4
3
2
Sr^{85}
20
40
60
80
100
TIME, (days)

(e) Palladium from Rhodium.

The irradiated rhodium rod was placed into a thick wall glass vessel containing some "aqua regia". The glass vessel was sealed with a flame and placed in a pressurized steel bomb which was placed into a oven and heated at 300°C. for about 100 minutes. The apparatus for this method was developed and applied by G.R. Grant of this laboratory. After dissolution, the solution of rhodium containing the radioactive palladium, was dried three times and subsequently redissolved in 3M HCl.

To separate the palladium from the rhodium, a method due to Berman and McBryde (137) was applied. Fig. 11(a) show the elution of Pd^{103} when the column was eluted with 9M HCl.

(f) Cadmium from Silver.

The irradiated silver foil was dissolved in conc. HNO_3 and the dried salt was redissolved in 0.001M HCl. Then, the solution was passed through the column which had been previously washed with 0.001M HCl. The radioactive cadmium came out at the very beginning while a brown ring of silver oxide formed at the top of the column. The silver could be eluted with conc. HCl. Ag^{110} was added to $Cd^{107-109}$ as a tracer. The resulting separation is shown in Fig. 12(a).

Figure 11

(a) Elution of Palladium

(b) Half-life Determination of Pd^{103}: 17.0 days.

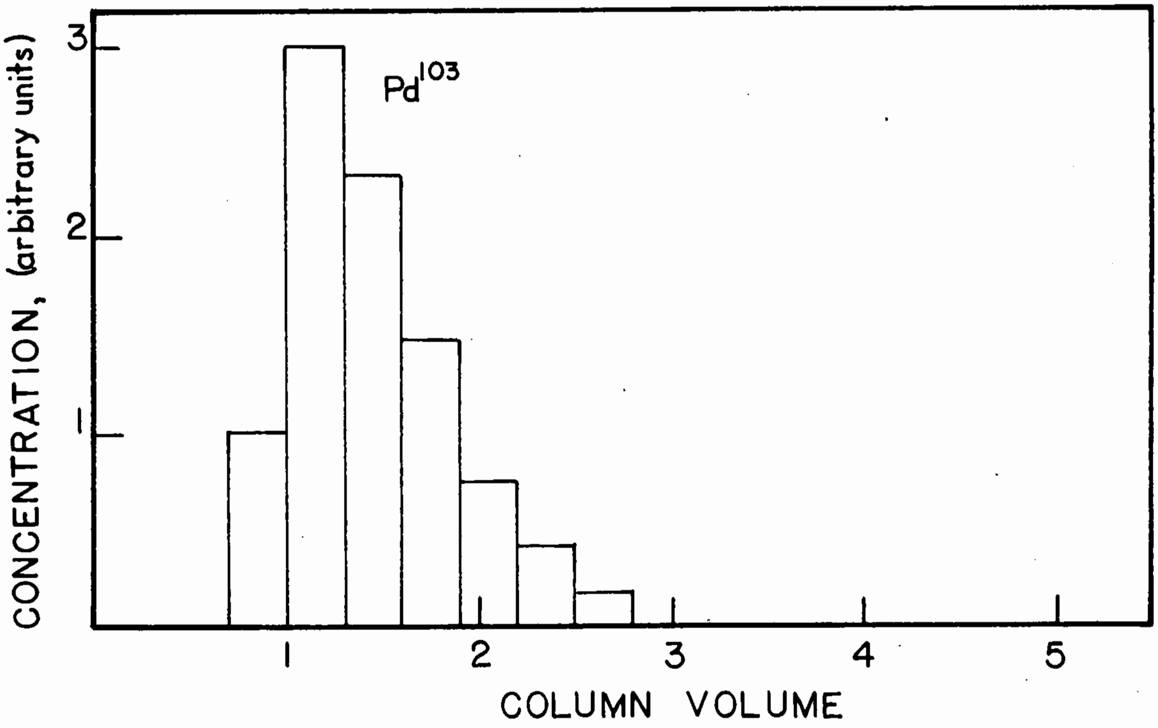
Pd^{103}
CONCENTRATION, (arbitrary units)
3
2
1
COLUMN VOLUME
1
2
3
4
5

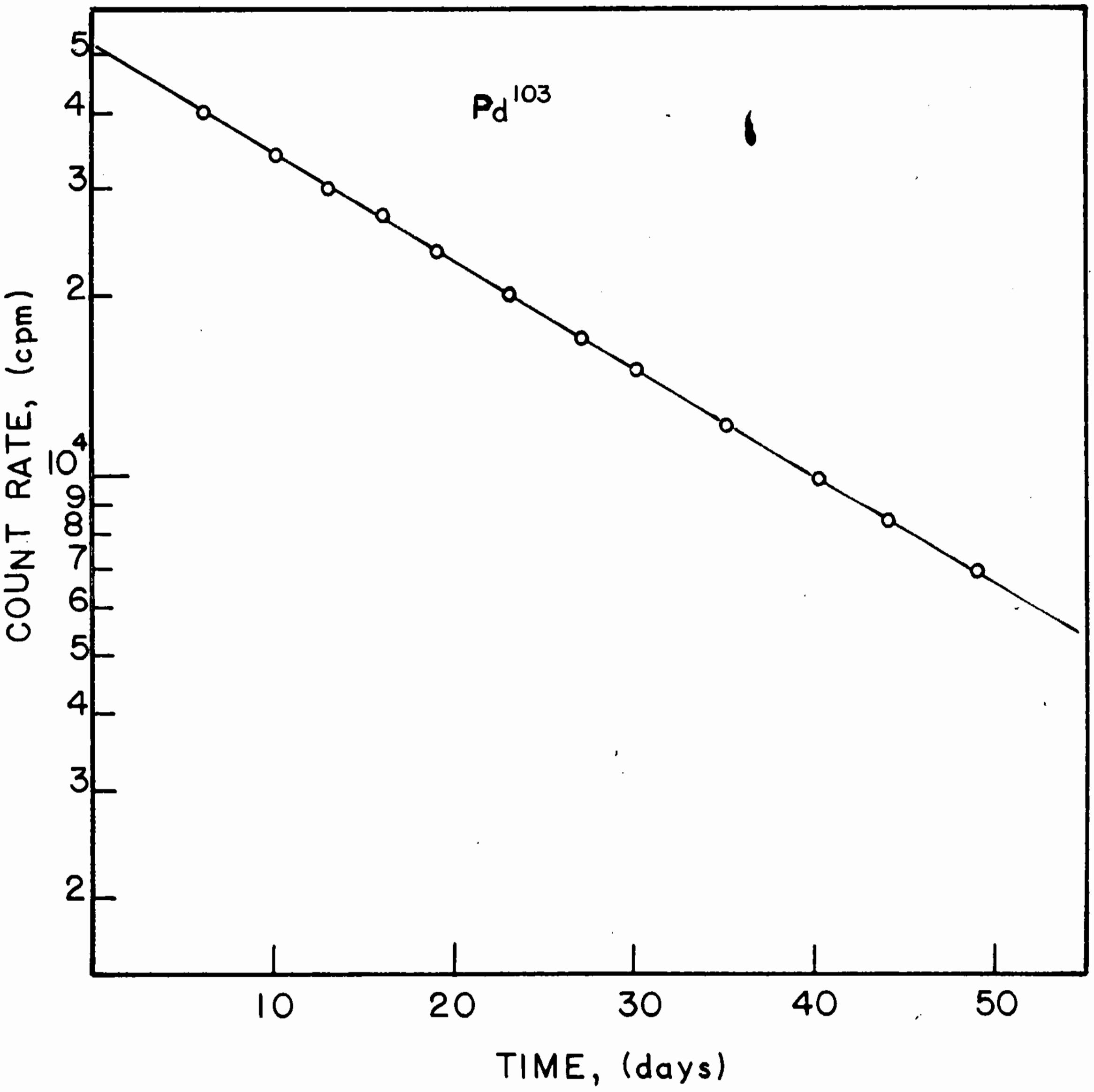
Pd^{103}
COUNT RATE, (cpm)
5
4
3
2
10^4
9
8
7
6
5
4
3
2
TIME, (days)
10
20
30
40
50

Figure 12

(a) Elutions of Cadmium and Silver

(b) Half-life Determination of Cd^{107}: 6.7 hrs.

76a

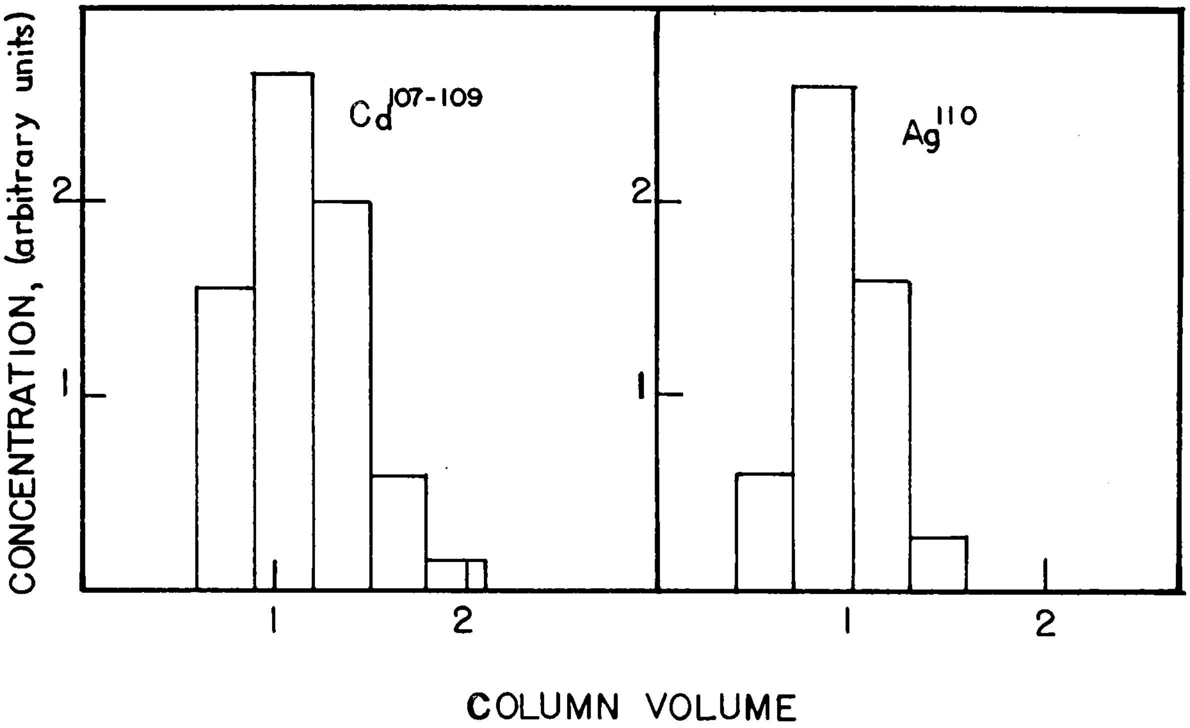

CONCENTRATION, (arbitrary units)
$Cd^{107-109}$
Ag^{110}
1
2
1
2
1
2
1
2
COLUMN VOLUME

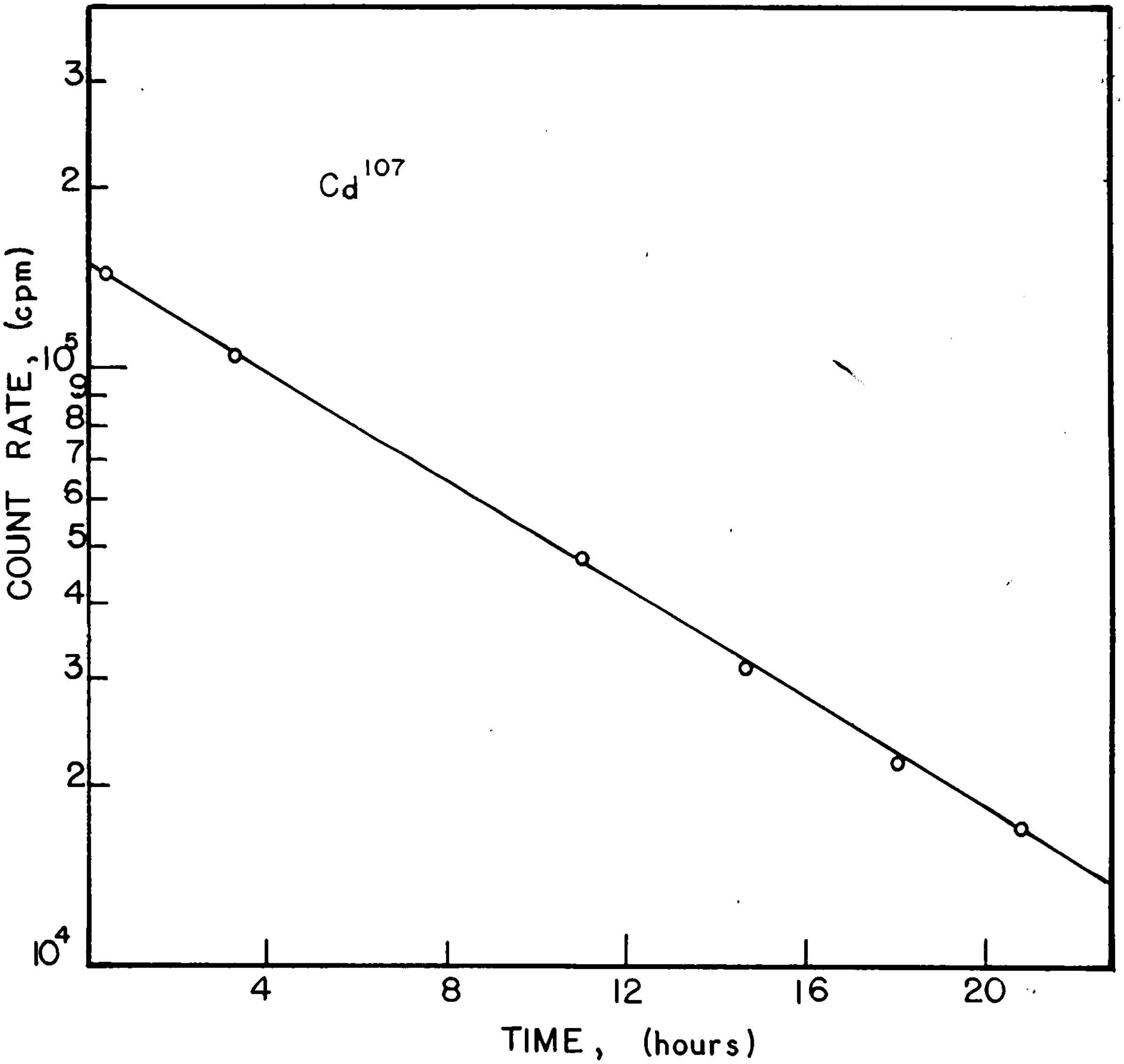

Cd^{107}
COUNT RATE, (cpm)
3
2
10^5
9
8
7
6
5
4
3
2
10^4
4
8
12
16
20
TIME, (hours)

(3) DISCUSSION

In the carrier-free separations described above, an attempt was made to keep the chemical separations to a minimum. With the exception of Pd^{103}, every separations could be realized within 15 minutes. However, the separation of Pd^{103} from the metallic rhodium target could be achieved within 20 minutes, if a soluble salt of rhodium would be used as a target.

Recently, one of few papers on cyclotron-produced carrier-free radioisotopes was published by Kruverman and Kruger (138). These authors have utilized the technique of co-precipitation with non-isotopic carriers. This can lead to large reagent volumes and concentrations, and poor separation yields or incomplete decontaminations might result. The time of separations for various nuclides (17 of them) is reported as being between 2 and 12 hours.

With the exception of Be^7 and Sr^{85}, the half-lives of the separated nuclides were followed until the activity died away. According to the Table III, a fair agreement with the most recent values published in the literature was obtained.

The Be^7 activity measurements are still in progress after a period of 268 days. The decay of Sr^{85} was followed only for a period of 120 days and no attempt was made to repeat the decay curve.

Appendix IV gives complete details of the total decay curves. In the case of Cd^{107} and V^{48}, long lived components presumably due Cd^{109} and V^{49}, were found and substracted from the main component.

TABLE III

Experimental Half-life Determinations

Nuclide	Detector	$t_{1/2}$ ours	$t_{1/2}$ others
Be^7	a*	53.5 days	53.6 days(152) 52.9 days(153) 53.0 days(154)
V^{48}	b*	16.5 days	15.9 days(155) 16.4 days(156) 16.1 days(157)
Cr^{51}	b*	27.7 days	27.8 days(158) 27.7 days(159) 27.9 days(160)
Sr^{85}	b*	65.0 days	64.0 days(161) 65.0 days(162) 65.0 days(163)
Pd^{103}	a*	17.0 days	17.0 days(164) 17.0 days(165)
Cd^{107}	b*	6.7 hours	6.7 hours(166) 6.7 hours(167)

*a: 1 in. by 1 in. NaI(Tl) Well-type Counter.

*b: Proportional Counter described in this Thesis.

C. COUNTING APPARATUS

(1) INTRODUCTION

The second part of the experimental work will be especially devoted to the description and discussion of the construction of a proportional counter and its preliminary calibrations. Also, various auxiliary apparatus such as vacuum and electronic accessories will be mentioned. Some importance will be given to an evacuation and filling system and two cathode followers, namely a conventional and a White type that were constructed and calibrated for optimum performances.

Much of the investigations which are now considered as secondary were achieved with the help of a commercial soft X-ray proportional counter originally obtained from "Beta Counter Laboratories", Patchogue, N.Y. It had an outside window made of beryllium (1 in. diameter by 0.040 in. thick) which was affixed on to the cylindrical brass cathode. The anode wire, commonly called the collector, had a diameter of 0.004 in. while the cylinder had a length of 12 in. by 4 in. inside diameter.

Although the operational characteristics of the above mentioned counter were found to be essentially the same as those of the counter calibrated in this thesis, some inherent disadvantages of the former were caused by the presence of the beryllium window (thickness and size) and its geometrical position which lead to a reduction of the sensitive aperture. These undesirable features did not correspond to the desiderata expressed in the general introduction, and for this reason, another proportional counter was subsequently constructed.

The results which will be reported in the next following pages will concern the basic calibrations of (a) an evacuation and filling system, (b) two cathode followers, and (c) either one of the two proportional counters constructed. The calibrations concerning the evacuation and filling system, in particular, are called primary because they can be applied for routine work with either of the counters which were constructed.

Unless otherwise mentioned, a mixture of argon-methane (9:1) at a pressure of one atmosphere was usually employed as counter gas. The ionization inside the sensitive volume of the counter was induced by a source of iron-55 ($\sim 6 \times 10^4$ cpm.) which emitted the characteristic X-rays of manganese with an energy of 5.9 kev.

(2) CONSTRUCTION AND PRELIMINARY CALIBRATIONS

(a) Evacuation and Filling System

The glass and metallic system shown in Fig. 13 was designed and constructed for the evacuation and filling of the

Figure 13

Evacuation and Filling Apparatus.

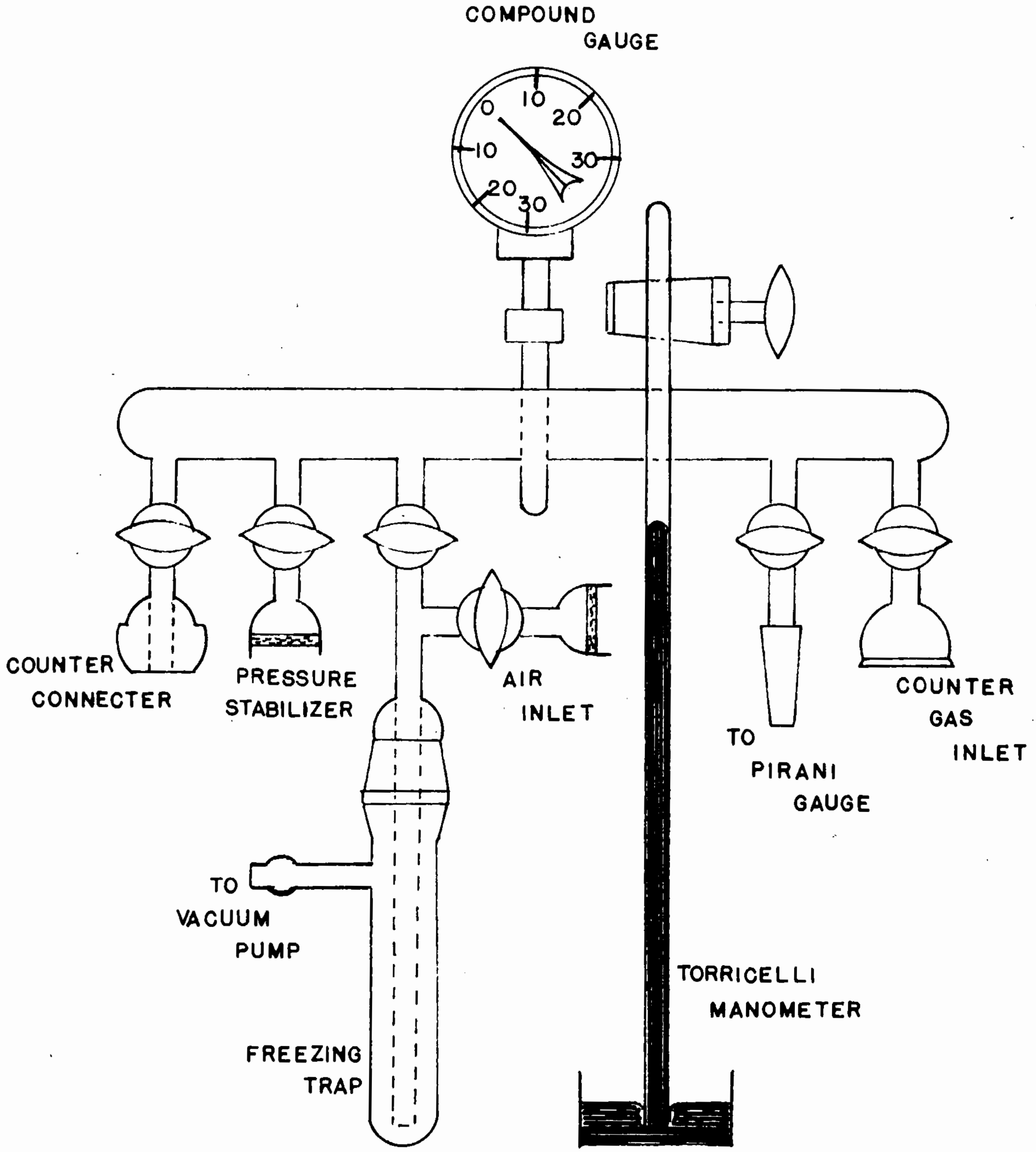

EVACUATION AND FILLING SYSTEM

proportional counter with various gases at different pressures. The commercial availability of counter gas mixture (154) in a chemically pure state enabled us to construct an apparatus which was not too elaborate in design and operation.

Before describing the apparatus, it might be interesting to point out that in 1939, Jentschke and Prankl (155) were the first to suggest the cycling of the counter gases over calcium turnings heated at about 300°C. This treatment would facilitate the removal of lowest traces of impurities which can have undesirable electronegative affinity. Although this extra precaution was recommended and applied by other investigators (91), (93), (156) and (157), it has been disregarded during the past few years (26), (27), (115), (158), (159), and (160). This is probably due to the advent of commercial availability of chemically pure gases. For example, the argon has a guaranteed purity of 99.9 per cent, and a representative analysis (161) gave 99.92 per cent argon, 0.08 per cent nitrogen and 0.001 per cent each of hydrogen and oxygen. A sample of methane contained 99.2 per cent methane, 0.5 per cent ethane and 0.3 per cent nitrogen.

Moreover, during the course of this work, the reproducibility of our results, in a quantitative and a qualitative manner, did not suggest the necessity of such a purification technique.

Regarding the description of the apparatus shown in Fig. 13, all stopcocks were high vacuum stopcocks. The adapters for the counter and gas cylinder were interchangeable glass ball and socket joints (28 mm. ball diameter and 12 mm. inside diameter tubing). A spring-activated pinch clamp, with a screw-locking device which augmented the spring action, provided a tighter joint between the socket and the ball. For the reliability of the operations of the system, waxes, cements or rubber tubing must be omitted, and glass-to-kovar seals are recommended.

A Welch Duo-Seal No. 1405 evacuation pump, having an air-free capacity of about 58 liters per minute was used as a forepump. As will be demonstrated later, the duration during which the counter must undergo evacuation and the number of flushings are important criteria for optimum performances. Accordingly, the rate of evacuation was plotted in Fig. 14, when the system was connected to the counter and the gas cylinder. A liquid-air trap was also used to accelerate the evacuation.

Accurate vacuum measurements were read either on a McLeod manometer or a Pirani gauge. For routine work, the pressures can be measured on metallic-Bourdon-type combination gauges which were adapted to the vacuum system and to the proportional counter. The vacuum side reads from 0 to 30 inches of Hg. while the pressure side reads from 0 to 30 pounds per

<u>Figure 14</u>

Rate of Evacuation of the Overall System. (counter and gas reservoir connected to the system).

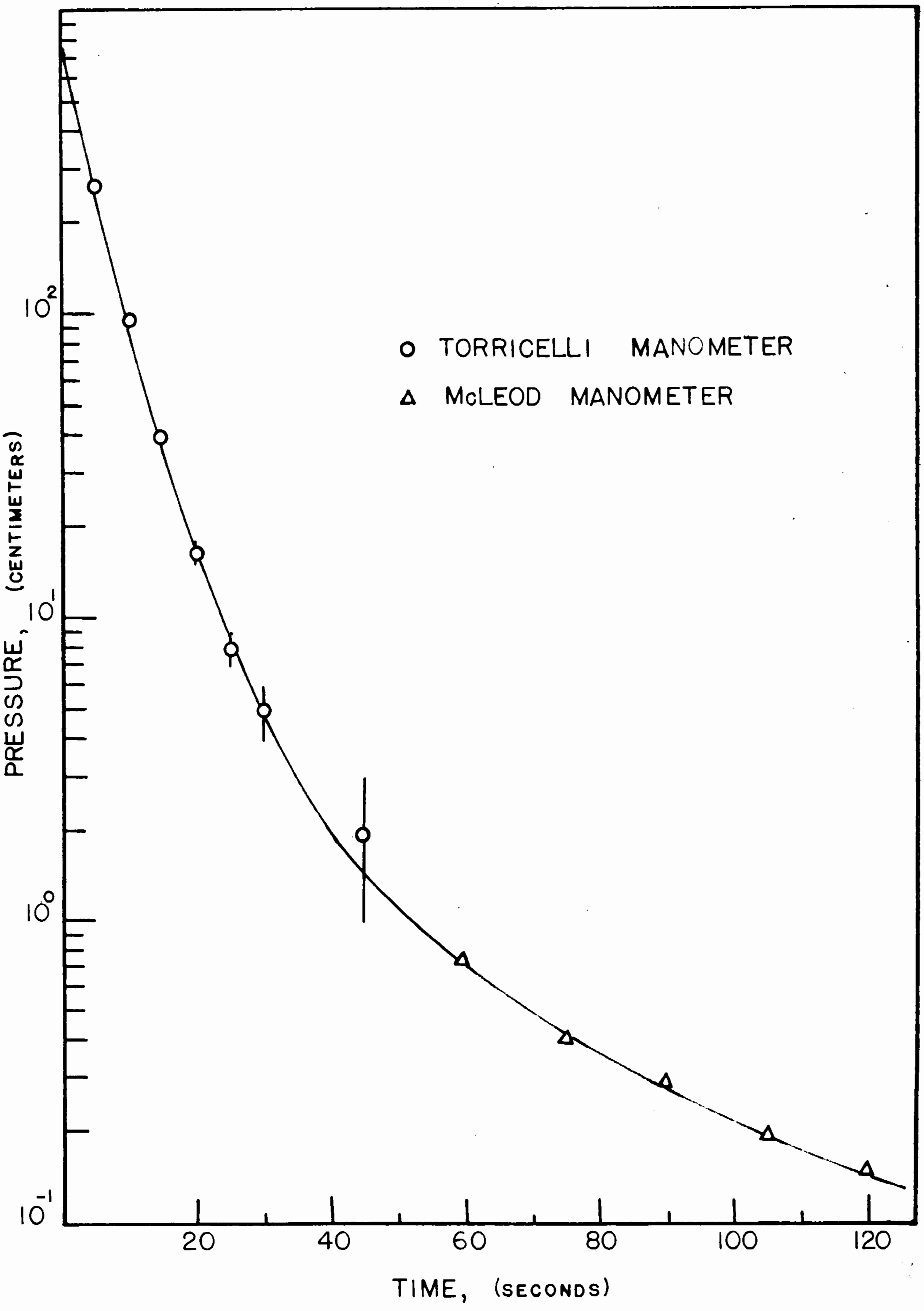
○ TORRICELLI MANOMETER
△ McLEOD MANOMETER
PRESSURE, (CENTIMETERS)
10^2
10^1
10^0
10^{-1}
20
40
60
80
100
120
TIME, (SECONDS)

square inch. The gauge was calibrated against an U-shaped tube filled with mercury and, according to Fig. 15, no departure from linearity was encountered either on the vacuum side or on the pressure side. This result applied for both combination gauges.

It has been recommended (91), (93), in order to secure an ultra high vacuum, that the counters be baked in order to drive off gases which might be occluded on the inner wall surfaces. This is probably correct for Geiger counters, but such requirements were found unnecessary when the counter was operated in the proportional region and at a pressure of one atmosphere or so. An exception to this was made for the first time when the counter was used. Prolonged evacuations were required. Otherwise, flushing (once or twice) of the counter was sufficient to give reproducibility. Every flushing was preceded by evacuation during short lapses of time (about 30 sec.). Applying this treatment, the results plotted in Fig. 16(a), (b), and (c) show three different ways of obtaining reproducible results when the counter was operated as shown in the block diagram in Fig. 22. The solid curves representing the plateaux and the spectra were fixed as standards of optimum operations. Everytime, before experimenting with a new evacuation condition, the counter was initially filled with air.

When the newly constructed counter was evacuated for the first time,

Figure 15

Calibration of Combination Gauges, (vacuum apparatus and counter).

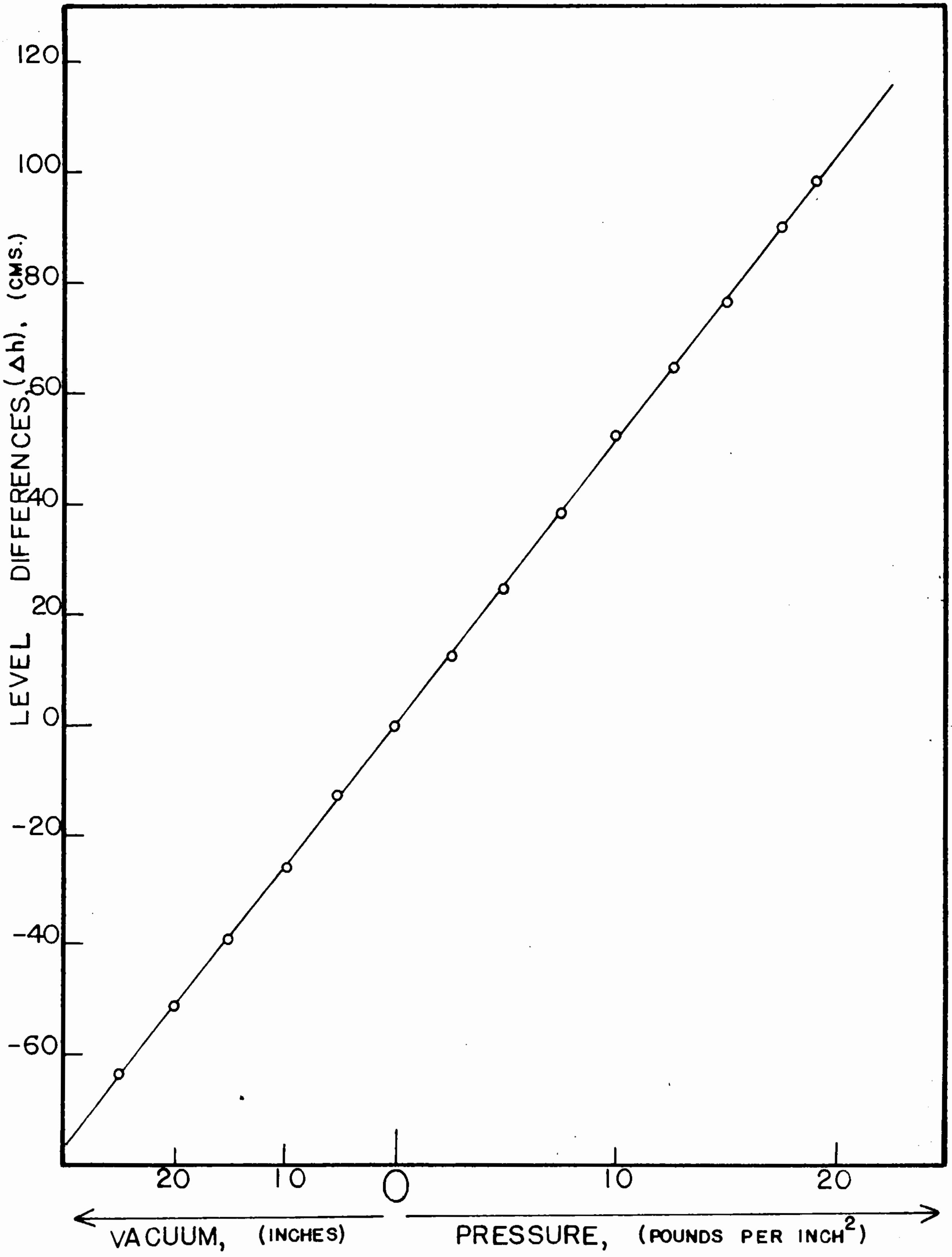

120
100
80
60
40
20
0
-20
-40
-60
LEVEL DIFFERENCES, (Δh), (CMS.)
20
10
0
10
20
VACUUM, (INCHES)
PRESSURE, (POUNDS PER INCH²)

Figure 16

Calibration of the Evacuation and Filling System for Proper Counter Operations.

(a) Three 15 second evacuations with intermediate (twice) gas filling.

—·—·—· after first gas filling.
- - - - - - - after second gas filling.
———— after third gas filling.

(b) Two 30 second evacuations with intermediate (once) gas filling.

- - - - - - - - after first gas filling.
———— after second gas filling.

(c) 60 second evacuation without gas flushing.

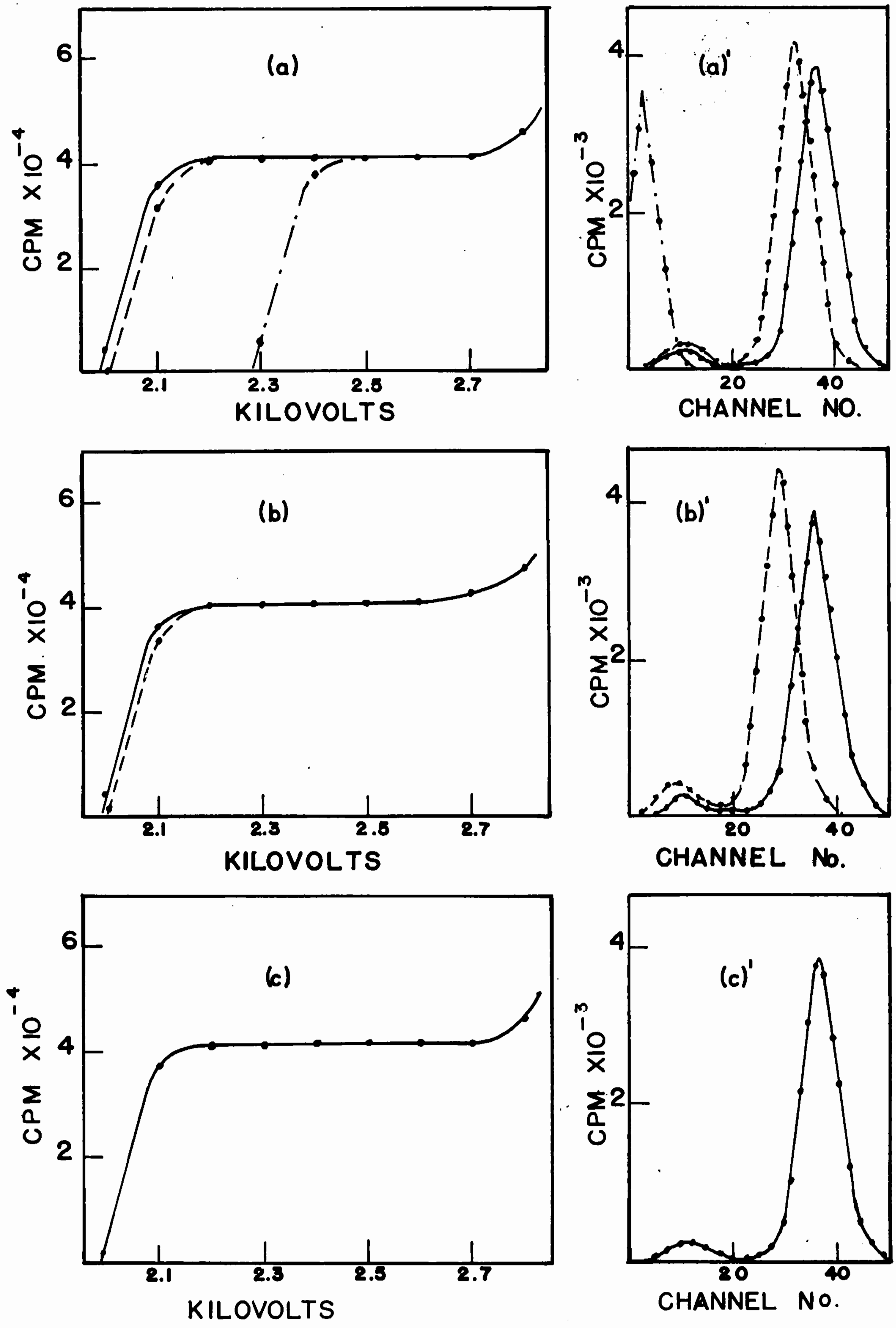
(a)
CPM X10^{-4}
6
4
2
2.1
2.3
2.5
2.7
KILOVOLTS
(a)'
CPM X10^{-3}
4
2
20
40
CHANNEL NO.
(b)
CPM. X10^{-4}
6
4
2
2.1
2.3
2.5
2.7
KILOVOLTS
(b)'
CPM X10^{-3}
4
2
20
40
CHANNEL No.
(c)
CPM X10^{-4}
6
4
2
2.1
2.3
2.5
2.7
KILOVOLTS
(c)'
CPM X10^{-3}
4
2
20
40
CHANNEL No.

the evacuation was carried out for 5 or 6 hours. Simultaneously, the counter was heated with the radiations from an infrared lamp situated about 6 inches away from the counter.

(b) Cathode Followers

Normally, the drop of the anode voltages resulting from an ionizing event inside a chamber operated in the ion-chamber or proportional region are detected with the help of preamplifiers. These instruments consist of two or three stages of amplification having an overall gain of about 25. They are very sensitive to pulses of the order of microvolts and when matched with large counters, adequate shielding must be considered.

A preamplifier, Baird Atomic Instruments model 219A, was used for preliminary studies. When coupled with the counter and various electronic equipments described in Fig. 22, anomalously high voltage characteristics of the counter were obtained for counting rates of about 5 x 10^4 cpm. The higher the counting rates the more distorted were the plateau curves. Also, careful shielding of the counter did not prevent the preamplifier from picking up microvolt pulses.

Instead of trying to modify some of the electronic parts of the preamplifier, it was decided to construct two cathode followers which had a lesser sensitivity to small input pulses but were known to be very efficient and reliable. The first one which is shown in Fig. 17(a) is called the conventional cathode follower, (CCF). It utilizes a 6AK5 pentode tube and its output impedance is of the order of 200 ohms. The second one had intrinsic qualities which militated in favour of its application. It bears the name of White cathode follower (WCF) and was patented by E.L.C. White in 1944 (162). The details of the wiring diagram are shown in Fig. 17(b). This particular type employs a 6AN8 triode-pentode coupled with a VR150 acting as stabilizer. The output impedances are smaller than 50 ohms.

Some elementary tests such as rise time determination and linearity were applied to each of them. In Fig. 18, a comparative study of the rise time is shown for input pulses ranging between 2 and 16 volts. The pulses were obtained from a calibrated AEP pulse generator, model 1607. Concerning the pulse linearity dependence, Fig. 19(a) expresses the results of the investigation. The WCF followed a straight linearity for pulses up to 60 volts while the CCF started to show saturation at pulses of the order of about 20 volts. For both experiments, the shape and the size of the pulses were read on a Tetronix oscilloscope, model 532.

<u>Figure 17</u>

(a) Wiring Diagram of a Conventional 6AK5 Cathode Follower.

(b) Wiring Diagram of a White 6AN8 Cathode Follower.

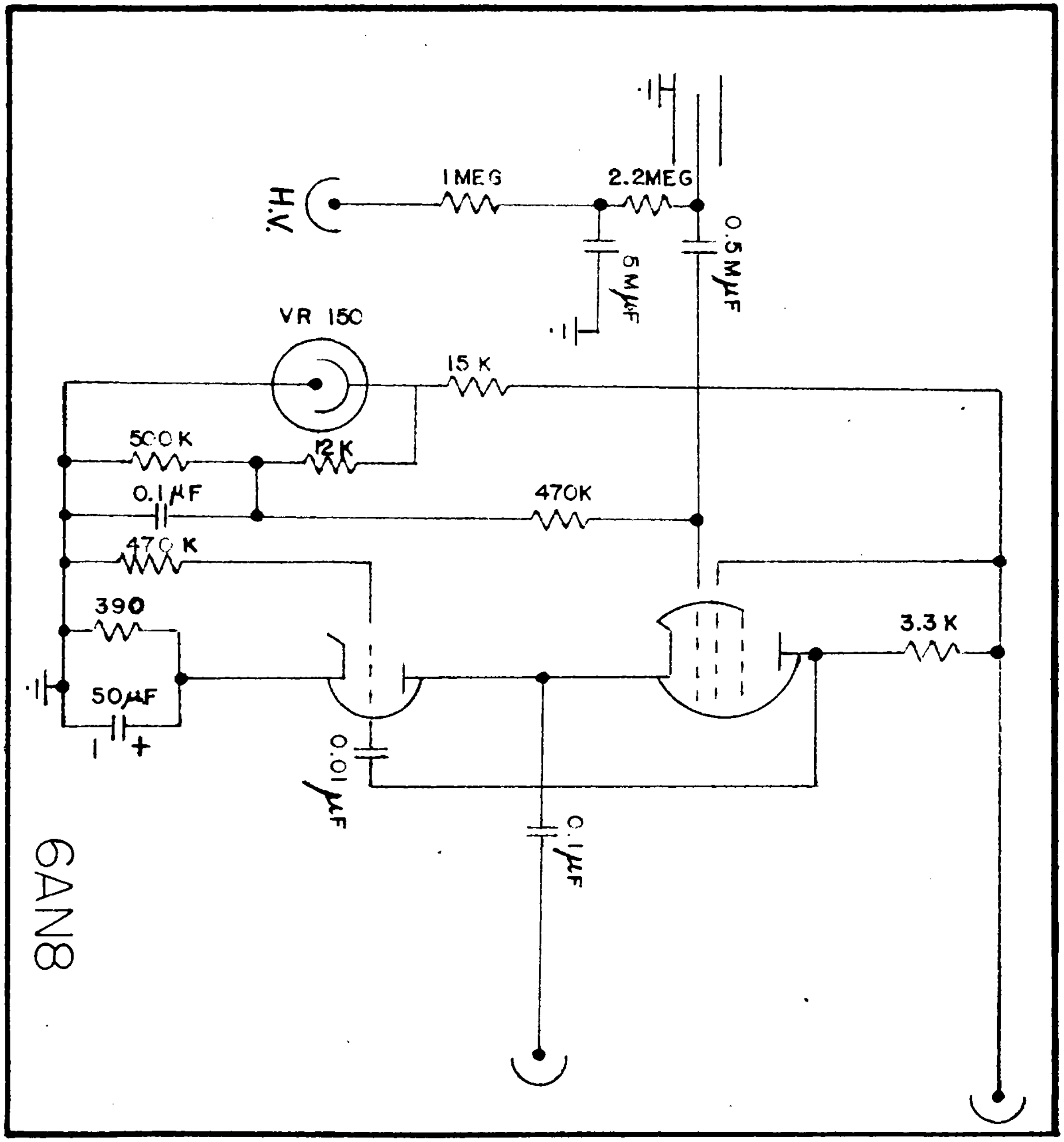
H.V.
1MEG
2.2MEG
5MμF
0.5MμF
VR 150
15 K
500K
12K
0.1μF
470K
470 K
390
50μF
3.3K
0.01μF
0.1μF

6AN8

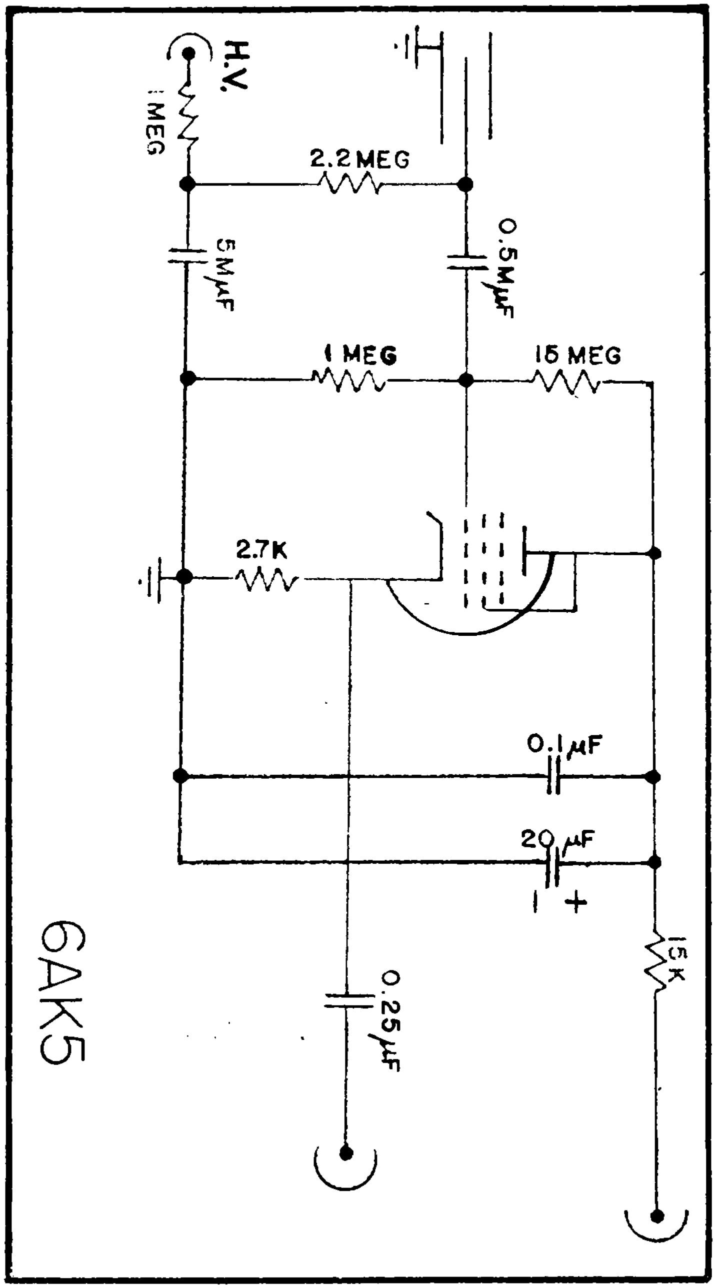
H.V.
1MEG
2.2MEG
5MμF
0.5MμF
1MEG
15MEG
2.7K
0.1μF
20μF
15K
0.25μF

6AK5

Figure 18

Study of the Conventional 6AK5 and the White 6AN8 Cathode Follower Rise Times.

△ 6AK5

○ 6AN8

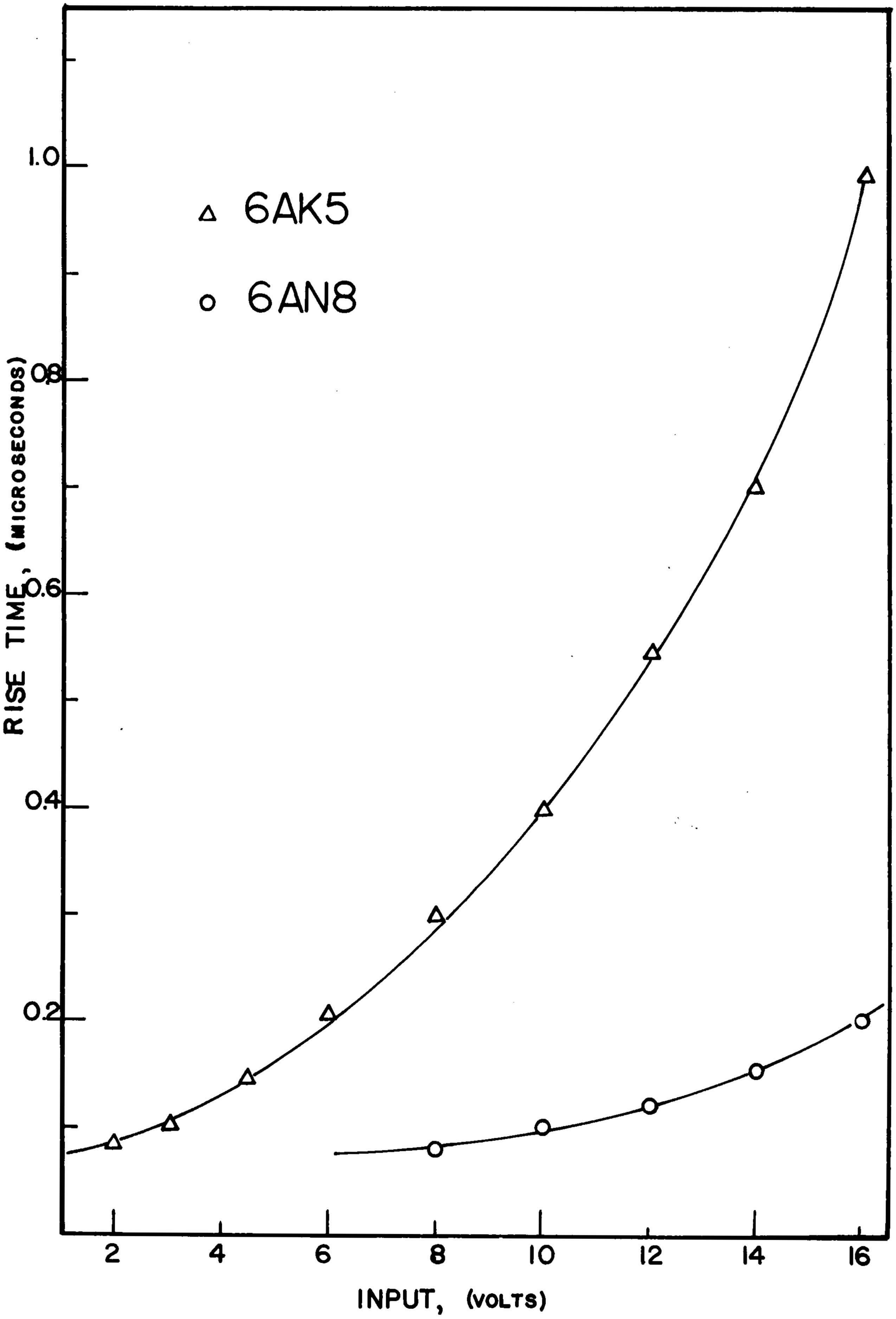

△ 6AK5
○ 6AN8
RISE TIME, (MICROSECONDS)
1.0
0.8
0.6
0.4
0.2
2
4
6
8
10
12
14
16
INPUT, (VOLTS)

Figure 19

(a) Linearity Response Comparison between a Conventional 6AK5 and a White 6AN8 Cathode Follower.

(b) Counter High Voltage Characteristics obtained with a Conventional 6AK5 and a White 6AN8 Cathode Follower.

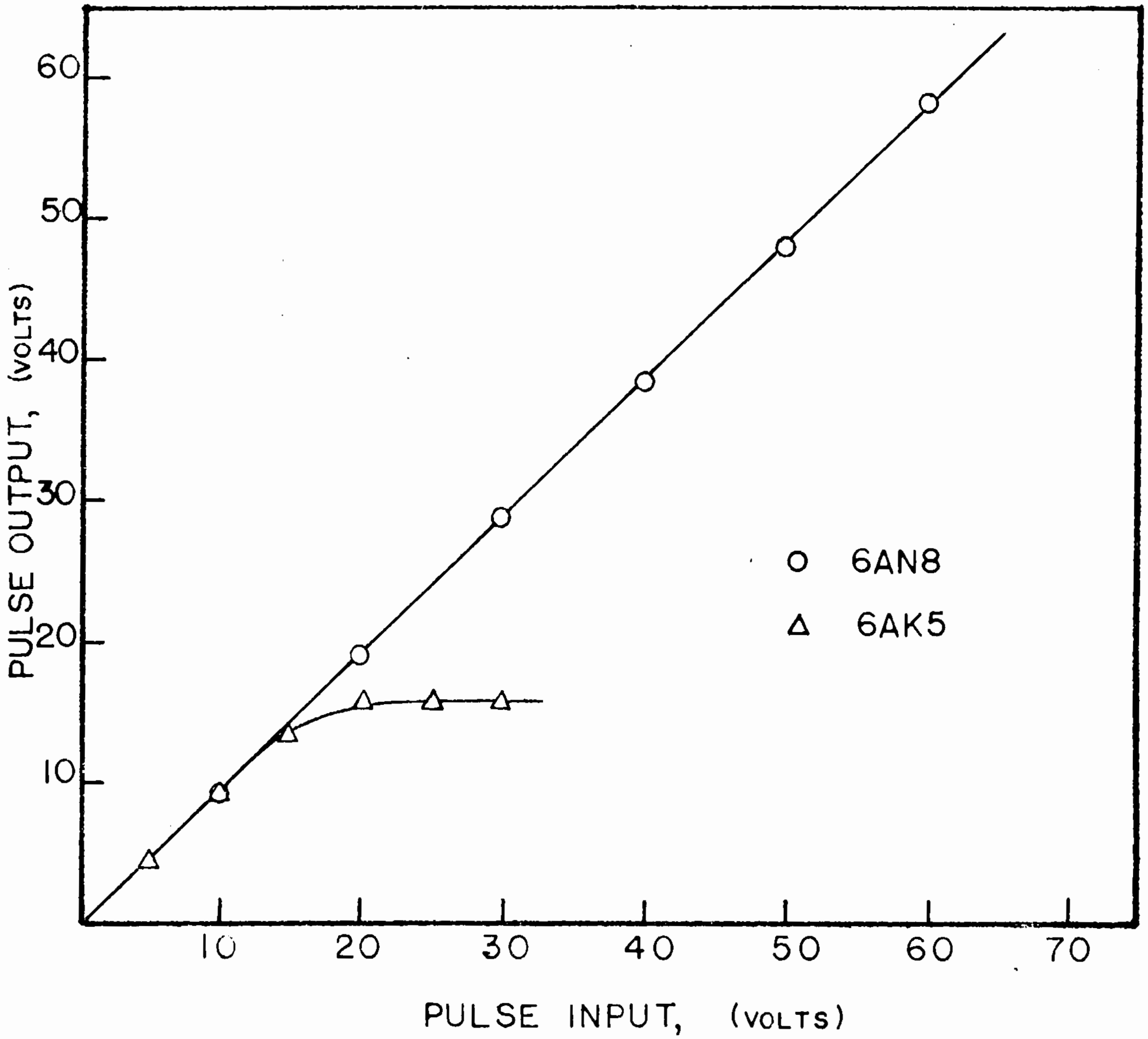
PULSE OUTPUT, (VOLTS)
60
50
40
30
20
10
PULSE INPUT, (VOLTS)
10
20
30
40
50
60
70
○ 6AN8
△ 6AK5

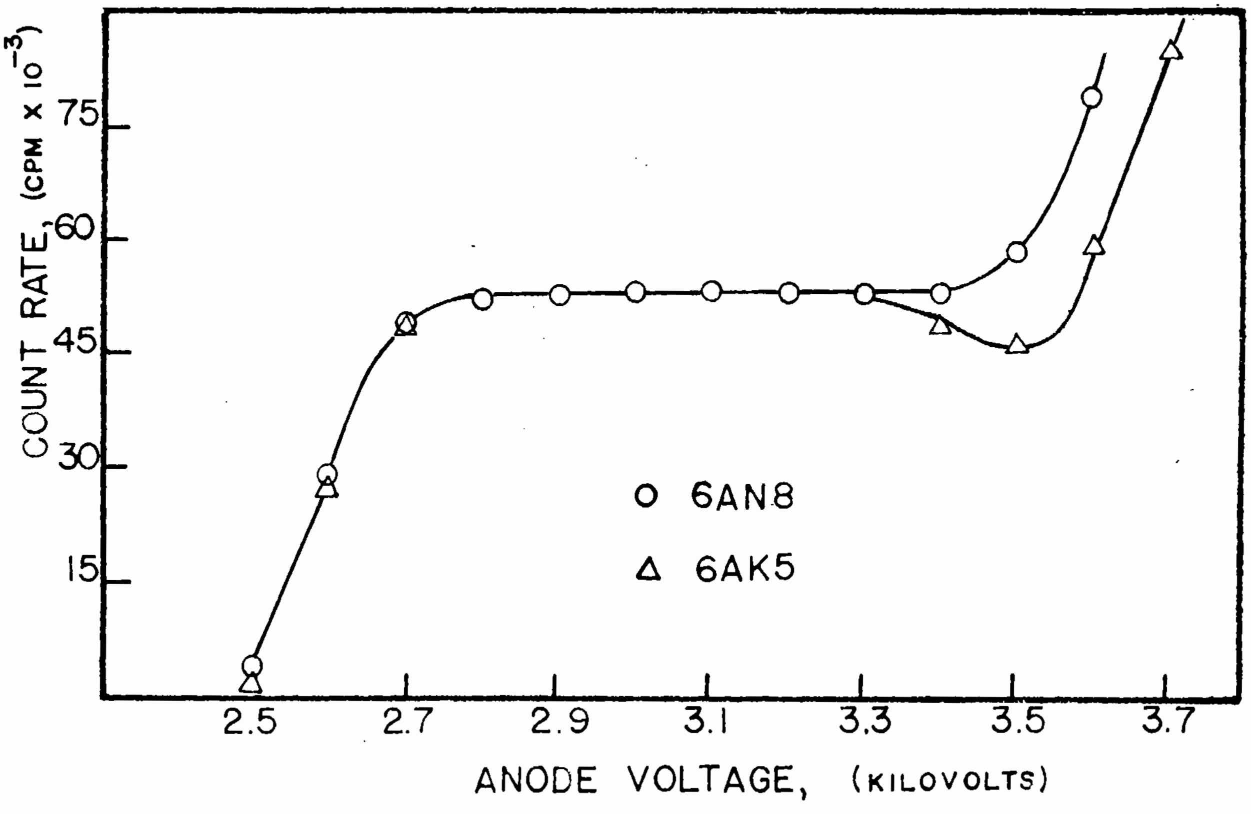
COUNT RATE, (CPM x 10⁻³)
75
60
45
30
15
ANODE VOLTAGE, (KILOVOLTS)
2.5
2.7
2.9
3.1
3.3
3.5
3.7
○ 6AN8
△ 6AK5

In Fig. 19(b), the high voltage characteristics of the counter are compared when the CCF and WCF are interchanged in the block diagram shown in Fig. 22. As can be noticed, the CCF model gave some distortion in the upper limit of the plateau. More distorted shapes were met at higher counting rates.

In addition to low output impedences, fast rise time, and linear response, the WCF has a push-pull circuitry permitting the transmission of pulses of either polarity with minimal distortion.

Very recently, a transient analysis of the WCF was compared to the CCF by Brown, (178). Quantitative aspects of the effect of various circuit parameters on the transient response are discussed in the paper. A few months later, another work was published in which Read (164) describes an ultra linear WCF. This instrument is said to be a WCF which was slightly modified and possesses an extremely linear response, a voltage gain of essentially unity and a calculated output impedance of 2×10^{-3} ohms.

(c) Proportional Counter

Proportional counters can be constructed with an astonishingly wide variety of characteristics and physical dimensions. To illustrate the possible ranges in sizes, counters 0.2 in. in radius and 1 in. long (108), may be contrasted with others 6 in. in radius and 36 in. long (161).

Usually, the nature of the problem to be studied determines the size and the shape of the counter to be used. If absolute standardization of nuclides decaying by electron capture is attempted with an end-window-type counter, three main desiderata must be fulfilled: (a) a relatively large sensitive area, (b) a thin window having a thickness which will virtually permit total transmission of the radiations, and (c) an accurately known source-to-counter geometrical efficiency. When the commercial counter with the beryllium window was used, desideratum (a) was met to a certain degree of satisfaction but (b), and (c) did suffer from severe limitations. For example, it was experimentally found that, at least, 50 per cent of the X-rays emitted by Fe^{55} were absorbed inside the thin beryllium window. Moreover, the reinforcement around the window did reduce the sensitive aperture by an additional 20 per cent. Also this correction is somewhat difficult to evaluate accurately through experimental means.

Furthermore, thin beryllium windows are very hard to obtain because of the brittleness of the metal. If obtained, they usually suffer from some physical imperfections which might lead to a possible source of error.

For routine work, the commercial counter was fragile to handle, was of inconvenient form, could not be used as flow counter unless the construction was altered, could not be employed for soft beta spectroscopy, did not possess an additional window which is recommended for simultaneous energy calibrations, and finally, the anode wire could not be interchanged in a simple manner.

Therefore, it was decided to construct two proportional counters, essentially the same, but with the following desirable features.

(a) A source-to-counter geometrical efficiency having a solid angle of 2π-steradians.

(b) A detector having no window. This would permit the entrance of all the radiations when required.

(c) An additional window made of beryllium, (thickness of 0.009 in.) thus permitting simultaneous calibrations without removal of the radioactive source under investigation.

(d) An adaptation to gas-flow system. This extra attachment became mandatory with energy linearity calibrations and with the measurement of some beta-spectra.

(e) A system whereby the anode wire can be interchanged readily. Sometimes, the collector must be changed or replaced for the optimum performance.

The design of the counter is drawn to scale in Fig. 20. The details of the construction of the most important parts are also shown in Fig. 21(a), (b), and (c).

During the construction of the counters, various precautions suggested by Korff (91) were scrupulously observed. However, the following considerations must be emphasized in addition.

(a) The cathode, made of hard drawn brass, was alternately washed with dilute nitric acid solution, buffed with some abrasive solution such as commercial "Brasso", and then cleaned with ethanol.

(b) The ends were soft soldered to the cylinder while the terminals were silver soldered to the ends in order to ensure good electrical and leak tight contacts.

(c) The weld between the collector and the support was made smooth and, as much as possible, freed from physical imperfections. Otherwise, these imperfections would create (as it was found in many cases) local irregularities in the electrical field, which in turn may cause local ionization, leading to the formation of spurious pulses. For further protection, insulating sleeves were used.

<u>Figure 20</u>

Description of the Proportional Counter.

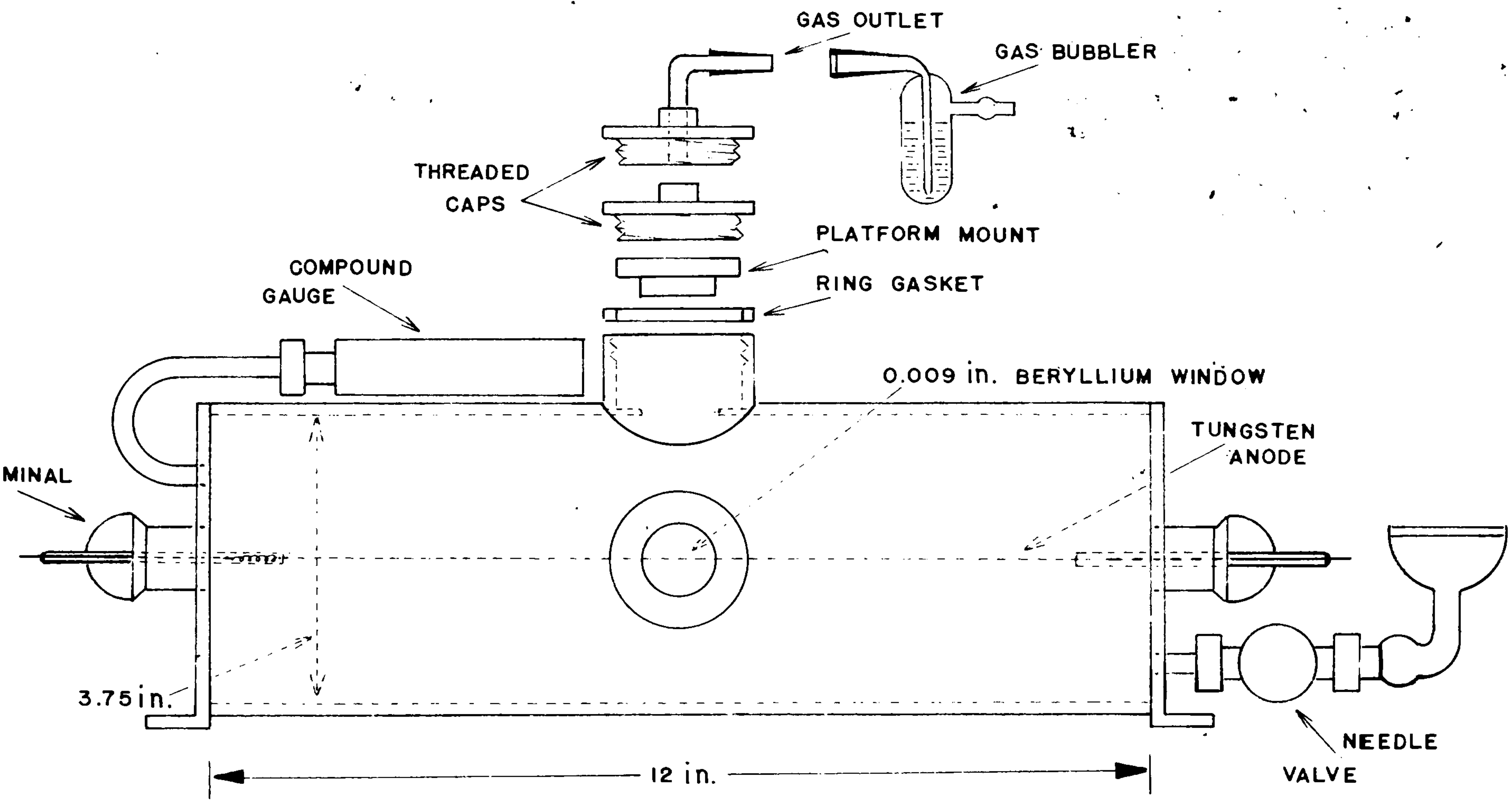

PROPORTIONAL COUNTER

97a

Figure 21

Construction Detail of the Proportional Counter.

(a) Counter Aperture,

(b) Additional Beryllium Window,

(c) Terminal Arrangement.

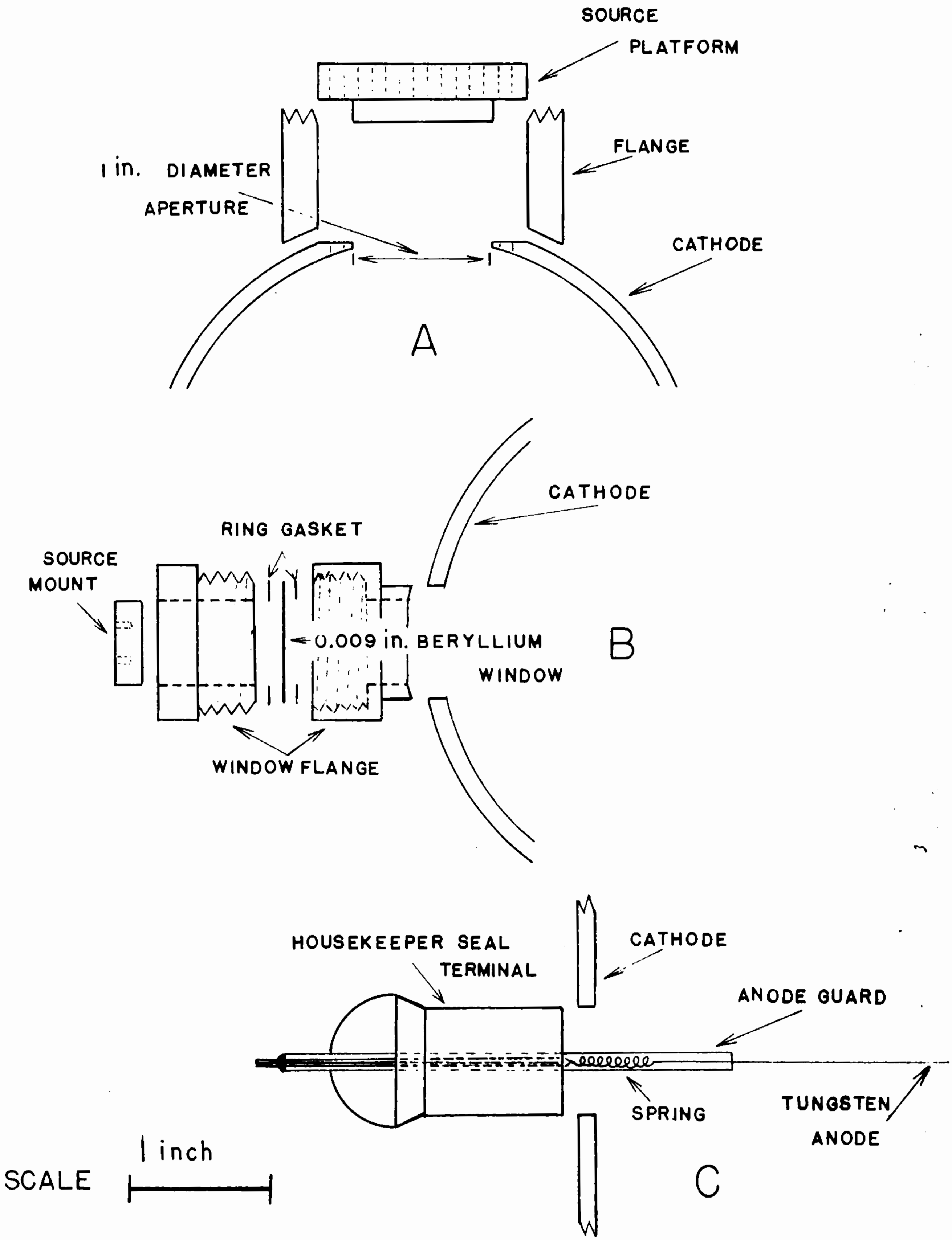
SOURCE
PLATFORM
FLANGE
1 in. DIAMETER
APERTURE
CATHODE
A
CATHODE
RING GASKET
SOURCE
MOUNT
0.009 in. BERYLLIUM
WINDOW
B
WINDOW FLANGE
HOUSEKEEPER SEAL
TERMINAL
CATHODE
ANODE GUARD
SPRING
TUNGSTEN
ANODE
C
1 inch
SCALE

Once all the parts were assembled, the thoroughly cleaned counter was attached to the evacuation and filling system. During the evacuation which lasted overnight, the cathode was heated with an infrared lamp situated about six inches underneath the counter. This treatment facilitated the removal of gas molecules or atoms that might be occluded on the inner surface of the cathode. Likewise, both ends of the anode were connected in series to a Variac and a few volts were enough to produce incandescence. In order to see the process, the beryllium window was replaced by a window transparent to light (lucite). The importance of heating the anode has been emphasized by Locher (165) who points out that it not only burns off dust and sharp edges on the wire but also alters the crystalline structure to give greater uniformity and reduces die-scratches on the wire.

Finally, the counter was tested for pinholes. No noticeable variation in the readings of the combination gauge was registered when the counter was left either under vacuum or pressure ($\sim$2 atm.) for a period of 48 hours.

After proper evacuation and flushing, the counter was coupled with the auxiliary electronic circuits represented in Fig.22. This block diagram shows how the pulses could be measured, controlled, and recorded. The electric field

<u>Figure 22</u>

Block Diagram of the Overall Assembly.

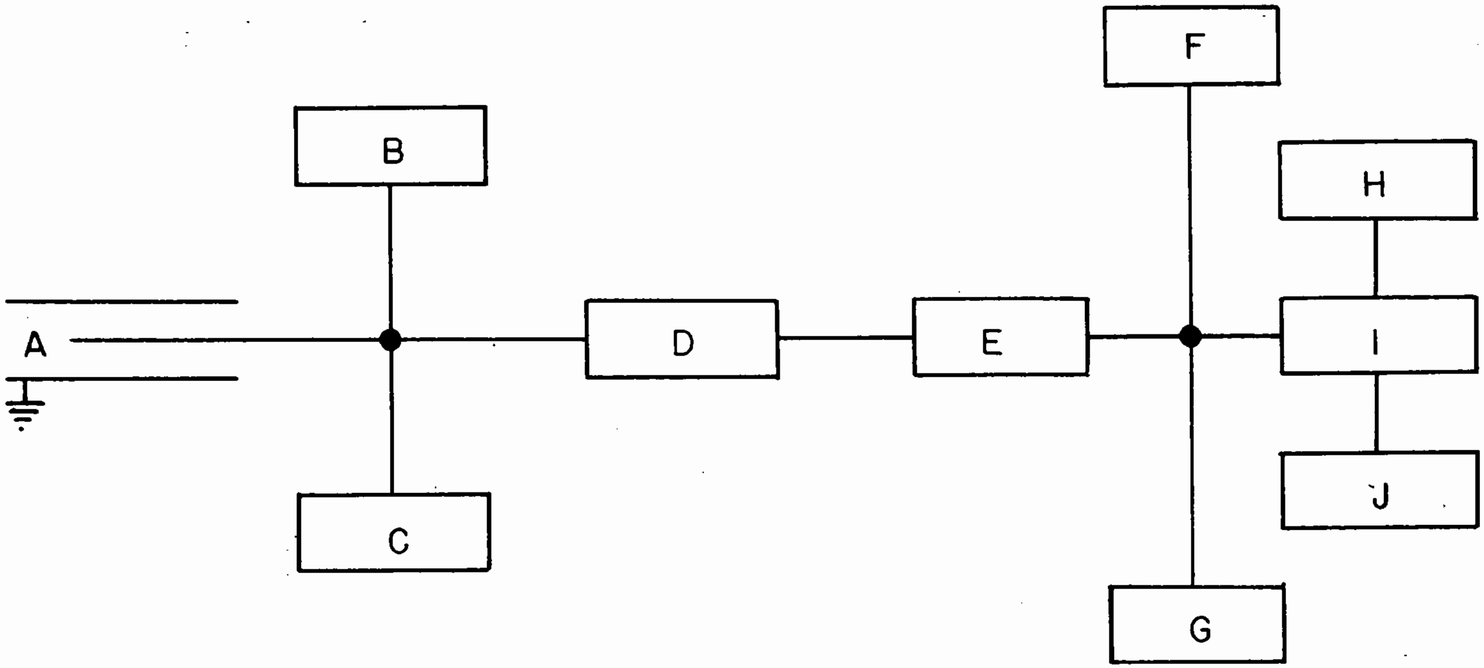

A : COUNTER
B : PULSE GENERATOR
C : D.C. POWER SUPPLY
D : CATHODE FOLLOWER
E : AMPLIFIER

F: OSCILLOSCOPE
G: SCALER
H: RECORDER
I: PULSE HEIGHT ANALYSER
J: PRINTER

across the chamber is provided by a 0 to 5000 volts D.C. power supply produced by John Fluke, Seattle, Wash. As required for this type of work, this set is highly stable. In fact, it has about 5 millivolts ripple at any output voltages. The linearity of the output voltages was calibrated against a voltmeter and according to Fig. 23, very little departure from linearity was found.

When an electric field was applied across the chamber, the pulses resulting from ionizing events inside the counter were detected with the help of a White cathode follower previously discussed. Thereafter, they were fed into a non-overloading 215A Baird Atomic Instrument amplifier. A C.D.C. 100 channel pulse-height analyser differentiated the pulses and the spectrum could be automatically recorded or printed. Alternatively, the number of pulses could be integrally counted if the output of the White cathode follower fed the pulses into a A.E.P. 1448 amplifier and finally into a A.E.P. 2005B scaler.

We now propose to calibrate the counter and investigate its characteristics.

(I) Background.

Any ionization detector will exhibit a certain background and it is the statistical fluctuation in this background which setsthe fundamental limit to the smallest amount of ionization detectable in the instrument. Normally this background

<u>Figure 23</u>

Output Voltage Linearity of the High D.C.
Voltage Power Supply.

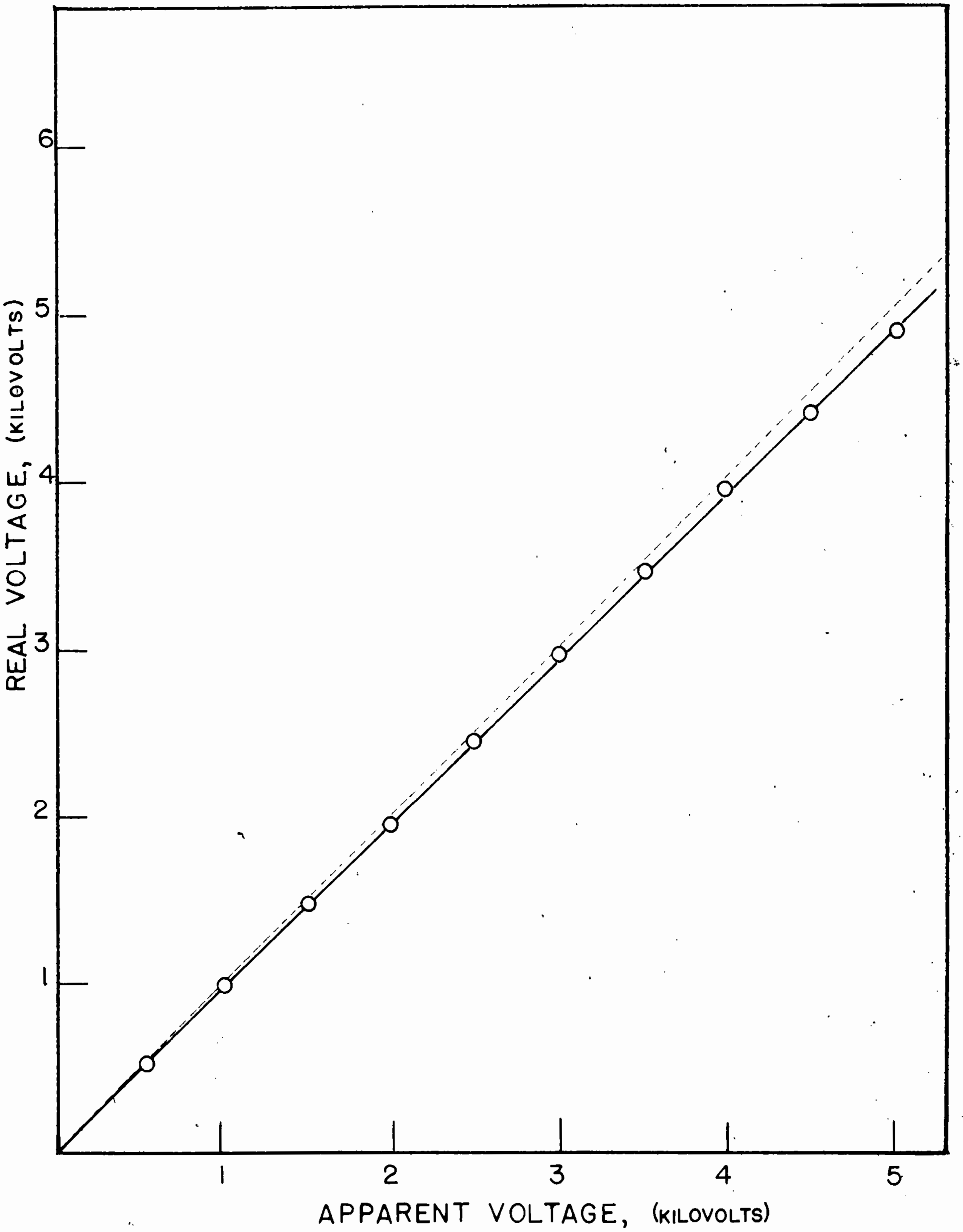

REAL VOLTAGE, (KILOVOLTS)
1
2
3
4
5
6
APPARENT VOLTAGE, (KILOVOLTS)
1
2
3
4
5

is caused by three types of radiations; (a) alpha particle contamination of the inside of the chamber, (b) cosmic radiations and (c) the radioactivity of the surroundings (natural and artificial).

Burden (166) has studied the amount of natural alpha radioactivity in various materials used to construct ion chambers. For example, brass gave an average counting rate of 5 alphas per 100 cm^2 per hour. This, of course, is of negligible importance when compared to the experimental backgrounds shown in Fig. 24 (a) and (b). However, when a lead housing having a thickness of 1.5 in. shielded each counter, an effective decrease of about 65 per cent was attained. From these results, it is fair to assume that some contribution to the background counting rate must be due to the radioactivity of the surroundings.

A spectrometric study of the background was made during a period of eight hours. The results are shown in Fig. 25 and gave an average background counting rate of 2 to 3 counts per minute per channel. This background was studied for the range of energy which concerns the problem under investigation.

The use of a lead housing for the lowering of the background counting rates has supplied an additional feature which is important in the realizations of our aims. In fact, one can now apply electronic amplification gain of 6,000 without any pick up of microphonic noises. Otherwise, the

Figure 24

(a) Background Study of Counter I.

(b) Background Study of Counter II.

○: Without Lead Shielding.

△: With Lead Shielding.

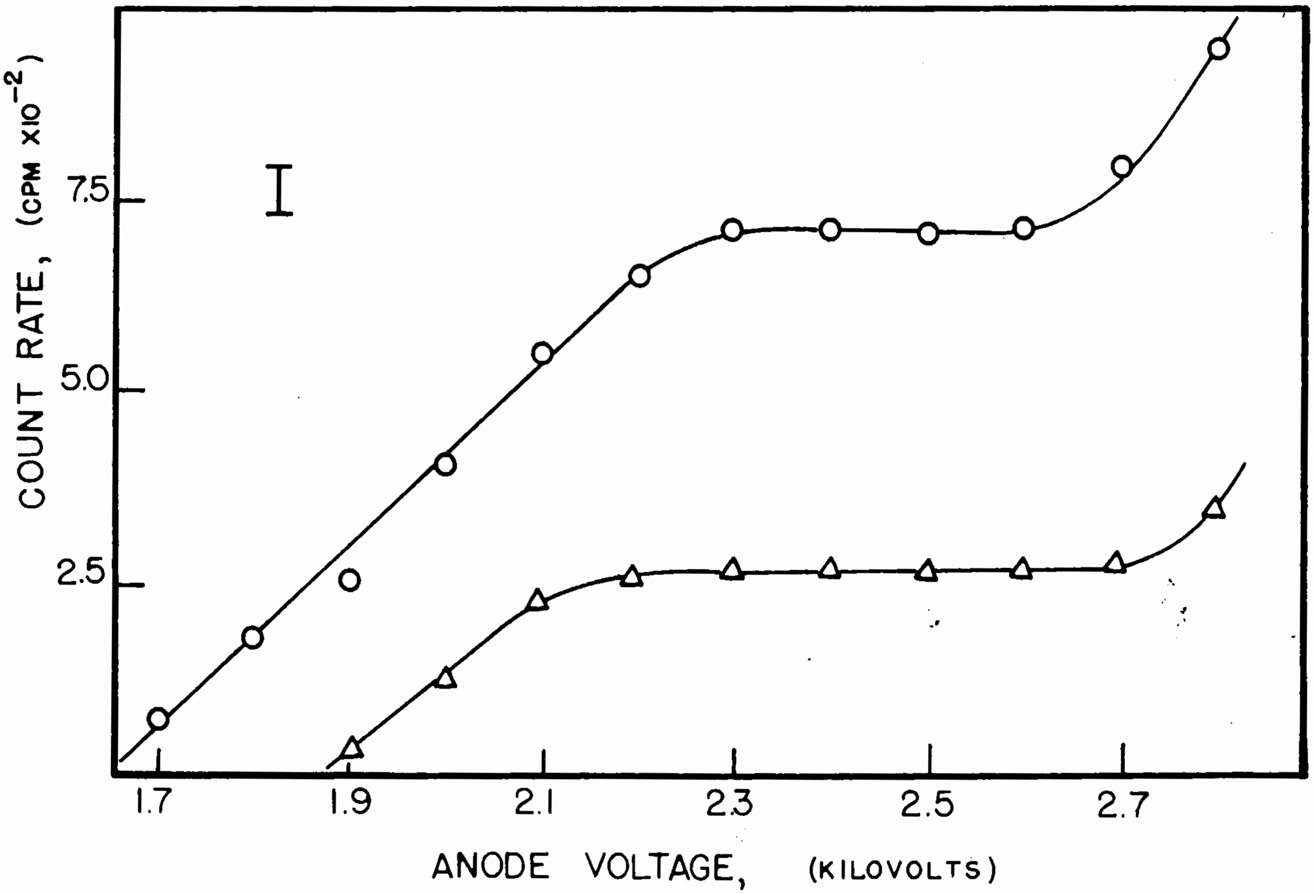
I
COUNT RATE, (CPM X10^{-2})
7.5
5.0
2.5
1.7
1.9
2.1
2.3
2.5
2.7
ANODE VOLTAGE, (KILOVOLTS)

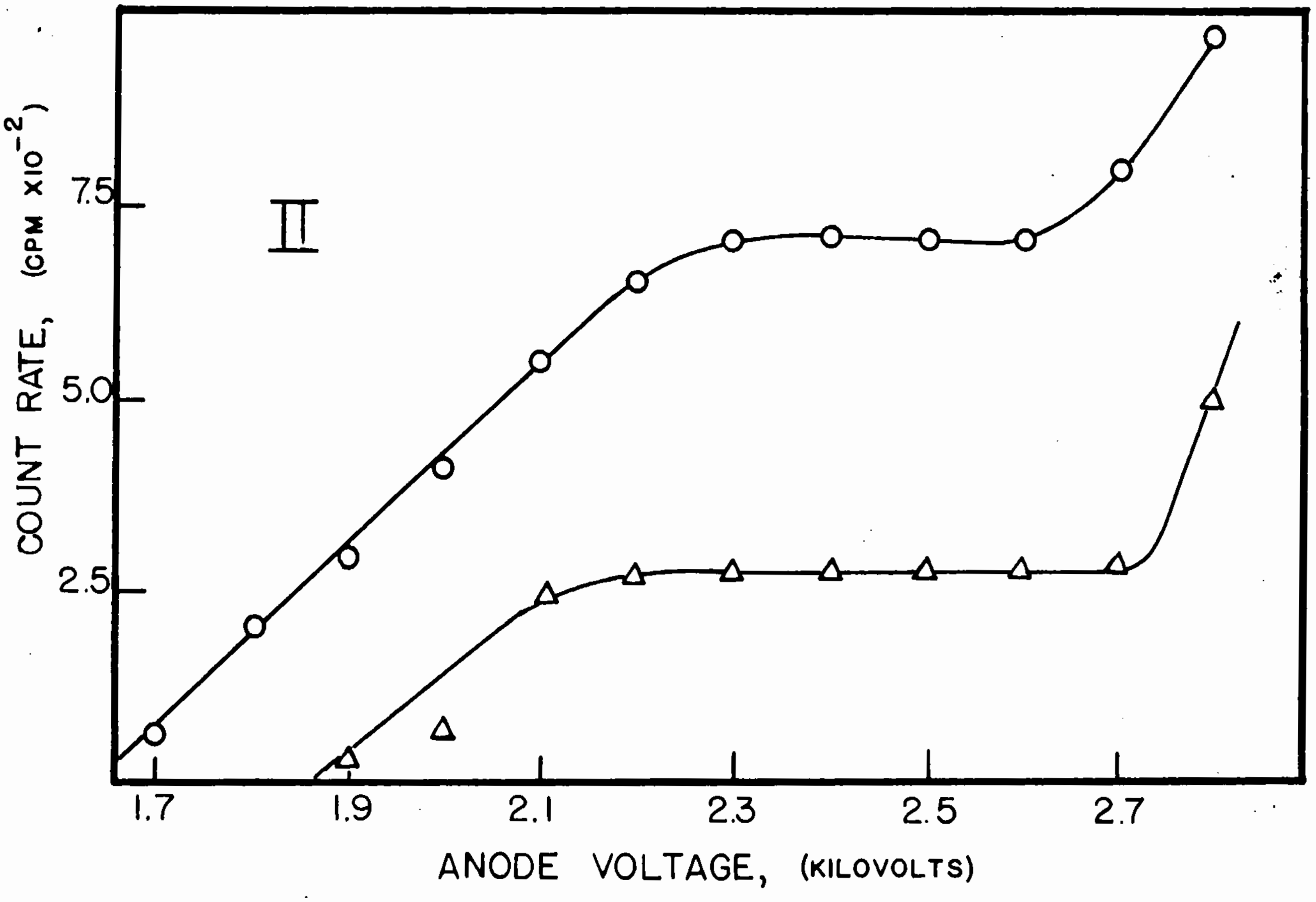
II
COUNT RATE, (CPM X10^{-2})
7.5
5.0
2.5
1.7
1.9
2.1
2.3
2.5
2.7
ANODE VOLTAGE, (KILOVOLTS)

Figure 25

Spectrometric Analysis of Background.

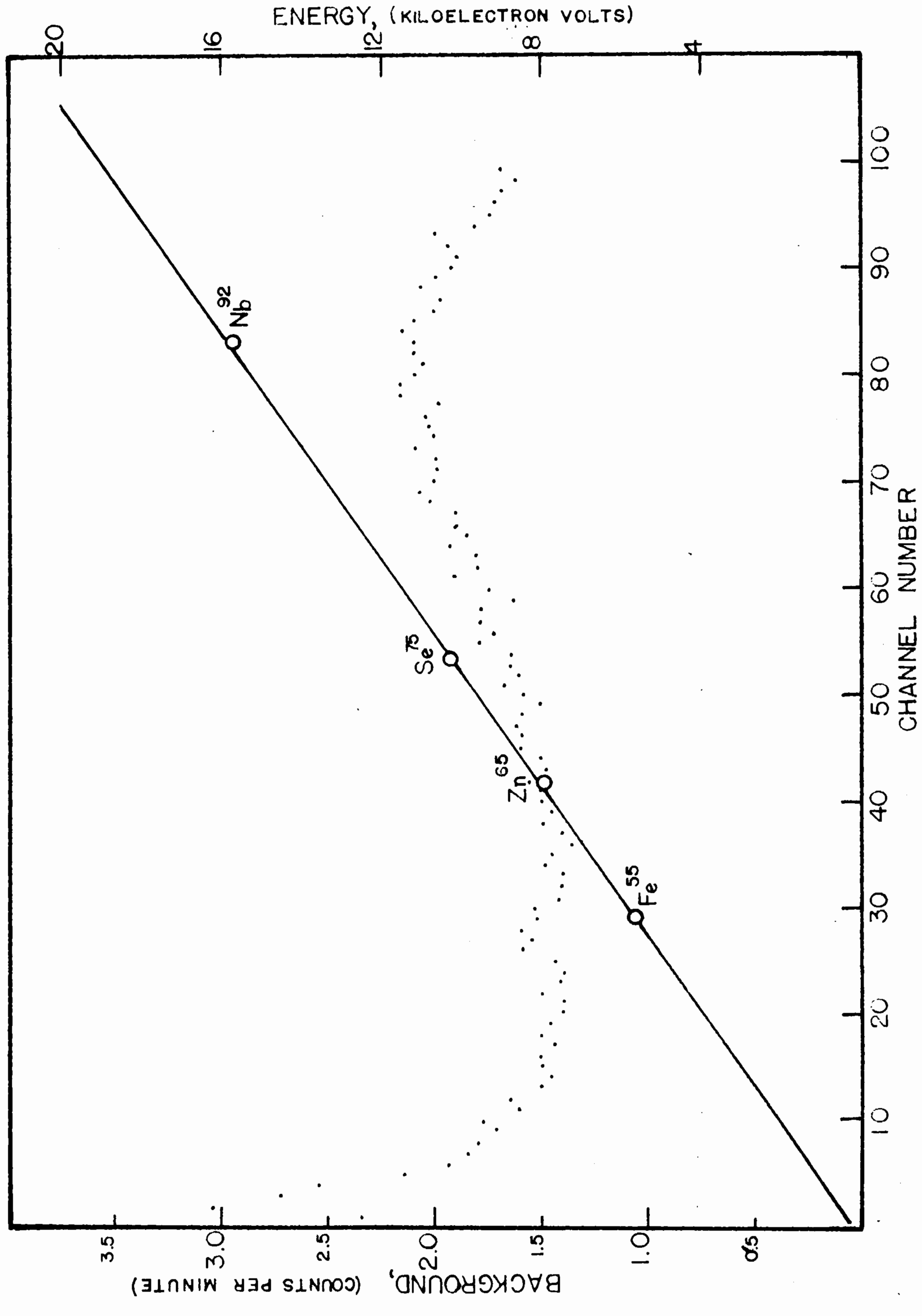
ENERGY, (KILOELECTRON VOLTS)
20
16
12
8
4
^{92}Nb
^{75}Se
^{65}Zn
^{55}Fe
10
20
30
40
50
60
70
80
90
100
CHANNEL NUMBER
BACKGROUND, (COUNTS PER MINUTE)
0.5
1.0
1.5
2.0
2.5
3.0
3.5

maximum gain amplifier could not be higher than 2,000. Now, this additional feature will enable us to use smaller anode voltages, hence better performances of the counter in the proportional region.

(II) Choice of Counter Gas

The operation of an ionization chamber depends mainly on the four following characteristics: (a) the auxiliary electronic circuits, (b) the size of the anode wire, (c) the pressure of the counter gas, and (d) the nature of the counter gas.

The auxiliary electronic equipment has already been discussed. The characteristics resulting from the variation of the size of the anode and the variation of the pressure will be discussed in the next section. The remaining variable, namely the nature of the counter gas was studied and we now propose to give some general results.

First of all, there are at least five desirable criteria which must be realized when a counter is used with a particular gas. These are (a) low operating voltage of the chamber, (b) long operating voltage range of the plateau, (c) flatness of the plateaux, (d) high efficiency of the counter gas, and (e) stability of the counter gas with use and time.

Among these desiderata, (c) and (e) did not concern us appreciably since all the plateaux which were obtained had a negligible slope and the counter was always rejuvenated with some fresh counter gas for every experiment. Consequently, attempts were made to fulfil the requirements (a), (b), and (d). For the purpose of the experiments the counter had an anode diameter of 0.002" and the counter was operated at a pressure of one atmosphere. Four different gases were employed, and inspection of Table IV shows that no gas in particular corresponded to the three requirements together. However, the mixture of A-CH_4 (9:1) seemed to be the sensible choice for the following reasons.

(a) Relative high efficiency.
(b) Reasonable plateau length.
(c) Reasonable operating voltage.
(d) Commercial availability and relatively low cost.

In Table IV the mixture of Kr-CH_4 (9:1) was assumed to have a relative X-ray efficiency of 100 per cent for energy radiation of 5.9 kev. This assumption enabled us to compare the efficiency of the counter gases. However, involved experiments were carried out for the absolute determination of the X-ray efficiencies and the results will be treated in part F of this thesis.

TABLE IV

Relative Counter Gas Efficiency

Counter Gas	V_s Starting Voltage	ΔV Plateau Length	Relative Efficiency
	Kilovolts	volts	per cent
He-C_4H_{10} (9:1)	1.2	700	8
A-CH_4 (9:1)	2.1	300	97
Kr-CH_4 (9:1)	2.6	400	100
CH_4	3.3	500	6

(III) Anode Diameter and Counter Gas Pressure Effects

In the investigations of the characteristics of proportional counters, some attention must be paid to the influence caused by the variation of the anode diameter and/or the pressure. In order to get a clear picture of the effects caused by these factors, they were treated independently.

The study was also undertaken because of the lack of helpful data available in the literature. Authoritative books (91), and (93), in the field of proportional counter construction suggest the use of anode wires of 0.003" or 0.004" diameter and recommend operating the counter at a pressure of one atmosphere. Nevertheless, in the following investigations, we have covered anode diameters ranging from 0.001" to 0.005" and pressures from 0.33 to 2.0 atmospheres.

In Fig. 26, a mixture of A-CH_4 (9:1) was used as counter gas, and a study of the starting voltages, (V_s), of the plateaux is shown for various anode diameters and pressures. By "starting voltages" of the plateaux are meant the "foot" of the plateau which corresponds to the intercept on the voltage axis. At this intercept, it was experimentally found that pulses had a voltage height of 3 millivolts. Similar experiments on plateau starting voltages were done with a mixture of Kr-CH_4 (9:1). The results are shown in Fig. 27.

Figure 26

Plateau Starting Voltages, (V_s), for various Anode Wires and Pressures of A-CH_4 (9:1).

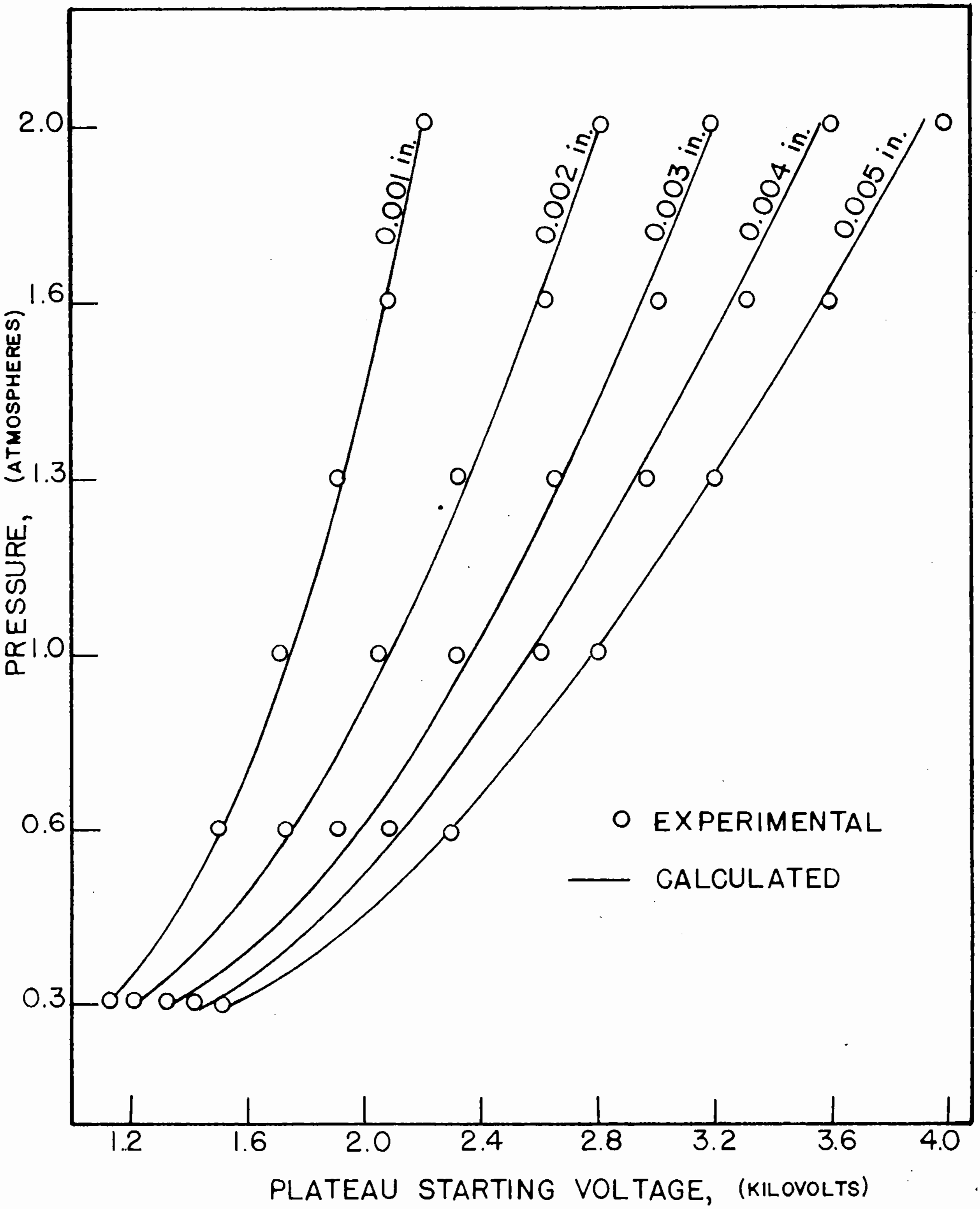

PRESSURE, (ATMOSPHERES)
2.0
1.6
1.3
1.0
0.6
0.3
0.001 in.
0.002 in.
0.003 in.
0.004 in.
0.005 in.
O EXPERIMENTAL
CALCULATED
1.2
1.6
2.0
2.4
2.8
3.2
3.6
4.0
PLATEAU STARTING VOLTAGE, (KILOVOLTS)

Figure 27

Plateau Starting Voltages for various Anode Wires and Pressures of $Kr-CH_4$ (9:1).

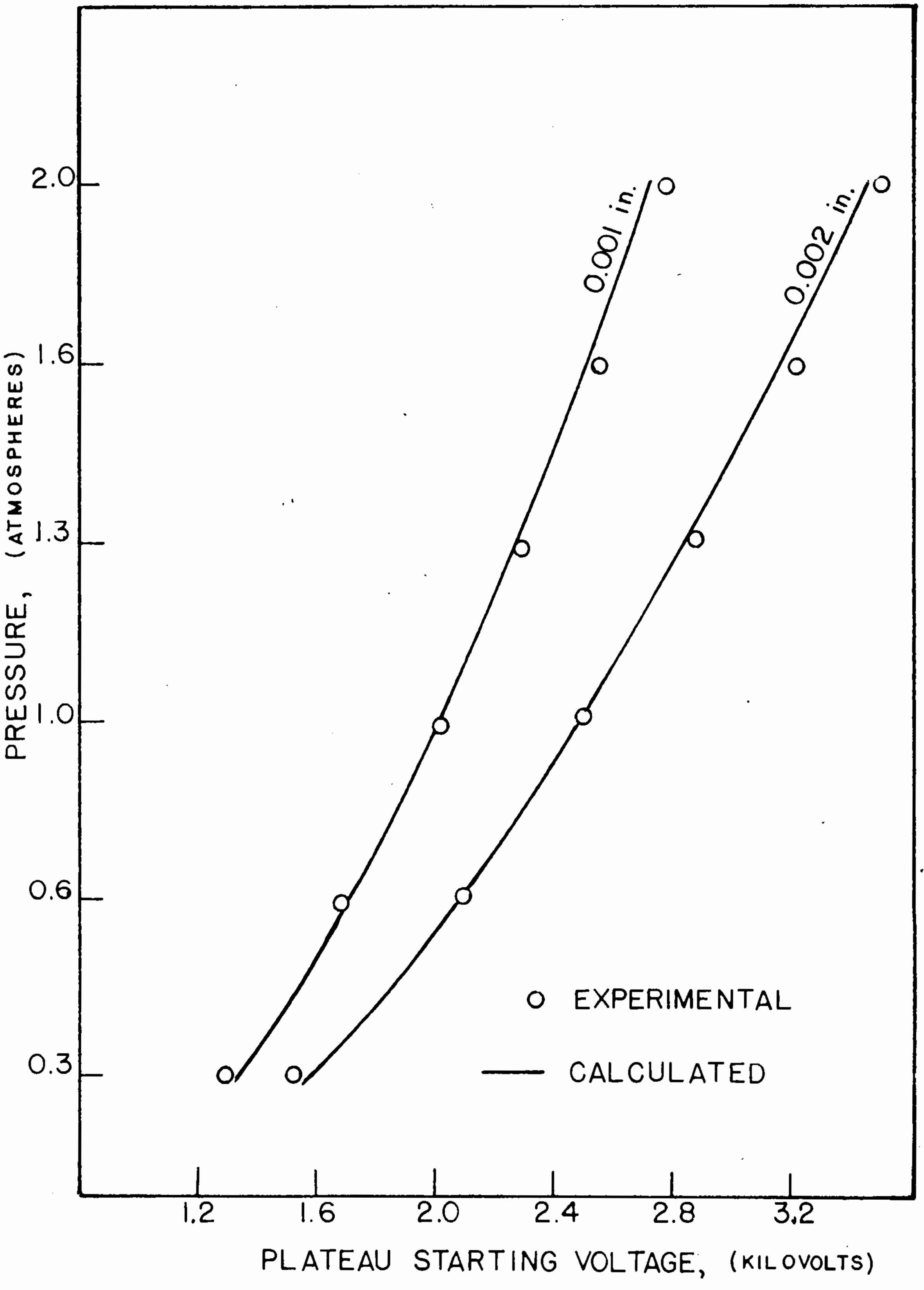
PRESSURE, (ATMOSPHERES)
2.0
1.6
1.3
1.0
0.6
0.3
1.2
1.6
2.0
2.4
2.8
3.2
PLATEAU STARTING VOLTAGE, (KILOVOLTS)
0.001 in.
0.002 in.
○ EXPERIMENTAL
— CALCULATED

The solid curves represented in Fig. 26 and 27 are the results of calculations based on the application of Eq. (12) derived by Rose and Korff (108). However, the exponential factor of the equation had to be modified for correct application. This modification will be extensively treated in part D of this thesis.

Another desirable characteristic for the proper functioning of a counter is the plateau length. A study of this was made when the anode size and pressure were varied in 41 different ways. According to the experimental results shown in Fig. 28, these conditions gave plateaux whose lengths were as short as 100 volts while some were as long as 1.7 kilovolts.

Up till now, we have discussed background counting rates, high voltage characteristics, V_s and ΔV, and choice of counter gas as important factors for the quality of the counter. Since the determination of disintegration rates is intended to be based on an instrument used as a detector and a spectrometer, these three criteria are not completely adequate tests. A more thorough investigation depends on the examination of the formation of the pulses produced by a soft monoenergetic radiation when the anode size and pressure are varied. This examination leads to the discussion of the energy resolution, $\frac{\Delta E}{E}$, which is related to the statistical fluctuation in the formation of the pulses.

Figure 28

Plateau Lengths (ΔV) for various anode Wires, Counter Gases and Pressures.

▲: Kr-CH_4 (9:1), 0.002" diameter.

●: Kr-CH_4 (9:1), 0.001" diameter.

△: A-CH_4 (9:1), 0.002", 0.003", 0.004", 0.005" diameter.

○: A-CH_4 (9:1), 0.001" diameter.

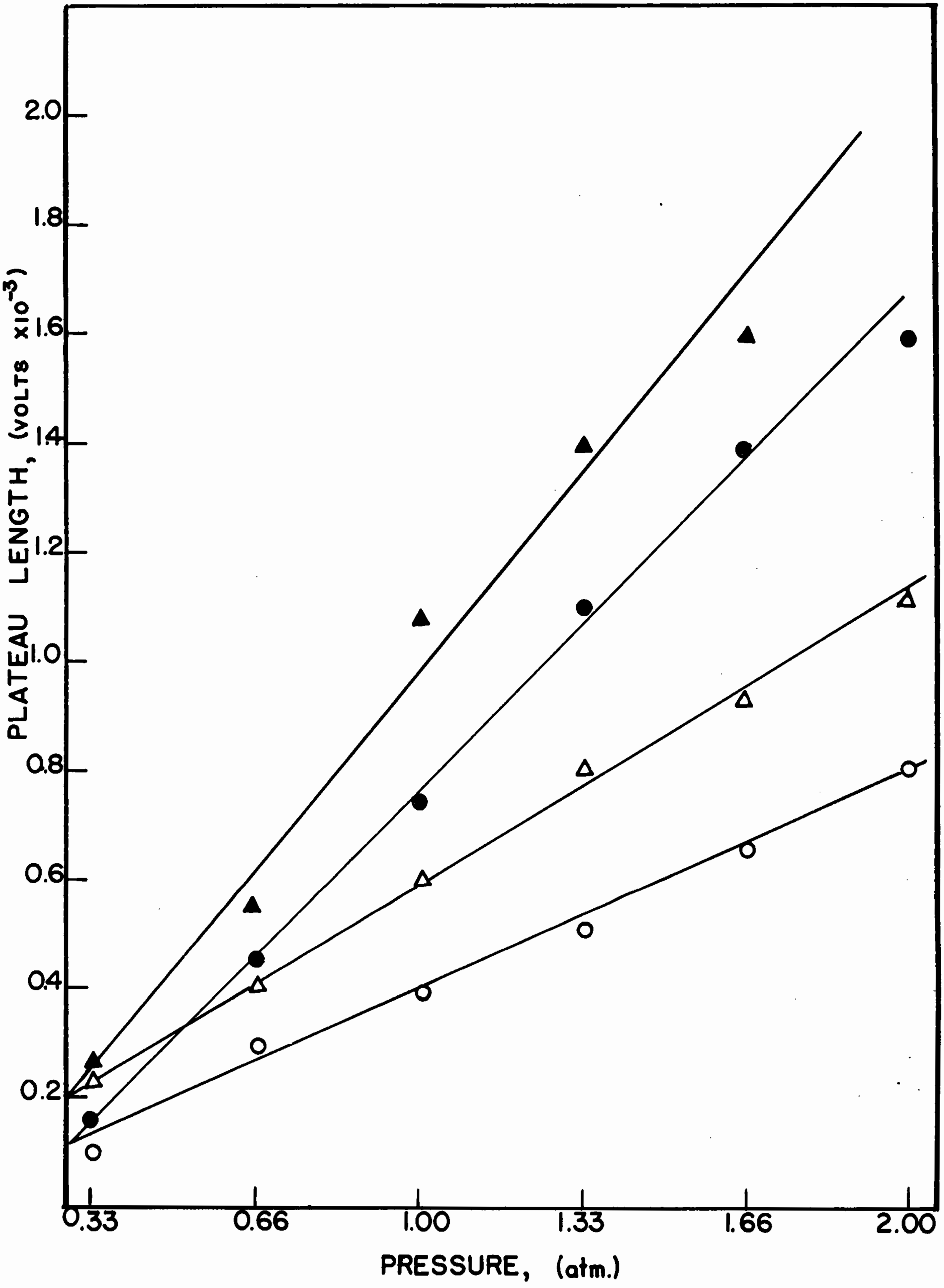
PLATEAU LENGTH, (VOLTS x10^{-3})
0.2
0.4
0.6
0.8
1.0
1.2
1.4
1.6
1.8
2.0
0.33
0.66
1.00
1.33
1.66
2.00
PRESSURE, (atm.)

According to Fig. 29(a), it was experimentally found that the energy resolution varied linearly with increase in the anode wire diameter. This phenomenon is presumably due to the variation in the distribution of the electric field when the anode radius is changed. The smaller the diameter of the wire, the shorter the critical radius, r_c, will be. Hence, on this crude assumption, one can predict less perturbation in the Townsend avalanche. The critical radius, as defined in the general introduction, is the radius where the avalanche in the proportional region is initiated. In this particular experiment the counter was operated at one atmosphere.

On the other hand, if the anode diameter is kept constant and the pressure is varied, the mean free path of the electrons producing secondary ionization will invariably be altered. In some calculations made on ionization of gases by Korff (91), the average mean free path is assumed to be approximately inversely proportional to the pressure. Then, as the pressure is decreased, the statistical fluctuation in the pulse formation would increase in the fashion described in Fig. 29(b).

During the course of these studies, it was interesting to note the reproducibility of the plateau counting rates when the conditions were changed. The results are summarized in Table V. As mentioned previously, a source of Fe^{55} was used as a reference.

Figure 29

(a) Energy Resolution versus Anode Wire diameter.

(b) Energy Resolution versus Pressure.

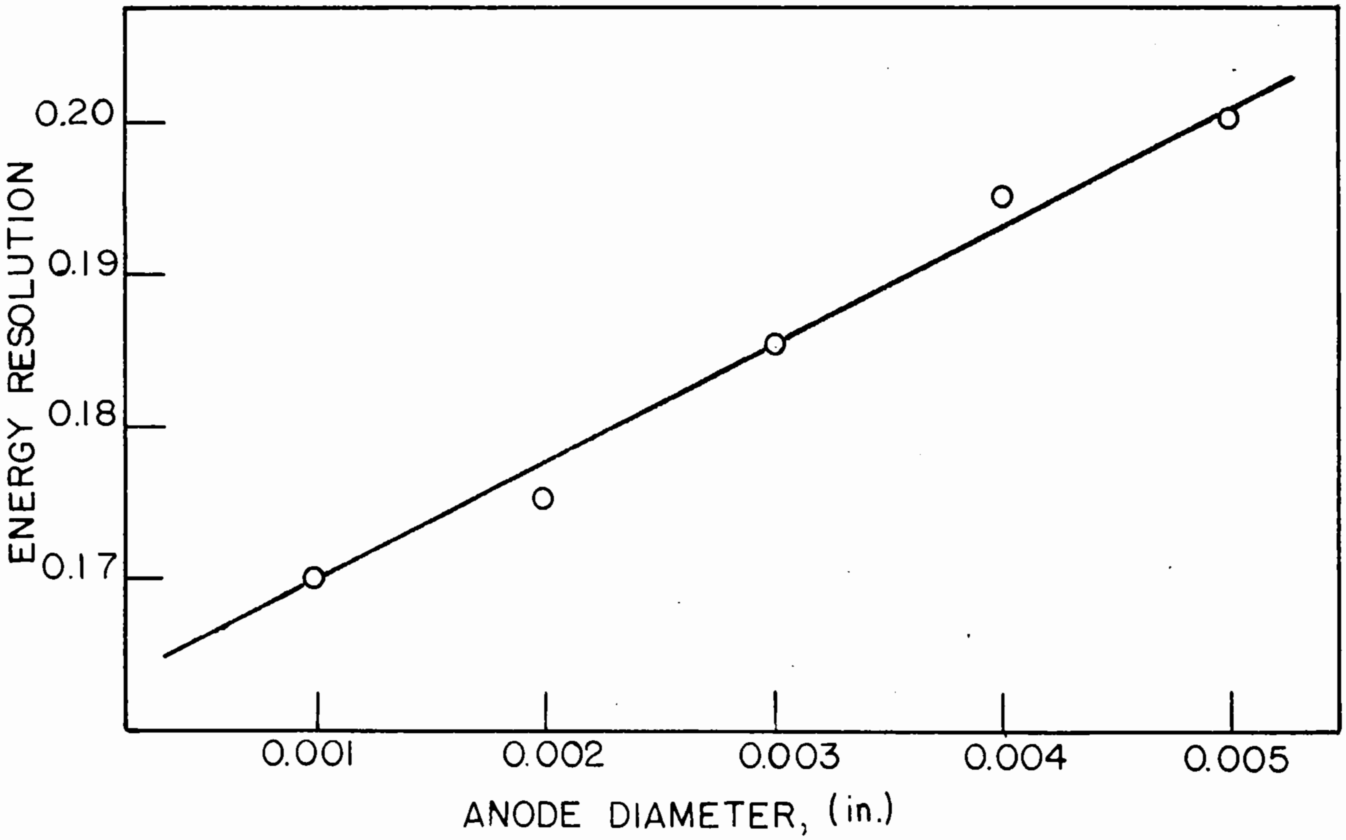
ENERGY RESOLUTION
0.20
0.19
0.18
0.17
0.001
0.002
0.003
0.004
0.005
ANODE DIAMETER, (in.)

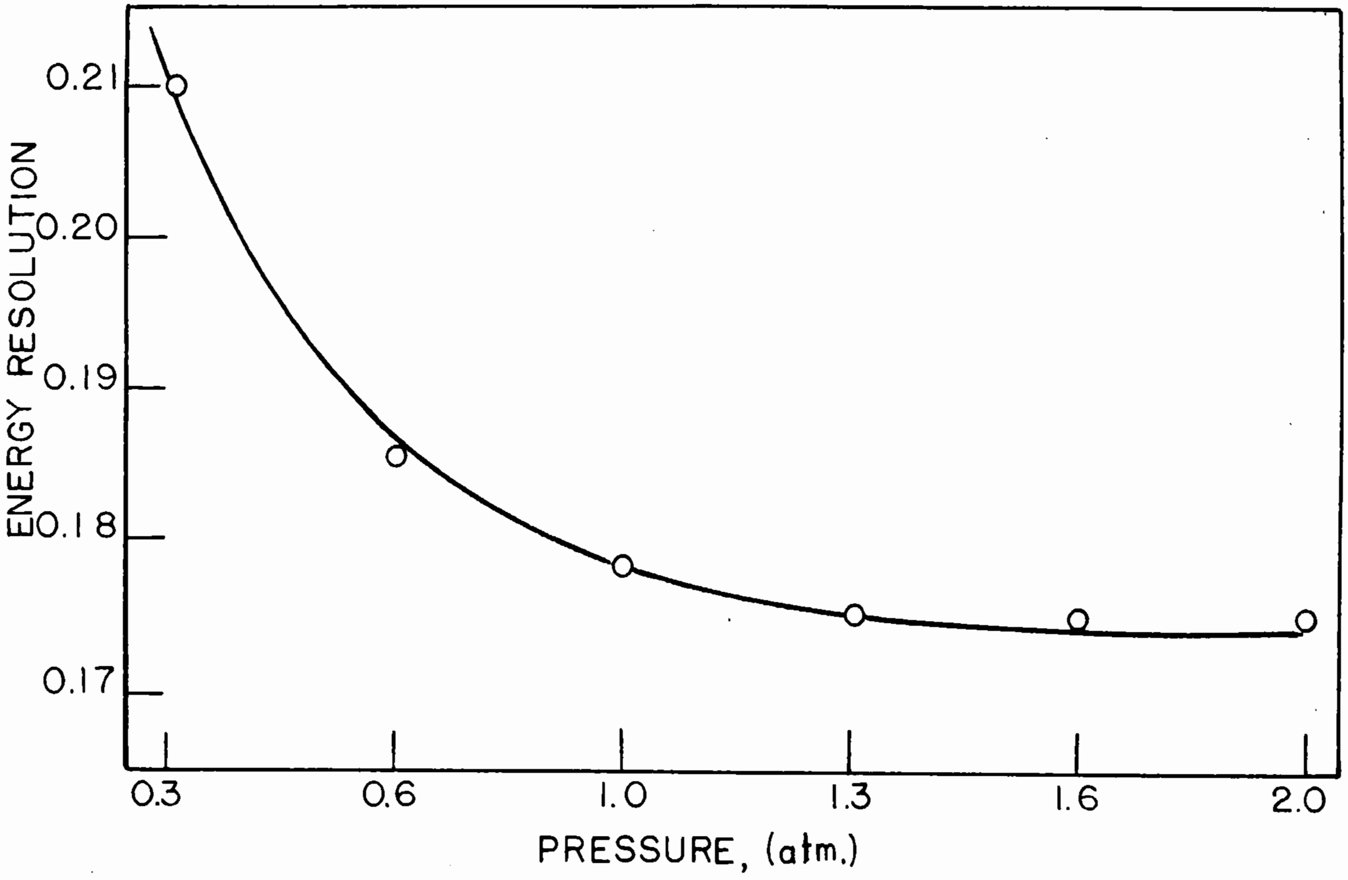
ENERGY RESOLUTION
0.21
0.20
0.19
0.18
0.17
0.3
0.6
1.0
1.3
1.6
2.0
PRESSURE, (atm.)

TABLE V

Reproducibility of Counting Rates

Anode Diameter Pressure atm.	0.001"	0.002"	0.003"	0.004"	0.005"
	cpm x 10^{-3}	cpm x 10^{-3}	cpm x 10^{-3}	cpm x 10^{-3}	cpm x 10^{-3}
0.33	29.5	30.6	29.7	30.3	30.5
0.66	40.6	40.5	40.7	40.3	40.8
1.0	44.3	44.6	44.6	44.8	44.7
1.33	46.7	46.6	46.5	46.5	46.5
1.66	47.1	47.2	47.0	47.3	47.2
2.0	47.7	47.7	47.7	47.6	47.8

(IV) Gas-flow Counter Characteristics

Although the principle of the gas-flow counter does not restrict it to the proportional region, many of these detectors are operated as proportional counters. For instance, the application of this principle is in wide use for detectors of particular geometrical forms and for counters detecting radiations of high specific ionization. Obviously, the geometrical form of our counter and the nature of the radiations under investigation do not militate in favour of the application of such a system. However, it has been found necessary to use the counter as a gas-flow at least in two cases, namely for energy measurements and for the study of beta spectra. The application of a gas-flow system would enable a constant pressure inside the counter. Hence, at constant anode voltages, slight changes in ambient temperature would not essentially alter the magnitude of the gas-multiplication factor. The counter was initially filled with air and then operated with the gas flowing at a rate of 2 bubbles per second. According to Fig. 30, the plateau counting rates became reproducible after 80 minutes of gas-flow. On the other hand, the plateaux could be superposed after a period of about 220 minutes.

Although the flow rate could be increased and less time would be required for more adequate flushing, this is not very good for routine work. A way to remedy the situation would be to

Figure 30

Gas-flow Counter, (counter initially filled with air).

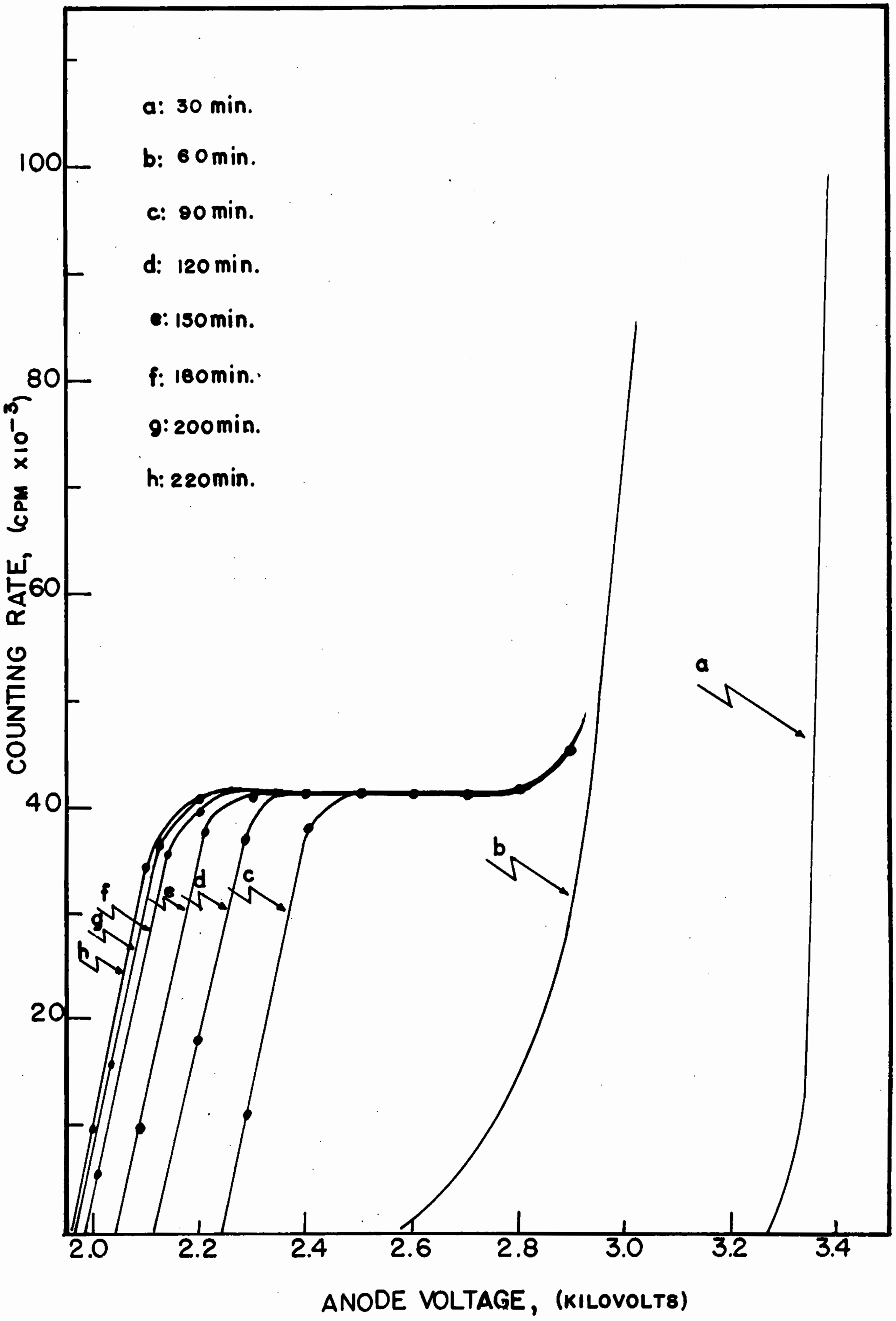
a: 30 min.
b: 60 min.
c: 90 min.
d: 120 min.
e: 150 min.
f: 180 min.
g: 200 min.
h: 220 min.
COUNTING RATE, (CPM X10^{-3})
100
80
60
40
20
2.0
2.2
2.4
2.6
2.8
3.0
3.2
3.4
ANODE VOLTAGE, (KILOVOLTS)
a
b
c
d
e
f
g
h

flow the gas through the counter which was initially filled with the same gas. This treatment was applied and in Fig. 31, improved results were obtained. The manipulations involved were the following.

(a) Filling the counter through the evacuation and filling apparatus at a pressure of one atmosphere.

(b) Removal of the threaded cap and placing the source in position for measurement.

(c) Replacement of the cap by the one especially designed for gas-flow system.

(d) Starting the flow at a rate of about 2 bubbles per second.

The results shown in Fig. 31 (a) show that the plateau counting rates were reproducible any time after the operation of flowing the gas had started. The plateaux could be superposed after about 10 minutes.

Spectra were also taken at different intervals and the results are shown in Fig. 31 (b). Reproducibility could be achieved after about 35 minutes.

In both figures (a) and (b), the solid curves are considered as standard and they were reproducible unless the conditions for operation are changed.

Figure 31

Gas-flow Counter, (counter initially filled with the counter gas).

(a) High Voltage Characteristics.

- - - - - 4 minutes

—·—10 minutes

———standard, (15 minutes).

(b) Fe^{55} spectra.

- - - - -10 minutes

—·—20 minutes

——— standard, (35 minutes).

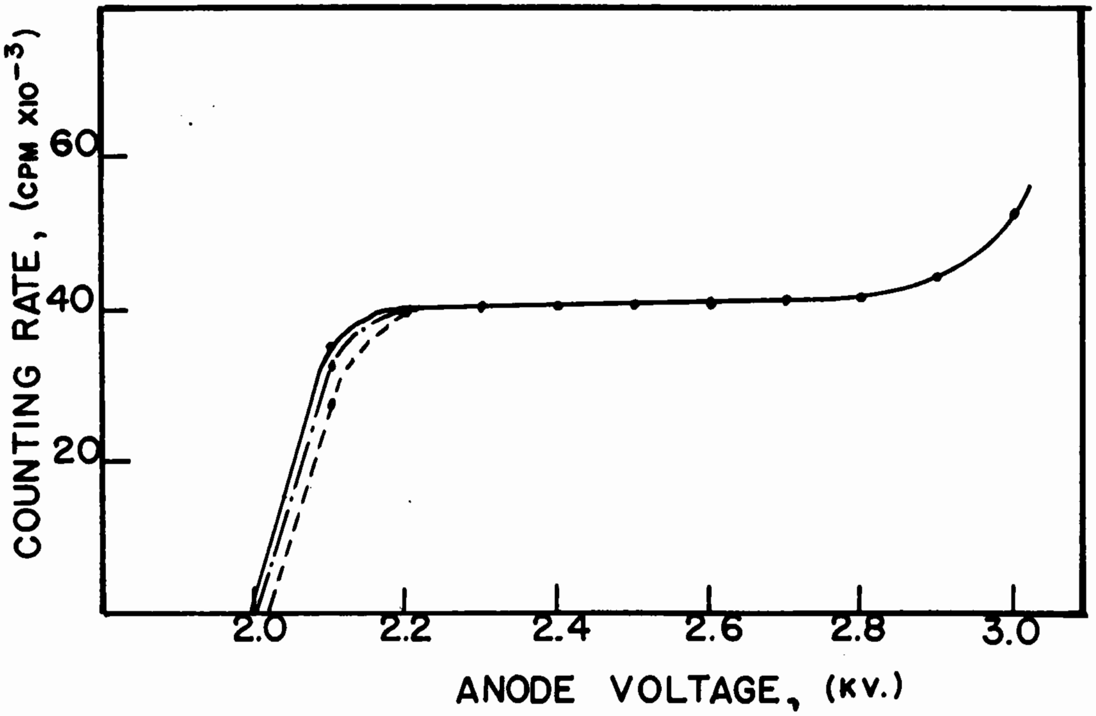
COUNTING RATE, (CPM X10^{-3})
60
40
20
2.0
2.2
2.4
2.6
2.8
3.0
ANODE VOLTAGE, (KV.)

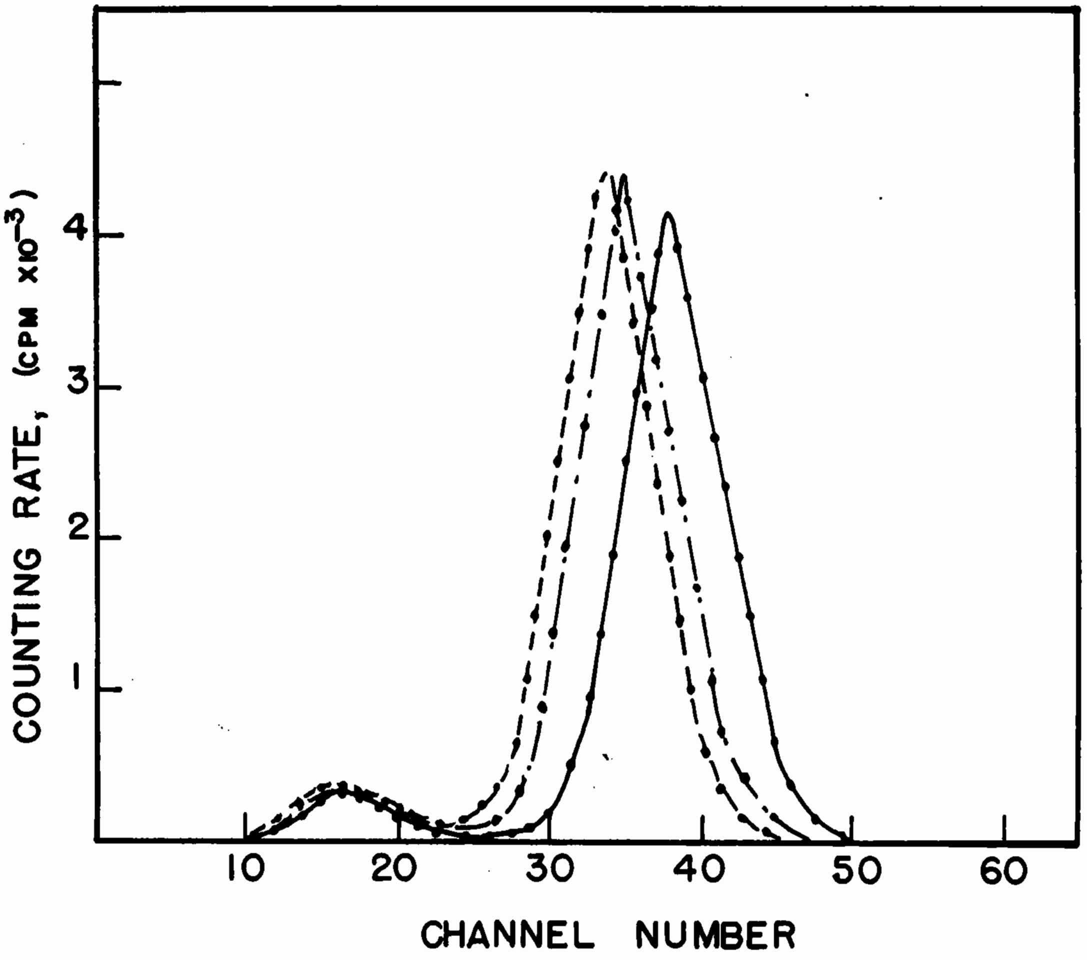
COUNTING RATE, (CPM X10^{-3})
4
3
2
1
10
20
30
40
50
60
CHANNEL NUMBER

(V) Air Tolerance in Counter Gas

One should always be aware of gas impurities in the counter gases. The most are those having high electronegative affinities, such as oxygen, nitrogen, halogen, etc.

In 1954, Wakefield (167) investigated the operation of a proportional counter when increasing amounts of air were mixed to chemically pure CH_4 counter gas. He found that for concentrations up to 14 per cent, plateaux having a length of 300 volts were still obtainable.

Similar experiments were made in this laboratory with the counter herein described, but the counter gas used was a mixture of A-CH_4 (9:1). The detector was initially filled with various partial pressures of air and then equilibrated at atmospheric pressure with the pure counter gas. As suggested by Korff (91), one hour at least was allowed for diffusion equilibrium to be established after the mixture was made.

The experimental results obtained show a set of plateaux having reproducible counting rates when the counter gas was "contaminated" with air for concentrations up to 10 per cent.

A comparison between Wakefield and our results was made and it may be pointed out that the effect of addition of air is more pronounced in the shifting of the starting voltages, V_S, and the plateau lengths, ΔV, when a mixture of A-CH_4 (9:1) is used. However, in both cases and for reasonable percentage of

Figure 32

Effect on the High Voltage Characteristics of the Counter when the Counter Gas is Contaminated with air.

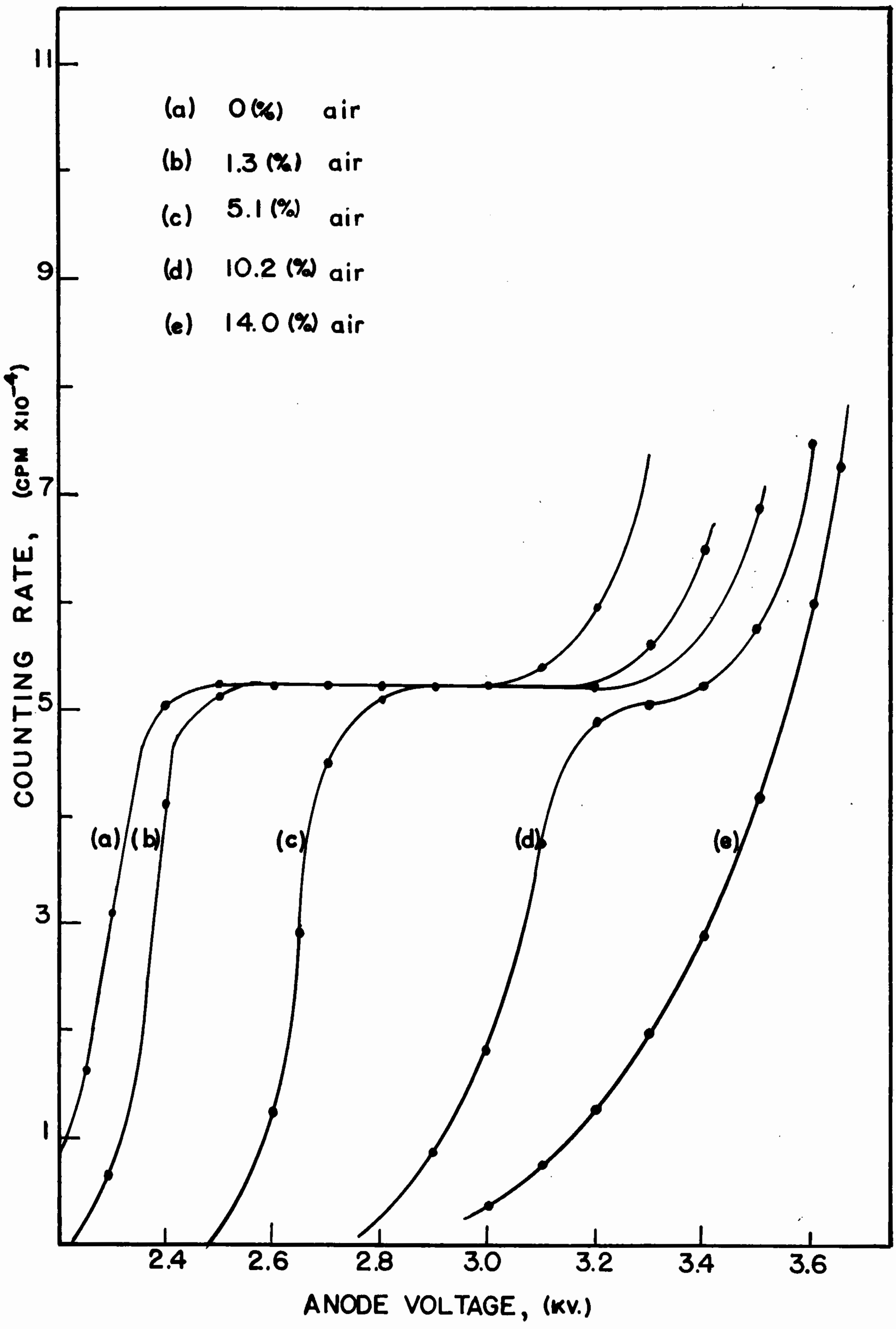
(a) 0 (%) air
(b) 1.3 (%) air
(c) 5.1 (%) air
(d) 10.2 (%) air
(e) 14.0 (%) air
COUNTING RATE, (CPM x10⁻⁴)
11
9
7
5
3
1
(a)
(b)
(c)
(d)
(e)
2.4
2.6
2.8
3.0
3.2
3.4
3.6
ANODE VOLTAGE, (KV.)

air, the flatness of the plateau is not materially reduced.

(VI) Pulse Amplifier Discriminator Calibrations

The apparatus for measurement can be considered as consisting of three different units. These units were (a) a AEP 1448 amplifier, (b) a built in discriminator, and (c) a 2005 B scaler. Through the amplifier, the pulses are usually shaped. Thereafter, the amplifier discriminator will pass only the desired pulses. Finally, the scaler counts the pulses passed through the amplifier and the discriminator.

On account of its crucial importance in the study of the intrinsic properties of proportional counters, some consideration must be given to the pulse-amplitude discriminator. First of all, the linearity was verified when varying pulse amplitudes were fed into the amplifier. The pulses were supplied by a mercury-wetted-contact-relay pulse generator. Simultaneously, the linearity of the amplifier could be checked. The results in Fig. 33 show no deviation from linearity when the discriminator bias was varied.

Now, that it had been established that the properties of the electronic measuring apparatus were reliable at least in the range of pulse heights corresponding to our counter, further studies of the properties of the counter could be made.

In Fig. 34 is shown a series of characteristics obtained

Figure 33

Pulse Amplitude Discriminator Bias Calibration.

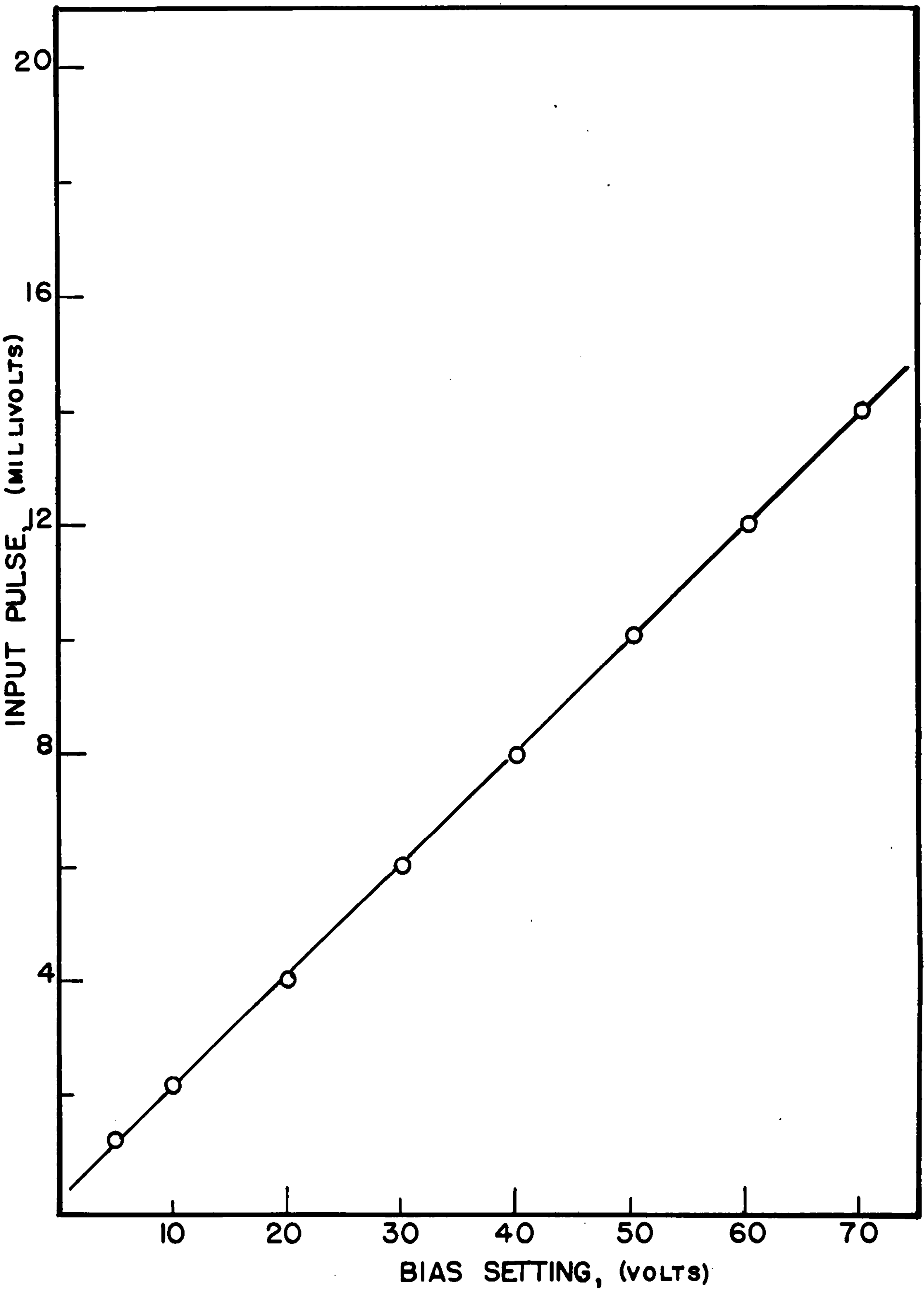

20
16
12
8
4
INPUT PULSE, (MILLIVOLTS)
10
20
30
40
50
60
70
BIAS SETTING, (VOLTS)

Figure 34

High Voltage Characteristics of the Counter as a Function of Applied Discriminator Bias.

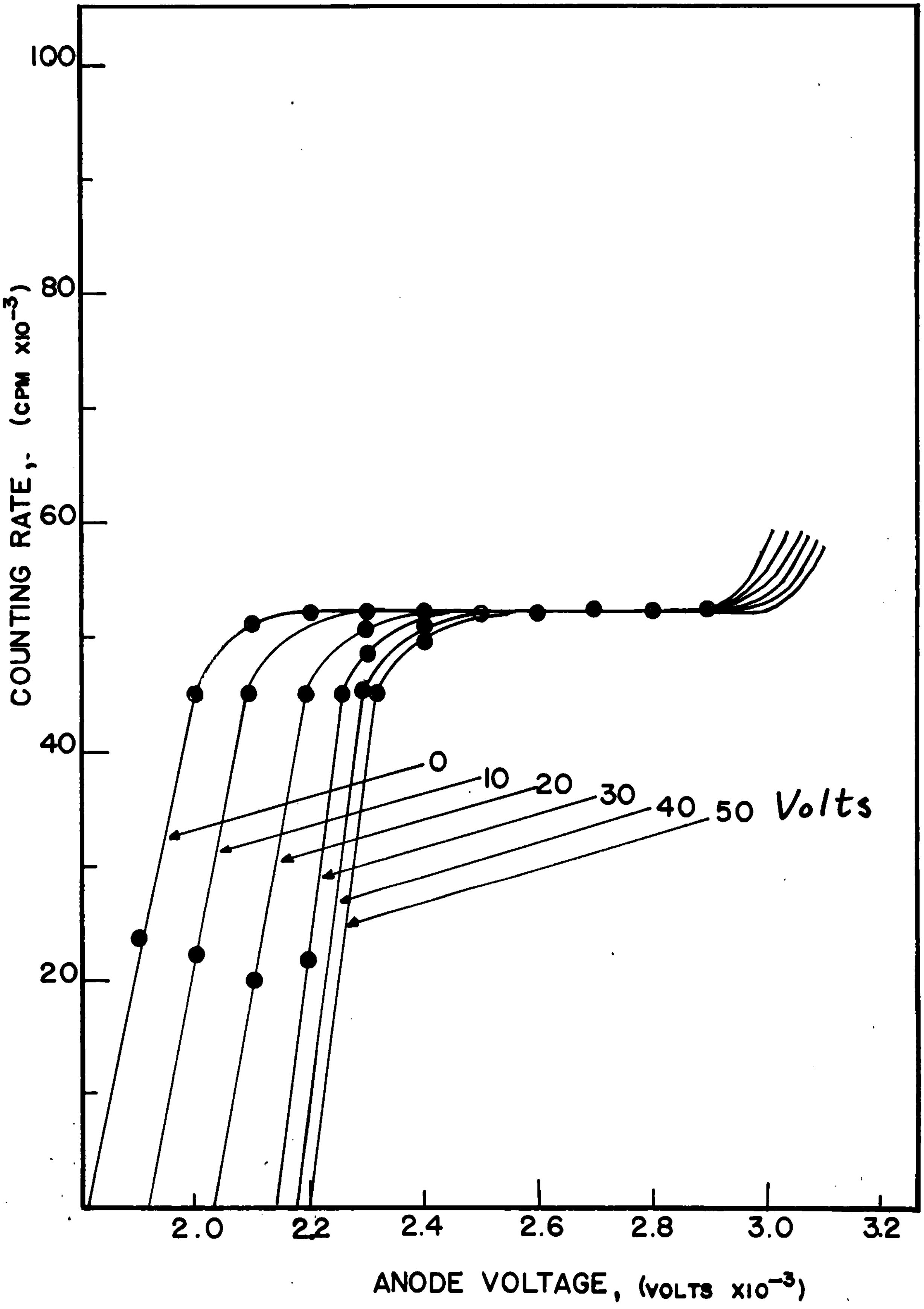
100
80
60
40
20
COUNTING RATE, (CPM X10^{-3})
2.0
2.2
2.4
2.6
2.8
3.0
3.2
ANODE VOLTAGE, (VOLTS X10^{-3})
0
10
20
30
40
50 Volts

using a source of Fe^{55} and anode diameter of 0.002 in. The readings were taken at increasing discriminator bias values. It is noticed that the plateaux are displaced to higher anode-voltage values since increased gas multiplication factors are necessary to produce pulses larger than the increased bias level.

From the same experiment, the discriminator bias characteristics for the same nuclide are shown in Fig. 35 when the anode voltage is kept at 2.6 kilovolts. This voltage is typical of those needed with this equipment. The results demonstrate the usual absence of low amplitude spurious pulses and show a constant counting rate.

An important application of discriminator bias is the study of the pulse amplitude distribution. The anode voltage was adjusted so that the bias voltage at maximum setting was sufficient to screen out all pulses. Then, the counting rates were determined with decreasing settings. The so-called "integral bias curve" was differentiated with respect to bias settings and Fig.36 (b) shows the distribution on an energy scale. This demonstrates that with an elementary instrument such as a simple discriminator, fundamental properties of a counter operating in the proportional region can be investigated.

Figure 35

Discriminator Bias Characteristics at an Anode Voltage of 2.6 Kilovolts.

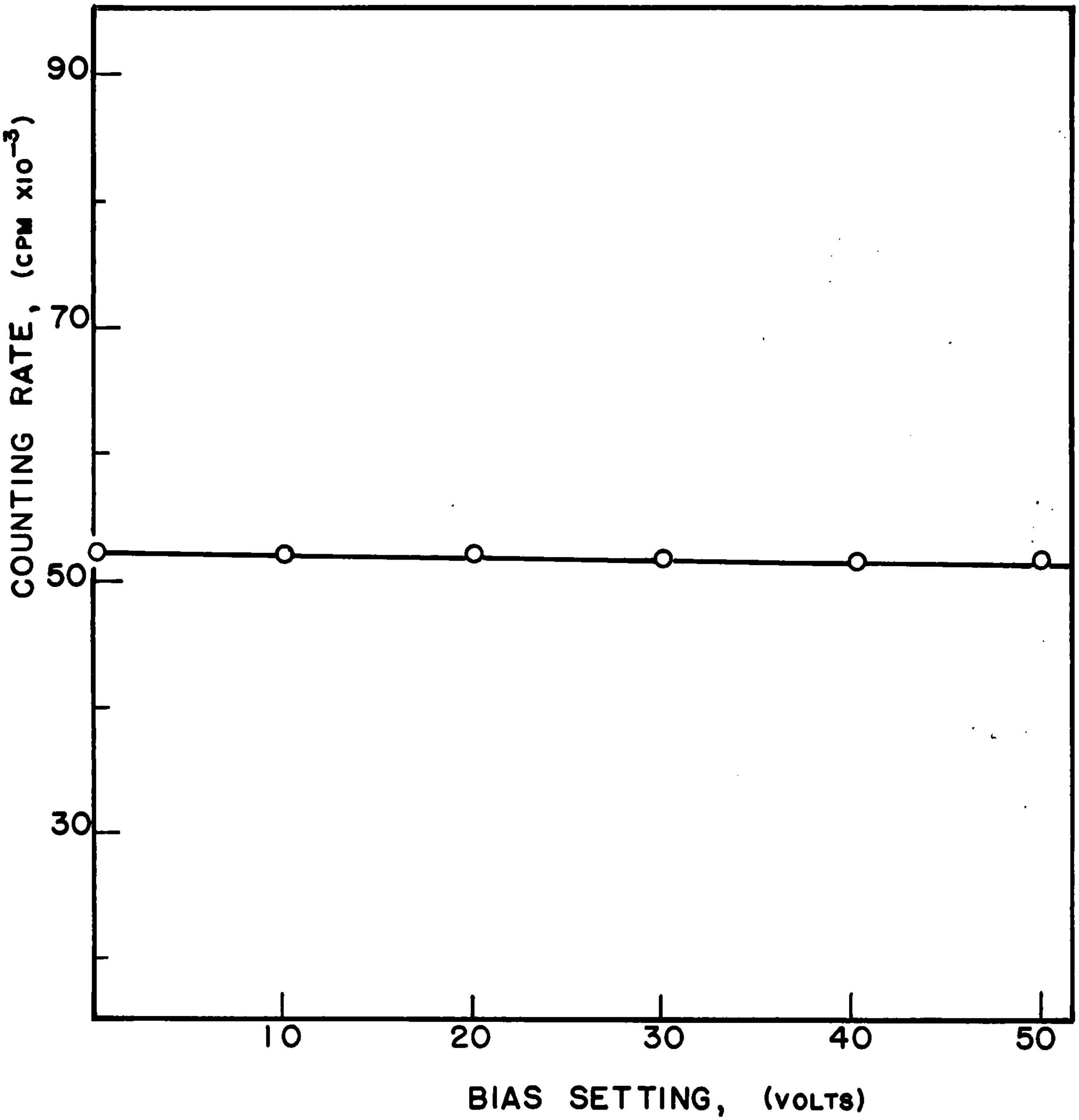
90
70
50
30
COUNTING RATE, (CPM X10^{-3})
10
20
30
40
50
BIAS SETTING, (VOLTS)

Figure 36

Discriminator Bias Characteristic for a Sample of Fe^{55} at an Anode Voltage of 2.35 Kilovolts.

(a) "Integral Bias Curve" of the Pulse Heights.

(b) "Differential Bias Curve" of the Pulse Heights.

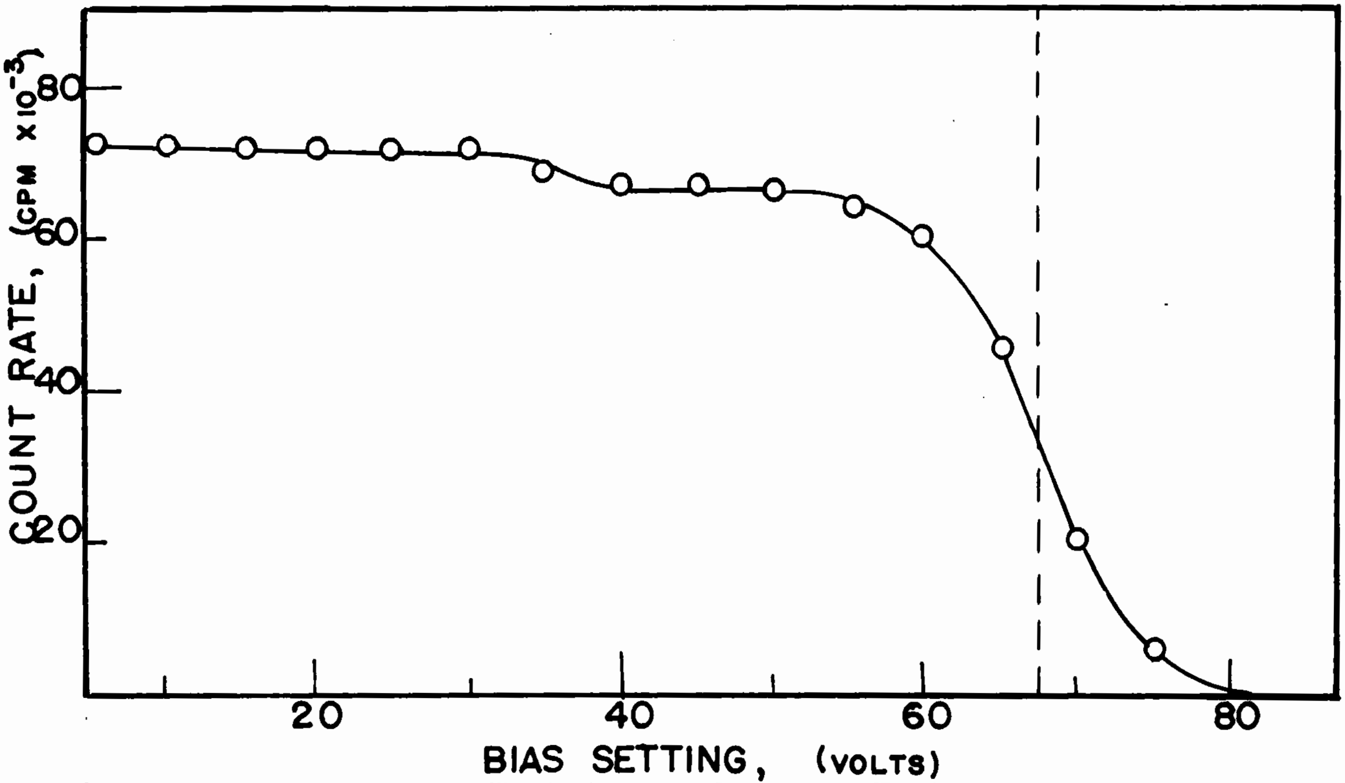
COUNT RATE, (CPM X10^{-3})
80
60
40
20
20
40
60
80
BIAS SETTING, (VOLTS)

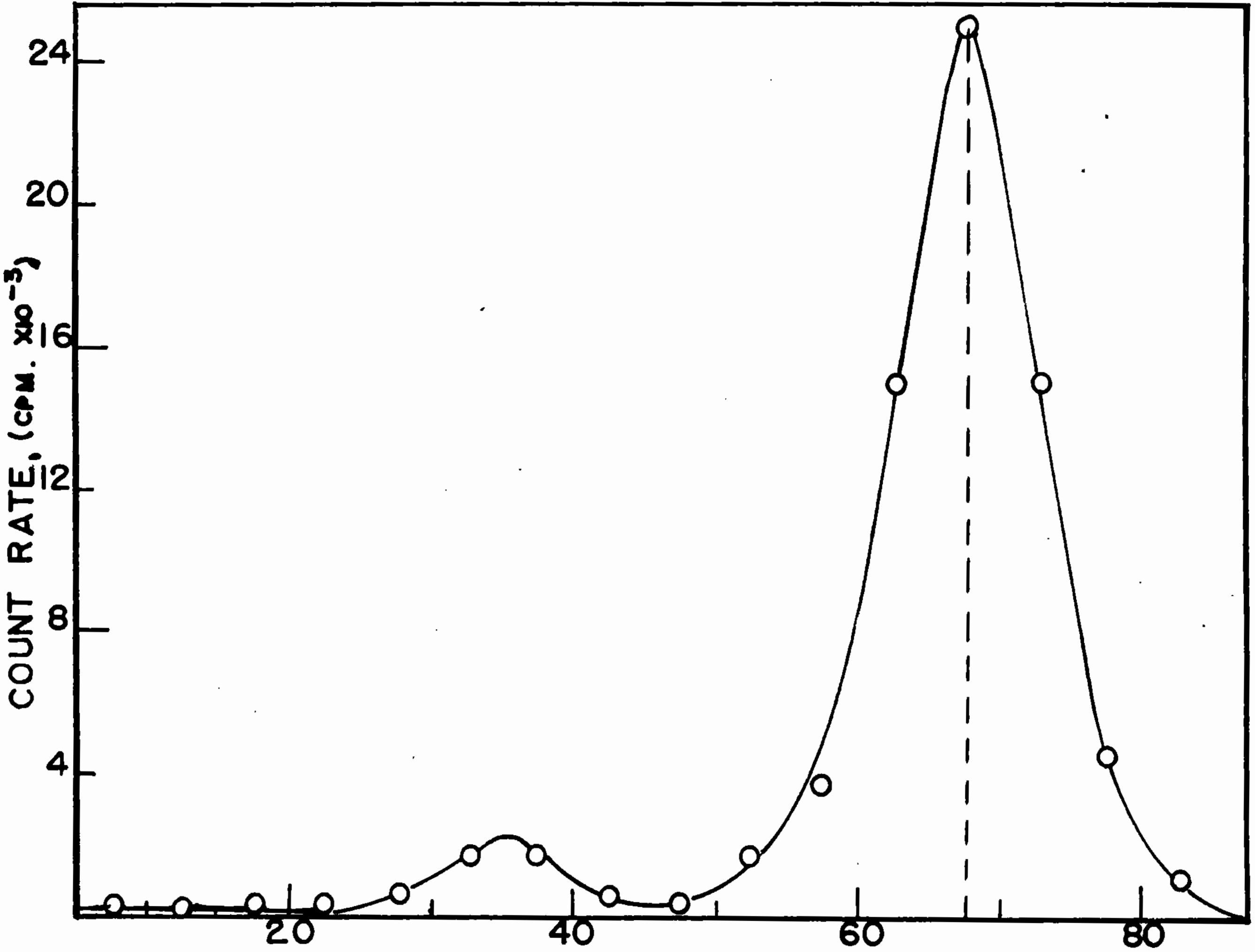
COUNT RATE, (CPM. X10^{-3})
24
20
16
12
8
4
20
40
60
80
BIAS SETTING, (VOLTS)

(VII) Pulse shape and Dead Time of the Counter.

Pulse Shape.

The most important property of a proportional counter, apart from its gas amplification, is the fact that the pulse size is independent of the position of the track within the sensitive volume of the counter. This follows at once from the fact that most of the ionization occurs very close to the wire. The pulses which are formed have the same form and the same fraction is always recorded even though the auxiliary electronic may have a "clipping" time much shorter than the pulse length.

Although no information can be obtained as to the orientation of the ionized track, it will be of interest to calculate, on the basis of electrostatics, the profile of the pulse. This would enable a verification of our ideas concerning counter mechanism and the design of correct electronic equipment to be matched with the counter.

From energy considerations, one can obtain a description of the mechanism of pulse formation. Since the gas multiplication, for practical work is about 10^3, the work done by the field in moving the electron into position for the initiation of the Townsend avalanche can be neglected in comparison to the work done by the field in moving the ions after the avalanche has taken place. Considerations of mean free path, gas ionization potential and electric field strength have lead Korff (91) to say that the positive ion sheath's outer periphery is within a wire diameter from the center wire.

Let us assume that the center of gravity of the positive ion sheath is at a point $r = (a + a/4)$ as shown in Fig. 37 (a).

The energy of the system can be written as

$$1/2\ CV^2 + \int_{a + a/4}^{b} QdV = 1/2\ CV_o^2 \qquad \ldots\ldots\ (19)$$

where,

C = capacity of the collector electrode with respect to the high voltage electrode, which has an initial potential V_o with respect to the collector.

V = new potential between the electrodes.

Q = total electronic charge collected on the collector.

a = collector radius.

b = cathode radius.

When Eq. (19) is rewritten, it gives,

$$1/2\ C(V_o^2 - V^2) = \int_{a + a/4}^{b} QdV \qquad \ldots\ldots\ldots\ (20)$$

Let

$$V_P = (V_o - V)$$

where V_P is the proportional counter pulse. Then,

$$V_P = \frac{1}{CV_o} \cdot \int_{a+a/4}^{b} QdV = \frac{Q}{CV_o} \int_{a+a/4}^{b} Edr = \frac{Q}{CV_o} \int_{a+a/4}^{b} \frac{V_o dr}{r \ln\frac{b}{a}} \quad \ldots\ldots (21)$$

where E is the electric field.

The voltage pulse due to the motion of the positive ions will be

$$V_{P^+} = \frac{Q}{C\ln\frac{b}{a}} \cdot \int_{a+a/4}^{b} \frac{dr}{r} = \frac{Q}{C\ln\frac{b}{a}} \cdot \ln\frac{4b}{5a} \quad \ldots\ldots (22)$$

Similarly, the voltage pulse due to the motion of the electrons will be,

$$V_{P^-} = \frac{Q}{C\ln\frac{b}{a}} \int_{a+a/4}^{a} \frac{dr}{r} = \frac{Q}{C\ln\frac{b}{a}} \cdot \ln\frac{5}{4} \quad \ldots\ldots (23)$$

Therefore the ratio of the pulse amplitude due to each component is,

$$\frac{V_{P^-}}{V_{P^+}} = 0.031$$

when b = 1.875 in.

a = 0.001 in.

Obviously, from the results of these calculations, the electrons contribute only a few per cent to the total pulse height. The relative pulse shape and the amplitude can be calculated from considerations of only the positive ion motion.

Consequently, the concepts on heavy ion mobilities must be known.

Wilkinson (97) in some elaborate discussions on ionization chambers and counters wrote that the heavy-ion mobilities, v, are found to be related to E/p (E is the electric field and p is the gas pressure) through the expression

$$v = KE \qquad \ldots\ldots\ldots\ldots\ (24)$$

where K is the ionic mobility. During the argument, the pressure will be considered as one atmosphere.

Eq. (24) can be rewritten as,

$$\frac{dr}{dt} = K \frac{V_o}{r \ln\frac{b}{a}} \qquad \ldots\ldots\ldots\ldots\ (25)$$

or

$$\int_a^r r dr = \int_0^t K \frac{V_o}{r \ln\frac{b}{a}} dt \qquad \ldots\ldots\ldots\ldots\ (26)$$

whence

$$r^2 - a^2 = \frac{2KV_o t}{\ln\frac{b}{a}} \qquad \ldots\ldots\ldots\ldots\ (27)$$

Since

$$V_{p^+} = \frac{Q}{C \ln\frac{b}{a}} \cdot \int_a^r \frac{dr}{r} = \frac{Q}{C \ln\frac{b}{a}} \int_0^t \frac{1}{r} \frac{dr}{dt} dt \qquad \ldots\ldots\ldots\ (28)$$

when Eq. (25) is substituted into Eq. (28), then,

$$V_{p^+} = \frac{Q}{C \ln\frac{b}{a}} \int_0^t \frac{KV_o}{\ln\frac{b}{a}} \cdot \frac{1}{\frac{2KV_o}{\ln\frac{b}{a}} + a^2} \qquad \text{.........} \; (29)$$

$$V_{p^+} = \frac{Q}{C \ln\frac{b}{a}} \int_0^t \left(\frac{1}{r^2} \cdot \frac{KV_o}{\ln\frac{b}{a}} \right) dt \qquad \text{.........} \; (30)$$

When Eq. (27) is substituted in Eq. (30), then

$$V_{p^+} = \frac{Q}{C \ln\frac{b}{a}} \cdot \int_0^t \frac{KV_o}{\ln\frac{b}{a}} \cdot \frac{1}{\frac{2KV_o}{\ln\frac{b}{a}} + a^2} \, dt \qquad \text{.........} \; (31)$$

Integrating Eq. (31) yields

$$V_{p^+} = \frac{Q}{2C \ln\frac{b}{a}} \ln \left(1 + \frac{t}{\frac{a^2 \ln\frac{b}{a}}{2KV_o}} \right) \qquad \text{..........} \; (32)$$

Since the final pulse height is given by

$$V_f = \frac{Q}{C} \qquad \text{..........} \; (33)$$

the time taken for the pulse to rise one half of its final height calculated from Eq. (32) and Eq. (33)

$$t_{\frac{1}{2}} = 0.9 \text{ x } 10^{-6} \text{ sec.}$$

if b = 1.875 in.
a = 0.001 in.
V_o = 2,300 volts, and
K = cm/sec per volt/sec for argon (168).

From the above discussion, one may say that all proportional counter pulses will have the same rise time and that the rise time is independent of the location of the initial ionization in the counter. To confirm this, experimental work carried out with various beta emitters for instance have indicated on the oscilloscope that the pulses had approximately the same rise time.

Combining Eq. (32) and Eq. (33) and using the same parameters as above, the time required for a full pulse length (unclipped) was calculated at about 1,700 microseconds.

In Fig. 37(b) two pulse profiles are shown, namely (a), which was derived from calculations and (b) which was the trace of Fe^{55} obtained on the oscilloscope.

Dead Time

From the preceeding paragraphs, one can assume that gas-filled devices acting as counters will have the inherent disadvantage that the response rate will be limited by the de-ionization time of the tube. This limitation leads us into the discussion of a new concept, namely the dead time of a counter,

<u>Figure 37</u>

(a) Proportional Counter and Input Circuit.

(b) "Clipped" and "Unclipped" Pulse Profile of the Proportional Counter.

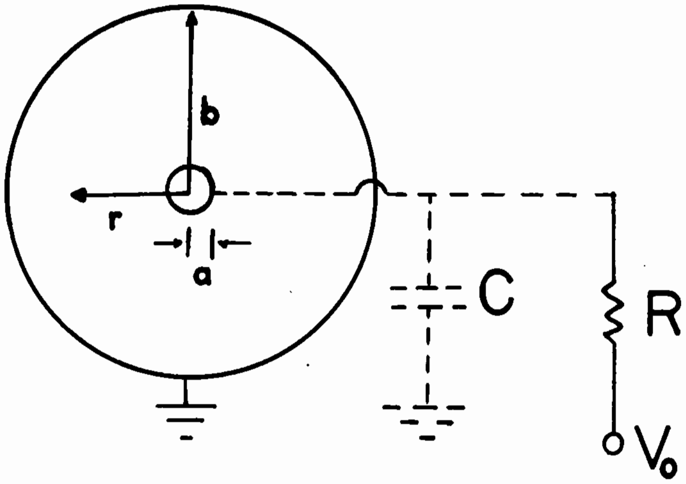

b
r
a
C
R
V_0

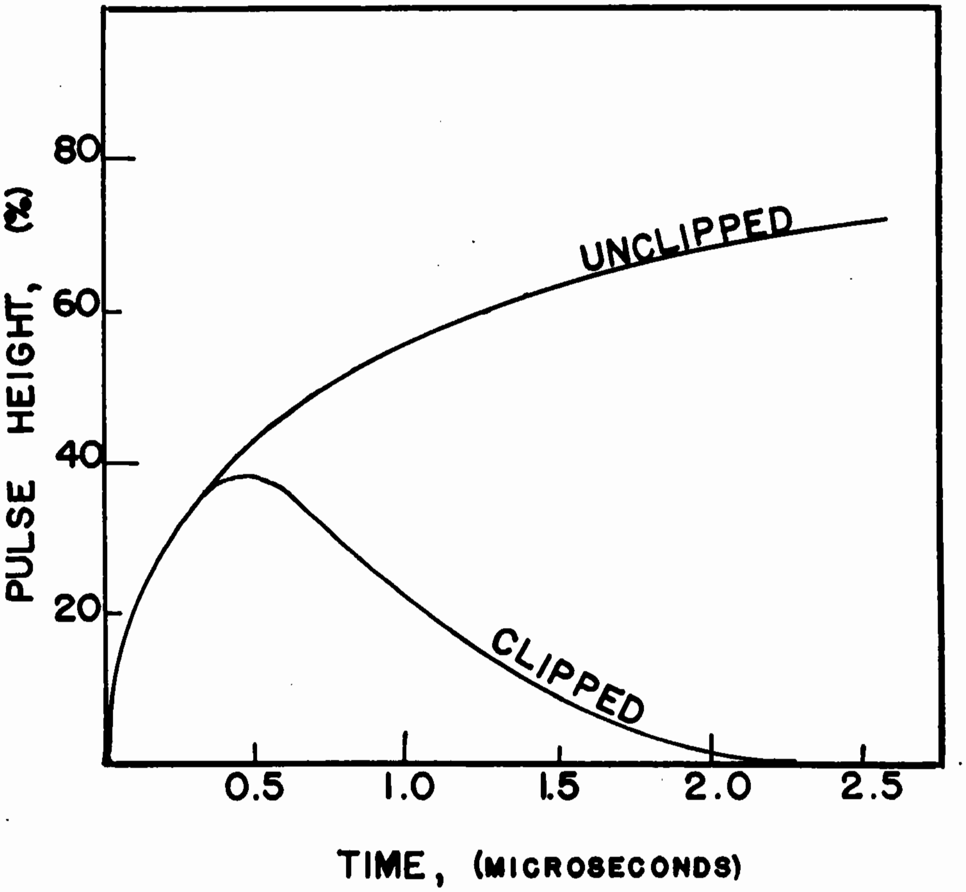

80
60
40
20
PULSE HEIGHT, (%)
UNCLIPPED
CLIPPED
0.5
1.0
1.5
2.0
2.5
TIME, (MICROSECONDS)

which corresponds to the minimum time elapsed between the start of two pulses if they are to be measured electronically as two pulses. Evidently the electronic circuit should have a resolving time smaller than the counter dead time. Otherwise, the response rate would be limited by the electronic circuitry.

In the determination of the disintegration rate of a source, a correction will be made if two radiations entering the counter within the time required to detect them separately.

To investigate the ability that a counter possesses to resolve consecutive ionization events, five different methods can be applied.

(a) The dilution technique. A source having a high disintegration rate (about 10^6 cpm) is diluted and the activities are measured independently.

(b) The "paired-source" technique. Two sources are mounted and measured individually and totally.

(c) The direct picture given on a triggered oscilloscope.

(d) The delayed count measurement. This method was applied by Curran and Rae (169) and in it, the output pulse of the counter is sent to two channels, one of which is delayed. The pulses are mixed at the output and coincidences measured; they will be observed when the delay is greater than the dead time.

(e) Decay of a short-lived radionuclide. The decay of an intense source of a radionuclide, whose half-life is known accurately is measured. The departure from linearity on a semi-logarithmic plot is taken as the loss due to resolution.

The method (b) was applied and an empirical calibration is given in Fig. 38. The coincidence losses and the observed counting rate are plotted on a "log-log" scale. The data obtained clearly illustrate the loss in counting rates of this counter assembly with increasing disintegration rate. When disintegration rates of nuclides decaying by electron capture are to be determined, the correction curve for Fe^{55} can be used for our arrangement up to an apparent counting rate of 2×10^5 counts per minute.

(VIII) Energy Calibration.

The energy expended by a primary radiation may affect some important aspects of the counter performance. For example, we have first to consider whether there is any variation of the energy expended in the production of an ion-pair as the energy of a primary radiation changes. If such an effect would be present, then the counter would not give pulses linearly proportional to the energy of the radiations detected. It is also important to consider another aspect of energy expenditure, the value per ion pair may be different for different types of primary radiations and this would mean that direct comparison of pulse amplitude could not be made. The first of these possibilities can be discounted at least for electrons in the range of investigation here. A great deal of work has been done on the second aspect.

Figure 38

Coincidence Loss of the Counter.

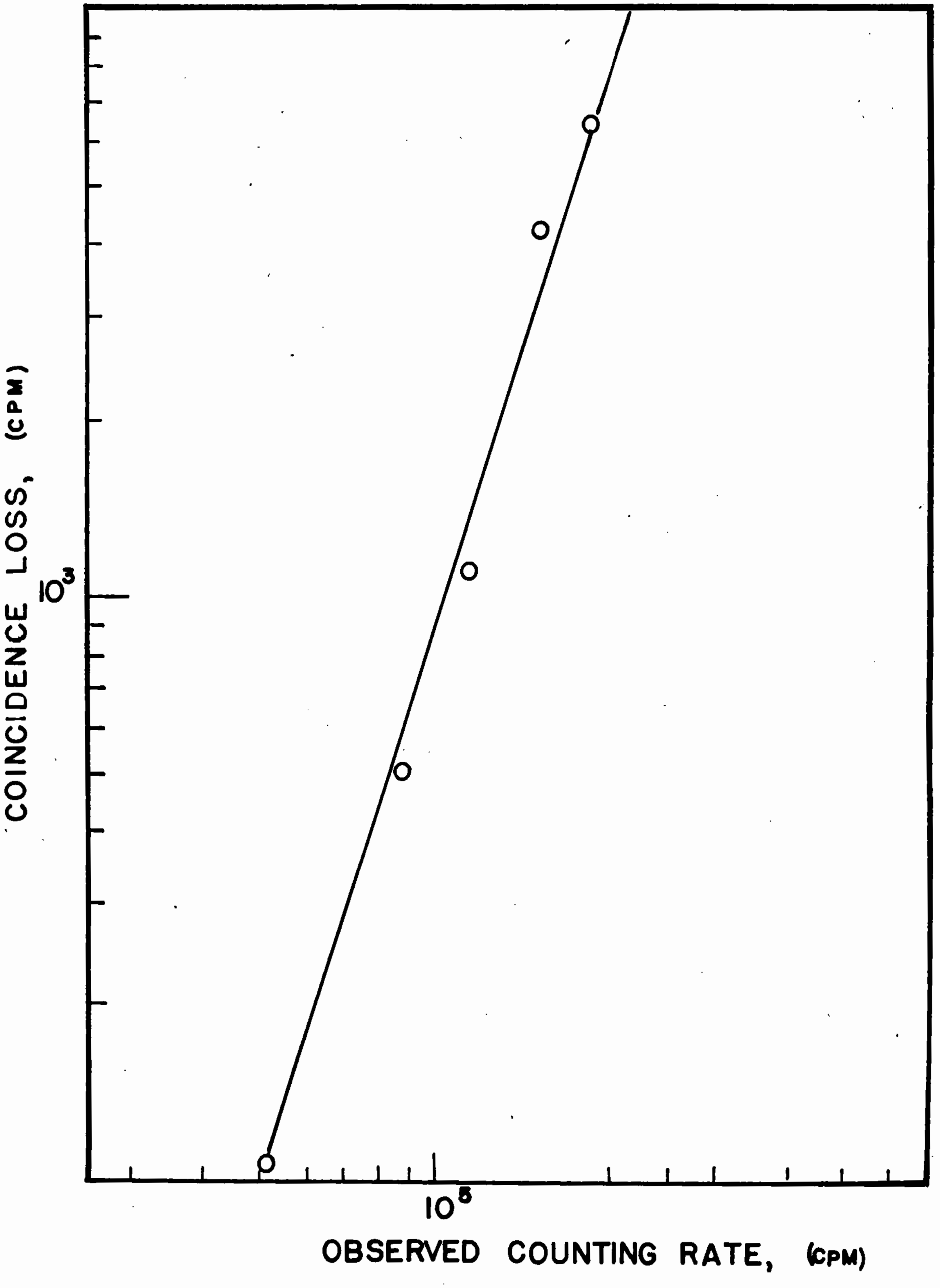
COINCIDENCE LOSS, (CPM)
10^3
10^5
OBSERVED COUNTING RATE, (CPM)

Work prior to 1944 has been reviewed by Gay (170) and since then a series of accurate studies have been made which were possible to a large extent by virtue of the introduction of the modern proportional counter. In fact, relatively recent work (116), (171), (172), and (173) report new and very direct series of measurements failing to reveal any clear evidence of departure from constancy, at least for the following gases: argon, helium, hydrogen, nitrogen, air, oxygen and methane. It is probably safe to assume that for electrons, (photoelectrons in our case), as primary particles and for energies in the range of 200 ev to at least 200 kev, the energy per ion pair is constant to within 2 per cent.

However, the energy required for the formation of one ion-pair is different for different primary particles in the same gas and care must be exercised when comparing amplitude of pulses produced by different radiations. Thus, alpha particles often show a slight decrease in the energy required to form one ion pair when compared to electrons in the same gas. A remarkable feature is the approximately consistent decrease which is observed (174), (175), and (176). Values of the energy per ion pair are listed in Appendix V, together with values relative to that of argon as standard. It follows from this work that the proportional counter can be calibrated with radiations of well-defined energy and the energies of other radiations deduced directly from the observed ratios of the pulse amplitudes.

Regarding this work, we have confined ourselves to photoelectrons as primary radiations. Various sources emitting characteristic X-rays ranging from 3 to 24 kev were prepared. The solid sources were measured internally with the counter operated as a gas-flow system. Employing a mixture of A-CH_4 (9:1) as counter gas, the known quantum energies of the emitters are plotted in Fig. 39 against the average output pulse size read on a pulse-height analyzer. Apart from a slight departure at higher energies, it is observed that the points lie on a straight line which passes close to the origin. The departure may be due to the finite range needed by photoelectrons for total absorption inside the sensitive volume.

At these energies, the majority of the quanta will initially produce photoelectrons in the K-shell of argon. These photoelectrons will be emitted with energies less than those of the quanta by about 3 kev. The characteristic X-rays which would be emitted subsequently by the atoms are very largely internally converted in the outer shells, thus producing one or more Auger electrons. The Auger yield is about 93 per cent (177). This high value together with the fact that the few X-rays which appear will be rapidly absorbed in neighbouring atoms of the gas means that in the absorption process the total energy of the photoelectrons will appear as Auger electrons with energy very close to the energy of the original quantum.

Figure 39

Energy Calibration with A-CH_4 (9:1) as Counter Gas.

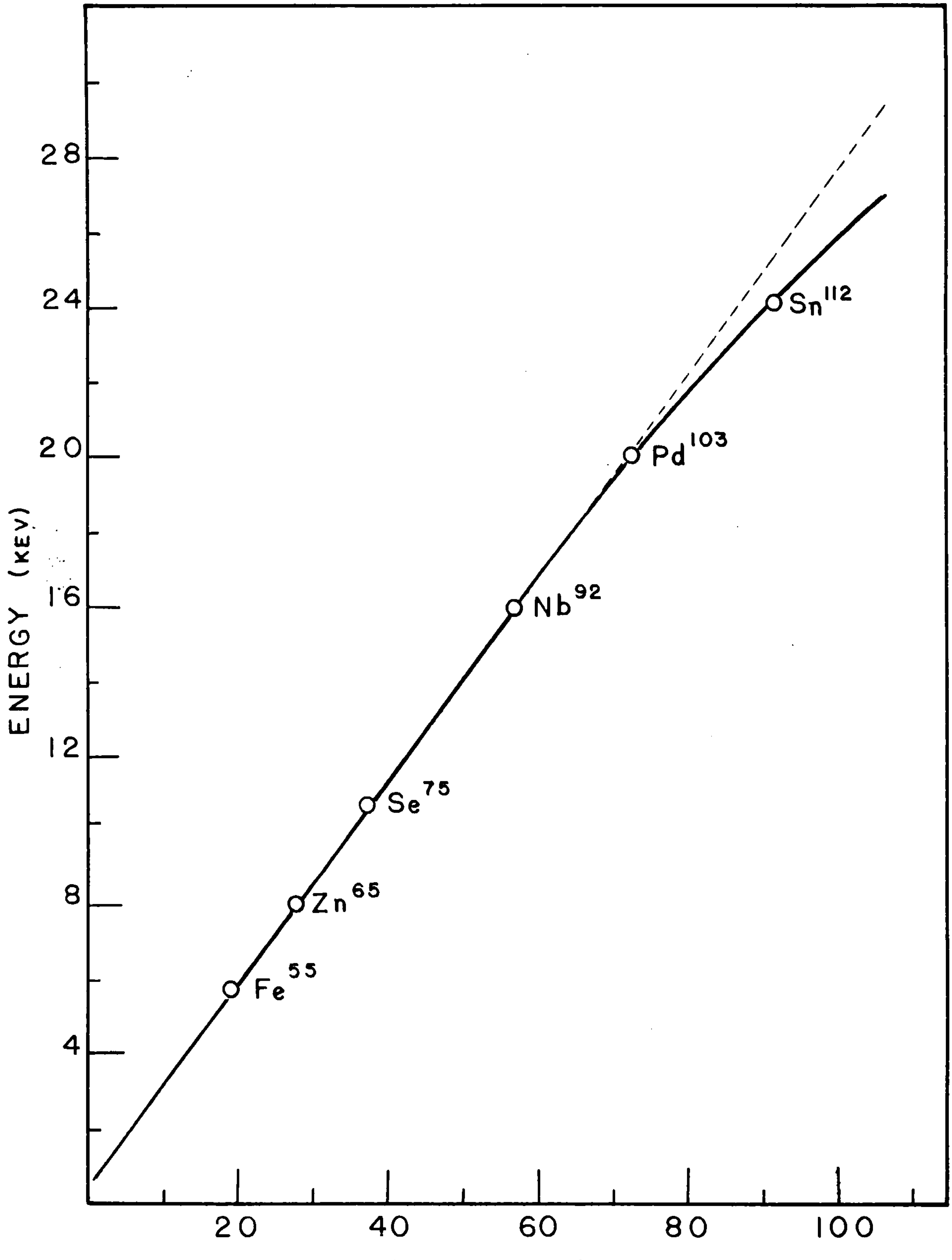
ENERGY (KEV)
4
8
12
16
20
24
28
20
40
60
80
100
CHANNEL NUMBER
Fe^{55}
Zn^{65}
Se^{75}
Nb^{92}
Pd^{103}
Sn^{112}

We have likewise investigated the variation of the pulse size with quantum energy for a mixture of Kr-CH_4 (9:1). The experimental conditions were as previously described. In this case, Fig. 40 demonstrates that the variation is remarkably close to linearity including high energy quanta. This is probably due to the relative higher atomic number of the counter gas leading to a greater reabsorption of the photoelectrons inside the sensitive volume. The straight line also provides evidence in favour of the view that the energy expenditure per ion pair by a photoelectron in this case is constant with increasing energies.

(IX) Gas Multiplication Linearity

The photoelectrons which are produced by the impinging radiations are accelerated towards the anode. As these photoelectrons are accelerated, they collide with the gas atoms and in turn excite these atoms. In the high field regions near the centre wire, the electrons will gain enough energy in the mean free path to ionize the counter gas. As previously, discussed, the production of secondary electrons has been described as the Townsend avalanche. The magnitude of this discharge was defined by the first Townsend coefficient, α, which can be defined as the average number of ion pairs produced by an electron falling through a potential difference of one volt. If the quantity α which is a function of the field strength, the nature of the gas and its pressure, is

Figure 40

Energy Calibration with Kr-CH_4 (9:1) as Counter Gas.

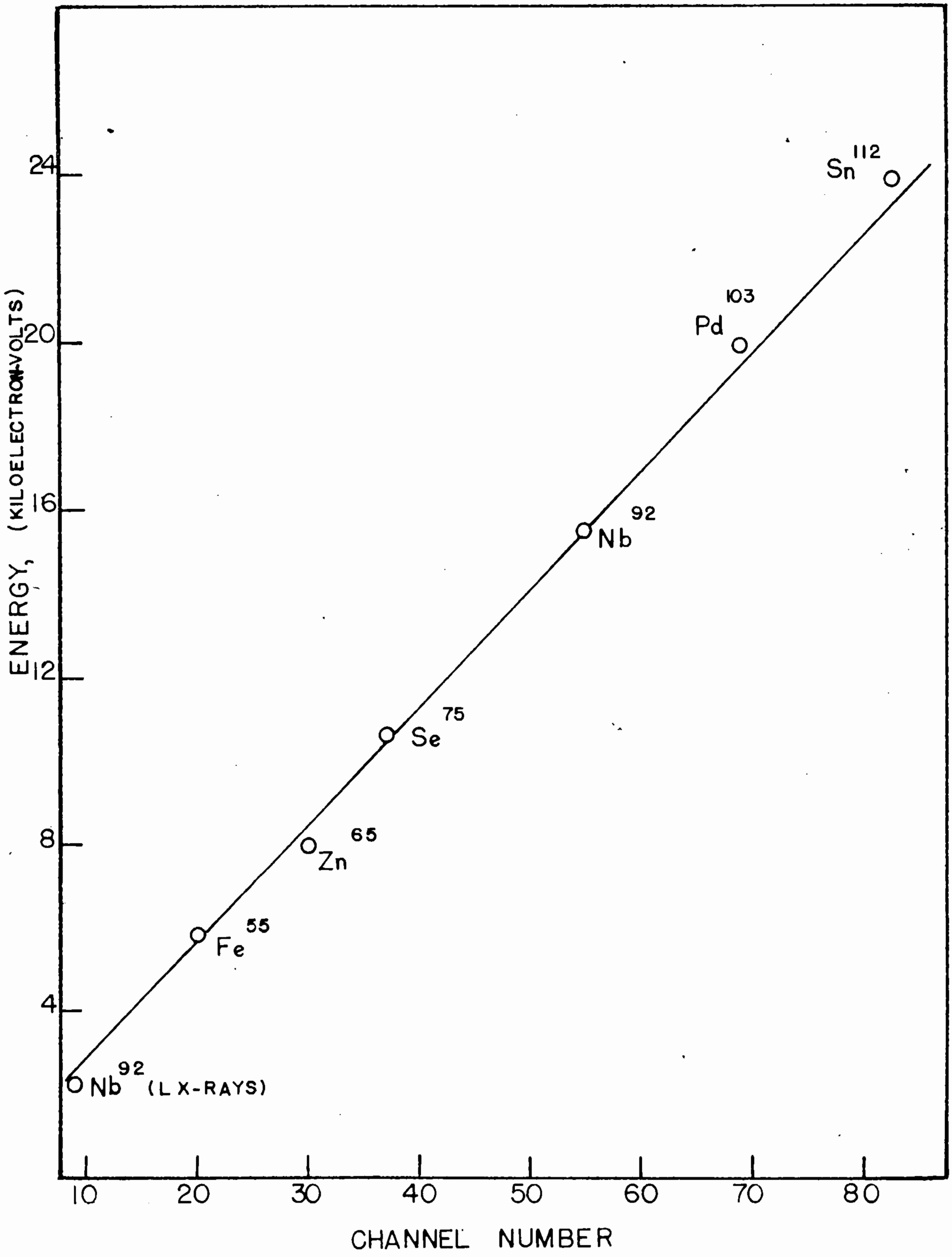
ENERGY, (KILOELECTRON-VOLTS)
24
20
16
12
8
4
CHANNEL NUMBER
10
20
30
40
50
60
70
80
Sn112
Pd103
Nb92
Se75
Zn65
Fe55
Nb92 (L X-RAYS)

independent of x the distance from the anode where the avalanche is initiated, we can assume the following equation.

$$N = N_o e^{\alpha x} \qquad \dots\dots\dots (34)$$

where N_o is the initial number of electrons and N, the final number after the avalanche. From this, it can be resolved that N/N_o will equal the gas multiplication factor A and it will also be an exponential function of the distance x or the voltage across the chamber. Hence, the pulse height from the proportional counter will vary exponentially with the voltage as shown in Fig. 41(b). These results were obtained from a pulse height analyzer when the gain of the amplifier, the discriminator bias and anode voltages were varied. The high voltage characteristic of the counter is shown in Fig. 41(a). A point of consideration in Fig. 41(b) suggests the use of a well-regulated high voltage supply for the proportional counter when used as a spectrometer. This would assure stability of the pulses when energy measurements are required.

(X) X-ray Backscattering

A phenomenon which is often met in photon spectrometry is the Compton scattering. This effect depicts the scattering of a photon of initial energy α_o by an atomic electron, so that the photon has a degraded energy α, and the recoil electron has acquired a kinetic energy equal to $(\alpha_o - \alpha)$. The expression for α as a function of α_o and the angle of photon scattering θ is usually given

Figure 41

(a) High Voltage Characteristics with a Source of Fe^{55}.

(b) Linearity of Gas Multiplication Factor when the Impressed Voltage on the Anode is Varied.

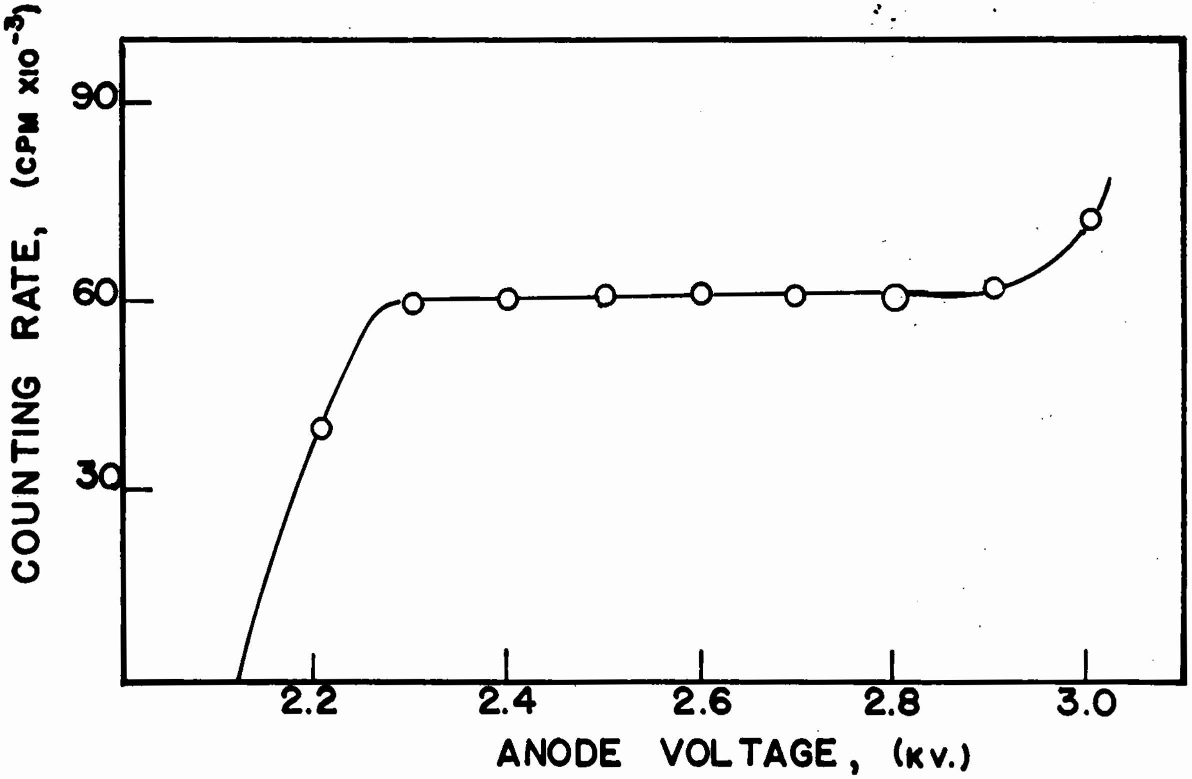
COUNTING RATE, (CPM X10^{-3})
90
60
30
2.2
2.4
2.6
2.8
3.0
ANODE VOLTAGE, (KV.)

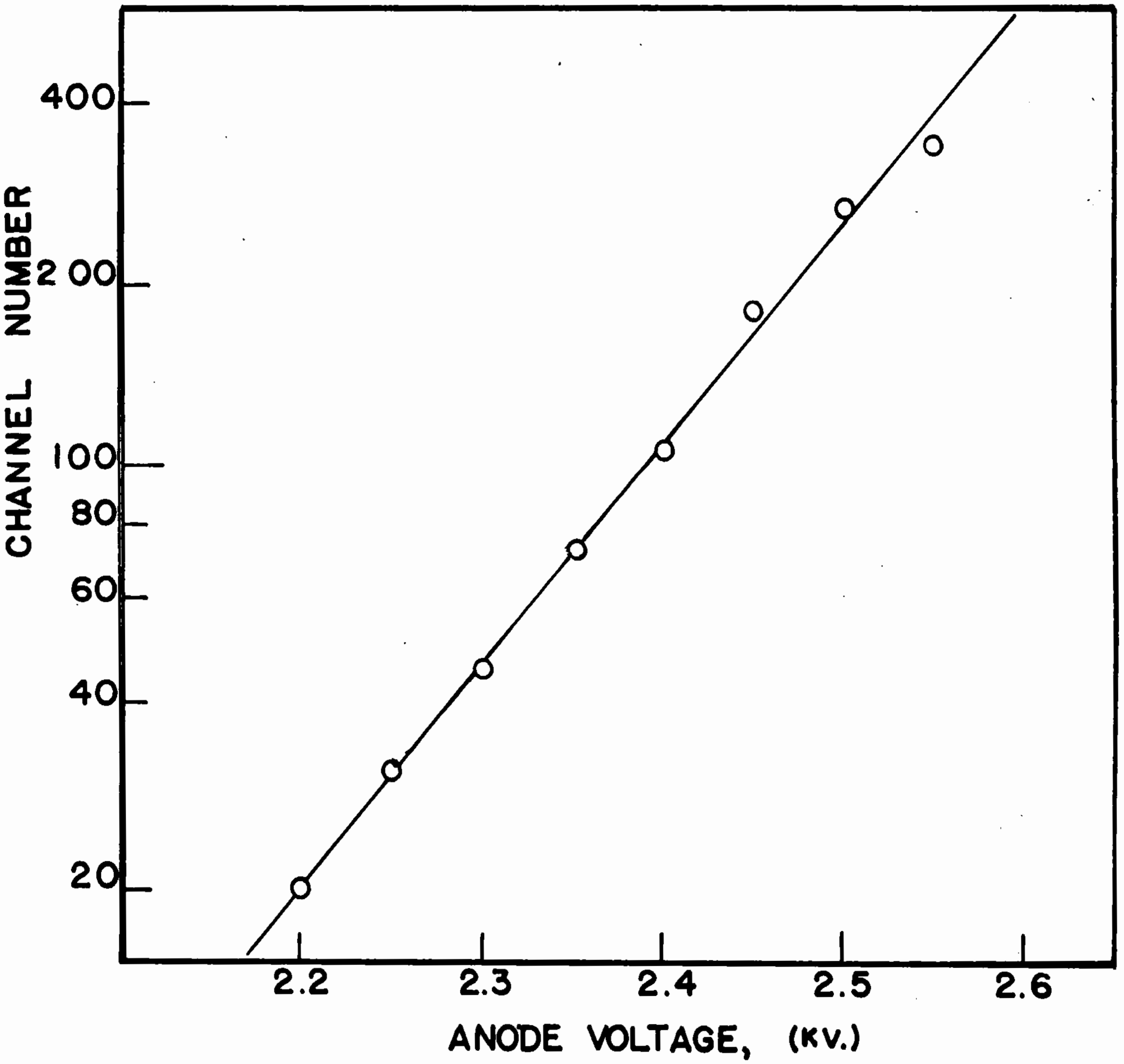
CHANNEL NUMBER
400
200
100
80
60
40
20
2.2
2.3
2.4
2.5
2.6
ANODE VOLTAGE, (KV.)

by the following non-relativistic equation

$$\alpha = \frac{\alpha_0}{1 - \alpha_0(1-\cos\theta)} \qquad \text{..........} \ (35)$$

In 1929, Klein and Nishina (83) derived an expression giving the differential cross-section for the scattering of a photon in the direction θ per unit solid angle. The theory assumes photon energies so great compared to the electron binding energies and motion within the atom that the electrons are considered as free and initially at rest. Unfortunately, this assumption limits the application to the theory especially for low energy photons.

To overcome this limitation Nelms (178) in 1953 started a survey of the literature. The available information was applied and calculations were derived permitting the tabulation of the Compton energy versus angle relationship and differential and integral Klein-Nishina cross-section for high and low energy unpolarized photons.

Accordingly, for energies below 30 kev, incoherent scattering (Compton Effect) was reported as negligible. This was experimentally confirmed when nuclide decaying by electron capture were spectrometrically studied.

Further investigations were made for the detection of coherent backscattering (Rayleigh Effect). The source of radioactive Fe^{55} was mounted on an aluminum foil thick enough (about 0.8 micron) to filter out the Auger electrons. The activity was measured and more measurements were taken when aluminum backscatterers were added. According to these measurements, which are shown in Table VI, no noticeable increases in the counting rates were found within the standard deviations. These results merely confirm that the backscattering of soft X-rays can be disregarded.

(XI) Auger Electron Distribution of Fe^{55}

As has already been mentioned, the probability of internal conversion of the characteristic X-rays after a K-capture event becomes larger for low atomic number. Problems due to self-absorption of these soft radiations will become important when these are to be measured absolutely. To demonstrate the importance of this phenomenon, an attempt was made to measure a source of Fe^{55} with and without an absorber for the Auger electrons. A drop of Fe^{55} solution was evaporated to dryness on an aluminum mounting. The results spectrometrically studied are shown in Fig.42. The spectrum (a) represents the K X-ray (5.9 kev) photopeak when the source is covered with an aluminum absorber while the spectrum (b) corresponds to the same source but unfiltered. In the latter case, the Auger electrons are uniformly distributed in energy from zero to the maximum energy. This experimentally demonstrates a loss of energy of the electrons from the source.

Moreover, this absorption was confirmed when K-fluorescence yield of iron was derived by comparison of the two spectra. The

TABLE VI

X-ray Backscattering

Anode Voltage	Al Backscatterer				
Kv.	0	0.8 x 10^{-4}cm.	1.6 x 10^{-4}cm.	2.4 x 10^{-4}cm.	3.2 x 10^{-4}cm.
	cpm x 10^{-3}	cpm x 10^{-3}	cpm x 10^{-3}	cpm x 10^{-3}	cpm x 10^{-3}
2.3	88.1	87.7	87.1	87.6	87.5
2.4	88.0	88.0	88.1	87.9	88.0
2.5	88.1	88.5	88.1	88.4	88.4
2.6	88.4	88.4	88.6	88.3	89.0
2.7	88.5	88.1	87.8	88.2	88.6

Figure 42

Comparison of Fe^{55} Spectra.

(a) With Auger Electron Absorber, (0.8μ of Al).

(b) Without Auger Electron Absorber.

149a

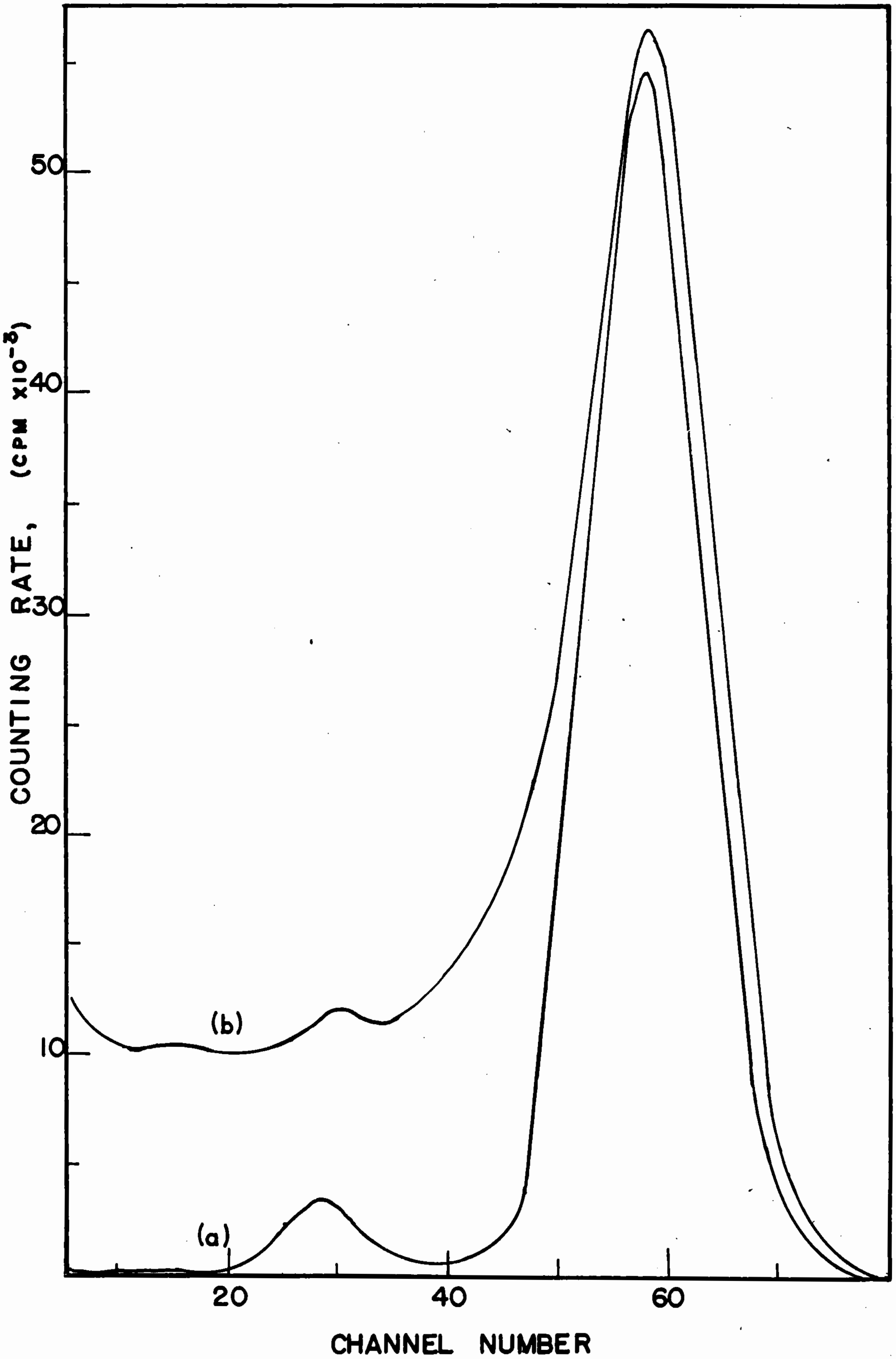
COUNTING RATE, (CPM x10⁻³)
50
40
30
20
10
(b)
(a)
20
40
60
CHANNEL NUMBER

results of the calculations gave a yield of 50 per cent which is about 20 per cent higher than the value known according to the literature.

(XII) Counter Wall Effects.

If the counter is operated with a mixture of A-CH_4 (9:1) at one atmosphere, the probability of transmission of the photons will increase exponentially with energy for X-ray energies greater than 3 kev. Hence, the proportion of these photons hitting the wall of the counter would increase accordingly. For transmitted photons having an energy greater than about 8 kev, a new secondary effect will take place. This effect is essentially due to a photoelectric phenomenon inside the wall of the counter leading to the rise of fluorescence excitation radiations. As a result of this, additional characteristic X-rays and/or photoelectrons will be detected inside the sensitive volume.

The source of origin of these radiations is schemetically represented in Fig. 43(a) and (b). Obviously, the effect (b) will be more important than the effect (a) for photons having low energies, but it will decrease more rapidly than (a) when the energy increases.

Calculations of the dependence of the coefficient of absorption (μ) for the photoelectric effect on the atomic number (Z) and the energy ($h\nu$) of the impinging photon have been made

Figure 43

Description of the Counter Wall Effect.

(a) Secondary Photoelectrons

(b) Secondary X-rays.

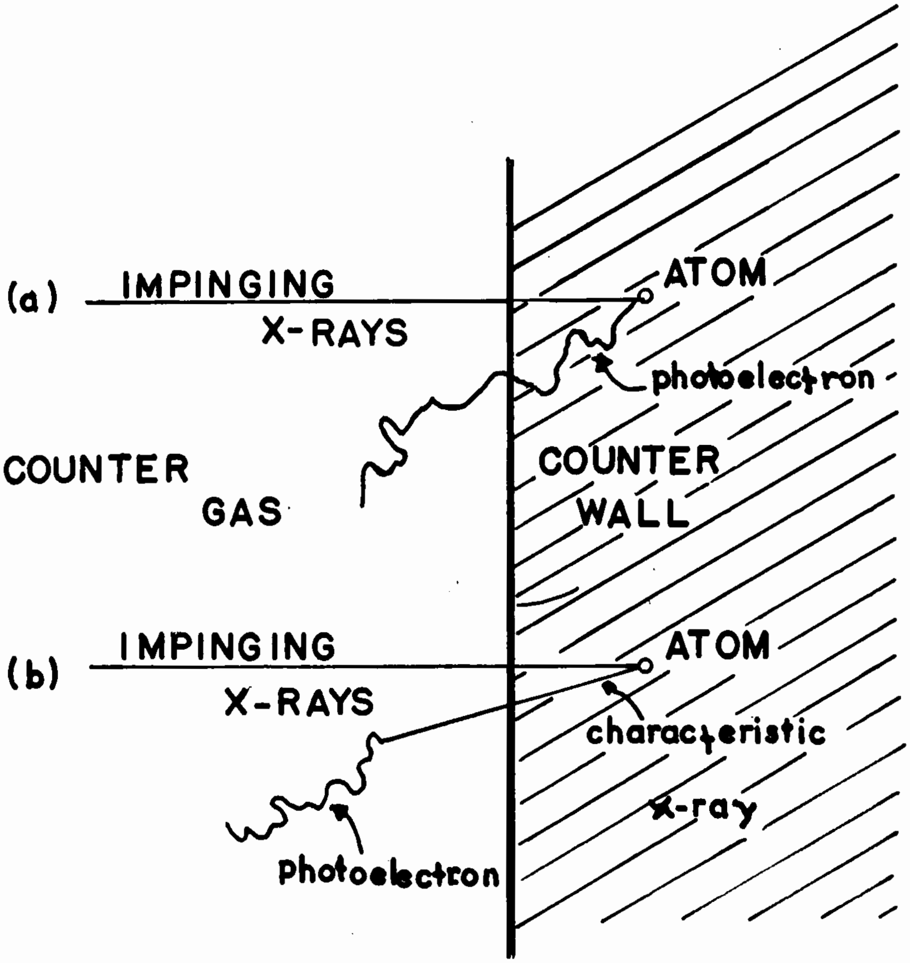
(a)
IMPINGING
X-RAYS
ATOM
photoelectron
COUNTER
GAS
COUNTER
WALL
(b)
IMPINGING
X-RAYS
ATOM
characteristic
x-ray
photoelectron

by Heitler (80) and others (179). A special case which holds for $E_K \ll h \ll mc^2$ is

$$\mu \sim NZ^5(h\nu)^{3.5} \qquad \ldots\ldots\ldots\ldots \quad (36)$$

where N is the number of atoms per unit volume and E_K is the binding energy of the K-orbital electrons.

During the course of this work, the effect (b) when compared to (a) was always predominant. This, of course, is due to the low energy range under investigation.

A typical example of the effect (b) is shown in Fig. 44. The main photopeak is the distribution of the characteristic X-rays of Sr^{85} (13.3 kev). The second peak, less in intensity, is due to the secondary effect which is the fluorescence excitation radiations due to the counter wall.

3) CONCLUSIONS

On the basis of the preliminary investigations discussed in this part C, one can say that the above described proportional counter can be used as a detector and a spectrometer for the measurement of soft X-rays.

For routine work, the 6AN8 White cathode follower was used in conjunction with the counter and various auxiliary electronic components.

Figure 44

Counter Wall Effect with 13.3 kev X-rays.

(a) Secondary (Wall) Effect.

(b) Counter Gas Escape Peak.

(c) K X-ray Photopeak.

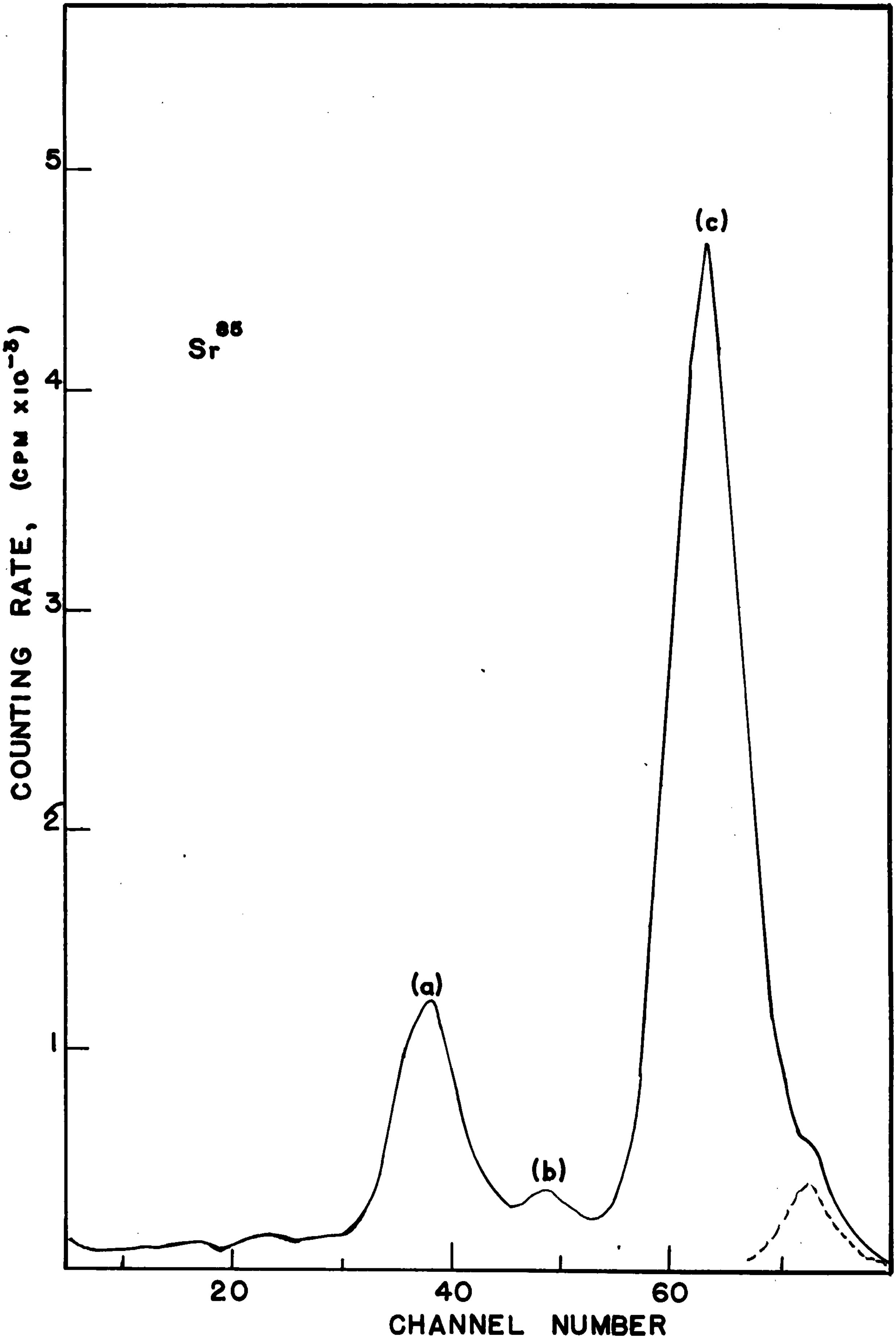
Sr^{85}
(a)
(b)
(c)
COUNTING RATE, (CPM x10^{-3})
1
2
3
4
5
20
40
60
CHANNEL NUMBER

The evacuation and filling system which was calibrated for operations with the proportional counter could be used to fill the detector at various pressures. Within 60 seconds after changing the source, the counter could be ready for use.

Also, the investigation of the properties of the counter has revealed that the counter with its proper attachments could be used either as a flow-gas counter or a variable pressure counter. However, when the flow-gas system is applied, it is recommended that the counter be filled initially with the counter gas.

The anode wire which was selected for routine work had a diameter of 0.002 in. This diameter was chosen because (a) it gives a flat and long plateau (~600 volts), (b) it requires a reasonable operating voltage, (c) it gives a good energy resolution (~17 per cent with 5.9 kev X-rays) when the counter was operated at atmospheric pressure, and (d) it produces a gas multiplication factor "A" which did not vary too rapidly when the anode voltage was changed.

The counter gas which is suggested for determination of disintegration rates of nuclides decaying by electron capture is a mixture of A-CH_4 (9:1). This is mainly due to (a) its relatively high efficiency which was determined for X-ray energies between 3 and 24 kev, (b) to the small escape probability of the characteristic X-rays of the counter gas after its atom underwent ionization in the K-shell, and (c) its relatively low cost.

D. GAS MULTIPLICATION FACTOR

1) INTRODUCTION

Gas discharge tubes operated in region III of Fig.5 have received considerable experimental study from various investigators (116), (181), (182), (183), and (184). They have established that for voltages well below the Geiger threshold and over most of the sub-threshold region, the pulse size on the central system would be proportional to the initial ionization produced by the primary particle. Consequently, the intensification of the initial ionization was only considered to be directly due to the passage of the radiation through the gas and the movement of the primary electrons in an electric field which was sufficiently intense to give them energies adequate to create an avalanche of secondary electrons.

In 1941, Rose and Korff (105) became interested in the gas discharge mechanism in proportional counters. They investigated the following two questions, namely the more qualitative question as to what type of gas (nature of gas) fillings should be used and the quantitative dependence of counter properties on gas pressure, relative concentration in the case of a mixture and on geometry, (cathode, anode diameter). In their original discussion (105), they made four important assumptions.

(a) The emission of photoelectrons or ultra-violet light of low energy photons at the cathode was negligible.

(b) The recombination and electron attachment to neutral molecules was negligible.

(c) There was no fluctuation in energy loss and in specific ionization.

(d) The rate of increase of ionization cross-section with the electron energies is linear for energies above the ionization potential threshold of the counter gas. According to the literature (105) and (185), it is indeed linear for energies up to 40 to 50 volts.

Experimental and theoretical data were found to be compatible by Rose and Korff for gas multiplication factors between 10^2 and 10^3 and for the investigation of various parameters of a counter. We have attempted to extend the application of their theory to a proportional counter operated at gas multiplication factors ranging between 10^3 and 10^6. For this purpose, different counter gases were used, namely pure CH_4, mixture of A-CH_4 (9:1), and mixture of Kr-CH_4 (9:1). With a mixture of A-CH_4 (9:1) in particular, the following anode wire diameters were studied: 0.001 in., 0.002 in., 0.003 in., 0.004 in., and 0.005 in. Likewise, the following pressures were also investigated: 0.3 atm., 0.6 atm., 1.0 atm., 1.3 atm., 1.6 atm., and 2.0 atm.

Comparison of experimental results with the theory were substantially correct if an additional variable was placed in the exponential factor of the theoretical equation. This will be subsequently described.

2) DERIVATION OF ROSE AND KORFF'S THEORETICAL EQUATION

When the primary radiation has produced the initial ionizing event, the electrons and positive ions will find themselves in the field produced by the voltage V_o across the chamber. Accordingly, they will start to drift toward the appropriate electrode. If V_o is greater than V_p, the threshold voltage of a proportional counter or the minimum voltage required for secondary processes, the electrons resulting from the primary ionizing event will gain enough energy in one mean free path between collisions to produce further ionizations. The total number of electrons will increase rapidly, and we will have the beginning of the familiar Townsend avalanche.

The arrival of this avalache of electrons on the central wire will produce a change in the potential of the wire. The voltage of the central wire will change by an amount given by ΔV volts.

$$\Delta V = \frac{A.N.G.q}{C} \qquad \text{..........} \quad (37)$$

where,

A = additional number of electrons produced by collisions processes plus the original one.

N = number of ion-pairs produced in the initial ionizing event.

G = voltage gain of the allied electronic circuits.

q = electronic charge.

C = distributed capacity of the central wire and those portions of the detecting circuit connected electrically to it.

The gas multiplication factor "A" may vary from unity up to many millions. Naturally, for voltages smaller than the proportional threshold voltage and high enough to prevent recombination of primary ion-pairs, this factor will be equal to unity.

Prior to 1941, secondary processes occuring in ionization chambers were well known in gas discharge phenomena. As early as 1900, Townsend in his discussion on the formation of an electron avalanche leading to a spark, was utilizing basic arguments similar to those given by Rose and Korff (186). For instance, he believed that at sufficiently high electrical field, the "negative ions" received enough energy from the field so that they could ionize neutral atoms or molecules on impact. Thus he argued that, if the negative ions could create α new ions in a path of one centimeter in the field direction, the increase in number of ions dN produced by N ions in a distance dx in the field could be written as,

$$dN = N \alpha dx \qquad \ldots\ldots\ldots\ldots (38)$$

whence,

$$N = N_o e^{\alpha x} \qquad \ldots\ldots\ldots\ldots (39)$$

where the constant of integration N_o is the initial number of electrons and α is the first Townsend coefficient, empirically found by himself, which is independent of the distance x.

If the process starts with a single electron the N_o is unity, and the number N is, by definition, the same as the gas multiplication factor. Then,

$$A = e^{\alpha x} \qquad \ldots\ldots\ldots\ldots (40)$$

More generally, since in a counter, α may depend on the distance x, and since the number of ionizing collisions will depend on the energy, which in turn will increase as the electron enters the high-field region near the wire, then the equation

$$A = e^{\alpha dx} \qquad \ldots\ldots\ldots\ldots (41)$$

may serve to relate the first Townsend coefficient to the gas multiplication.

Rose and Korff (105) applied the above reasoning to the problem of proportional counters to evaluate the factor A in terms of the parameters usually known in the case of proportional counters. They assumed an ionization cross-section of the counter gas linear with the electron energy above the threshold and the added assumption that the electron-energy spectrum shows a monotonic decrease at the ionization potential. This leads to an effective α of the form

$$\alpha = \left(\frac{a.N.C.V_o}{r}\right)^{1/2} \quad \ldots\ldots. \ (42)$$

where,

a = the rate of increase of ionization cross-section with electron energy.

N = the number of atoms or molecules per centimeter cube in the counter.

C = the capacitance of the counter per unit length. It is equal to $\dfrac{1}{\ln \frac{r_2}{r_1}}$ where r_2 and r_1 are the radii of the cathode and anode.

V_o = the operating voltage across the chamber.

r = the distance between the cathode and the anode.

Before going into further discussions, we must introduce another term r_c which is the critical radius where the avalanche starts. At the threshold, r_c is equal to the wire radius r_1. Now, r_c in the region of proportional counting never becomes very much greater than r_1, and we may therefore assume an approximately linear dependence with the voltage. Hence, we may relate the radius r_c, at which the avalanche starts when the voltage applied is V_o, to the threshold voltage V_P by the relation,

$$\frac{r_c}{r_1} = \frac{V_o}{V_P} \qquad \ldots\ldots\ldots \ (43)$$

Thus r_c is defined in terms of the directly measurable voltages and wire radius.

If an electron which started to produce ions at a radius r_c created $N(r)$ ion-pairs by the time it arrived at a distance r from the axis, and since α is the average number of collisions per unit path, then,

$$-dN(r) = N(r)\,\alpha\,dr \qquad \ldots\ldots\ldots \ (44)$$

Integrating over the whole path from r_c to r_1,

$$\ln N(r_1) = \ln A = \int_{r_1}^{r_c} \alpha\,dr \qquad \ldots\ldots\ldots \ (45)$$

and

$$\int_{r_1}^{r_c} \alpha\,dr = \int_{r_1}^{r_c} \left(\frac{aNCV_o}{r}\right)^{\frac{1}{2}} dr = 2(aNCr_1V_o)^{1/2}\left[\left(\frac{V_o}{V_P}\right)^{1/2} - 1\right] \qquad \ldots\ldots \ (46)$$

when Eq. (42) and (43) are used.

Hence,

$$A = e^{2(aNCr_1V_o)^{1/2}} \cdot \left[\left(\frac{V_o}{V_p}\right)^{1/2} - 1\right] \quad \text{......} \quad (47)$$

Eq. (47) is the one which Korff and Rose used in the limited range of gas multiplication factor "A".

3) EXPERIMENTAL TECHNIQUES

At least three different methods can be applied to measure the gas multiplication factor "A".

The first method was suggested by Rossi and Staub (99). They have assumed that both the primary ionization and the gas multiplication are suffiently small so one can neglect the modification of the electric field near the wire which is caused by the space charge. Then the gas multiplication factor, for a given gas, will be a function of the diameter a of the wire, of the diameter b of the cathode, of the pressure p, and of the voltage V_o across the counter. All significant phenomena will take place at a very small distance from the wire and the factor "A" will not change if V_o and b are changed without altering the field at the wire. It follows that the factor A can be expressed as a function of the ratio $V_o/\ln\frac{b}{a}$ and of the product pa:

$$A = A\left(\frac{V_o}{\ln\frac{b}{a}}, (pa)\right) \quad \text{.........} \quad (48)$$

The second method makes use of an oscilloscope. When the sweep of the oscilloscope is triggered at the beginning of the count and the delay circuit insures that the pulse height, ΔV, appears on the oscilloscope screen in its entirety, then Eq. (37) may be applied and the factor A derived from it.

The last method compares the total electronic charge collected on the wire to the charge liberated by the initial ionizing event. Referring to Fig. 5, this method compares the charges collected in region III to those in region II when the same radiation is used.

The application of the second method will necessitate the measurement of the capacitance C of the system and this should be avoided when good accuracy is required. Moreover, it will involve accurate measurements of the other parameters of Eq. (37). In practice, the gas multiplication factor is usually experimentally determined and not calculated. Therefore, the second method is very rarely used. On the other hand, application of the first method will imply accurate knowledge of the gas multiplication factor for a given counter geometry and will be especially suitable for low multiplication factors. This, of course, cannot serve our purposes since we are interested in the application of Rose and Korff's theoretical equation. Consequently, the third method was employed.

The instrumentation used in obtaining the gas multiplication factor "A" is shown in the block diagram of Fig. 22. The following parts were employed.

(a) Counter with sources of Po^{210} and Fe^{55}.

(b) Two high voltage supplies, namely a Dynatron set for voltages between 250 and 500 volts and a Fluke set for voltages higher than 500 volts.

(c) Cathode Follower 6AN8.

(d) A Baird Atomic Inst. 215A linear and non-overloading amplifier.

(e) A Tetronix oscilloscope, type 532.

The pulse heights were measured on the screen of the oscilloscope and the gas multiplication factor A was derived when comparing the pulses in the proportional region to the pulses in the ionization chamber region.

To perform experimental investigation in the ion-chamber region (region II of Fig. 5) a source emitting radiations having a high specific ionization was prepared. Po^{210} was electrochemically deposited on polished silver foils (5 by 5 by 0.5 mm.) according to a method described by Bouissieres (187). The procedure was as follows:

(a) The dried salt of RaDEF chloride was dissolved in absolute ethanol, and the activity of the RaF (or Po^{210}) present in the solution was about 6×10^3 cpm per microliter.

(b) A volume of 10 microliters was transferred from the stock solution into each of 5 vials (screw-cap type, 15 mm. outside diameter and 45 mm. in length) and each one initially contained the silver foil and 200 microliters of absolute ethanol.

The rate of electroplating was determined by measuring the activity of each foil in a 2π-counter for different durations of plating. The results are shown in Fig. 45.

However, at higher gas multiplication values, a source of Fe^{55} which has a lower specific ionization was used.

4) COMPARISON OF EXPERIMENTAL RESULTS WITH THEORY

For gas multiplications greater than 10^3, it was possible to use a form of Rose and Korff's equation if an additional variable, f(o), was inserted into the exponential factor according to the following fashion:

$$A = e^{2(aNCr_1V_of(o))^{1/2} \cdot \left[\left(\frac{V_o}{V_P}\right)^{1/2} - 1\right]} \qquad \ldots\ldots (49)$$

The factor f(o) was experimentally determined for various pressures and anode wire diameters.

The first experiment was performed with pure CH_4 as counter gas and 5.3 mev alpha particles from Po^{210}. In this particular case, the anode wire was kept constant at 0.002 in. in diameter. The change of f(o) is shown in Fig. 46 and comparison between the experimental results and Eq. (49) is expressed in Fig. 47.

<u>Figure 45</u>

Rate of Electrochemical Deposition of Po^{210}
on to Silver Foils.

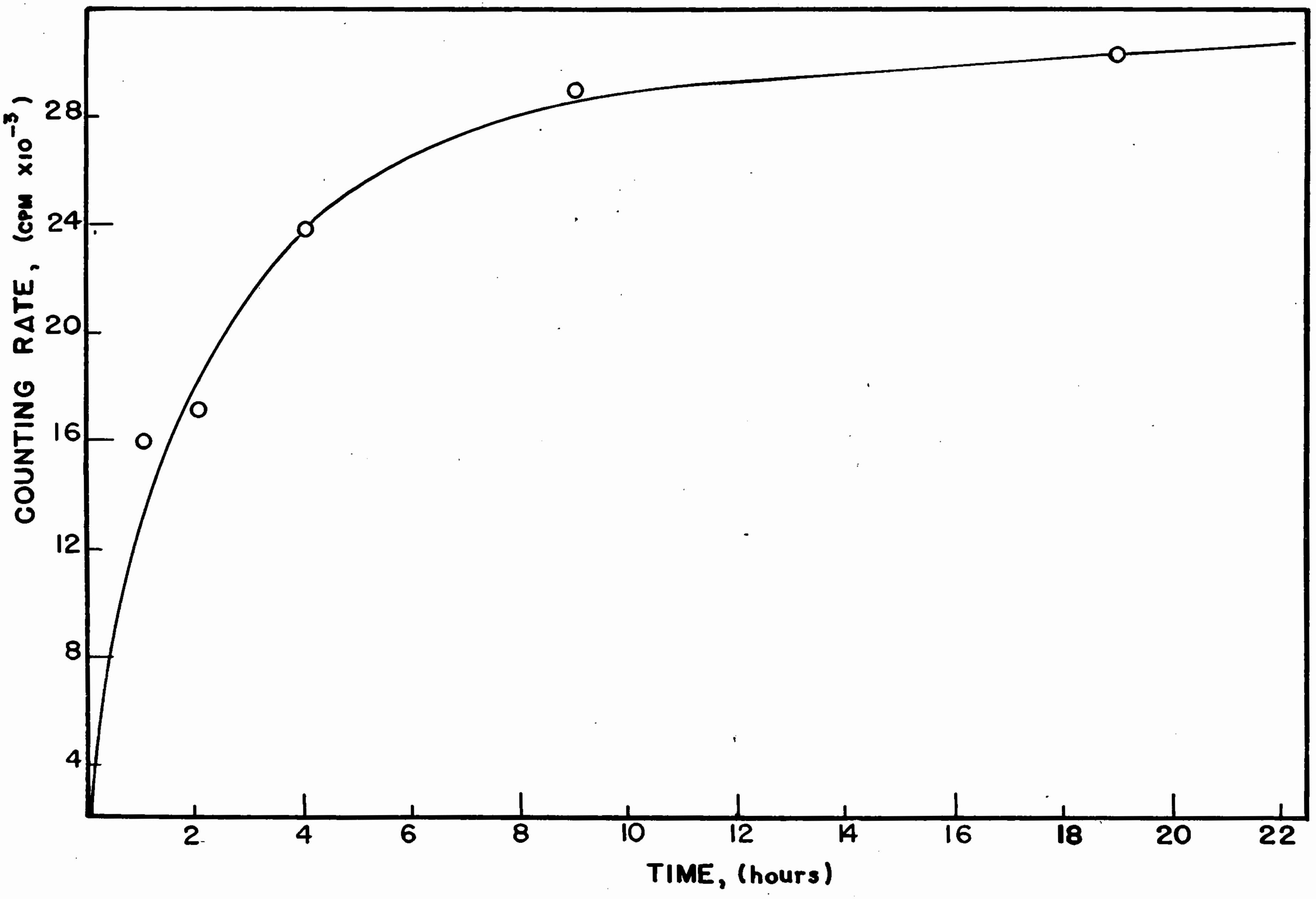
COUNTING RATE, (CPM x10^{-3})
4
8
12
16
20
24
28
2
4
6
8
10
12
14
16
18
20
22
TIME, (hours)

Figure 46

Variation of f(o) for Various Pressures of CH_4. Anode Diameter: 0.002 in.

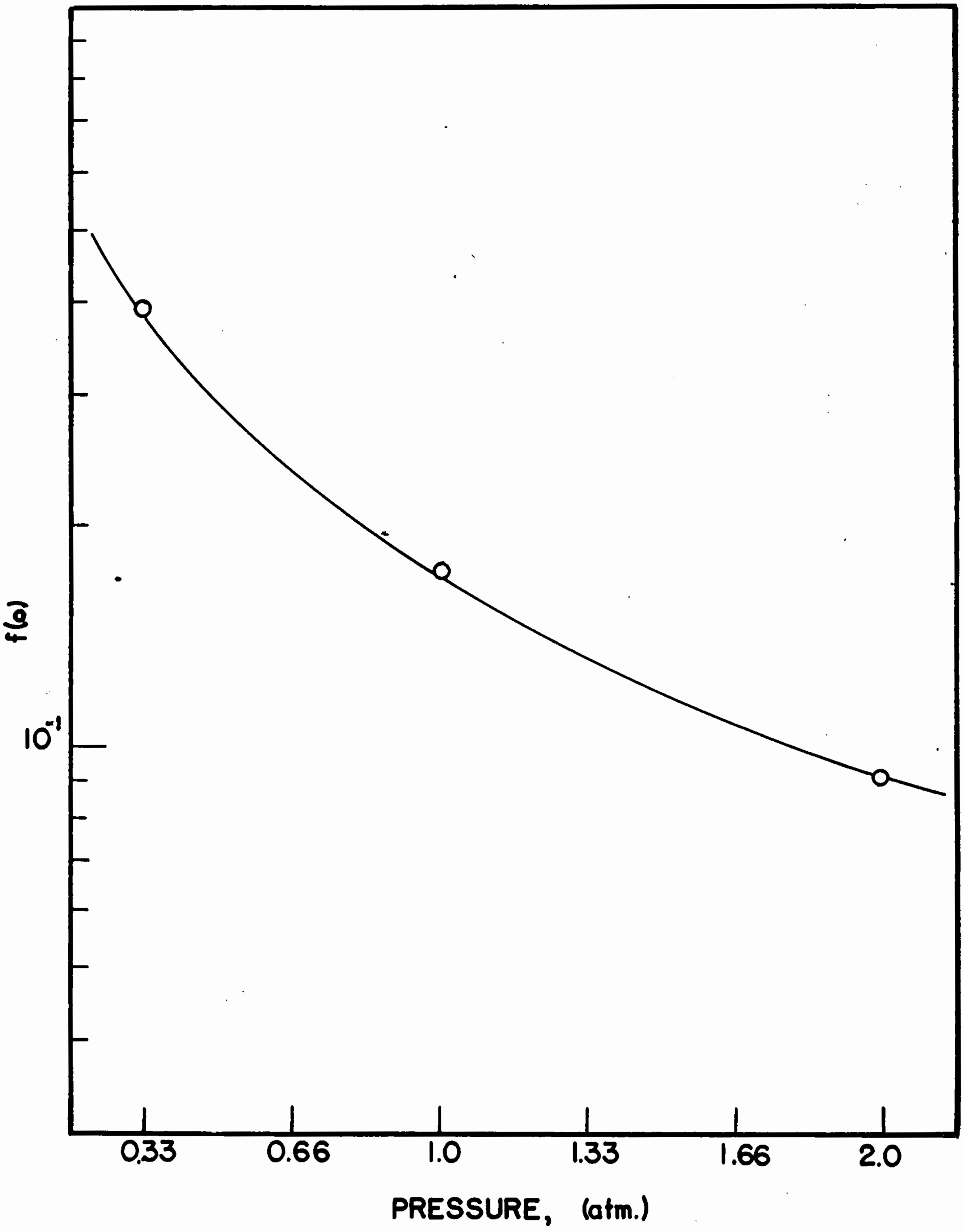
f(a)
10⁻¹
0.33
0.66
1.0
1.33
1.66
2.0
PRESSURE, (atm.)

Figure 47

Comparison between Experimental and Semi-theoretical Gas Multiplication Factor, "A", (Eq. 49) when CH_4 is used as Counter Gas.

——— Semi-theoretical

○ Experimental

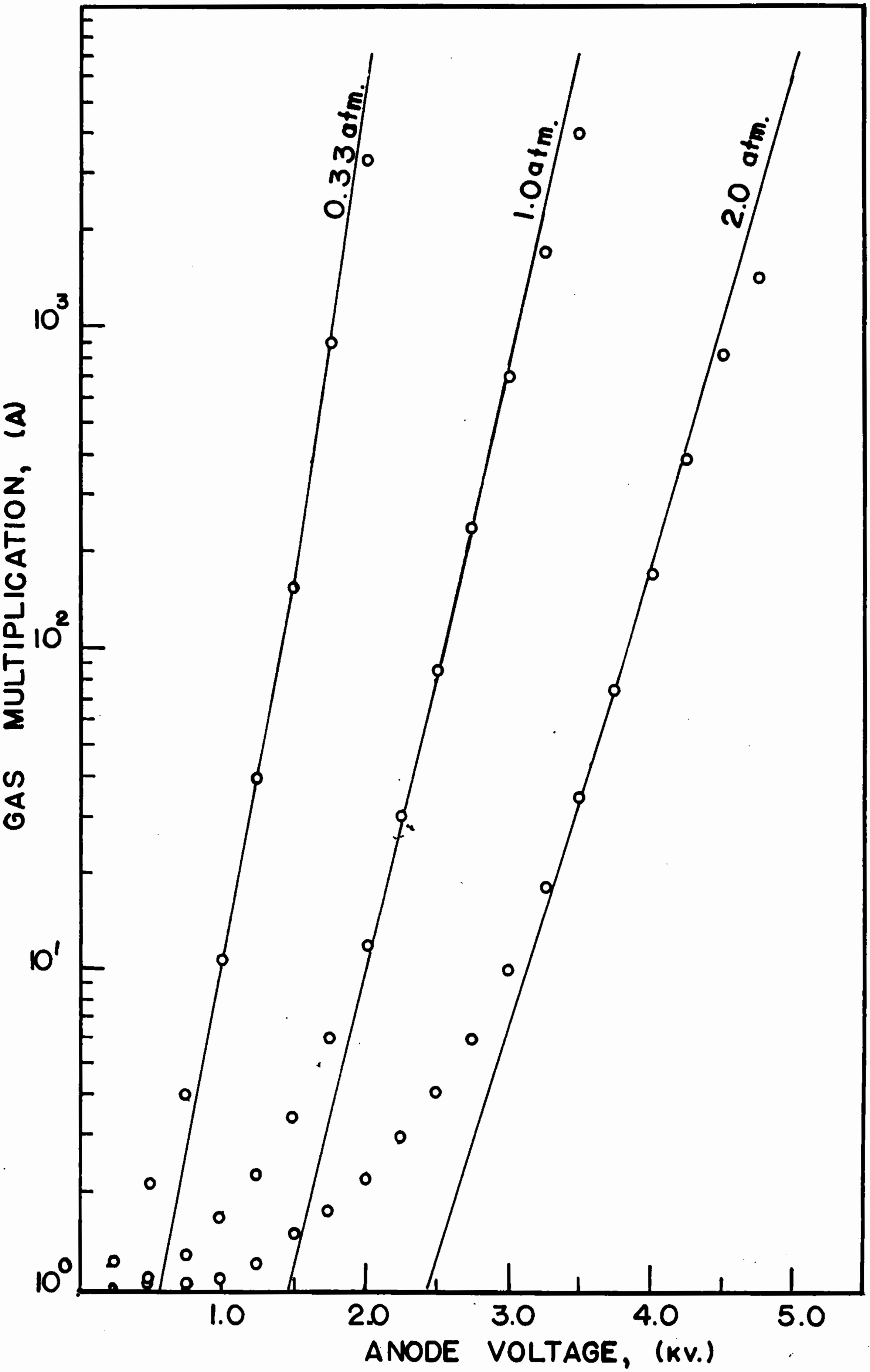
0.33 atm.
1.0 atm.
2.0 atm.
GAS MULTIPLICATION, (A)
10^0
10^1
10^2
10^3
1.0
2.0
3.0
4.0
5.0
ANODE VOLTAGE, (KV.)

At a pressure of two atmospheres, the observed pulse amplitude was independent of the anode voltage between 250 and 800 volts. Here the chamber was acting as a saturation ion-chamber and the gas multiplication was unity.

However, if the CH_4 gas was substituted for a mixture of A-CH_4 (9:1), and Po^{210} and Fe^{55} being alternatively used, f(o) varied according to Fig. 48 when the anode diameter was 0.002 in. Comparison between experimental results and the modified Rose and Korff's equation is shown in Fig. 49.

Using Fe^{55}, a series of experiments were made for various anode diameters and pressures of A-CH_4 (9:1). The values corresponding to the experimental term f(o) are represented in Fig. 48 while the comparisons are shown in Fig. 50 (a), (b), (c), (d), and (e). The proportional threshold voltages were obtained through extrapolation of the linear region for various experimental gas multiplication factors. The results of these extrapolations are shown in Fig. 51.

Similar experiments were carried when the counter was operated at various pressures of Kr-CH_4 (9:1) and for an anode diameter of 0.002 in. The variation of f(o) is shown in Fig. 52 and comparison between experimental results and Eq. (49) is expressed in Fig. 53.

The rate of increase of cross-section ionization of krypton was derived from recent experiments made by Tozer and Craggs (185). According to these authors, this was the first publication of measurements of the ionization cross-section of

Figure 48

Variation of f(o) for Various Pressures of A-CH_4 (9:1) and Anode Diameters.

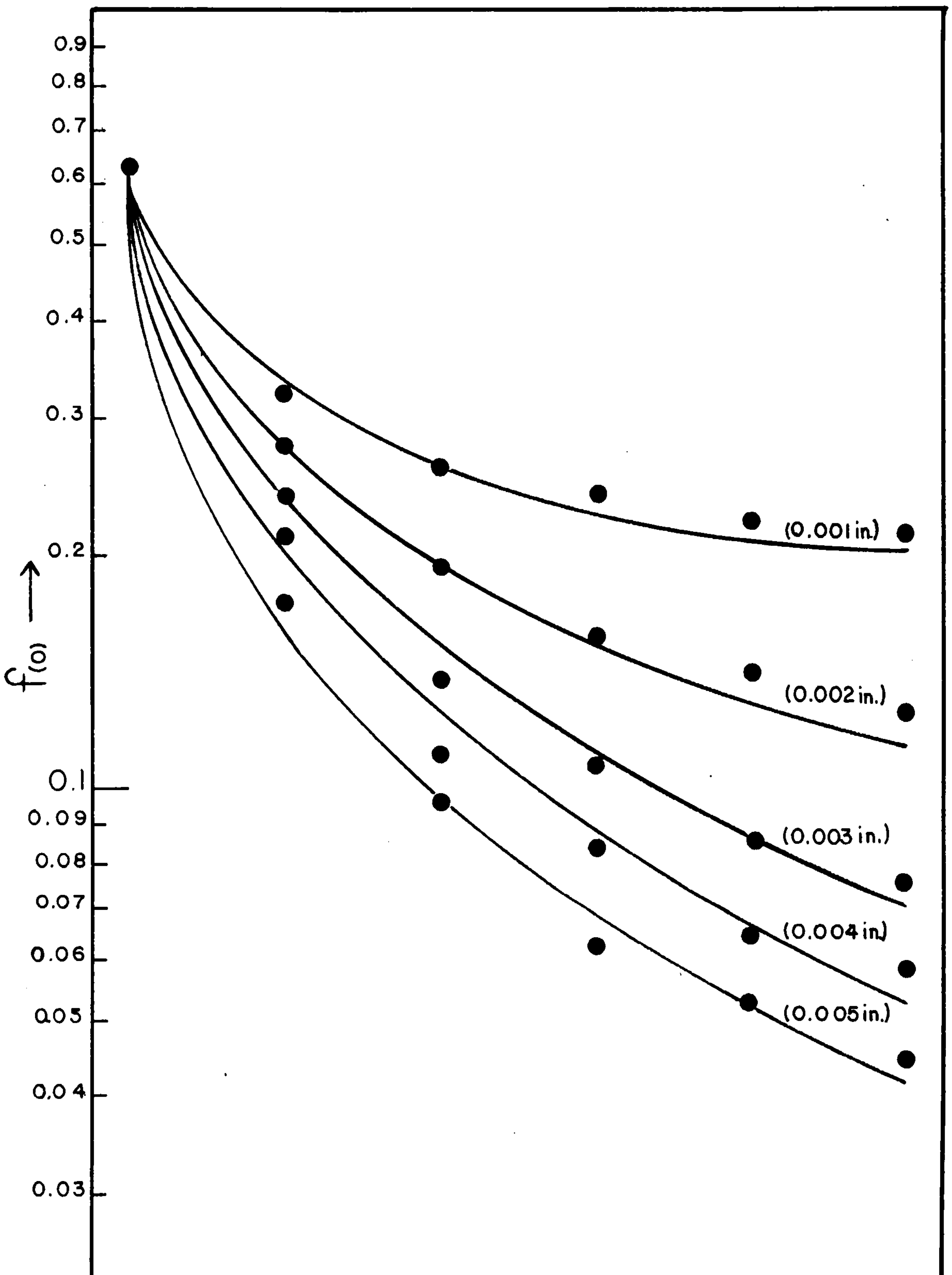
0.9
0.8
0.7
0.6
0.5
0.4
0.3
0.2
0.1
0.09
0.08
0.07
0.06
0.05
0.04
0.03
$f_{(0)}$ →
(0.001 in.)
(0.002 in.)
(0.003 in.)
(0.004 in.)
(0.005 in.)
0.3
0.6
1.0
1.3
1.6
2.0
PRESSURE, (atm.)

Figure 49

Comparison between Experimental and Semi-theoretical Gas Multiplication Factor, "A", (Eq. 49) when A-CH_4 (9:1) is used as Counter Gas.

——— Semi-theoretical

• ○ Experimental

171a

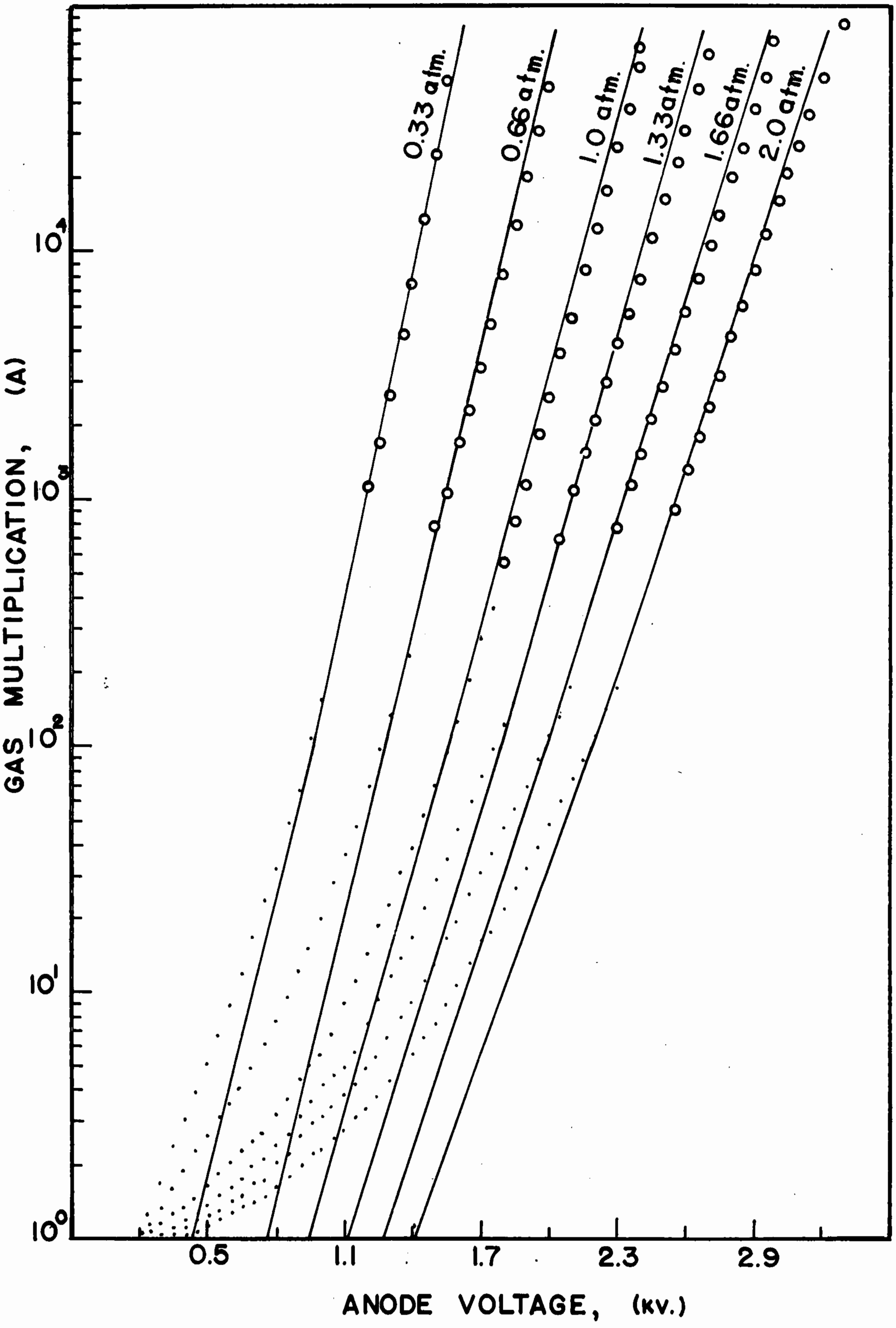

0.33 atm.
0.66 atm.
1.0 atm.
1.33 atm.
1.66 atm.
2.0 atm.
10⁴
10³
10²
10¹
10⁰
0.5
1.1
1.7
2.3
2.9
GAS MULTIPLICATION, (A)
ANODE VOLTAGE, (KV.)

Figure 50

Comparison between Experimental and Semi-theoretical Gas Multiplication Factor, "A", (Eq. 48) when A-CH_4 (9:1) is used as Counter Gas.

(a) anode diameter: 0.001 in.
(b) anode diameter: 0.002 in.
(c) anode diameter: 0.003 in.
(d) anode diameter: 0.004 in.
(e) anode diameter: 0.005 in.

—— Semi-theoretical
○ Experimental

172a

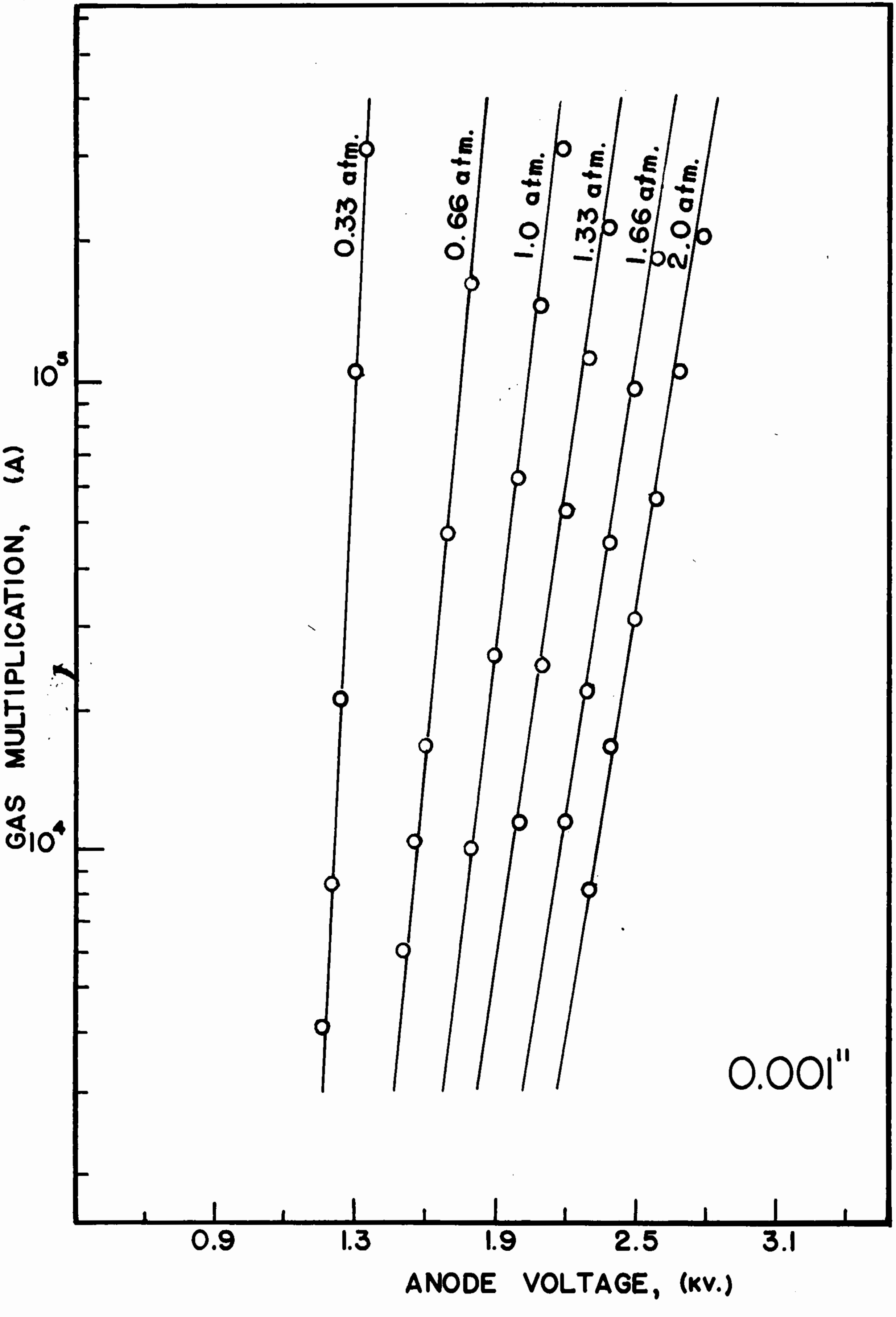

0.33 atm.
0.66 atm.
1.0 atm.
1.33 atm.
1.66 atm.
2.0 atm.
10^5
10^4
GAS MULTIPLICATION, (A)
0.9
1.3
1.9
2.5
3.1
ANODE VOLTAGE, (KV.)
0.001"

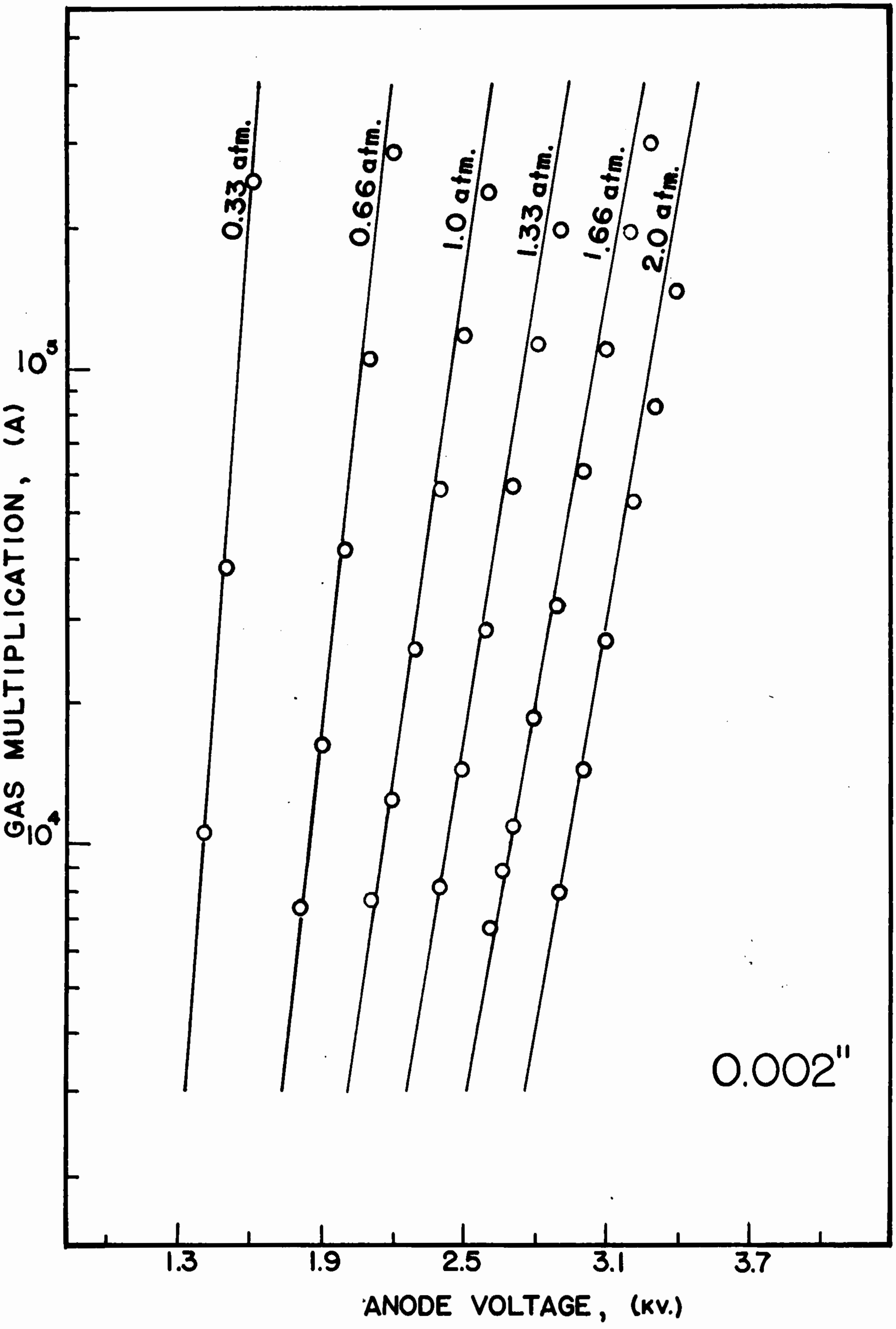
0.33 atm.
0.66 atm.
1.0 atm.
1.33 atm.
1.66 atm.
2.0 atm.
10^5
10^4
GAS MULTIPLICATION, (A)
0.002"
1.3
1.9
2.5
3.1
3.7
ANODE VOLTAGE, (KV.)

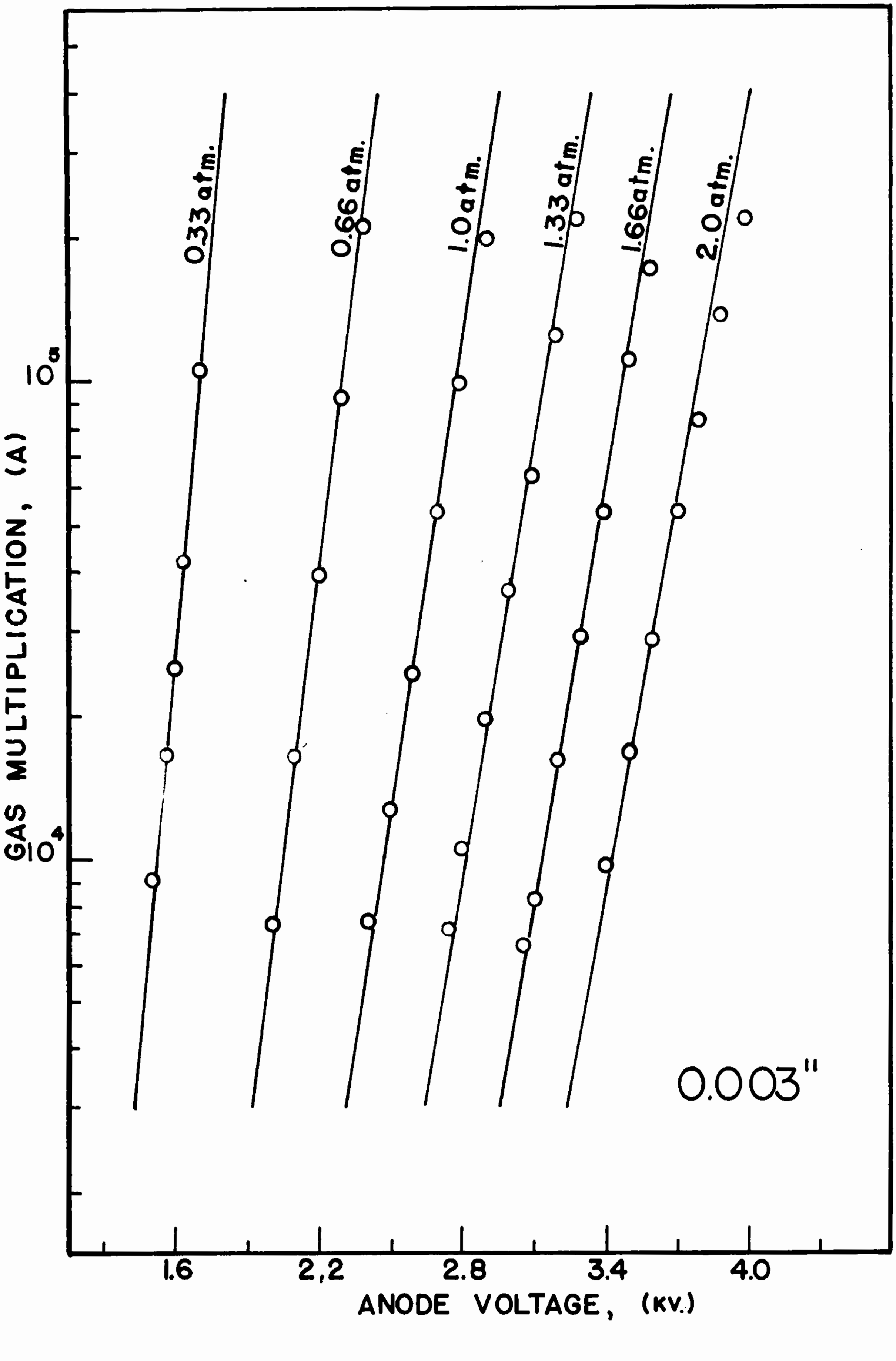
GAS MULTIPLICATION, (A)
10⁵
10⁴
0.33 atm.
0.66 atm.
1.0 atm.
1.33 atm.
1.66 atm.
2.0 atm.
0.003"
1.6
2.2
2.8
3.4
4.0
ANODE VOLTAGE, (KV.)

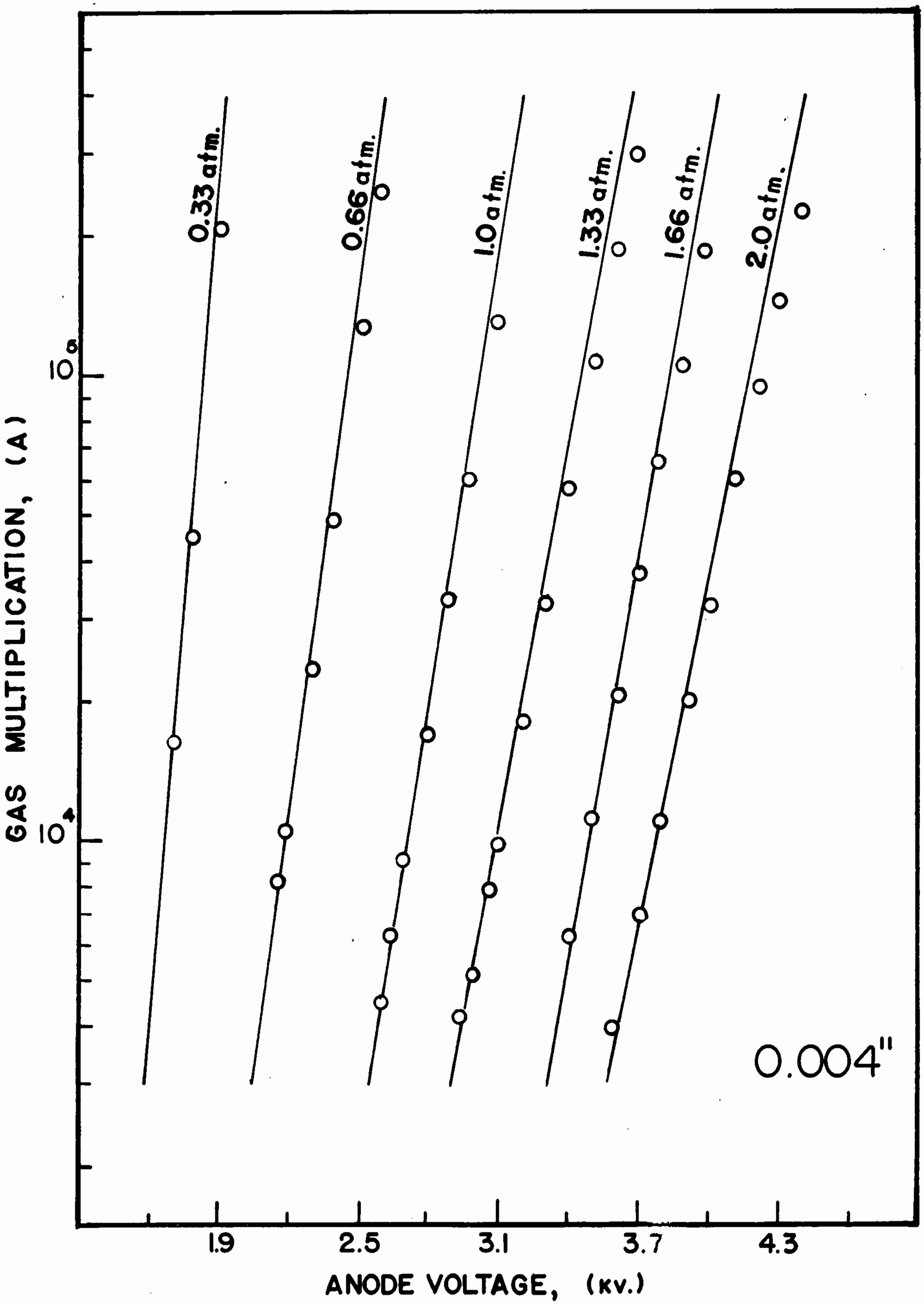

0.33 atm.
0.66 atm.
1.0 atm.
1.33 atm.
1.66 atm.
2.0 atm.
10^5
10^4
GAS MULTIPLICATION, (A)
1.9
2.5
3.1
3.7
4.3
ANODE VOLTAGE, (KV.)
0.004"

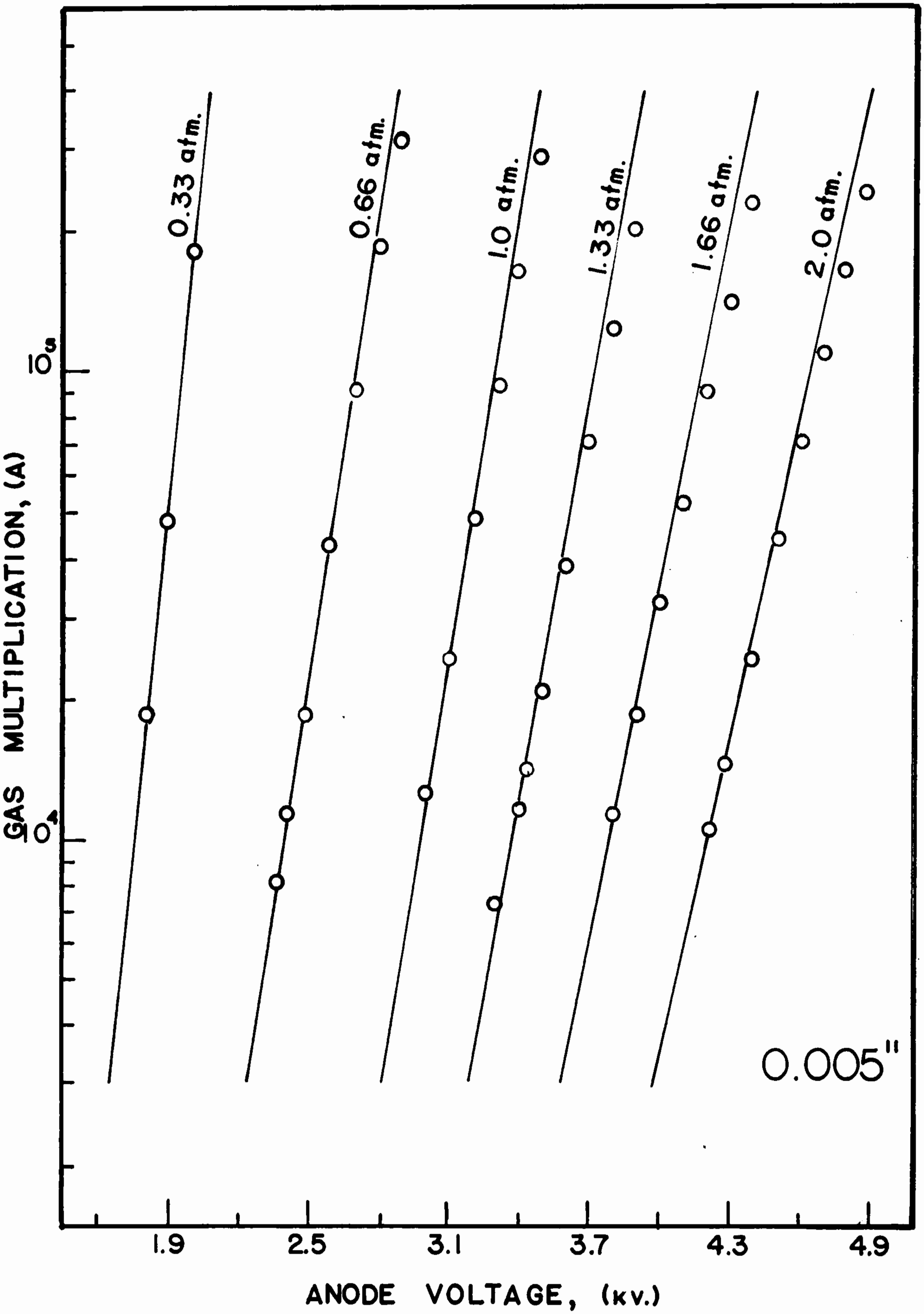
0.33 atm.
0.66 atm.
1.0 atm.
1.33 atm.
1.66 atm.
2.0 atm.
10^5
10^4
GAS MULTIPLICATION, (A)
0.005"
1.9
2.5
3.1
3.7
4.3
4.9
ANODE VOLTAGE, (KV.)

<u>Figure 51</u>

Proportional Threshold Voltages for various pressures of A-CH_4 (9:1) and Anode Diameters.

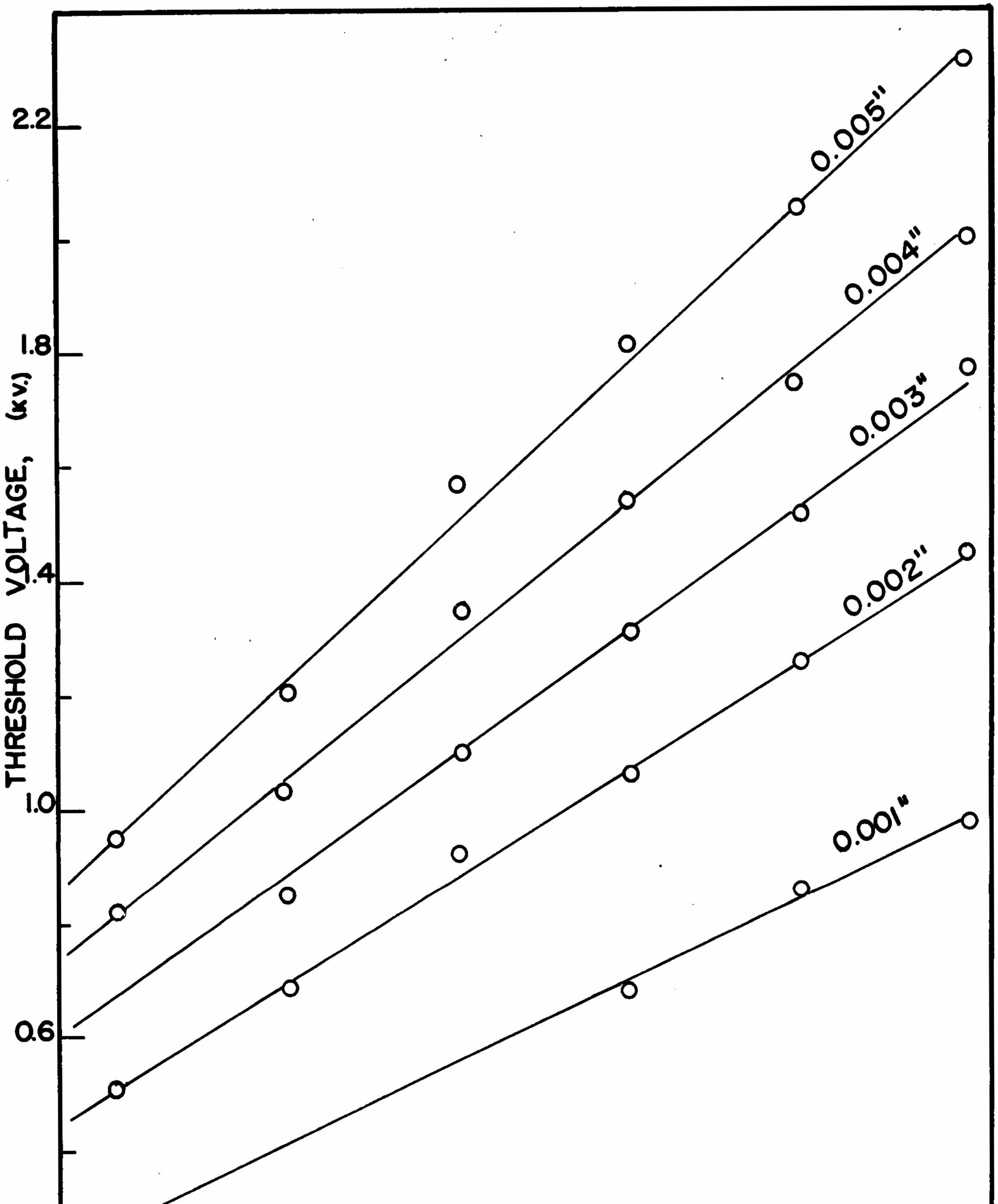

THRESHOLD VOLTAGE, (KV.)
2.2
1.8
1.4
1.0
0.6
0.33
0.66
1.0
1.33
1.66
PRESSURE, (atm.)
0.005"
0.004"
0.003"
0.002"
0.001"

<u>Figure 52</u>

Variation of f(o) for Various Pressures of Kr-CH_4 (9:1).

Anode diameter: 0.002 in.

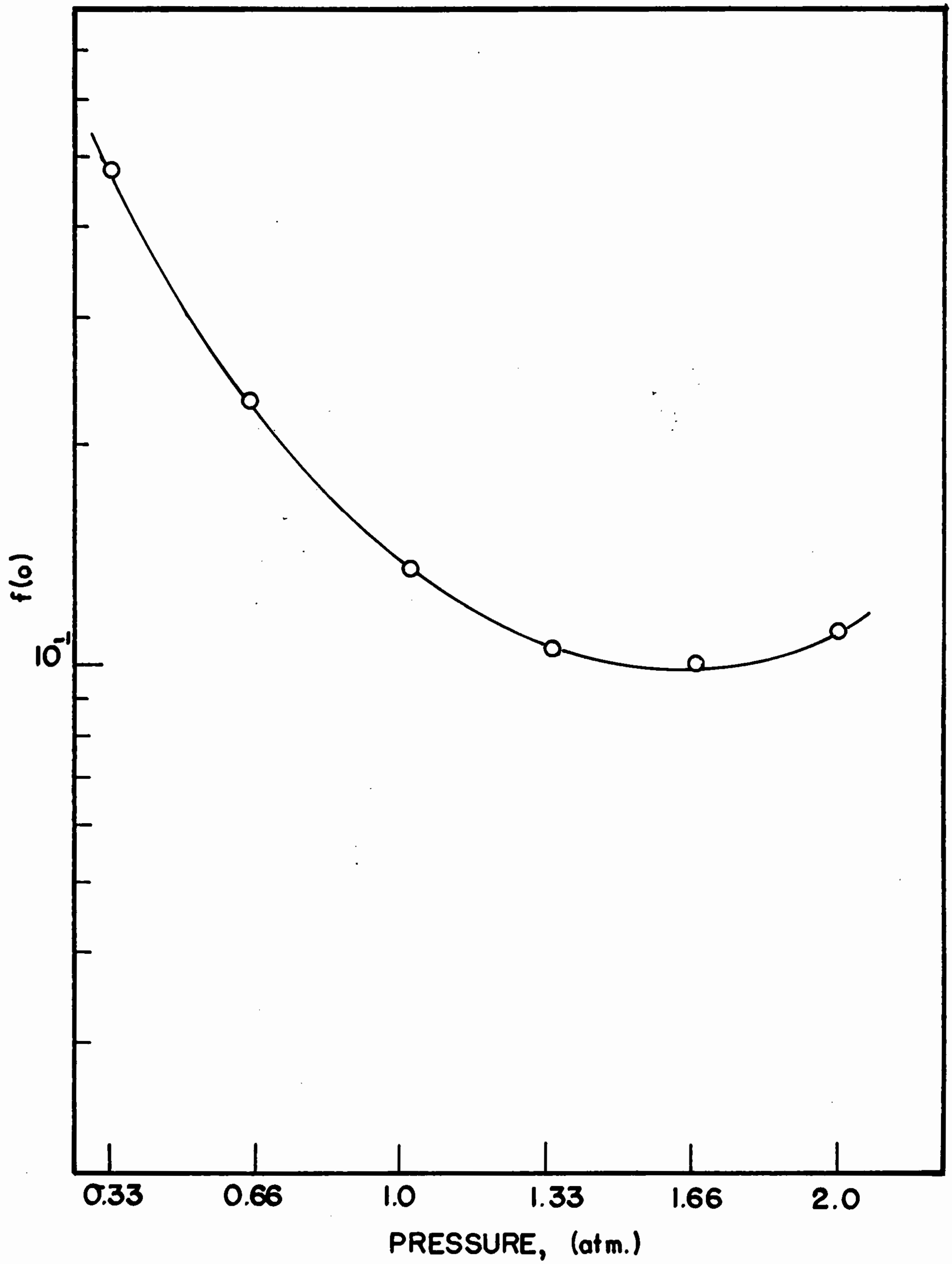
f(o)
10^{-1}
0.33
0.66
1.0
1.33
1.66
2.0
PRESSURE, (atm.)

Figure 53

Comparison between Experimental and Semi-theoretical Gas Multiplication Factor, "A", (Eq. 48) when Kr-CH_4 (9:1) is used as Counter Gas.

——— Semi-theoretical

○ Experimental

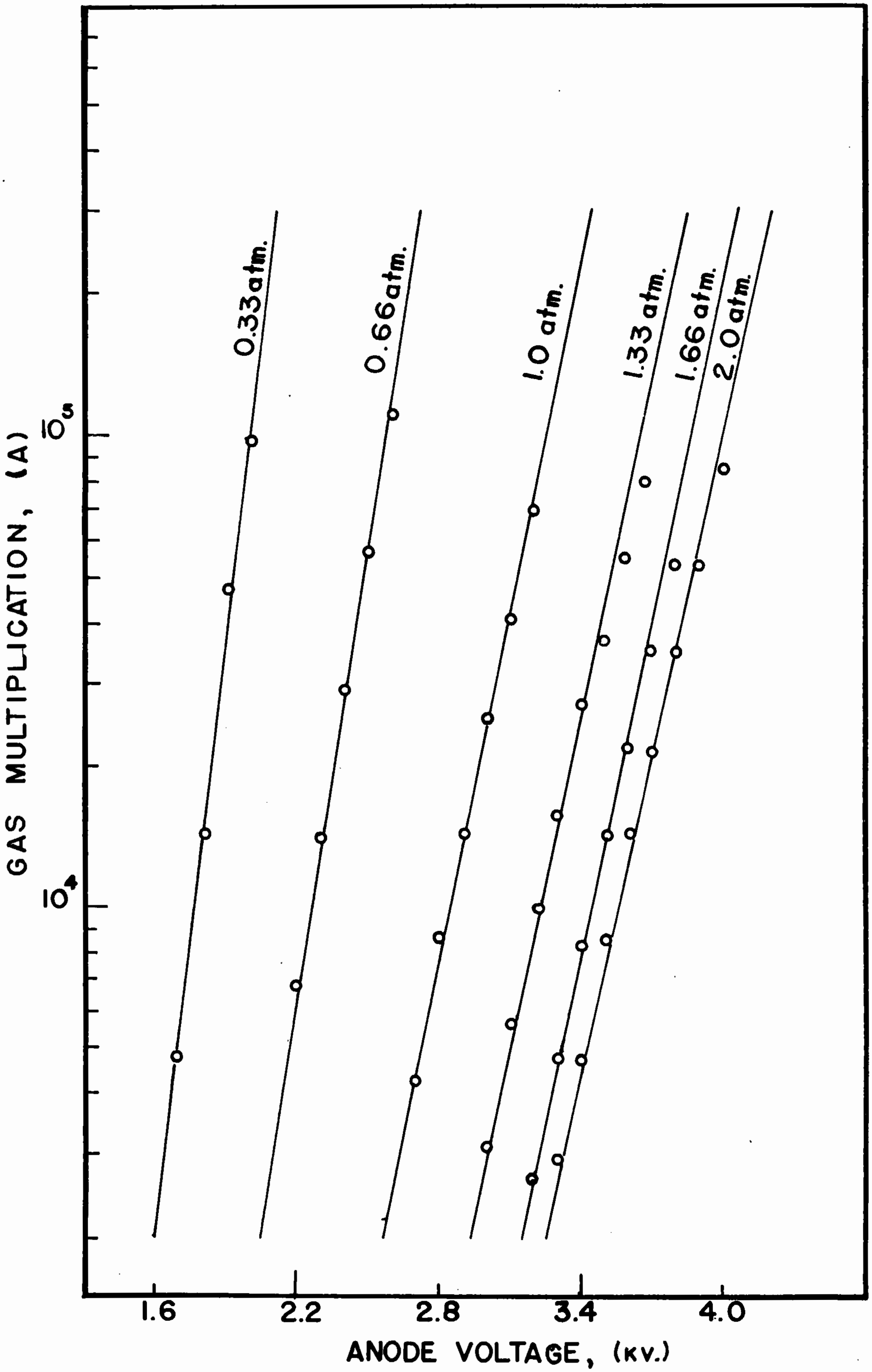

GAS MULTIPLICATION, (A)
10⁵
10⁴
0.33 atm.
0.66 atm.
1.0 atm.
1.33 atm.
1.66 atm.
2.0 atm.
1.6
2.2
2.8
3.4
4.0
ANODE VOLTAGE, (KV.)

krypton. It was assumed that their value for krypton was reliable since similar experiments under same experimental conditions were made with other rare gases and agreed very well with reliable data published by other investigators.

An empirical equation was derived to satisfy the experimental points shown in Fig. 50 (a), (b), (c), (d), and (e). This equation which is written below relates the gas multiplication factor "A" to (a) pressure of A-CH_4 (9:1), (b) anode diameter, and (c) the operating voltage across the counter.

$$\log A = mV_o + b \qquad \text{..........} \quad (50)$$

where,

$m = e^{2.3(m_m \log d^{-1} + k_m)}$

$b = e^{2.3(m_{-b} \log d + k_{-b})}$ where d is the anode wire diameter.

V_o = operating voltage

For various pressures, the values for m_m, m_{-b}, k_m, k_{-b} are summarized in Table VII.

Calculations resulting from application of the empirical Eq. 50 are shown in Fig. 54 (a), (b), (c), (d), (e), and (f). The experimental points are compared to the calculated solid curves.

TABLE VII

Determination of the Variables of Eq. 50 for Various Pressures.

	$P \geq 1$ atm.	$P \leq 1$ atm.
m_m	0.155	$0.04\ P^{-2} + 0.12$
m_{-b}	$0.057\ P + 0.29$	$-0.391\ P^{-1} + 0.739$
k_m	$-0.140\ P - 2.77$	$-0.02\ P^{-3} - 2.89$
k_{-b}	$0.13\ P - 1.3$	$-0.92\ P^{-1} + 2.34$

Figure 54

Comparison between Experimental Points and Calculations derived from an Empirical Equation, (Eq. 50).

(a) pressure : 0.33 atm.
(b) pressure : 0.66 atm.
(c) pressure : 1.00 atm.
(d) pressure : 1.33 atm.
(e) pressure : 1.66 atm.
(f) pressure : 2.00 atm.

——— Calculated
○ Experimental Points.

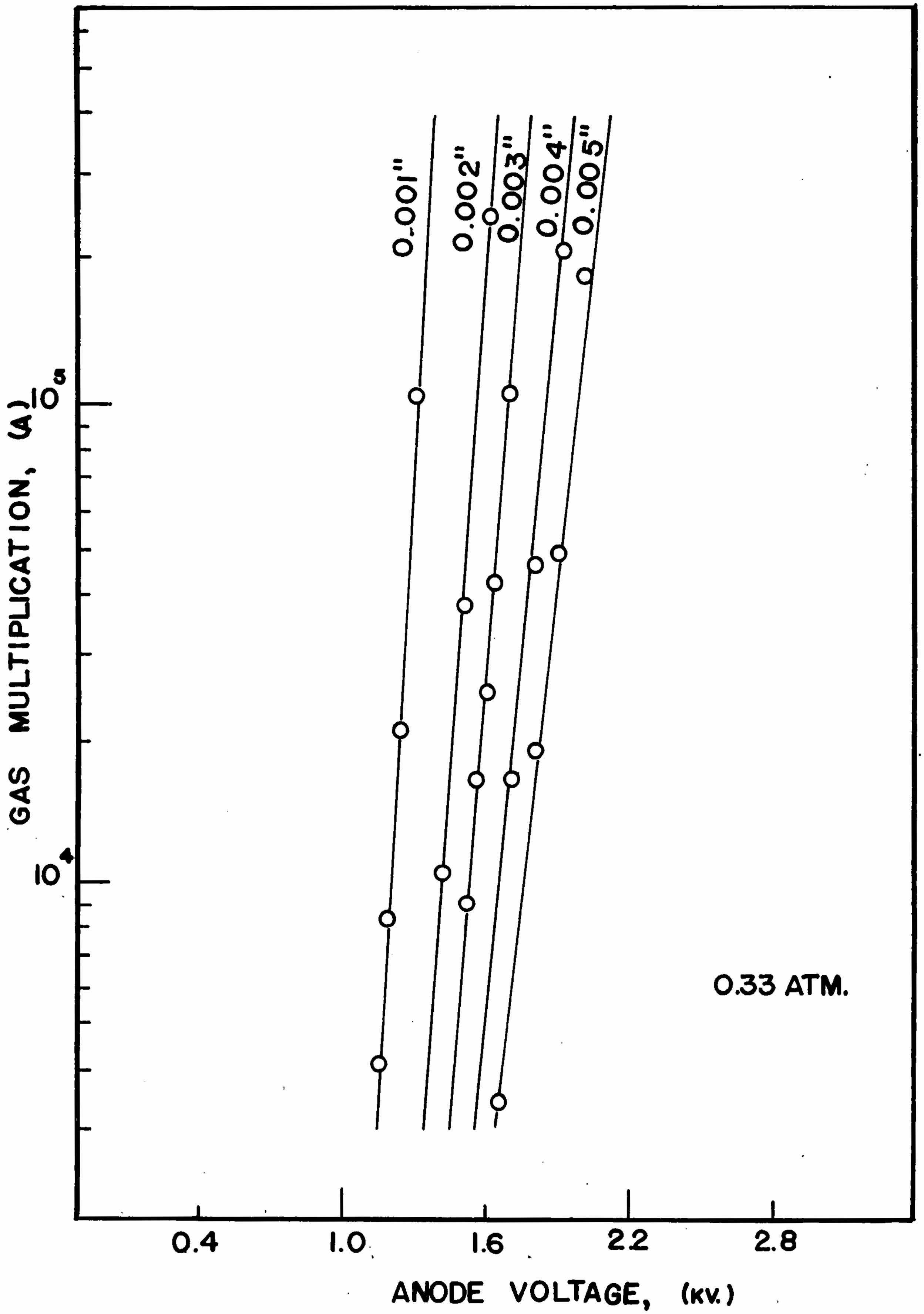
GAS MULTIPLICATION, (A)
10^5
10^4
0.001"
0.002"
0.003"
0.004"
0.005"
0.33 ATM.
0.4
1.0
1.6
2.2
2.8
ANODE VOLTAGE, (KV.)

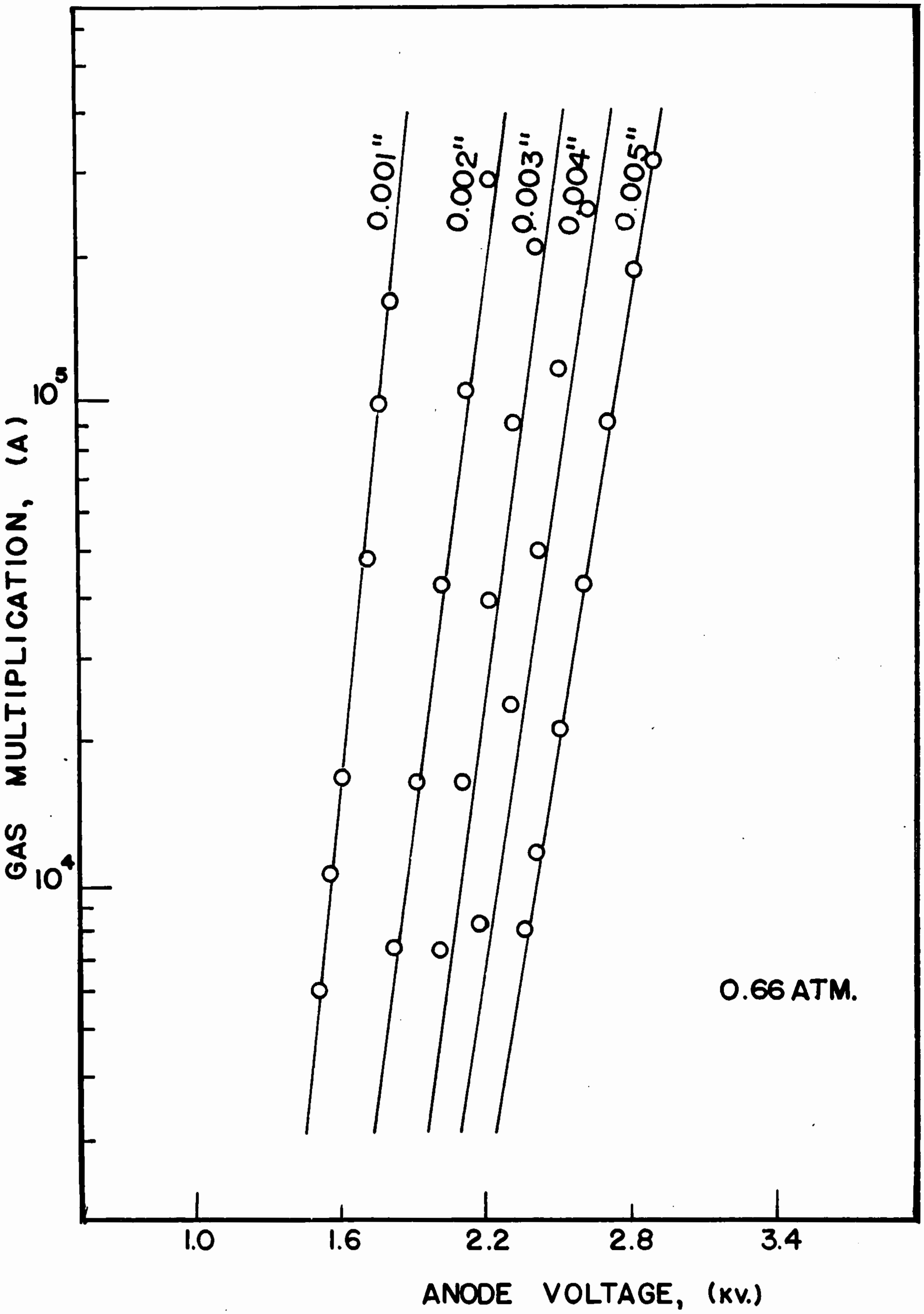
0.001"
0.002"
0.003"
0.004"
0.005"
GAS MULTIPLICATION, (A)
10^5
10^4
0.66 ATM.
1.0
1.6
2.2
2.8
3.4
ANODE VOLTAGE, (KV.)

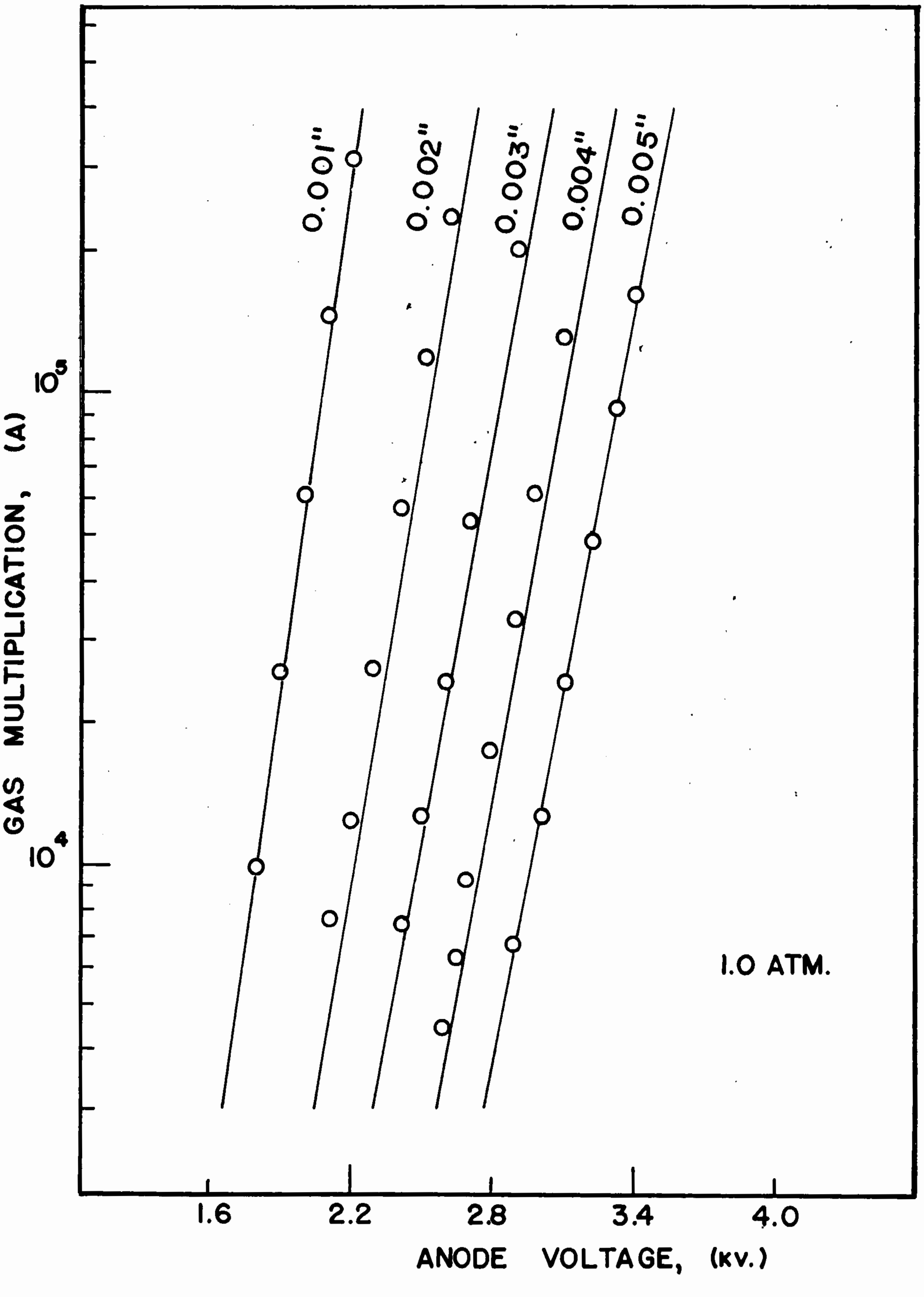
0.001"
0.002"
0.003"
0.004"
0.005"
GAS MULTIPLICATION, (A)
10^5
10^4
1.0 ATM.
1.6
2.2
2.8
3.4
4.0
ANODE VOLTAGE, (KV.)

178d

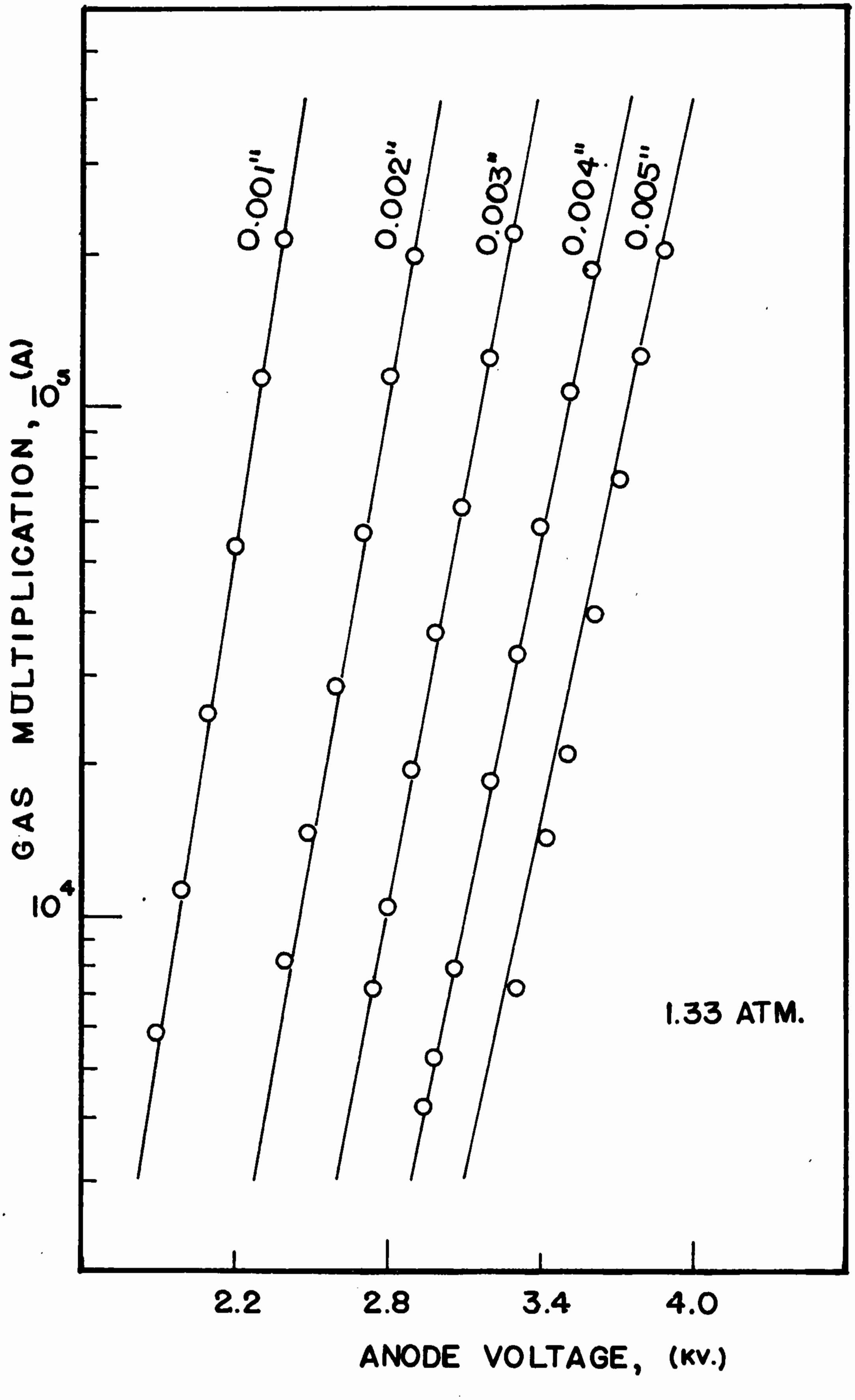

GAS MULTIPLICATION, (A)
10^5
10^4
0.001"
0.002"
0.003"
0.004"
0.005"
1.33 ATM.
2.2
2.8
3.4
4.0
ANODE VOLTAGE, (KV.)

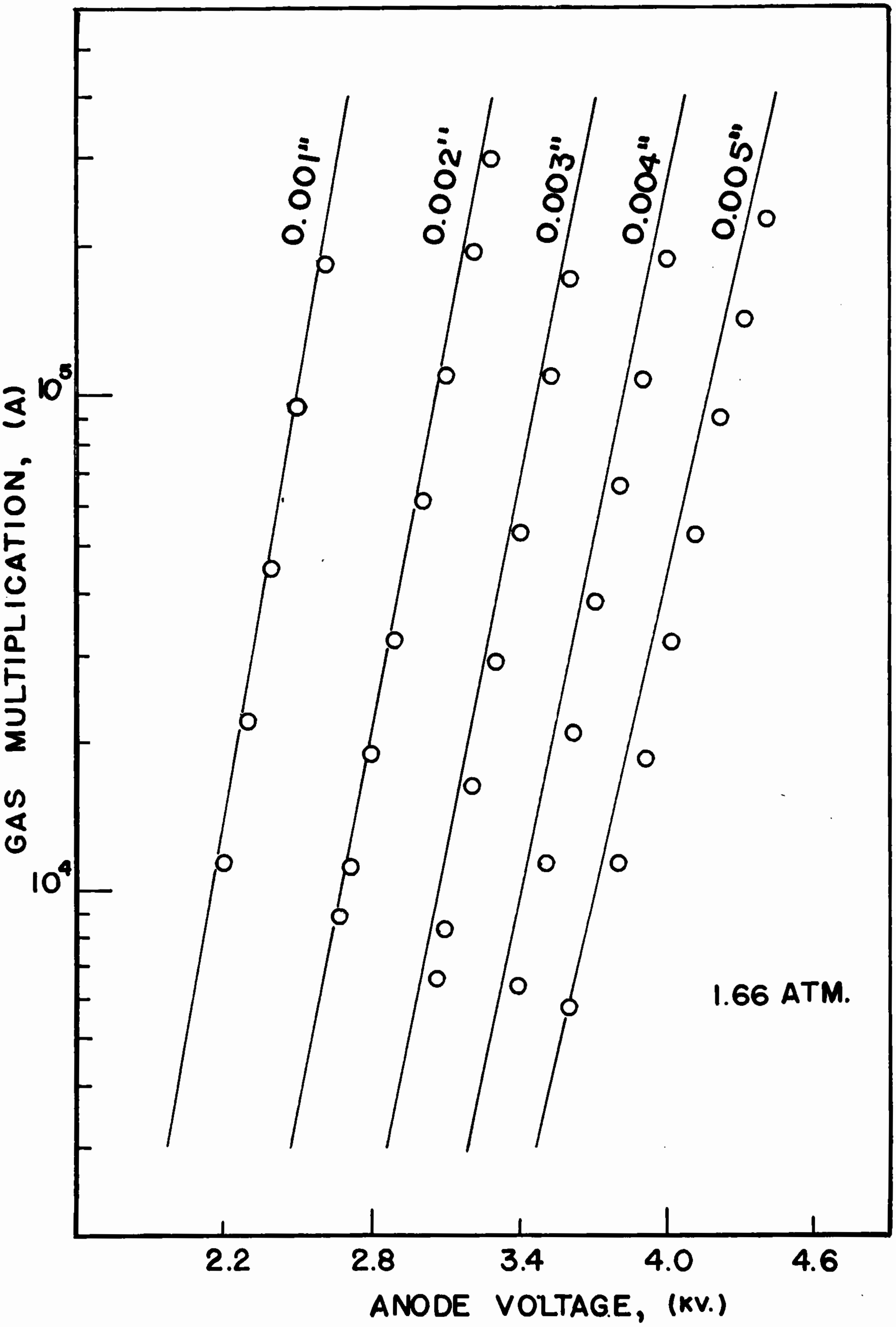
0.001"
0.002"
0.003"
0.004"
0.005"
10^5
10^4
GAS MULTIPLICATION, (A)
1.66 ATM.
2.2
2.8
3.4
4.0
4.6
ANODE VOLTAGE, (KV.)

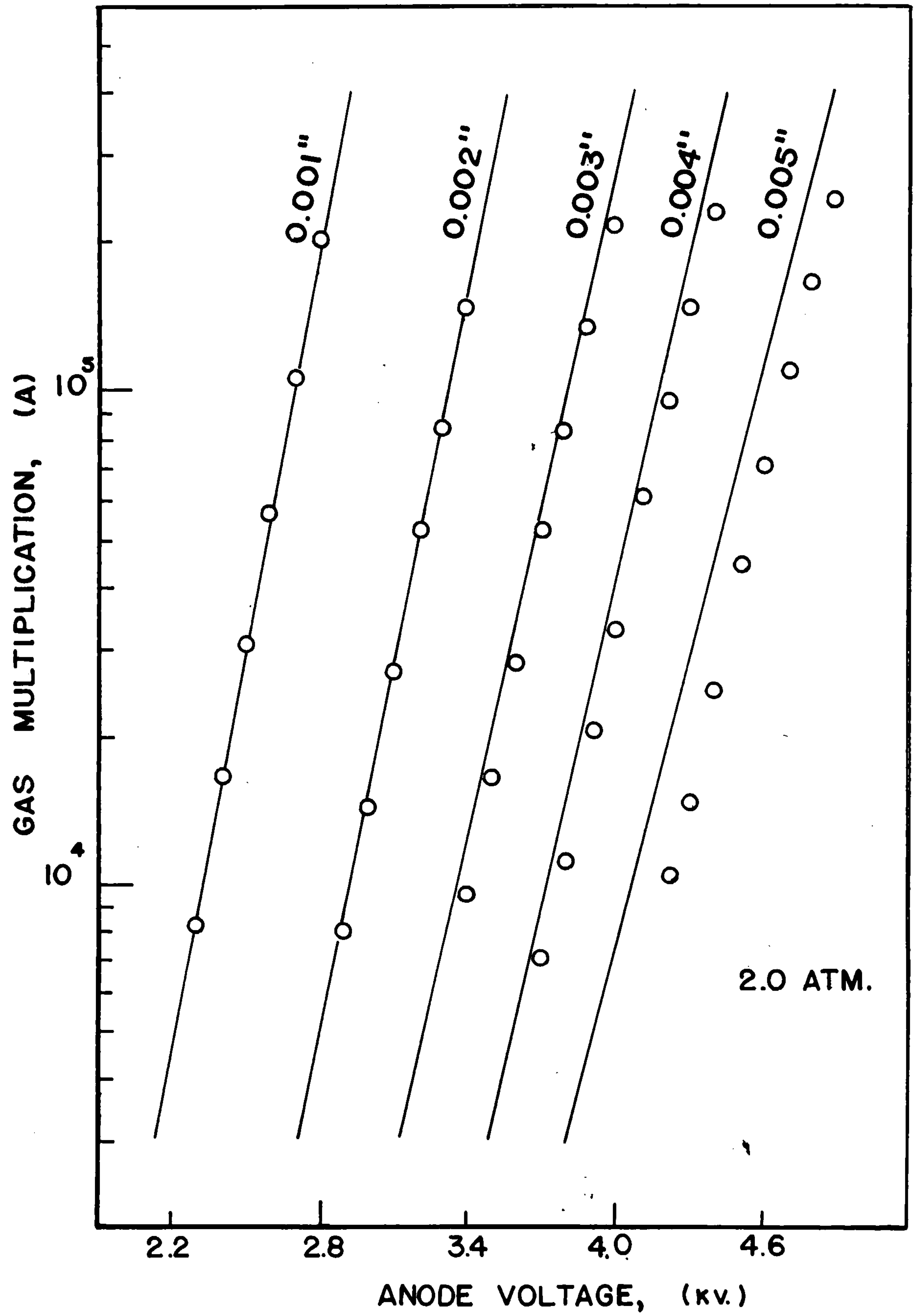
0.001"
0.002"
0.003"
0.004"
0.005"
2.0 ATM.
GAS MULTIPLICATION, (A)
10^5
10^4
2.2
2.8
3.4
4.0
4.6
ANODE VOLTAGE, (KV.)

5) DISCUSSION

As suspected, the above experiments have demonstrated a reasonable linearity of the gas multiplication factor "A" when low energy radiation measurements were made.

However, it was noted that when the pressure and anode wire diameter were decreased, the magnitude of the factor A became more drastically dependent on the voltage V_o across the chamber. In practice, a rapid rate of increase of A is not recommended when V_o is varied slightly, and for this reason, the use of an anode diameter of 0.002 in. and of the counter operated at atmospheric pressure was suggested.

On the other hand, if the pressure is increased to two atmospheres, for instance, a stronger departure from linearity is met for low gas multiplication factors, ($A < 10^2$). This phenomenon is depicted in Fig. 47 and 49. This is probably due to (a) recombination and electron attachment to neutral molecules, (b) fluctuation in energy loss and in specific ionization, and (c) some distortion of the electric field, especially at both ends of the counter.

For high energy radiation measurements, smaller gas multiplications will be required to trigger the input electronic amplification circuits. Under these conditions and according to Fig. 47, a lack of linearity in the factor A became apparent and it was particularly more pronounced as the pressure of the counter was increased. The deviation of the upper limit or more precisely, the space charge distortion was explained by Hanna et al. (188) by means of the following relation.

$$E_i \times A_c = \text{constant} \sim 10^8 \qquad \ldots\ldots\ldots (51)$$

They assumed that the multiplication factor A is independent of the energy of the impinging radiation (E_i), and tends towards a critical value equal to A_c.

When Fig. 46, 48, and 52 are compared, it may be noted that the variation of the factor f(o) has a similar trend. Naturally, if f(o) is equal to unity, the modified Eq. (49) will become equivalent to the theoretical equation derived by Rose and Korff, i.e., Eq. (47). The direct application of Rose and Korff's theoretical equation will become possible at pressures lower than 0.3 atmospheres. In their original paper (105), Rose and Korff have verified the theory for proportional counters operated at pressures smaller than 0.5 atmospheres and in particular at a pressure of 0.13 atmospheres.

Concerning the empirical Eq. (50) which enables the direct calculation of the factor "A" for various voltages, (V_o), anode diameter, (d), and pressure, (P), its practical application was limited to a mixture of A-CH_4 (9:1) as counter gas. Different gases will, of course, have different ionization cross-sections and will require appropriate empirical factors.

E. PULSE STATISTICAL FLUCTUATION

1) INTRODUCTION

The output pulse size of a proportional counter arising from full energy absorption of a monoenergetic radiation in the counter gas is subject to statistical fluctuations. Actually, there are fluctuations in the number of ion-pairs which are initially released by a monoenergetic radiation and in the size of the avalanche resulting from the secondary ionizing processes. The problem has been treated theoretically by Frisch (189). He established that the relative variance (mean square relative standard deviation) of the output pulse size, $(\sigma_P/P)^2$, was given by,

$$\left(\frac{\sigma_P}{P}\right)^2 = \frac{1}{N}\left(\frac{\sigma_A}{A}\right)^2 + \left(\frac{\sigma_N}{N}\right)^2 - \frac{1}{AN} \qquad \ldots\ldots (52)$$

where,

$\left(\frac{\sigma_A}{A}\right)^2$ = relative variance in the number of ions produced in an avalanche by a single ionization.

$\left(\frac{\sigma_N}{N}\right)^2$ = relative variance in the number of initial electrons.

A and N are respectively the gas multiplication factor and the primary number of electrons. For A equal to unity, (no gas multiplication) the last two terms will cancel, as they must. However, we are interested in working with A much greater than unity (about 10^4), and consequently, the last term can be ignored.

The contribution to the relative variance, $1/N(\sigma P/P)^2$, due to the gas multiplication was theoretically evaluated by Frisch (189) and Snyder (190) and found to be equal to 1/N. This was derived under the assumption that the instantaneous probability for an electron to make an ionizing collision was merely a function of the electric field and not of the previous history of the electron.

Hence, if $\sigma_N{}^2$ is equal to N, as for a Poisson distribution, the right hand side of Eq. (52) will become 2/N. This assumption will imply that the initial ionization has a normal Poisson distribution (191).

Using a proportional counter, Hanna et al. (188) have measured the fluctuations of the pulse size for various energies. They obtained fluctuations which were definitely less than predicted from Eq. (52). Also, they found that the relative variance of the output pulse size was practically independent of the multiplication factor.

On the other hand, Curran et al. (127) have measured, in a very ingenious manner, the fluctuation of the process alone. This was done by detecting single slow electrons liberated from a tungsten filament situated at the cathode. The photoelectrons were not sufficiently energetic to produce ionization so that, as far as the recorded pulses are concerned, $\sigma_N{}^2$ equals zero. The resulting pulse size distribution at high gas multiplication enables a direct determination of $\sigma_A^{\ 2}$ to be made. Their results showed that the relative variance was,

$$\frac{1}{N}\left(\frac{\sigma_A}{A}\right)^2 = \frac{0.68}{N} \qquad \text{........ (53)}$$

which is a value smaller than the theoretical estimate of Frisch (189) and Snyder (190).

If the value of Eq. (53) is inserted into Eq. (52) this will lead to,

$$\left(\frac{\sigma_P}{P}\right)^2 = \left(\frac{\sigma_N}{N}\right)^2 + \frac{0.68}{N} \qquad \text{........ (54)}$$

and this relation (semi-theoretical) will be employed to compare our experimental results.

Concerning the fluctuation of the number of primary ions for a given initial energy, this problem was theoretically treated by Fano (192). Its relative variance was due to the fact that some collisions are ionizing while others are not, and to the statistical fluctuation of energy loss in the ionizing and in the exciting collisions. His results were partially supported by measurements of the total fluctuations in pulse size made by Hanna et al. (188) and by Curran et al. (191). The energy of the radiations investigated were: 0.25 kev, 2.8 kev, and 17.4 kev, (Hanna et al.), 8.0 kev, and 17.4 kev, (Curran et al.).

In this present work, an investigation of Eq. (54) has been made and for energies ranging between 3 and 25 kev. Hence, the dependence of the total relative variance of the pulse size distribution and the relative variance in the number of initial electron were studied.

2) EXPERIMENTAL TECHNIQUES AND RESULTS

Before describing the experimental techniques, it should be mentioned that the spread of a pulse distribution might not be caused only by the statistical fluctuations but also by additional fluctuations arising from the experimental apparatus. Although they were neglected, the main ones are:

(a) Non-uniformity and eccentricity of the wire.

(b) End and wall effect.

(c) Electron attachment to gas molecules.

(d) Instability of D.C. power supply.

(e) Amplifier noise.

The radioactive species summarized in Table VIII were mounted on the platform of the counter and the Auger electrons were screened off with the proper aluminum thickness. The anode wire had a diameter of 0.002 in. while the counter gas was a mixture of A-CH_4 (9:1) at a pressure of one atmosphere.

Using Fe^{55}, in particular, the statistical spread in the pulse size was found to be independent of the multiplication

TABLE VIII

Results on the Statistical Spread of the Pulse Size from a Proportional Counter.

Nuclides	E_X kev	Theo. σ_P/P Per cent	Exp'l σ_P/P Per cent	Exp'l σ_N/N Per cent
Ca^{41}	3.3	13.9	9.8	7.5
Cr^{51}	4.9	10.8	7.8	4.7
Mn^{54}	5.4	10.3	7.7	4.7
Fe^{55}	5.9	9.9	7.5	4.8
Co^{57}	6.4	9.4	7.6	5.2
Zn^{65}	8.0	8.5	6.0	3.5
Se^{75}	10.5	7.4	5.0	4.3
Sr^{85}	13.4	6.5	5.2	3.5
Pd^{103}	20.2	5.3	4.0	2.5
Sn^{112}	24.0	4.9	3.4	1.9

factor A for values of A up to 10^5.

The observed distributions were gaussian over an energy range of ± 3 standard deviations. The standard deviation σ_P could therefore be obtained by measuring the width of the peak at half maximum through the following relation

$$\frac{\Delta E}{E} = \frac{\Delta P}{P} = 2.36 \frac{\sigma_P}{P} \qquad \text{..........} \; (55)$$

where,

ΔE = full width of the peak at half height.

E or P = energy of the impinging radiation.

σ_P = standard deviation of the pulse height distribution for a gaussian distribution around the most probable value.

The results of our measurements are summarized in Table VIII. For the purpose of the calculations of Eq. (54), we have assumed that the average energy loss in argon for the formation of one ion pair was 28.5 kev as did Curran (193). These results are shown in Fig. 55 (a) and (b).

3) <u>CONCLUSIONS</u>

As may be seen from Fig. 55 (a), the root mean square of the total relative variances for various output pulses are smaller than would be expected from a Poisson distribution. The simplifying assumptions used by Snyder (190) and Frisch (189) in the derivation of Eq. (52) are probably at fault. In fact, the probability that an electron can ionize in an avalanche depends on its previous history as well as on its position. Immediately after

Figure 55

Statistical Spread in Pulse Size and Primary Ionization.

(a) Total Relative Standard Deviation of Pulse Size as a Function of the Energy.

——— Theoretical or Poisson Distribution
○ - - - - Experimental
△ Curran et al. (127).
□ Hanna et al. (188).

(b) Relative Standard Deviation in the Number of Initial Electrons as a Function of the Energy.

——— Fano Theory
○ Experimental.

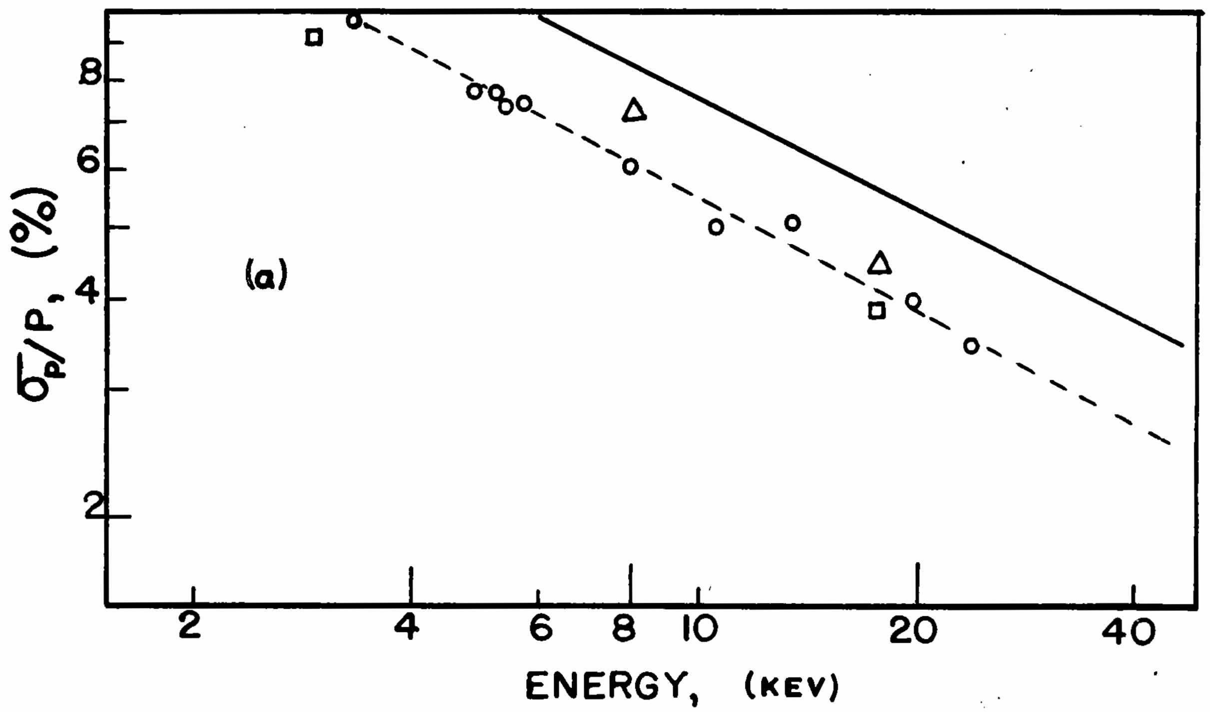

8
6
4
2
σ_P/P, (%)
(a)
2
4
6
8
10
20
40
ENERGY, (KEV)

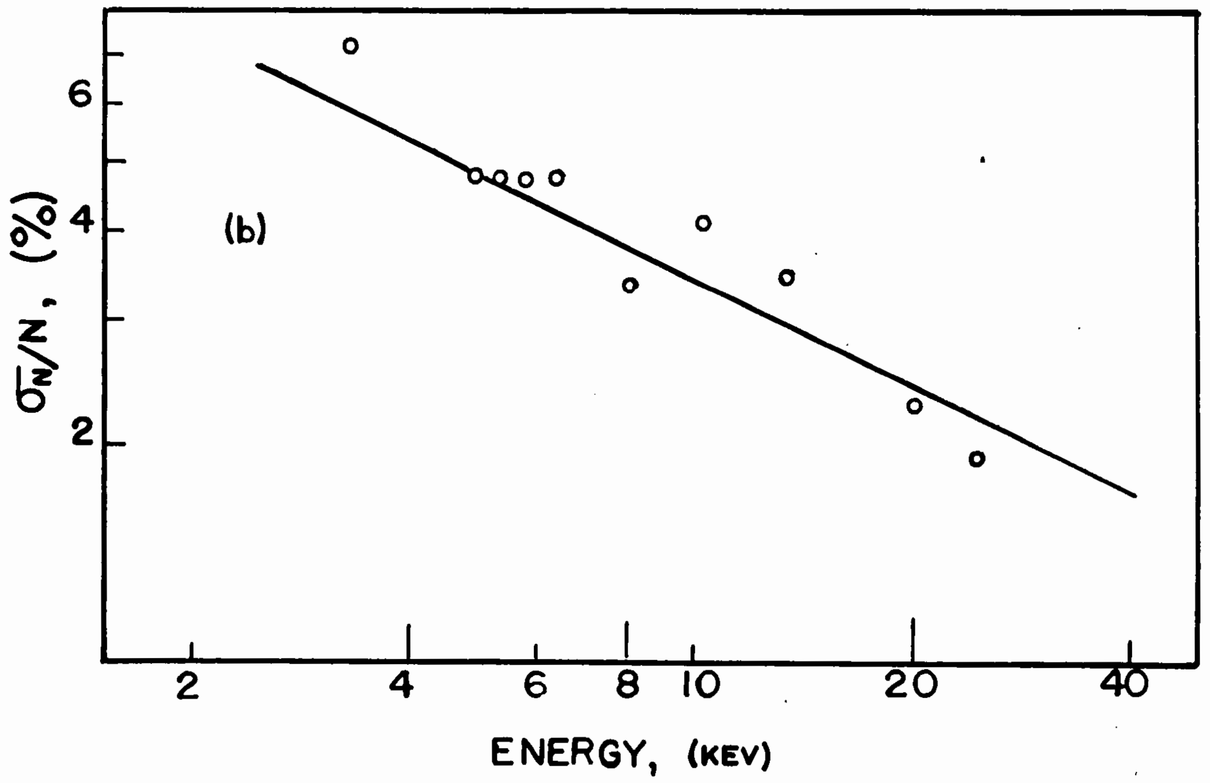

6
4
2
σ_N/N, (%)
(b)
2
4
6
8
10
20
40
ENERGY, (KEV)

having produced one ion pair, it will have to travel some distance towards the wire before its energy is sufficient to produce further ionization. If that distance was sharply defined, then the avalanche would be predictable (non-statistical) and σ_A^2 would be zero. For this reason, we have used Eq. (54) to derive our results illustrated in Fig. 55(a).

In the range of energy investigated, the total standard deviation of the pulse size was found to be related to the energy as follows:

$$\frac{\sigma_P}{P} = 0.17\ E^{-1/2} \qquad \text{.........} \ (56)$$

Thus,

$$\text{Resolving Power} = 0.42\ E^{-1/2} \qquad \text{.........} \ (57)$$

where the energy E is in kev.

Last January (1960), Husain and Jaffe (194) have described a sensitive proportional counter used as a charged particle spectrometer. They have found that the relation,

$$\text{Resolving Power} \cong 2.4\ N^{-1/2} \cong 0.415\ E^{-1/2} \qquad \text{......} \ (58)$$

held for proton energies up to 8 mev, in argon gas. Comparison between their relation and ours shows a striking similarity.

It is clear that in addition to the above uncertainty in the contribution due to the gas multiplication factor itself, there is a definite difference in the nature of the fluctuations in the primary number of ion pairs created along the complete track of a particle of definite energy. As mentioned previously, this fluctuation would be due to the fact that some collisions are ionizing while others are not, and to statistical fluctuations of energy loss in the ionizing and in the exciting collisions. According to the estimate of Fano (192), the relative variance $(\sigma_N/N)^2$ becomes 1/kN, with "k" between 2 and 3, that is, smaller than that obtained with a Poisson distribution.

From Eq. (52) and on the basis of the results of Curran et al. (127) concerning the relative variance of ions of a single avalanche, we have attempted to deduce the fluctuation of the primary ionizing event. The results shown in Fig. 55 (b) were in fair agreement with Fano's theoretical predictions. The value for "k" was taken as 2.5.

F. DISINTEGRATION RATE DETERMINATION

1) INTRODUCTION

In the general introduction, we have related the counting rate, R, to the disintegration rate, N_o, of nuclides decaying by orbital capture through the following equation,

$$R = N_o.G.f_e.f_a.f_t.f_{w_K}.f_r. \qquad \ldots\ldots\ldots \quad (59)$$

where,

G = source-to-counter geometrical efficiency,

f_e = correction for the counter gas escape radiations,

f_a = correction for the transmission of the X-rays through the gas,

f_t = correction for the absorption of the characteristic X-rays inside the Auger electron absorber,

f_{w_K} = K-fluorescence yield,

f_r = correction for the neglected L-capture events.

In this section, we will evaluate the factors which were experimentally obtainable in the scope of this work. These are: G, f_e, and f_a. To correct for the others, namely f_t, f_{w_K}, and f_r, the most recent and probably the most accurate data from the literature will be used. For instance, Campion and Merritt (27) have derived an accurate equation to evaluate f_t. Their relation uses the equation normally used for the transmission of photons through matter plus a factor correcting for the radiations traversing the Auger absorber in an oblique direction. A great amount of data regarding the factor f_{w_K}, have been published in the literature, and Broyles et al. (29) have reported the compilation of these data in a paper published in 1953. Their compilations are reported in Appendix I of this thesis. However, Robinson and Fink (66) have recently written that, for $26 < Z < 50$, the best measurements on K-fluorescence yield are probably those of Roos (195). These measurements delineate the rising portion of W_K vs Z and are given to some 2 to 3 per cent. Finally, the last factor, f_r, will correct for the contribution of L-capture events not being detected by the counter or being neglected in the spectral analysis. To correct for this factor, a great deal of experimental data were published in 1960 by Robinson and Fink (66). These data are in good agreement with the theoretical calculations made by Brysk and Rose (51).

The possible contributions due to M, N, ...-capture events will be neglected on account of the low probability of occurrence. This assumption is quite true for the range of atomic numbers which we are dealing with, (up to $Z = 50$).

To determine the counting rate, R, the two following procedures will be possible: (a) the summation of all pulses in all channels under the main photopeak, or (b) the comparison of the area under the main photopeak to the area of a gaussian distribution for the normal curve of errors, (196).

We will now proceed to the experimental evaluation of the first three factors, namely the geometrical, escape, and absorption factors.

2) CORRECTION FACTORS EXPERIMENTALLY EVALUATED

(a) Source-to-counter Geometrical Efficiency.

The correction factor, G, which appears in the Eq. (59) for the determination of disintegration rate of electron capture nuclides might lead to a source of error if not accurately evaluated. Normally, three different methods can be applied to determine the factor G. These are (a) mathematical calculations, (b) use of a solution where the specific activity is known absolutely and (c) comparison of the counter to be calibrated with another counter having a geometrical efficiency absolutely known.

Although the description of the counter shown in Fig. 18 and the details of the window in Fig. 19(a) seem to display an inherent geometry of 2π-steradians the third method was applied to verify it with more precision. For this purpose, the unknown geometry was compared with two 4π-steradian counters which are different in principle. These are (a) a 4π-beta proportional counter calibrated in this laboratory, (6) and (b) a high pressure 4π-proportional counter used for soft X-ray detection (27).

In both cases the bottom half was used, thus contributing to a geometry having a solid angle of 2π-steradians. Four nuclides, namely Fe^{55}, H^3, Ni^{63}, and C^{14}, were mounted on the platform which is sketched in Fig. 19(a). The beta emitters were measured in the 4π-beta proportional counter while the nuclide decaying by electron capture was measured in the high pressure 4π-proportional counter. The results of the comparisons are summarized in Table IX, and from these data, one can assume that, within the standard deviation of the counting rates, the counter has a source-to-counter geometrical efficiency, G, equal to a solid angle of 2π-steradians.

(b) Counter Gas Escape Radiations

A way of explaining the occurrence of counter gas escape radiations leading to an "escape peak" accompanying the main photopeak in soft X-ray measurements may be made through the following argument.

First of all, we shall consider an impinging radiation whose energy E is greater than the K-binding energy E_K of the counter gas. When this radiation interacts with the gas atoms, there is some probability that an electron from the K-shell will be released with a kinetic energy equal to $(E - E_K)$. Simultaneously, that is within a time which is not detectable with instruments normally used, the ionized atom in the K shell will

TABLE IX

Geometrical Efficiency

Nuclide	This work	High Pressure 4π-Prop'l Counter	4π - Prop'l β^- Counter
	cpm x 10^{-3}	cpm x 10^{-3}	cpm x 10^{-3}
Fe^{55}	34.00 ± 0.05	34.07 ± 0.07	--
H^3	41.2 ± 0.2	--	41.5 ± 0.2
Ni^{63}	47.3 ± 0.2	--	47.5 ± 0.2
C^{14}	46.2 ± 0.2	--	46.7 ± 0.2

re-organize itself either by emission of a characteristic K X-ray having an energy E_X, or by emission of Auger electron having an energy E_e. The energy of the Auger electron is slightly smaller than the energy of the characteristic X-ray. Evidently, this assumes that only one Auger electron is emitted when a radiationless transition occurs. Depending on the atomic number, the ratio of these two different modes of re-organization will vary. The higher the atomic number, the greater the probability of characteristic X-ray emission will be. Hence, the pulse height resulting from total absorption of the incoming radiation will be detected by the auxiliary electronic circuits and will be proportional to $(E - E_K)$ E_X or $(E - E_K)$ E_e. However, when the characteristic X-ray will be emitted in the re-organization of the K-ionized atom, there will be a distinct probability of escape of such radiation from the gas, (E_X is unobserved), and the energy expended in ionization will be less than E, (possibly $E - E_K$). Pulses arising in this way will give rise to an "escape peak" in the observed spectrum of the incident radiations. They can be identified by the fact that they occur at constant energy intervals below the main photopeak. With different counter gases, this phenomenon is depicted in Fig. 56 (a), (c) and (d). However, if the incoming radiation has an energy E which is greater than the K-binding energy of the gas, then the higher the atomic number the greater will be the magnitude of the "escape peak". This is

Figure 56

K X-ray Spectra.

(a) Fe^{55} (5.9 kev).

Counter gas: A-CH_4 (9:1), 1 atm.

(b) Fe^{55} (5.9 kev).

Counter gas: Kr-CH_4 (9:1), 1 atm.

(c) Nb^{92} (15.7 kev).

Counter gas: A-CH_4 (9:1), 1 atm.

(d) Nb^{92} (15.7 kev).

Counter gas: Kr-CH_4 (9:1), 1 atm.

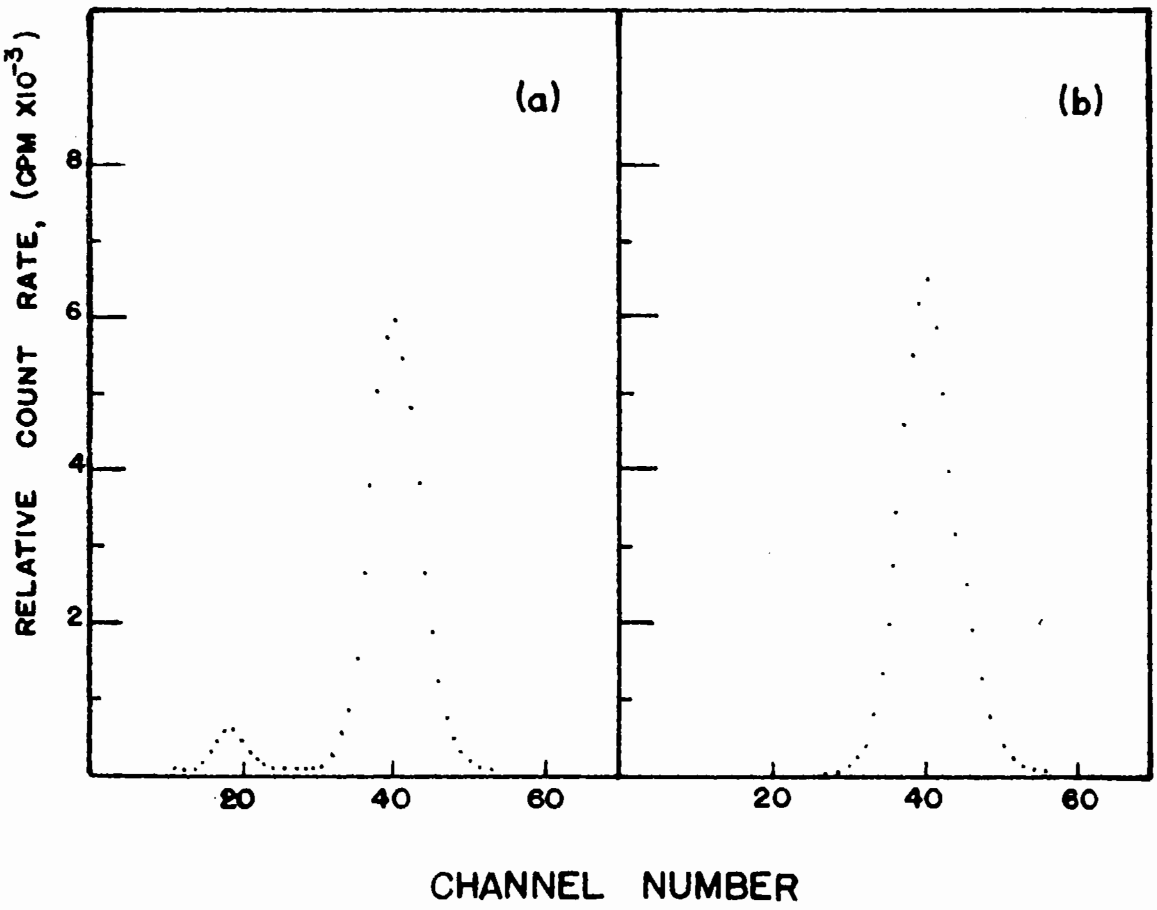
(a)
(b)
RELATIVE COUNT RATE, (CPM X10^{-3})
8
6
4
2
20
40
60
20
40
60
CHANNEL NUMBER

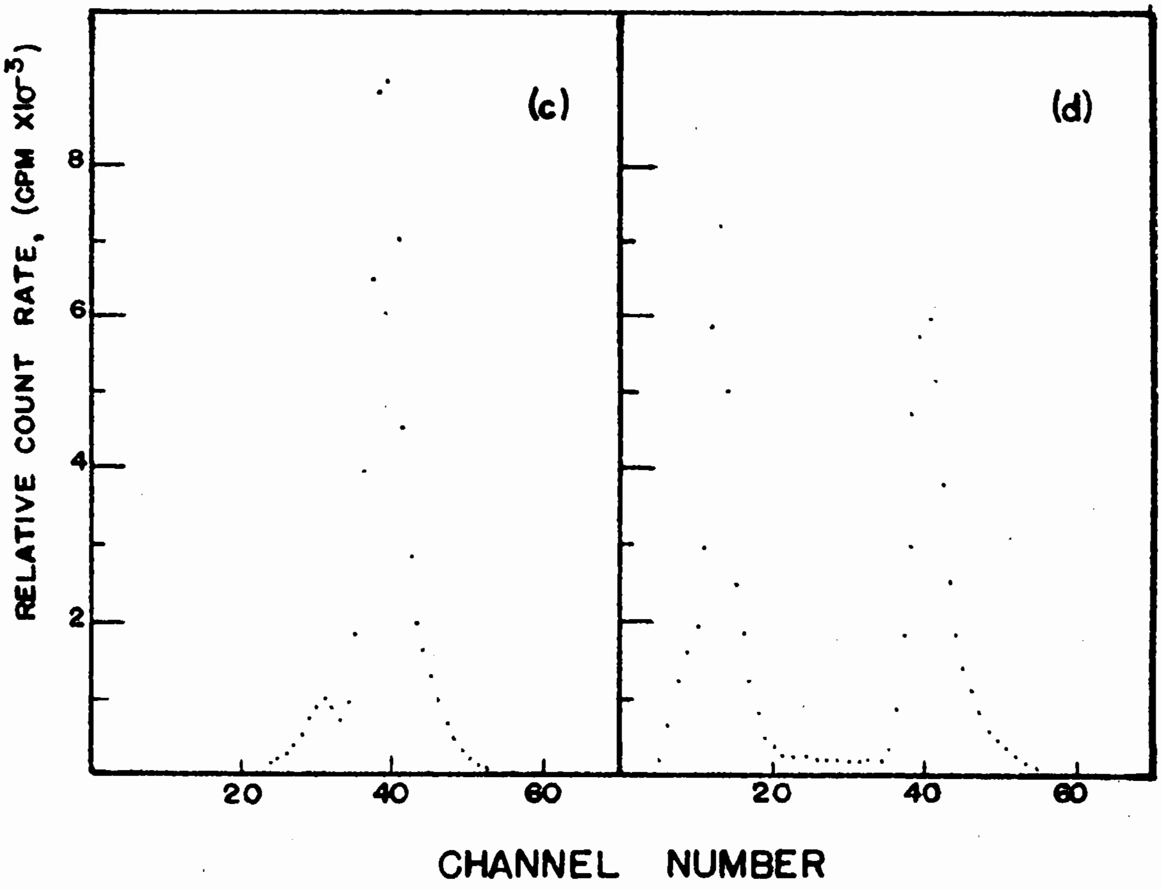
(c)
(d)
RELATIVE COUNT RATE, (CPM X10^{-3})
8
6
4
2
20
40
60
20
40
60
CHANNEL NUMBER

shown in Fig. 56 (c) and (d).

There are, at least, three different known methods of eliminating "escape peaks". They are the following.

(a) The utilization of a counter gas having a K-binding energy greater than the energy of the impinging photon.

(b) The use of a pressure high enough to absorb essentially all the X-rays resulting from the re-organization of the atom.

(c) The use of a multiwire counter such as was recently applied by Scobie et al. (197) in the determination of L/K capture ratio of Fe^{55}. This elegant method which already had incontestable applications was originally introduced by Drever et al. in 1957, (198).

Results from the application of the first method are shown in Fig. 56 where the diagrams (a) and (b) can be compared.

The second method was also attempted for different pressures of A-CH_4 (9:1). The pressures were varied from 0.3 atmospheres to 2.0 atmospheres while the X-rays were emanating from a source Co^{57} (6.4 kev). The results which are shown in Fig. 57, represent the variation of the ratio of "escape peak" to K-photopeak for various pressures.

The counter gas escape radiations were investigated for different X-ray energies. The results which are shown in Fig. 58 give the ratios of the "escape peak" to the K X-ray photopeak for energies between 4.8 kev and 20.2 kev. The counter gas was a mixture of A-CH_4 (9:1) at a pressure of one atmosphere.

Figure 57

Escape Peak to Photopeak Ratio of Co^{57} for Different Pressures.

Counter gas: A-CH_4 (9:1).

198a

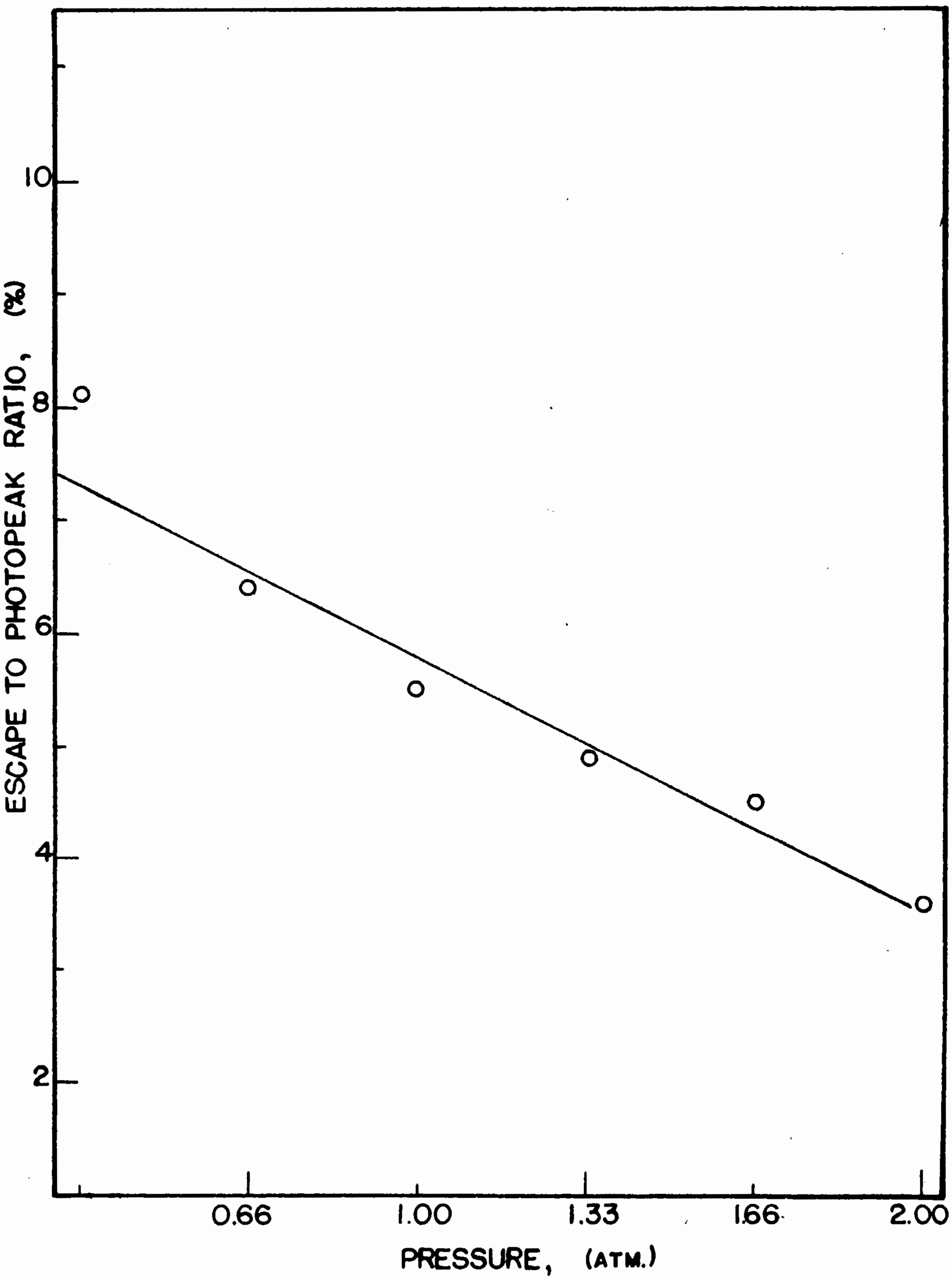

ESCAPE TO PHOTOPEAK RATIO, (%)
10
8
6
4
2
0.66
1.00
1.33
1.66
2.00
PRESSURE, (ATM.)

Figure 58

Escape Peak to Photopeak Ratio for Different X-ray Energies.

Counter gas: A-CH_4 (9:1) at one atm.

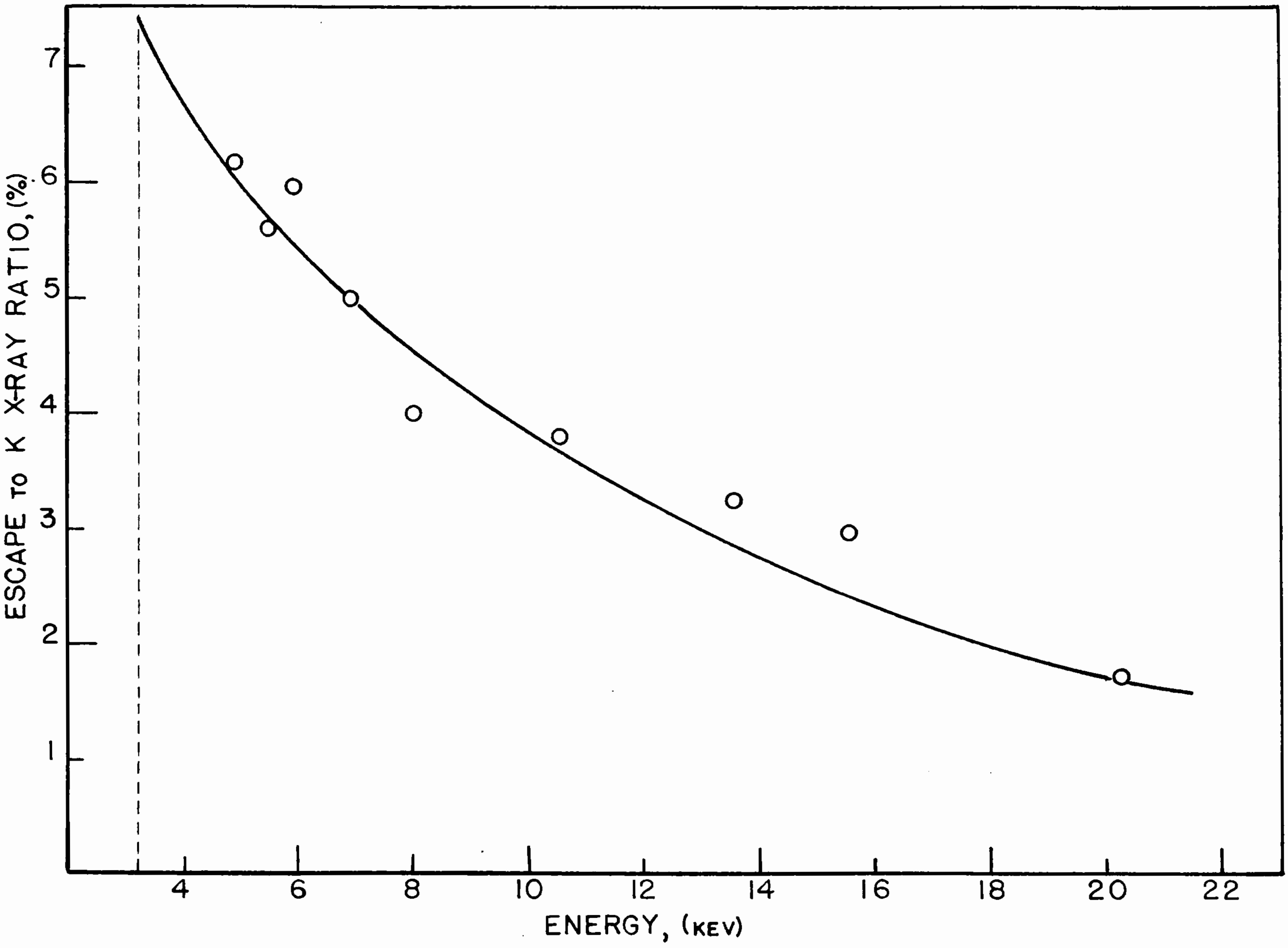
ESCAPE TO K X-RAY RATIO, (%)
7
6
5
4
3
2
1
ENERGY, (KEV)
4
6
8
10
12
14
16
18
20
22

1992

(c) Counter X-ray Efficiency

Due to the geometrical arrangement of the counter and the high power of transmission of X-rays through matter, there will be a finite probability that these X-rays will travel through the sensitive volume of the counter without producing ionization. From this phenomenon, a factor f_a which will correct for lack of total absorption of the photons in the counter will arise. To determine this factor, an average path length was derived. This was experimentally obtained when four different nuclides were used. These were: Mn^{54} (5.4 kev), Fe^{55} (5.9 kev), Co^{57} (6.4 kev), and Zn^{65} (8.0 kev). To enable the determination of these four individual path lengths the pressure of the gas, a mixture of A-CH_4 (9:1), was increased up to a value where, if the relative counting rates were plotted against the reciprocal pressures, a "plateau" occurred at high pressures. The results are shown in Fig.59 when the pressures were varied from 0.3 atmospheres to 3.0 atmospheres. The region where a "plateau" appeared was taken as total absorption of the X-rays in the counter. The idea of such plots was originally due to Allen (26) who, in 1957, published a paper in which he erroneously assumed a linear extrapolation of such curves.

From our experimental data, an average path length could be derived from the equation which relates the intensity of the incident photons, I_o, to the intensity of the transmitted

Figure 59

Relation between X-ray Counter Efficiency and Reciprocal Pressures.

Counter gas: A-CH_4 (9:1).

(Escape peak included).

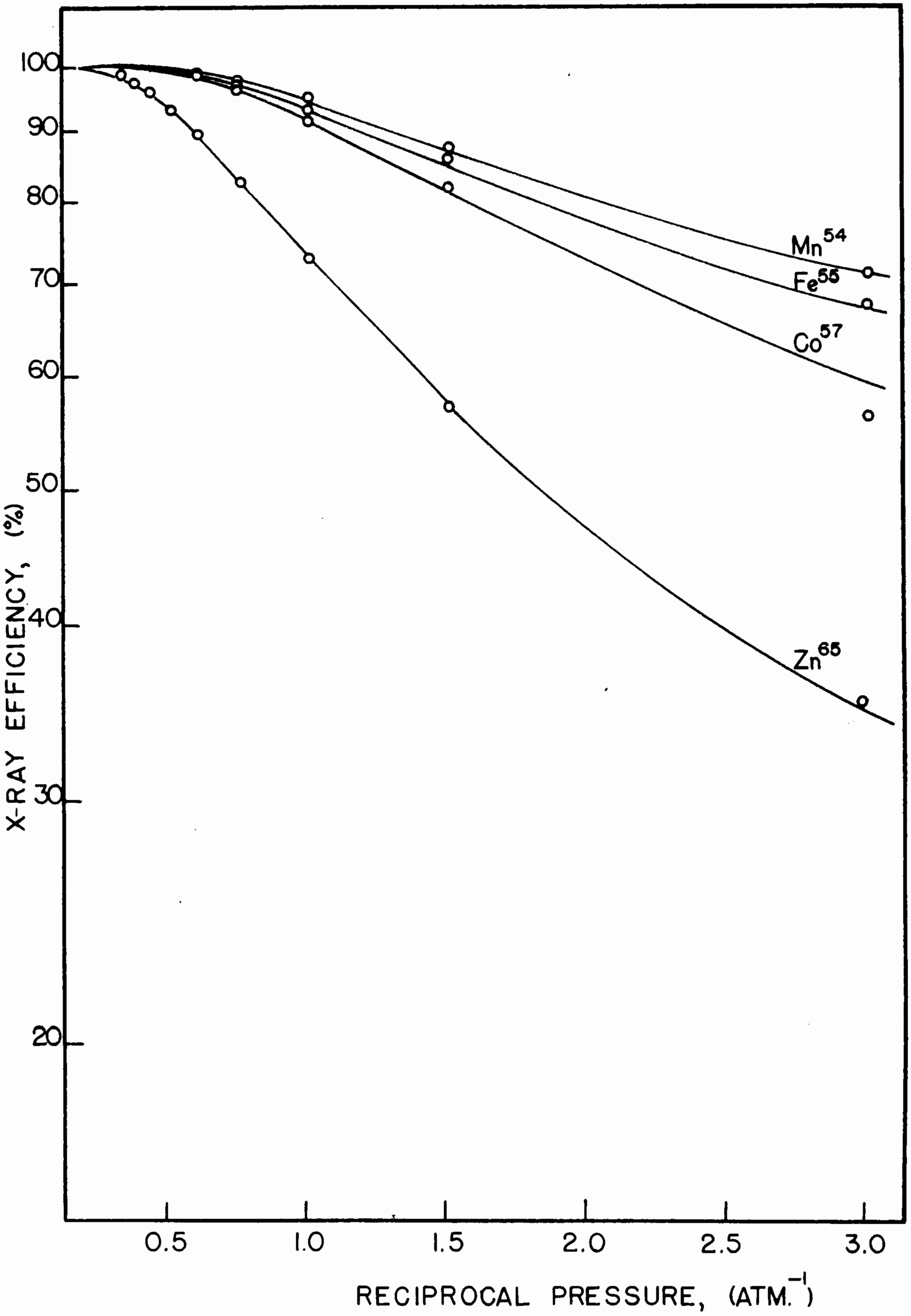
100
90
80
70
60
50
40
30
20
X-RAY EFFICIENCY, (%)
0.5
1.0
1.5
2.0
2.5
3.0
RECIPROCAL PRESSURE, (ATM.$^{-1}$)
Mn^{54}
Fe^{55}
Co^{57}
Zn^{65}

photons, I. The equation is the following.

$$I = I_o e^{-\mu t} \qquad .... (60)$$

where, μ is the linear absorption coefficient of the gas in cm^{-1}, and t, is the path length in cm. The linear absorption coefficients were obtained from reported data as shown in Appendix VI. However, since a gaseous mixture was used, a slight correction was applied for the contribution of methane. Values for μ can be obtained from the "Handbook of Chemistry and Physics" published in the 1957-58 edition.

The results of "t" which are summarized in Table X gave an average path length of 6.8 centimeters. Four of these path lengths were obtained from the plateau counting rates at total X-ray absorption while the other four were derived from integrating the counting rates beneath the K X-ray photopeak plus the escape peak.

Applying these above experimental path lengths, the efficiency of the 2π-proportional counter used as spectrometer was derived for K X-rays energies between 5 and 24 kev and this was evaluated for any pressure. When a mixture of $A-CH_4$ (9:1) was used, the results are shown in Fig. 60. The procedure was as follows: at a pressure of one atmosphere and for a particular energy between 5 and 24 kev, the area under the K X-ray photopeak plus the area under the escape peak were normalized to the

TABLE X

Average Path - Length Determination

Nuclide	t_P * cm.	t_S ** cm.	$\bar{t}$ cm.
Mn^{54}	6.18	6.05	
Fe^{55}	6.75	6.95	6.8
Co^{57}	7.35	7.10	
Zn^{65}	6.90	7.05	

* t_P = average path length based on calculations on the plateau.

** t_S = average path length based on calculations on the spectra.

Figure 60

Relation between X-ray Counter Efficiency and Reciprocal Pressures for A-CH_4 (9:1). (Escape peak included).

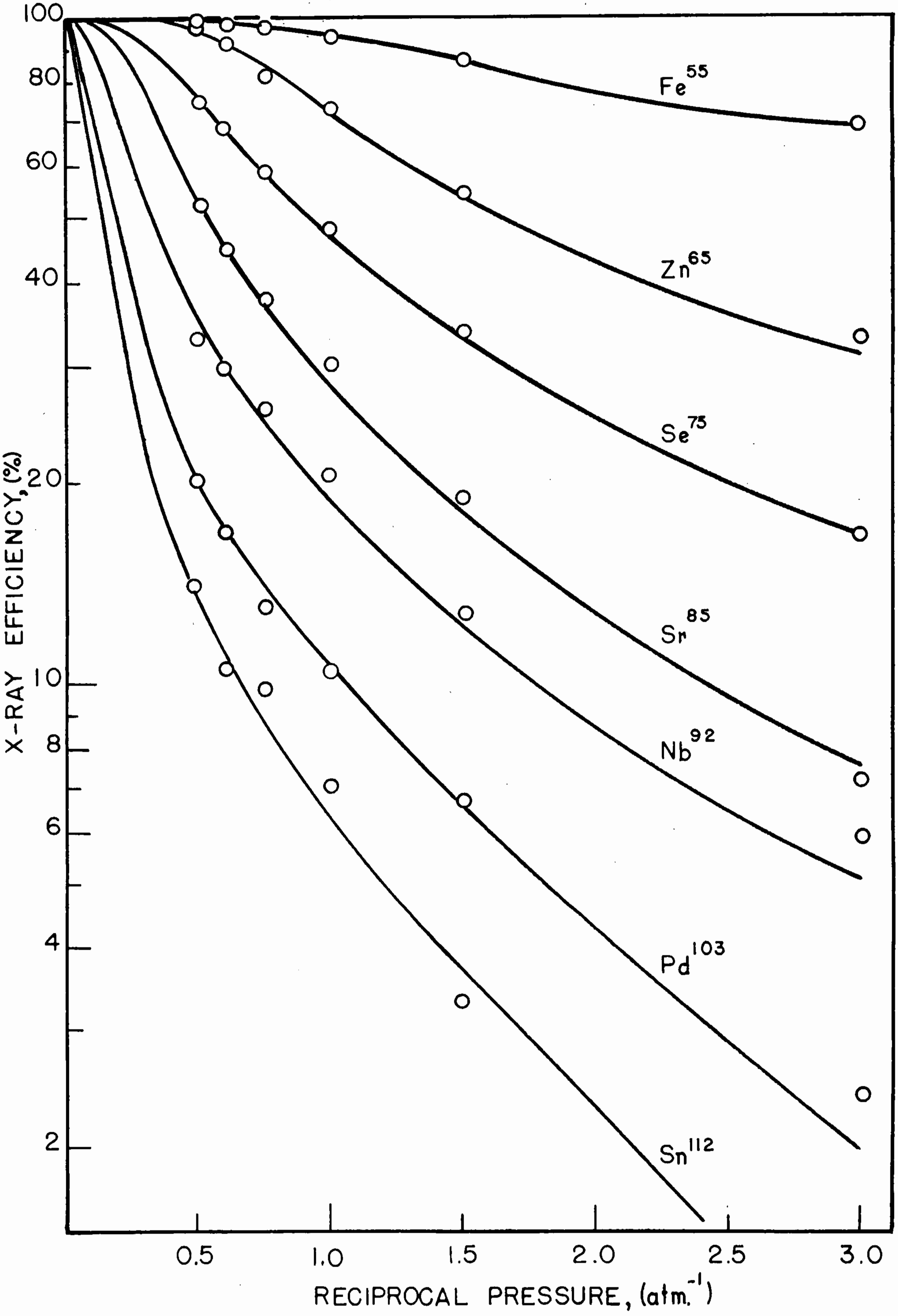
X-RAY EFFICIENCY, (%)
100
80
60
40
20
10
8
6
4
2
0.5
1.0
1.5
2.0
2.5
3.0
RECIPROCAL PRESSURE, (atm.$^{-1}$)
Fe^{55}
Zn^{65}
Se^{75}
Sr^{85}
Nb^{92}
Pd^{103}
Sn^{112}

corresponding efficiency obtained from Eq. (60). Then, the areas for various pressures were adjusted to the normalized area and plotted accordingly.

For X-ray emitters having energies greater than 14 kev., it was desirable to use a mixture of Kr-CH_4 (9:1) in order to take advantage of the enhanced absorption. The efficiencies were derived as before with the exception that the proper value for the parameter μ in Eq. (60) was applied. The result which were obtained are shown in Fig. 61.

To procure a picture of the enhanced efficiency of Kr-CH_4 (9:1) over A-CH_4 (9:1), the ratio of the X-ray efficiencies for the two counter gases as a function of the energy was experimentally derived and calculated with the help of Eq. (60). Comparisons between both results are expressed in Fig. 62.

3) DISCUSSION

To determine the disintegration rates of nuclides, ($Z < 50$), decaying by orbital capture, one will need to introduce the correction factors that were experimentally determined on the one hand and suggested from the literature on the other.

However, in the application of Eq. (59), it must be pointed out that the factor f_e which corrects for the gas escape radiations will be unity. In Figs. 60 and 61, the escape radiations were included in the K X-ray photopeak efficiencies. This was done for the two following reasons:

<u>Figure 61</u>

Relation between X-ray Counter Efficiency and Reciprocal Pressure for Kr-CH_4 (9:1).

(Escape peak included).

206a

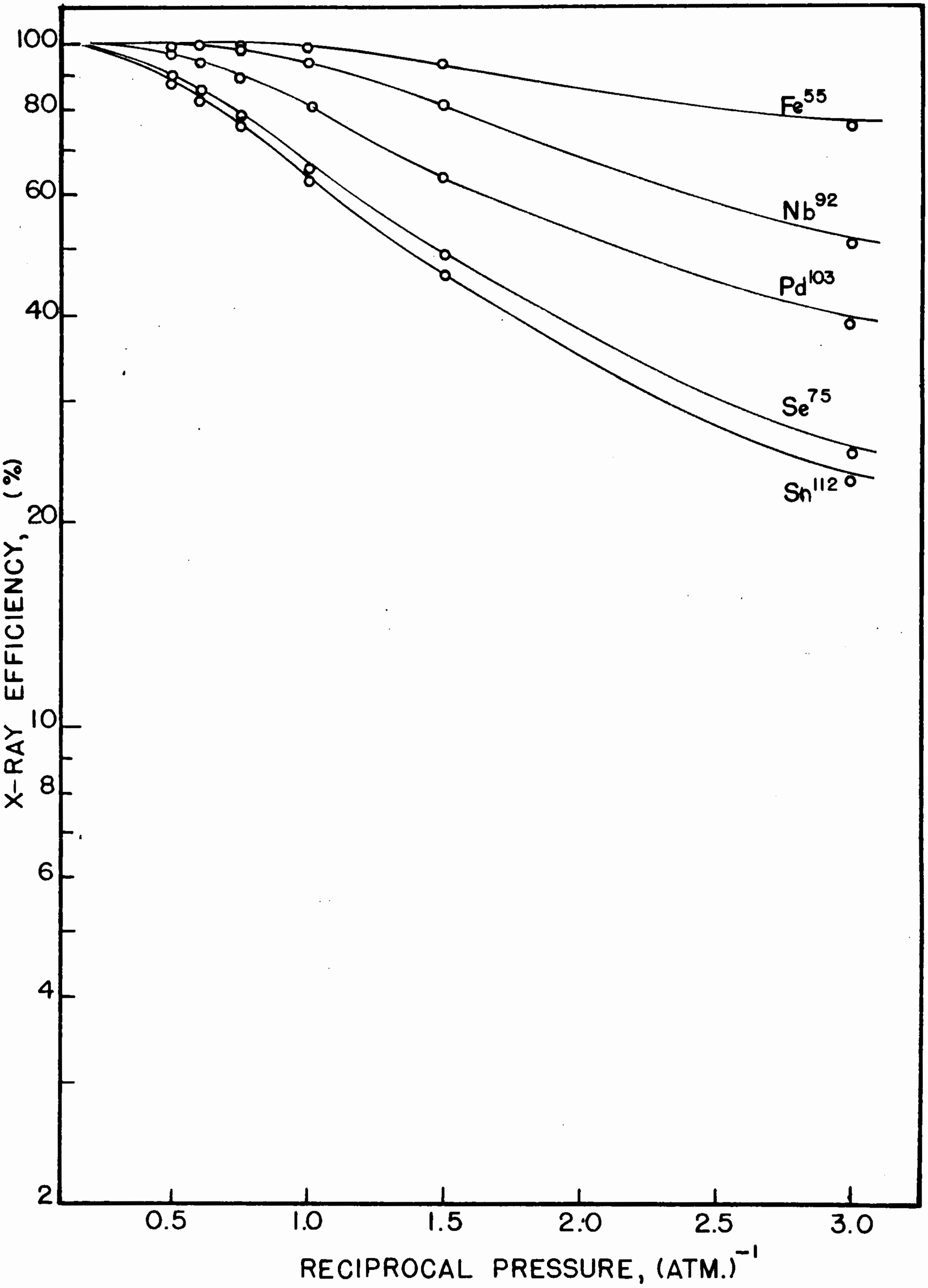

100
80
60
40
20
10
8
6
4
2
0.5
1.0
1.5
2.0
2.5
3.0
X-RAY EFFICIENCY, (%)
RECIPROCAL PRESSURE, (ATM.)⁻¹
Fe55
Nb92
Pd103
Se75
Sn112

Fig 11

Figure 62

Ratio of the X-ray Efficiencies for two Different Counter Gases for Various Energies.

○ Experimental

—— Calculated.

207a

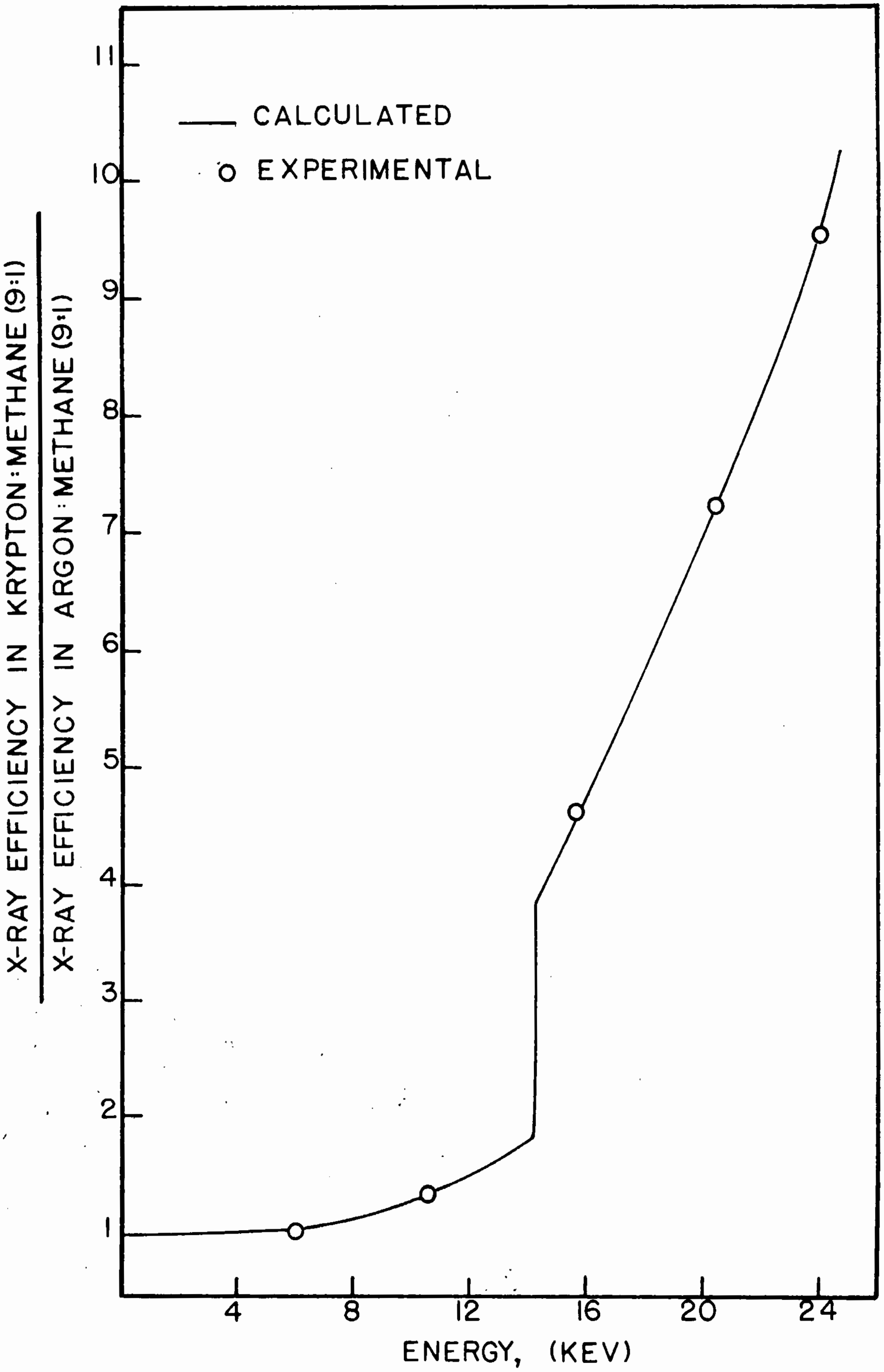
CALCULATED
EXPERIMENTAL
X-RAY EFFICIENCY IN KRYPTON:METHANE (9:1) / X-RAY EFFICIENCY IN ARGON:METHANE (9:1)
1
2
3
4
5
6
7
8
9
10
11
4
8
12
16
20
24
ENERGY, (KEV)

Fig 12

(a) Because of their dependence on pressure and energy. Otherwise, this factor would have to be evaluated using elaborate experimental methods.

(b) Because this secondary phenomenon is the result of the incomplete absorption of the K X-ray in the gas of the detector.

Then, Eq. (59) will become,

$$R = N_o.G.f_a.f_t.f_{w_K}.f_r. \qquad \ldots\ldots\ldots (61)$$

During the process of the above investigations, a report dealing with the standardization of nuclides decaying by electron capture was written by Campion and Merritt (27). These authors used an 8 in. diameter proportional counter having a 4π - geometry. It could be operated at elevated pressures, and the radioactive sources were sandwiched between aluminum foil being thick enough to screen off the Auger electrons. Standardization of Fe^{55} radionuclides was particularly successful. Using an equation similar to Eq. (51) but with the exception that the source-to-counter geometrical efficiency was unity, the overall accuracy was claimed to be ± 4.5 per cent. The K X-ray absorption efficiency was assumed to be 99.9 per cent.

Utilizing Campion and Merritt's instrument and alternatively the one which is calibrated in this thesis, a source of Fe^{55} was measured and the measurements were compared at various pressures. The results of the investigations are shown in Fig. 63 and, at pressures for total absorption of the X-rays (saturation pressures), the two detectors have shown the same efficiency. For the purpose of the experiment, the bottom part of the 4π counter was used.

According to Fig. 62, and for energies greater than the K-binding energy of krypton, (14.3 kev) a definite increase in X-ray efficiency is realized when Kr-CH_4 (9:1) is employed instead of A-CH_4 (9:1). However, on account of the relatively high value of the K-fluorescence yield for krypton (67 per cent) the probability of counter-gas escape radiations will be increased a great deal. In fact, it was experimentally found to be at least ten times greater than the escape radiations from A-CH_4 (9:1). A typical example of this increase is shown in Fig. 56 (c), and (d). When Kr-CH_4 (9:1) is used, the resulting escape peak may have a considerable nuisance value in the analysis of the X-ray spectra, so that the relatively clean results observed with A-CH_4 (9:1) are often desirable.

Figure 63

Comparison between Two Different High Pressure Counters used for X-ray Measurements from Fe^{55}.

Counter gas : $A-CH_4$ (9:1)

(a) Our Instrument.

(b) Campion-Merritt Instrument.

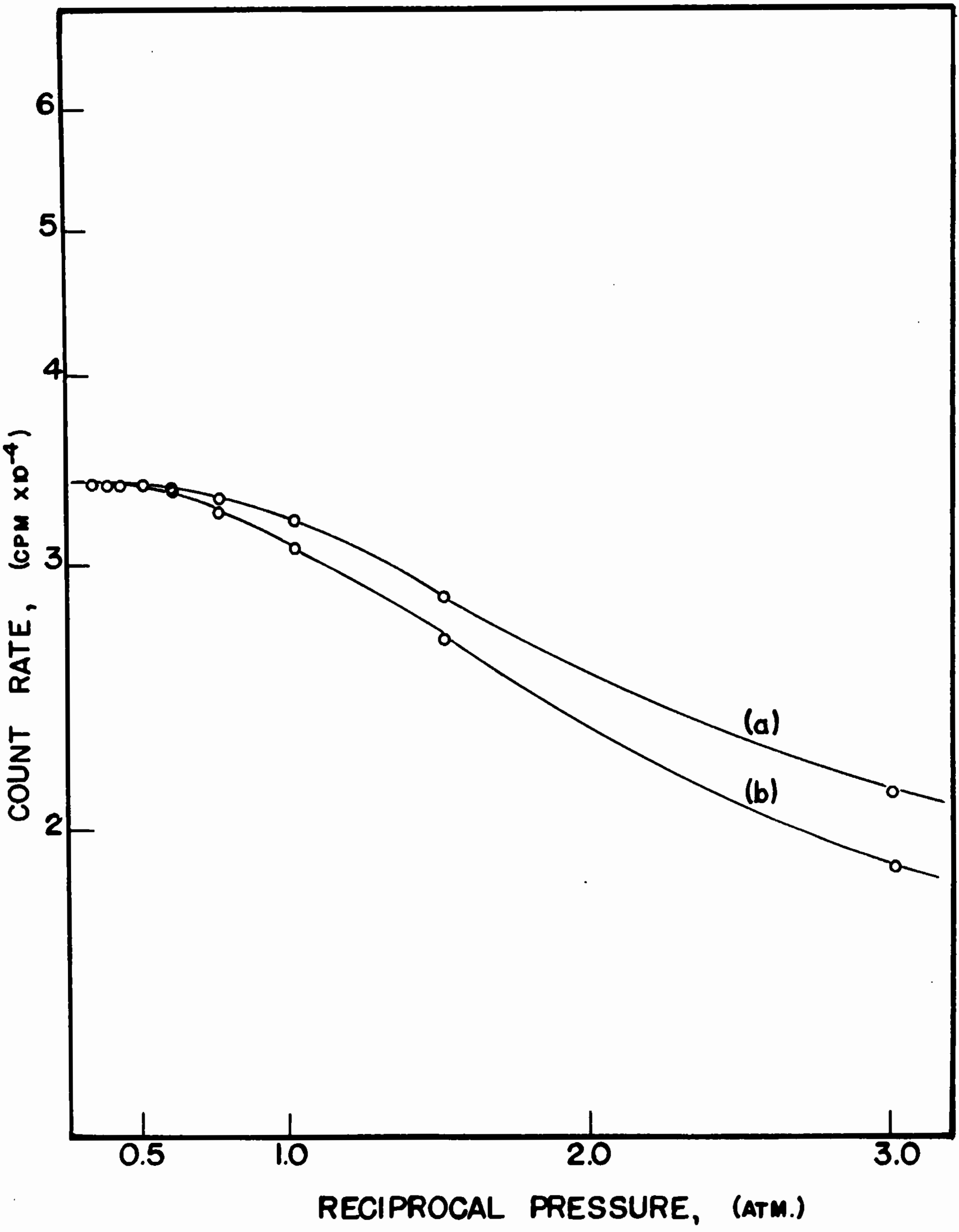
6
5
4
3
2
COUNT RATE, (CPM x 10^{-4})
0.5
1.0
2.0
3.0
RECIPROCAL PRESSURE, (ATM.)
(a)
(b)

G. SPECTROMETRIC APPLICATIONS

1) STANDARDIZATION AND HALF-LIFE DETERMINATION OF Ca^{41}

(a) Introduction

The currently accepted ideas of shell structure (199) suggest that the transition ($Ca^{41} \xrightarrow{K} K^{41}$) should be ($f_{7/2} \rightarrow d_{3/2}$), that is with a change of angular momentum of two units and with a change of parity, (-, +). The selection rules for beta decay would then predict the transition to be a first order forbidden (unique) having a value of ft of the order of 10^9 seconds.

In 1950, Richards et al. (200) measured the threshold of the reaction $K^{41}(p,n)Ca^{41}$ and have subsequently derived that the energy available for the decay of Ca^{41} by K-capture would be 0.440 ± 0.020 mev. This value was quoted by Way et al. (201) five years later. The half-life of Ca^{41} was experimentally evaluated by Brown, Hanna and Yaffe in 1953 (202). Under difficult conditions, due mainly to the presence of Ca^{45} ($t_{\frac{1}{2}}$ = 160 days) and the low specific activity of the Ca^{41} component (about 4.9 ± 0.7 counts per minute), the half-life of Ca^{41} was determined and found to be $(1.1 \pm 0.3) \times 10^5$ years.

When the aforementioned value for the transition energy and for the half-life were inserted in the nomographs published by Moszkowski (203), a value of ft of the order of 8×10^{10} seconds was derived. This value is higher than the one predicted by the selection rules derived from Fermi theory. With a view to re-examining this value, the half-life of Ca^{41} was re-measured with a sample in which the Ca^{45} had decayed to such an extent that it did not produce any interference. The disintegration rate was determined with the proportional counter described in this thesis.

In the following paragraphs, we shall give the experimental procedures that were applied and determine the disintegration rate of the radioactive Ca^{41}, thus enabling the evaluation of its half-life.

(b) Experimental and Results

(I) Irradiation

A sample of $CaCO_3$ was irradiated in the NRX nuclear reactor at Chalk River for a period of about 10 months. In Table XI the maximum fluxes and integrated fluxes are given for various time intervals which the sample was irradiated. The total integrated flux was calculated as 8.08×10^{20} neutrons/cm^2. In order to ensure complete decay of the Ca^{45} component ($t_{\frac{1}{2}}$ = 160 days), the determination of the disintegration rate of the Ca^{41} was performed about 9 years after the neutron activation.

TABLE XI

Irradiation History of $CaCO_3$

Time	Max. Flux.	Integrated Flux
days	$n/cm^2/sec.$	n/cm^2
10.20	1.8×10^{13}	1.59×10^{19}
12.166	3.2×10^{13}	3.36×10^{19}
6.366	1.84×10^{13}	1.01×10^{19}
46.63	3.82×10^{13}	15.39×10^{19}
88.80	3.87×10^{13}	29.69×10^{19}
66.466	2.79×10^{13}	16.02×10^{19}
40.966	3.87×10^{13}	13.70×10^{19}

(II) Chemical Analysis

The $CaCO_3$ target was dissolved in 0.3M HNO_3. The dried salt was re-dissolved in water and a master solution of 1 ml~~.~~ was made from it. The master solution was analyzed for calcium content through volumetric method analysis. For this purpose, a technique which is described by Welcher (204) was applied. Aliquots were diluted with distilled water to a volume of 100 mls., buffered to a pH of 11 and titrated with a solution of 0.01M EDTA (di-sodium ethylenediaminetetraacetic acid di-hydrate). The indicator used was made of 0.01 per cent solution of o-cresolphthalein complexone.

The solution of EDTA was standardized against an accurately known amount of calcium nitrate dissolved in distilled water. The results of the calibration are shown in Fig. 64.

The calcium content of the master solution was then evaluated. Two aliquots, namely 100 and 200 microliters were withdrawn from the master solution and analyzed with the standardized EDTA solution. The results shown in the bottom of Fig. 64 gave an accurate weight of 0.42 mg. of calcium per 100 microliters.

(III) Disintegration Rate Determination

A volume of 100 microliters was pipetted out from the master solution and mounted on the platform which has been shown

Figure 64

Standardization of EDTA Solution and Determination of Ca Content in the Master Solution.

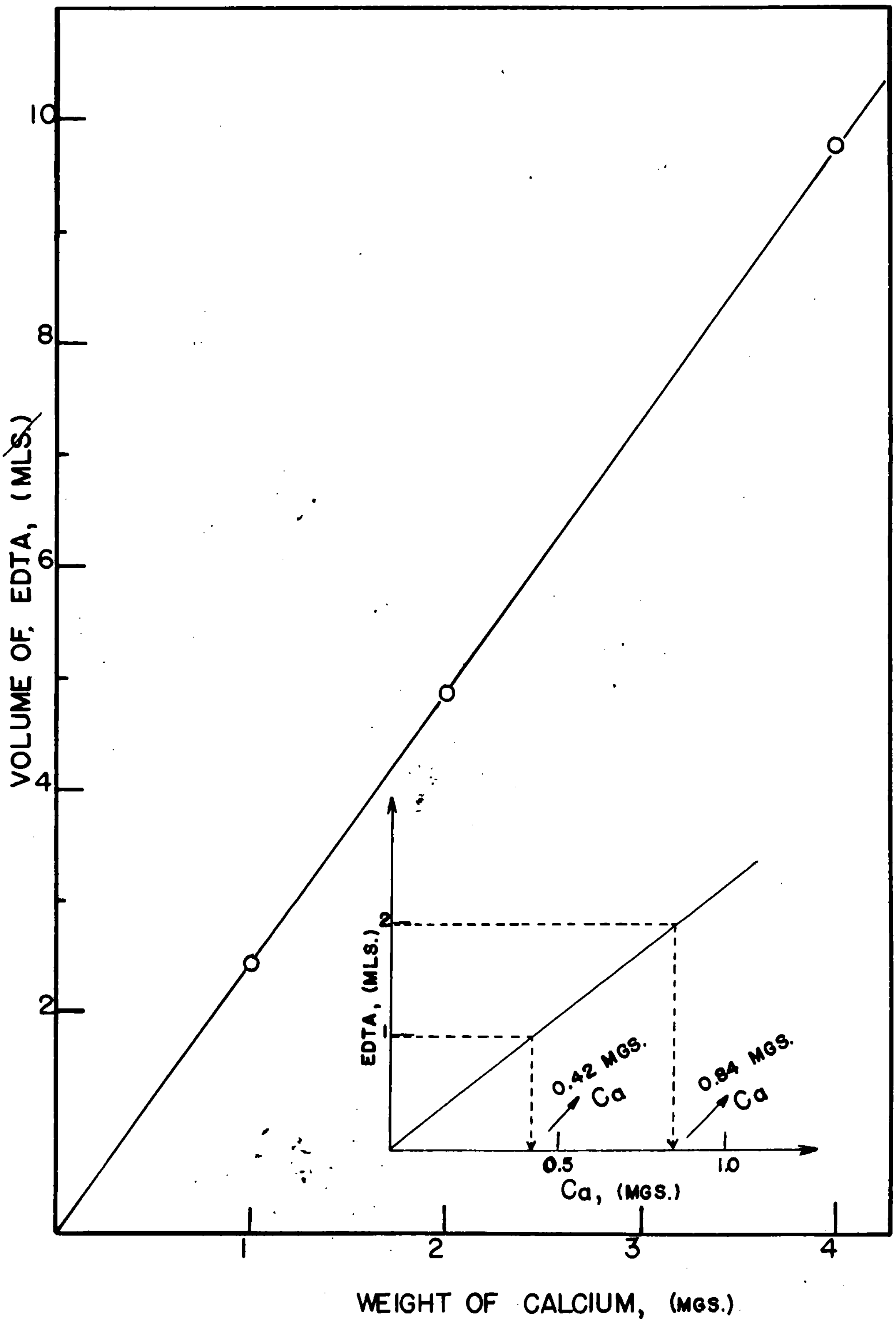
VOLUME OF, EDTA, (MLS.)
10
8
6
4
2
WEIGHT OF CALCIUM, (MGS.)
1
2
3
4
EDTA, (MLS.)
2
1
0.42 MGS. Ca
0.84 MGS. Ca
0.5
1.0
Ca, (MGS.)

in Fig. 20 and 21(a). Prior to this, the mount was treated with a solution of about 5 per cent of insulin and rinsed several times with distilled water. The aliquot of the counting solution was evaporated to dryness. During the process of evaporation, the mount was continually rocked in order to keep all parts of the area originally covered (1 cm^2) wet until the last possible moment. When the sample was dried, the radioactive source was covered with an absorber thick enough (0.8 micron of Al) to screen off all the Auger electrons emanating from the source, (see Appendix III for range of electrons in Al).

The source was placed in the counter, operated as a gas-flow system, and the characteristic K X-rays were identified when compared with various X-ray energies. The results are shown in Fig. 65.

The counting rate of the source was followed for a period of 3 hours and in Fig. 66 is shown the K X-ray photopeak resulting from the measurement. In this range of operation, the background was found to be slightly less than one count per minute per channel, and was automatically substracted by the instrument for the same period of time.

To obtain a disintegration rate, one will need to add another correction factor into the Eq. 61 which relates the counting rate to the disintegration rate. This factor which was found to be important for such low energy X-rays is due to the

Figure 65

Identification of Ca^{41} K X-rays.

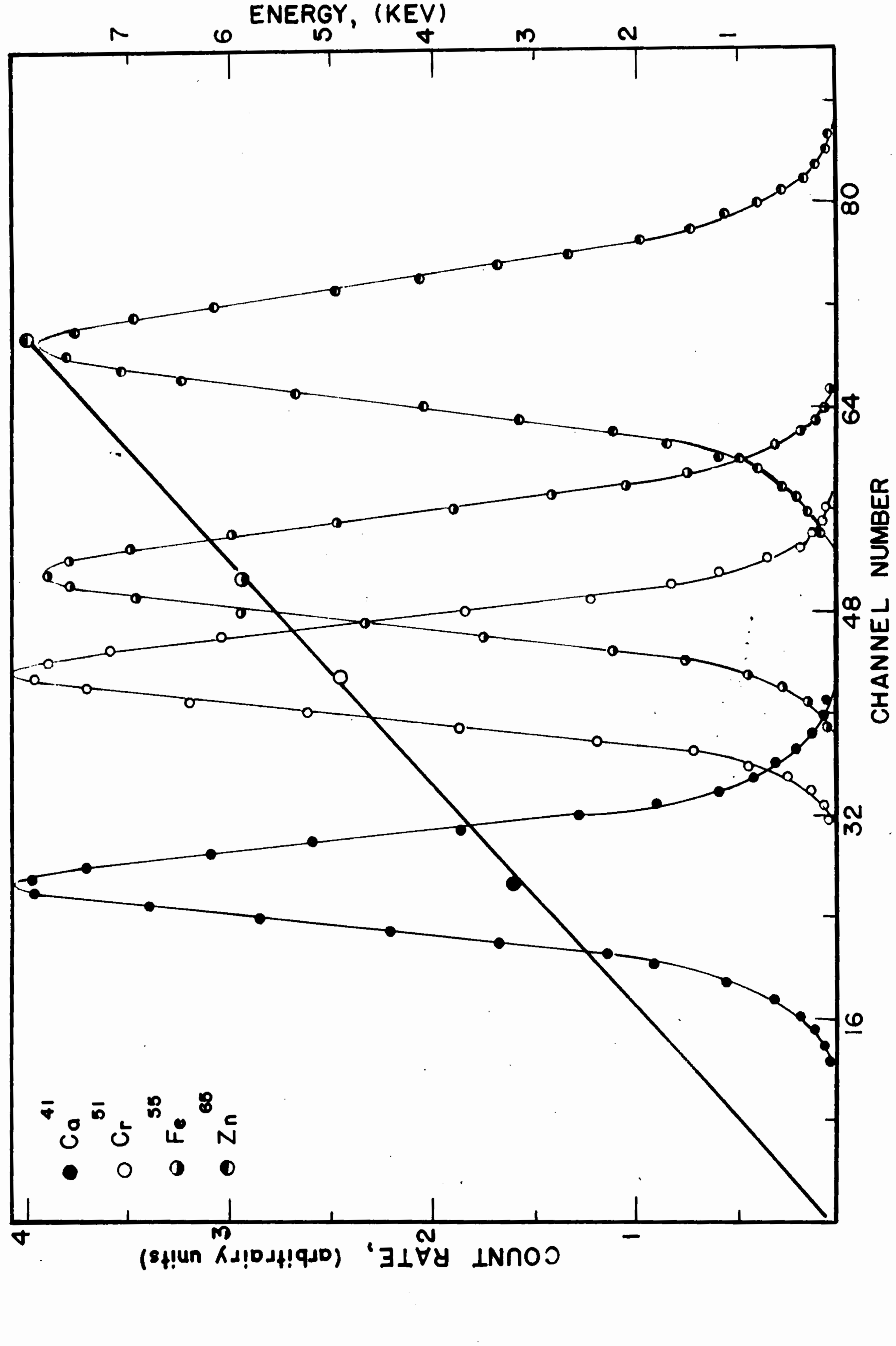
ENERGY, (KEV)
7
6
5
4
3
2
1
CHANNEL NUMBER
16
32
48
64
80
COUNT RATE, (arbitrairy units)
4
3
2
1
● Ca^{41}
○ Cr^{51}
◑ Fe^{55}
◐ Zn^{65}

<u>Figure 66</u>

Spectrum Resulting from a Source of Ca^{41}.

(K X-ray energy, 3.2 kev).

218a

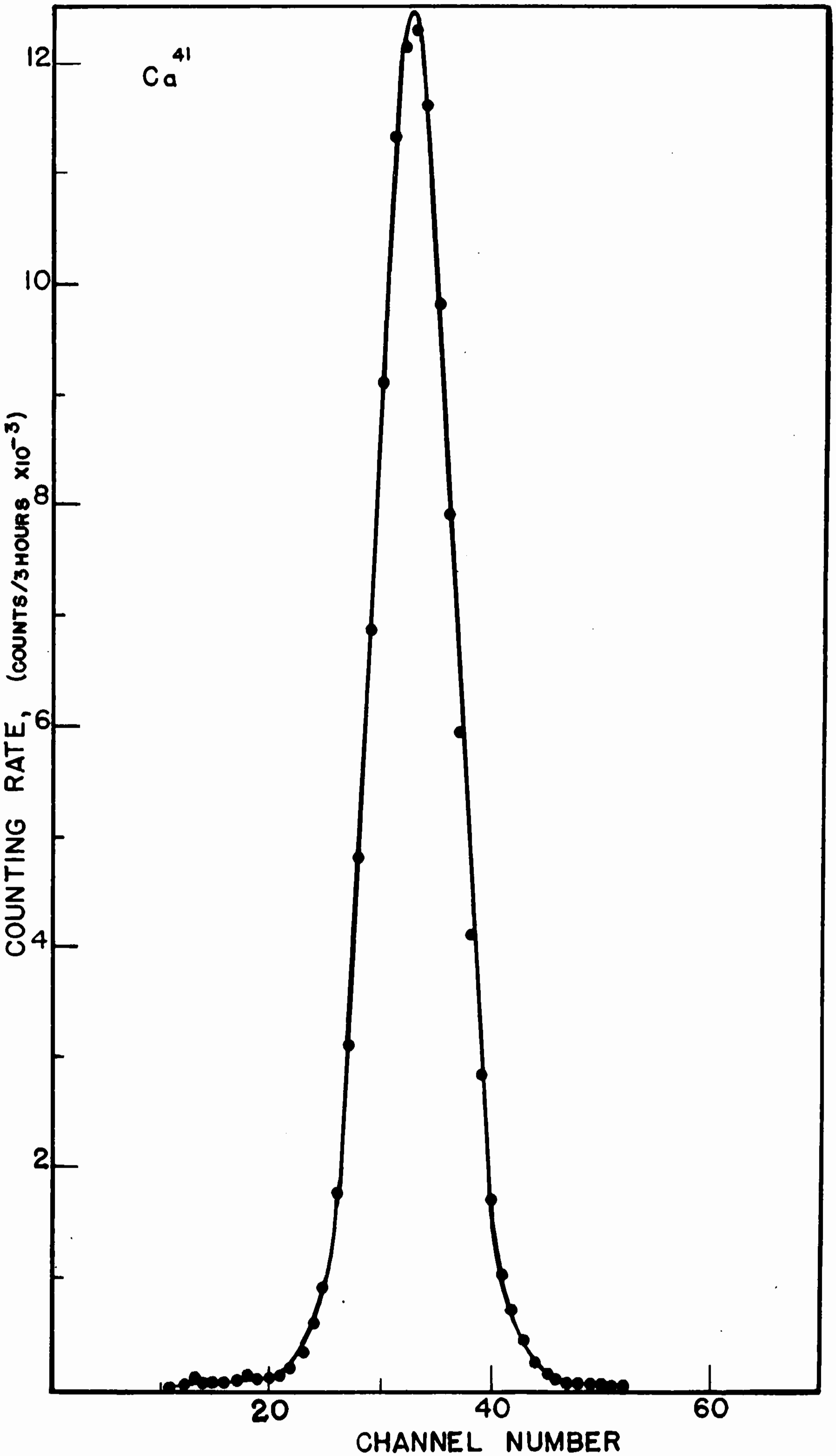

12
Ca^{41}
10
8
6
4
2
COUNTING RATE, (COUNTS/3 HOURS x10^{-3})
20
40
60
CHANNEL NUMBER

superficial density of the source, (0.42 mg.Ca/cm^2). This factor was evaluated when known amounts of an equimolar solution of inactive material were added to the source itself. For different amounts, the counting rate was determined and the results are shown in Fig. 67. From these results, one can estimate a value for the self-absorption equal to 14 per cent.

When the counter was operated at a pressure of one atmosphere and alternatively at two atmospheres, the counting rates were reproducible within the standard deviation. This implies that the factor which would correct for total absorption in the counter can be neglected.

The number of K X-rays beneath the photopeak in Fig. 66 was calculated as 594.1 counts/min. and the following correction factors were applied.

(a) Absorption of K X-rays in the Auger electron absorber. Utilizing the proper mass absorption coefficient for aluminum (see Appendix VIII), that is 600 cm^2/gr for 3.2 kev, and the equation which was derived by Campion and Merritt (27), an absorption of 33 per cent was found. If the usual equation for transmission of X-rays through matter was employed, an absorption of only 12 per cent would be found. This value assumes a collimated beam of X-rays and is definitely erroneous in this particular experiment.

Figure 67

Self-absorption Correction for 3.2 kev X-rays.
(counting rate versus superficial density).

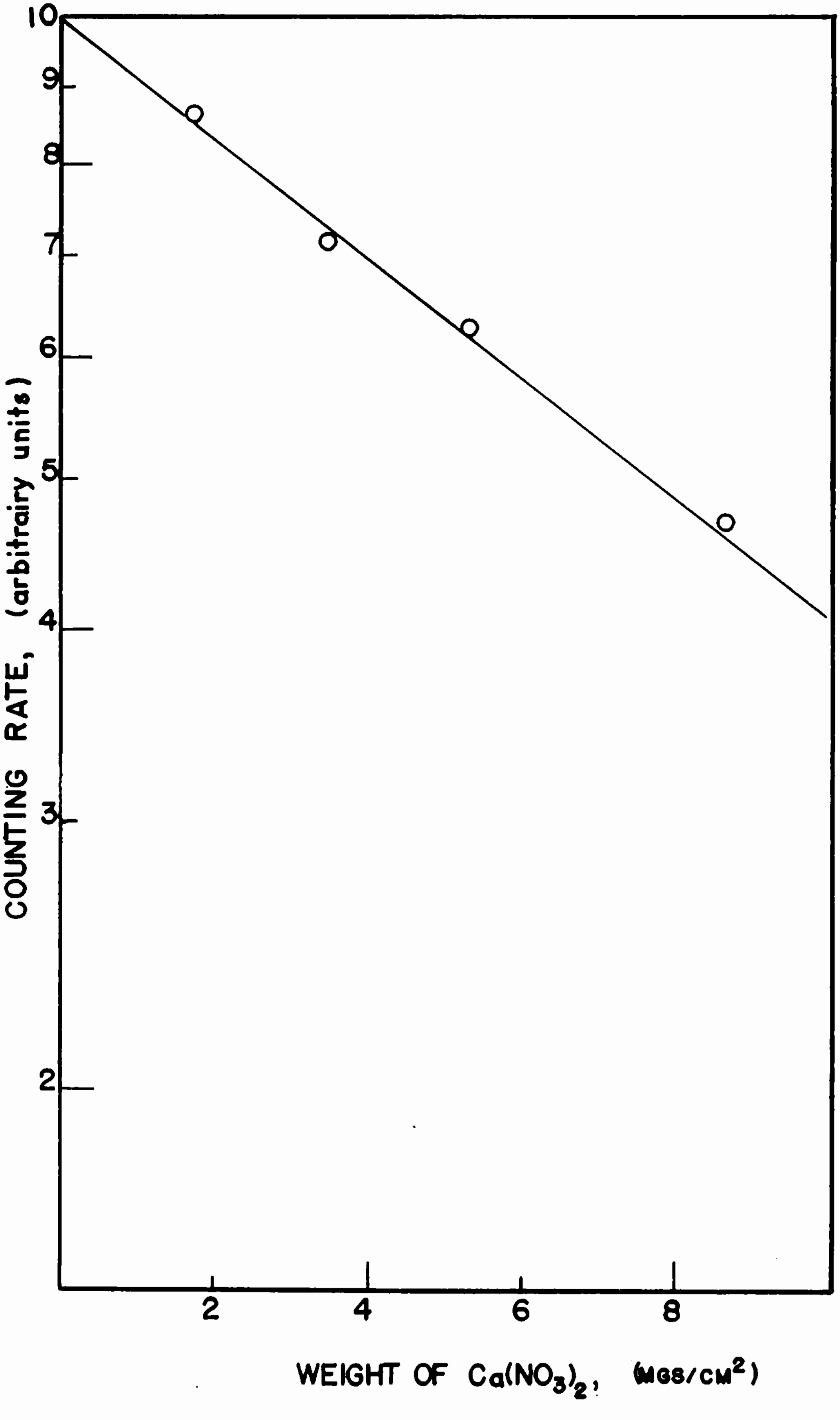
10
9
8
7
6
5
4
3
2
COUNTING RATE, (arbitrairy units)
2
4
6
8
WEIGHT OF Ca(NO3)2, (MGS/CM2)

(b) As experimentally derived, in Fig. 67, a factor due to the self-absorption must be used and the value as determined is 14 per cent.

(c) The latest, and presumably the most accurate, results of Hagedoorn and Wapstra (205) were applied for the K-fluorescence yield of calcium, ($W_K = 0.120$).

(d) Due to the forbidden nature of the transition, L_{II} and L_{III} - capture must be added to the L_I capture and from theoretical results of Brysk and Rose (51), the L/K capture ratio was 0.089.

(e) Finally, the results must be multiplied by a factor of two since the source-to-counter geometrical efficiency was already determined as 2π -steradians.

The results of the calculations are summarized in Table XII. From these, the specific disintegration rate of Ca^{41} was found to be 7.57×10^2 dps/mg.Ca.

(IV) Half-life Calculation

The specific activity was found to be 7.57×10^2 dps/mg.Ca. Contributions to the activity by other calcium isotopes (Ca^{45} and Ca^{47}) were neglected. The abundance of Ca^{40} relative to other calcium isotopes is 0.97.

TABLE XII

Disintegration Rate of Ca^{41} (0.42 mg.Ca)

K X-rays	$.594 \times 10^3$	cpm.
Al Absorber	$.886 \times 10^3$	cpm.
Self Absorption	1.031×10^3	cpm.
Auger Electrons	7.732×10^3	cpm.
K-events	8.763×10^3	dpm.
L-events	0.780×10^3	dpm.
(K+L) events	9.543×10^3	dpm.
Geometry	19.087×10^3	dpm.

Let,

N_{41} and N_{40} = number of Ca^{41} and Ca^{40} atoms.

σ = neutron cross-section for $Ca^{40}(n,\gamma)Ca^{41}$ reaction

($\sigma = 0.22 \times 10^{-24}$ cm^2. according to Pomerance (206).

(nv)t = integrated flux: 8.0763×10^{20} neutrons/cm^2.

λ = decay constant of Ca^{41}.

Therefore, since,

$$\lambda N_{41} = \frac{dN_{41}}{dt} = \text{Disintegration Rate} \quad \ldots\ldots \quad (62)$$

knowing $\frac{dN_{41}}{dt}$, one can calculate N_{41} and derive the decay constant λ from Eq. (62).

To calculate the number of Ca^{41} atoms, one can apply,

$$N_{41} = N_{40}.\sigma.(nv)t \quad \ldots\ldots\ldots \quad (63)$$

Therefore,

$$N_{41} = \frac{6.023 \times 10^{23}}{40} \times 10^{-3} \times 0.97 \times 0.22 \times 10^{-24} \times 8.076 \times 10^{20}$$

$$N_{41} = 2.59 \times 10^{15} \text{ atoms.}$$

If one uses this value in Eq. (62), then

$$\lambda \times 2.59 \times 10^{15} = 7.57 \times 10^{2}$$

therefore,

$$t_{1/2} = \frac{2.59 \times 10^{15} \times 0.693}{7.57 \times 10^{2} \times 3.65 \times 8.64 \times 10^{6}}$$

$$t_{1/2} = 7.53 \times 10^{4} \text{ years.}$$

(c) Discussion

Errors involved in the actual measurement are small, of the order of 0.3%. Other errors include neutron flux determination, the fluorescence yield value used, etc. An error of 15% is felt sufficient to cover these as well as systematic errors.

This gives a value of (7.53 ± 1.1) 10^4 years. This value is slightly lower than that found previously by Brown et al. (202) but the limits overlap.

When the value of 0.44 mev. (200) is used for the transition energy of $Ca^{41} \xrightarrow{K} K^{41}$, and also the new experimental half-life of 7.53×10^4 years, the "comparative half-life" was derived from Moszkowski's tables (203) as equal to 3×10^{10} sec. This value is in fair agreement with the value of ($\sim 10^9$) predicted by the Fermi selection rules for beta decay.

2) BETA RAY SPECTRUM FROM H^3.

(a) Introduction

As mentioned in the general introduction, the proportional counter with a coaxial geometry, is very well suited to the investigation of the beta spectra of radioelements. For this purpose very thin sources are necessary. A report on "Preparation of Thin, Uniform Sources for a Beta-ray Spectrometer" by Blanchard et al. (86) summarizes many methods. Also, one can enhance the use of this counter as a spectrometer if one uses counter gases possessing proper atomic numbers.

The first application of beta spectrometry with proportional counters was proposed by Curran et al. (115), in 1948. Thereafter, various investigators have pursued applications with the view of obtaining more refined results. In particular, Preiss et al. (207) have studied the spectrum of a "weightless" source of carrier-free Ni^{63}. A Fermi-Kurie plot applied to the spectrum was linear down to an energy of 7.5 kev, thus enabling more predictions to be made regarding the decay scheme.

Obviously, the study of beta spectra will be of interest because one can obtain from their shapes some information regarding the angular momentum change of the transition which is an important link in describing not only decay scheme but also nuclear structure.[*]

---

[*] Until late 1956, beta spectra were used in describing parity changes for certain nuclear transitions. However, Lee and Yang Phys. Rev. 104, 254, (1956) have shown that the laws of conservation of parity are violated by "weak" interactions of this type. However, this violation of parity rules does not affect the study of the spectrum of H^3 since in the old system, there is no parity change for ($H^3 \longrightarrow He^3$).

Also, a study of the shape of the spectrum gives data about a more or less unique type of nuclear interaction similar in many respects to electromagnetic processes of emission and absorption of light, that is, particles are created (or destroyed in the case of positron emission) at the instant the particle appears outside the nucleus (208). For instance,

$$n \longrightarrow p + \beta^- + \nu \qquad \text{..........} \; (64)$$

where, a nucleon in a neutron state (n) would disintegrate into a nucleon in a proton state (p).with the simultaneous creation of a pair of leptons (negatron and neutrino).

The theory of beta decay has been discussed extensively and developed by many authors (57),(208), (209), and (210). Here, we will describe it only in the following general terms.

As a basic principle, it is required that the process of beta decay be subject to the laws of conservation of energy, linear and angular momentum, statistics, and charge.

In 1933, Pauli (211) postulated an enigmatic particle, called the neutrino, which was associated with the beta decay. This assumption could explain the continuous energy distribution of the beta particles and hence the nucleons were existing in well-defined energy levels within the nucleus.

This strange particle (ν) which served to carry off the excess energy and to conserve spin of the reacting system of the nucleus and the beta particle was observed in 1953 by Reines and Cowan (212).

So, to have conservation of energy, momentum and spin, there must be an interaction between the beta particle and the neutrino.

In 1934, Fermi (57) expressed the intensity of emission of a given beta particle at a given energy, E, for allowed transitions by considering the distribution of the energy of the particles in phase space. The probability N(E) of the emission of an electron with energy E between E and dE was found to be:

$$N(E)dE = C\left(F(E,Z).(E_o - E)^2.(E^2 - 1)^{1/2}E\right)dE \quad \ldots\ldots\ldots \quad (65)$$

where,

C = constant.

F(E,Z) = correction for the Coulombic interaction of beta particles and the fields of the nucleus and electron clouds.

E_o = total energy of the transition in units of m_oc^2.

Z = charge of the product nucleus.

From Eq. (65), it is obvious that the probability of emission will approach zero for very low or very high values of E.

The constant C is given by,

$$C = \frac{g^2.m_o^5.c^4}{2\pi^3.h^7} \; . \; |M|^2 \quad \ldots\ldots\ldots \quad (66)$$

where g, is a universal constant equal to 4×10^{-50} cm^3/erg, h is Planck's constant, m_o is the rest mass of the electron and $|M|^2$, is the nuclear matrix element whose form is not known, but is essentially constant for a given system. Five forms of $|M|^2$ are consistent with the theory. These are: scalar, vector, tensor, axial-vector and pseudoscalar. All, but the scalar and axial vector interaction are of negligible magnitude.

From Eq. (65), converting the energy E into units of momentum (p) we get,

$$N(p)dp = C.p^2.(E_o - E)^2.F(Z,p)dp \qquad \ldots\ldots\ldots (67)$$

It is assumed that C and F(Z,p) are constant for a given value of Z and given daughter nucleus; therefore substituting a third constant, G, called the "coupling constant for beta decay", for these terms,

$$N(p) = G.p^2.(E_o - E)^2 \qquad \ldots\ldots\ldots\ldots (68)$$

or in the more commonly used form,

$$(E_o - E) = \left(\frac{N(p)}{p^2.G}\right)^{1/2} = \left(\frac{N(p)}{f}\right)^{1/2} \qquad \ldots\ldots\ldots\ldots (69)$$

In practice, values of G are calculated as functions of $(p)^2$, and their product is represented by f which is the so-called "Fermi Function".

Experimentally, it is almost impossible to determine E_o of the beta particles from a beta spectrum. This is mainly due to the infinitely small mass of the neutrino and the experimental conditions, i.e., the finite resolution energy of the instrument. To overcome this difficulty, by plotting $\left(\frac{N(p)}{f}\right)^{1/2}$ against energy, one can obtain a straight line for allowed transitions, so that extrapolation of this line to the energy axis will intercept values equal to E_o.

The selection rules are related to the "comparative half-life", (ft). This is a means of expressing half-life in a system comparable for all decays, since "f" converts the observed half-life by correcting for nuclear charge and energy effects. The product ft is defined as $f(Z,E_o).t_{1/2}$ where,

$f(Z,E_o)$ = time probability of the decay or the so-called "Fermi Function" f.

$t_{1/2}$ = observed half-life in seconds which is related to the interaction matrix $|M|^2$, through the mean life τ defined as (57).

$$\lambda = \frac{1}{\tau} = C.|M|^2.f(Z,E_o) \qquad \text{.........} (70)$$

where λ is the decay constant of the transition.

Since it can be shown that,

$$t_{1/2} = \frac{0.693}{|M|^2.f(Z,E_o)} \qquad \text{........} (71)$$

we may write

$$ft = \frac{0.693}{|M|^2} = \frac{\text{constant}}{|M|^2}$$

Usually, it is more convenient to speak of log(ft) rather than ft itself since these values are relatively large and generally change by factors of ten from one type of transition to another, (i.e., log(ft) for allowed transitions has values from 3 to 6 and for first forbidden, 6 to 8, etc.) (210).

(b) Experimental Technique and Results

Some dried tritiated benzidine was dissolved in absolute ethanol. The activity of the solution was about 4×10^3 cpm per microliter. Twenty microliters were withdrawn from the stock solution and mounted on a saturation thickness aluminum backscatterer. The use of ethanol as solvent allowed a very thin source to be mounted. This sample was then placed under the beryllium window counter.

With a gas multiplication factor of about 10^4 and the counter operated as a flow-gas system, the beta-ray spectrum of H^3 was obtained by pulse height analysis. The results are shown in Fig. 68. The energy calibration was made by using the beryllium window with the following external radioactive sources: Fe^{55} (5.9 kev), Zn^{65} (8 kev), Sr^{85} (13.4 kev), and Pd^{103} (20.2 kev). The background was automatically substracted by the pulse height analyzer

The appropriate tables were used to evaluate the Fermi functions (213), and the "Fermi-Kurie" plot was obtained from

Figure 68

Beta Spectrum of Tritiated Benzidine.

(background substracted).

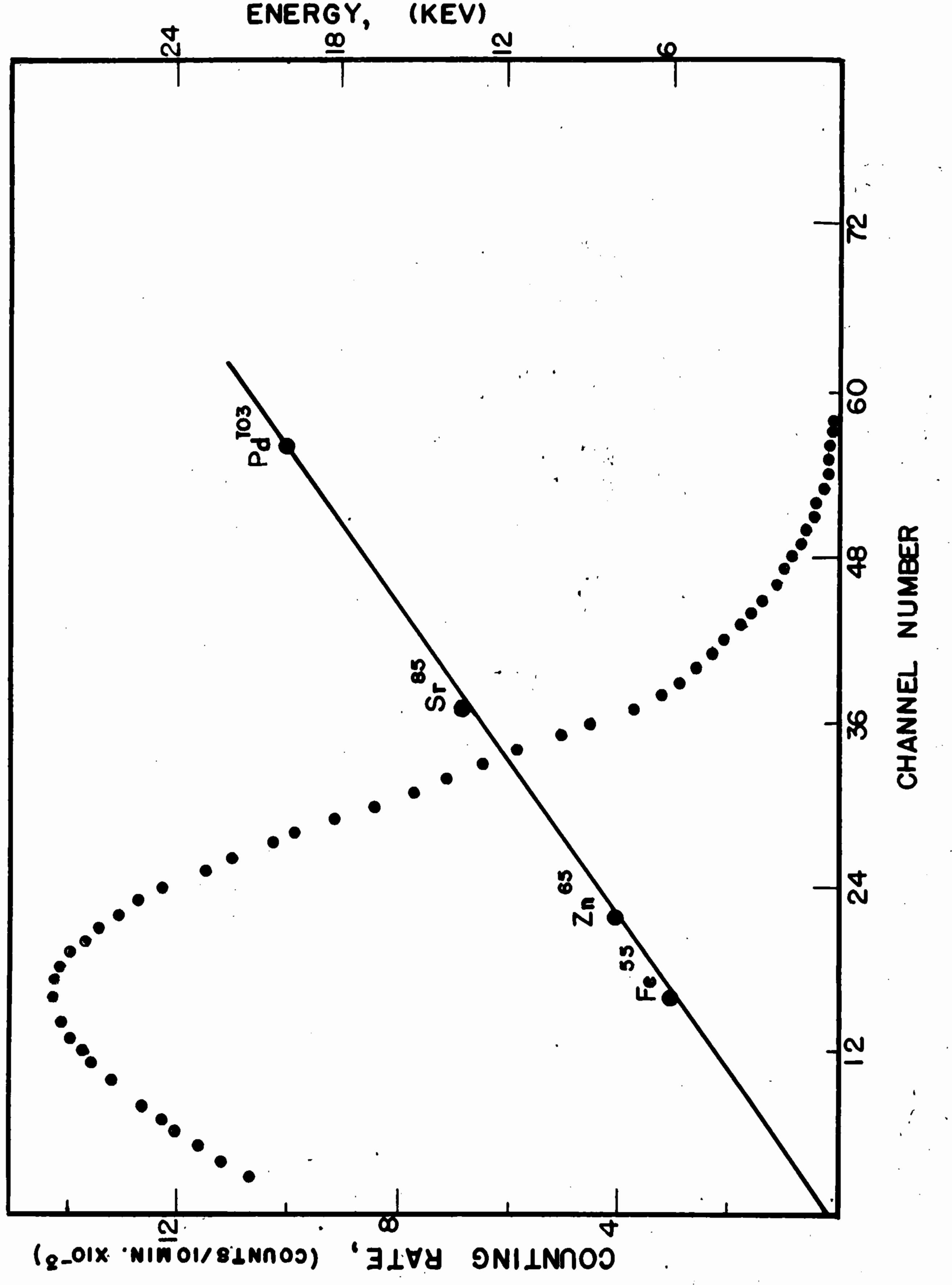
ENERGY, (KEV)
24
18
12
6
Pd^{103}
Sr^{85}
Zn^{65}
Fe^{55}
12
24
36
48
60
72
CHANNEL NUMBER
12
8
4
COUNTING RATE, (COUNTS/10 MIN. x10^{-3})

the beta spectrum. The plot of $\left(N(p)/f(p)\right)^{1/2}$ versus E (in kev) was constructed according to the results shown in Fig. 69. The plot was linear to a lower limit of about 3 kev and exhibited an endpoint energy of 18.2 kev. This result is consistent with the value of 18.0 kev which was found by Curran et al. (214).

(c) Discussion

The experimental energy transition of 18.2 kev and the half-life of 12.4 years (214) enabled us to make precise evaluation of the "comparative half-life" of the $(H^3 \xrightarrow{\beta} He^3)$ transition. The result from the calculations of ft* gave a "comparative half-life" of 1.08×10^3 seconds or log ft = 3.03. According to the selection rules for beta decay, this transition should be "super allowed". This is in agreement with the experimental "Fermi-Kurie" plot which was found to be linear in energy to energies down to 3 kev. Likewise, the nuclear shell model would predict a transition with no change of angular momentum and conservation of parity.

A theory of Owen and Primakoff (215) which demonstrates that the measured spectrum N(E) should be corrected to give the implied "true" spectrum M(E) was applied to the beta spectrum of

---

* The value of "f" was calculated from equation A6 and A7 given by E. Feenberg and G. Trigg in Rev. Mod. Phys. 22, 404, (1950).

Figure 69

"Fermi-Kurie" Plot from the Beta Spectrum of Tritiated Benzidine.

Maximum Energy, E_o = 18.2 ± 0.4 kev.

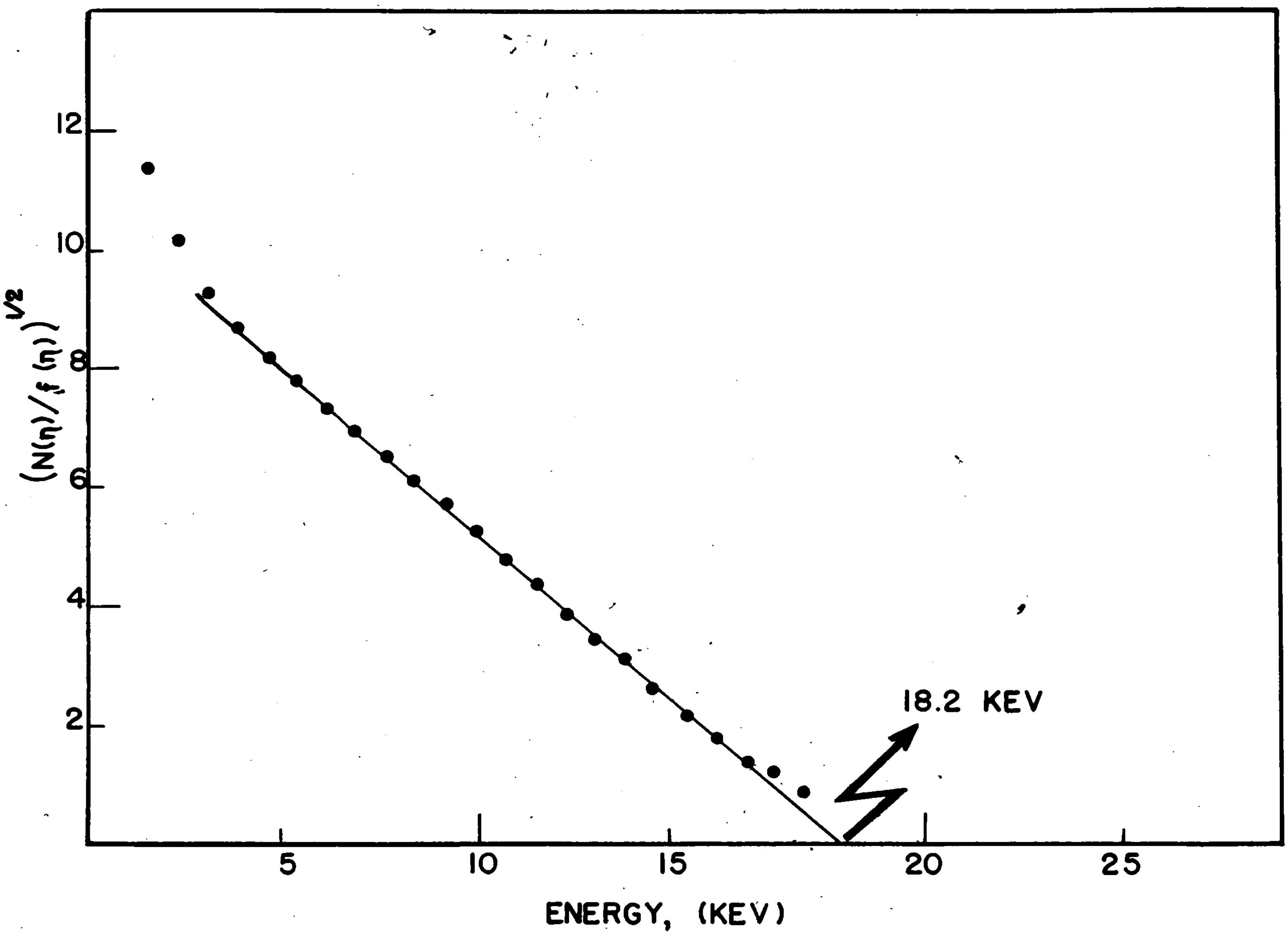
12
10
8
6
4
2
$(N(\eta)/f(\eta))^{1/2}$
5
10
15
20
25
ENERGY, (KEV)
18.2 KEV

H^3. The equation which would correct for this, is the following,

$$M(E) = N(E) - c.E_o. \frac{dN(E)}{dE} - \frac{g^2}{4} . \frac{d^2N(E)}{dE^2} \qquad \text{........} \ (72)$$

where,

c = full width a half maximum which was already investigated in part E of this thesis. (see Fig. 55a, where $2.36 \frac{\sigma_P}{P} = c$)

E_o = endpoint energy.

The second derivative term is usually considered as negligible, (216).

No significant effect on the spectral shape and endpoint energy were encountered when Eq. (72) was applied. The data, in Fig. 68, therefore were not corrected for changing resolution.

Further analysis of beta ray spectra were made with sources of Ni^{63}, and C^{14}, but the spectral shape were distorted in the low energy region. This distortion can probably be ascribedto the problems of self-absorption in the mounted sources.

For an allowed spectral shape, the "Fermi-Kurie" plot will be sensitive to slight deviations. From the spectrum obtained in Fig. 68, one can conclude that there was no marked backscattering effect leading to distortions. This is in agreement with the results on monoenergetic electron scattering presented by Schonland (217) who showed that the magnitude of saturation backscattering of monoenergetic electrons was independent of energy below 90 kev.

H. MISCELLANEOUS RESULTS

1) INTERNAL BREMSSTRAHLUNG PHOTON FROM Fe^{55}

(a) Introduction

As previously discussed, an element decaying by orbital electron capture to the ground state of the daughter element is principally detected by the characteristic X-rays or Auger electrons of the daughter element. There are, however, in addition an undetectable neutrino and a weak (in intensity) but detectable X-ray continuous spectrum. The origin of the latter is due to the sudden change of charge from atom to nucleus. This continuum was first investigated theoretically by Morrison and Schiff (67). It is analogous to the continuum accompanying beta decay (218), (219). In the former case, the spectrum extends to the transition energy E_o minus the energy obtained from a K-electron, (E_K), while in the latter, it extends up to the maximum energy of the beta particles.

By the use of highly simplifying assumptions, i.e., considering only K capture from allowed transitions, a spectrum from magnetic dipole radiations only, and neglecting Coulomb effects, Morrison and Schiff have derived a theoretical spectrum of the form $x(1 - x)^2$ where $x = E/E_{max}$. Later, Jaunch (220) extended the theoretical investigation with minor revisions.

The ratio of the total number of bremsstrahlung photons $N(E_\gamma)$ to the number of K-capture events N(K) was given for ls capture by the following relation (67),

$$\int_0^{E_{max}} \frac{N(E_\gamma)\, dE}{N(K)} = \frac{\alpha}{12\pi} \cdot \left(\frac{E_o - E_K}{m_o c^2} \right)^2 \qquad \ldots\ldots\ldots (73)$$

where $(E_o - E_K)$ is the available energy, $m_o c^2$ is the energy of the mass of an electron at rest, and α the usual fine structure constant.

From this relation, the ratio will be roughly proportional to $(E_o - E_K)^2$; therefore, it is easier to detect the bremsstrahlung from an electron capture process of high transition energy value.

However, experimental investigations (74), (221), (222), on the distribution of internal bremsstrahlung photons from electron capture processes have shown that the aforementioned calculations were not quite adequate in interpreting the low-energy region of the distribution. From these experimental pieces of evidence, Martin and Glauber (71) have reconsidered the Morrison-Schiff theory taking into consideration (a) both magnetic and electric radiations, (b) both s- and p-electron capture, and (c) all effects of the Coulomb field. In the low energy region, they have demonstrated that the electric dipole radiation accompanying the capture of p-electrons is primarily responsible for the large intensity increase. The processes of interest combine both radiation and capture; that is, an electron initially in an s or a p-state will ordinarily emit a photon during a virtual transition to an s-state from which it is subsequently captured by the nucleus. However, the virtual transitions to s-states already occupied in the atom are forbidden by the Pauli principle. Nevertheless, in their equation dealing with the summations over intermediate states, they have shown that the absence of these terms was compensated for by the occurrence of transitions in which the capture of an electron from an occupied state precedes the radiative transition.

In particular, the internal bremsstrahlung photons from Fe^{55} were studied with some precision, in 1954, by Madanski and Rasetti (74). At that time, the Martin-Glauber theory was not known and therefore, no comparison could be made. We have attempted to repeat the experiment and compare the results with both theories, namely Martin-Glauber and Morrison-Schiff. Also, a determination of the disintegration rate of the source and a determination of the absolute number of internal bremsstrahlung photons enabled us to compare the results with Eq. (73).

(b) Experimental Techniques and Results.

First of all a 3 in. by 3 in. NaI(Tl) crystal which was calibrated* for the absolute measurement of gamma rays having energies between 0.030 mev and 1.40 mev was utilized. Then, the crystal was calibrated for energy linearity and energy resolution. The results for various gamma-ray energies are shown in Fig. 70 (a) and (b). Also a correction must be applied to the continuous spectrum to correct for the iodine escape radiations. Experimental and theoretical data which are reported in Fig. 70 (c) were obtained from McGowan (223) and Axel (224).

The second part of the experimental work consisted in encapsulating an aqueous solution (2 mls.) of $Fe^{55}Cl_3$ in one of the standard vials which are normally used in this laboratory for the measurement of gamma rays. By means of the proportional counter, which was calibrated for standardization of nuclides decaying by orbital capture, the total activity of the solution was determined and found to be 2.28×10^8 disintegrations per minute. The vial containing the radioactive Fe^{55} nuclides was placed on the crystal and the energy distribution of the photons was recorded for a period of 60 minutes. The spectrum which was obtained, is expressed in Fig. 71 where the background has been automatically substracted.

---

* Calibrations of the crystal for total efficiency were made by G.R. Grant, G.V.S. Rayudu and M. May from this laboratory, (see Appendix VIII).

Figure 70

(a) Energy Calibration for Various Energies.

(b) Instrumental Resolving Power for Various Energies.

(c) Ratio of Iodine Escape Peak to Gamma-Ray Photopeak for Various Energies.

—— Theoretical, (224)

○ Experimental, (223)

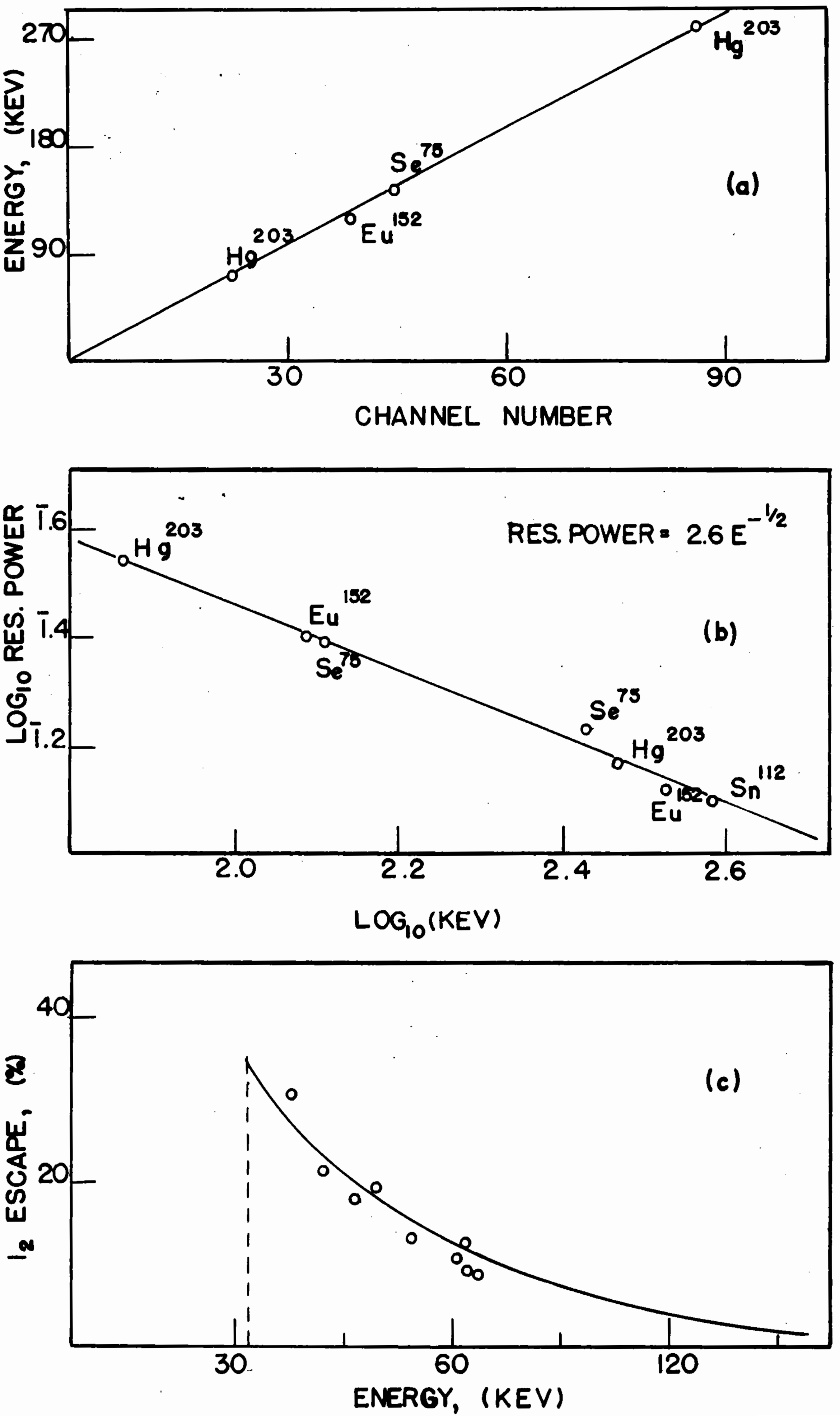
ENERGY, (KEV)
270
180
90
Hg^{203}
Se^{75}
Eu^{152}
Hg^{203}
(a)
30
60
90
CHANNEL NUMBER
LOG$_{10}$ RES. POWER
$\bar{1}$.6
$\bar{1}$.4
$\bar{1}$.2
RES. POWER = 2.6 E$^{-1/2}$
Hg^{203}
Eu^{152}
Se^{75}
Se^{75}
Hg^{203}
Sn^{112}
Eu^{152}
(b)
2.0
2.2
2.4
2.6
LOG$_{10}$(KEV)
I$_2$ ESCAPE, (%)
40
20
(c)
30
60
120
ENERGY, (KEV)

<u>Figure 71</u>

Continuous Photon Spectrum from Fe^{55}.

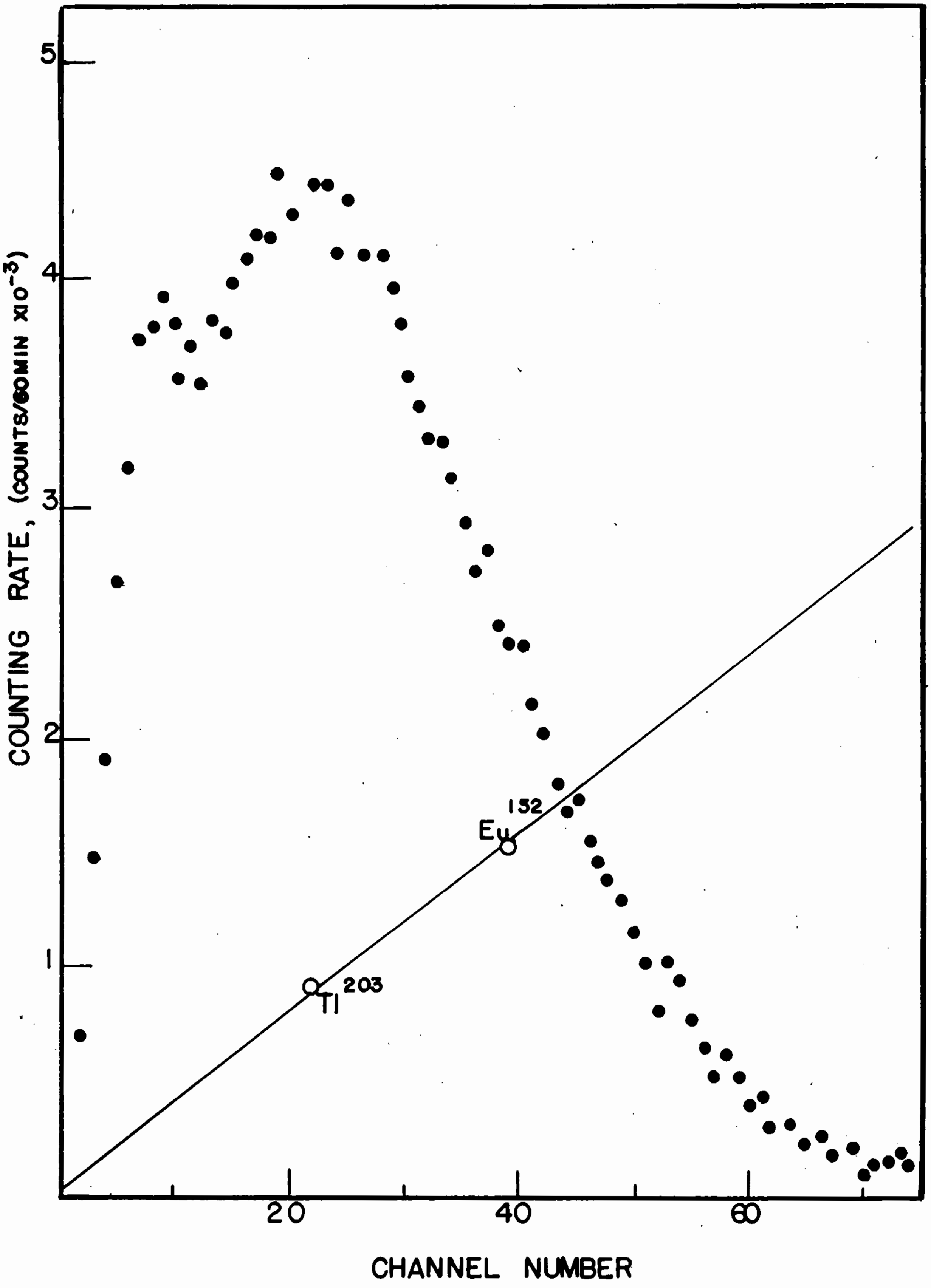
COUNTING RATE, (COUNTS/60MIN X10^-3)
5
4
3
2
1
20
40
60
CHANNEL NUMBER
Eu 152
Tl 203

An inspection of the continuous spectrum shown in Fig. 71 and of Eq. (73) shows the similarity to the relation for the beta-ray distribution given by Fermi theory. When the experimental distribution was treated the same way as done for beta rays by Kurie et al. (225), we derived a "Fermi-Kurie" type plot which is expressed in Fig. 72. The plot was approximately linear, thus demonstrating that the transition is allowed and intercepts the energy axis at $(E_o - E_K)$ equal to 220 kev which was the available energy for the transition. This experimental value is fairly consistent with 206 kev and 220 kev respectively found by Bell et al. (220) and Madanski and Rasetti (74).

The experimental spectrum in Fig. 71 was corrected for iodine escape effect and crystal efficiency. Then, the corrected spectrum was compared with the theoretical spectra derived from Martin-Glauber and Morrison-Schiff theory. The results which were obtained are shown in Fig. 73.

To correct for iodine escape effect, data reported in Fig. 70(c) were utilized while the data for total photopeak efficiency which are also reported in Appendix VIII were used for the second correction. Two theoretical spectra were obtained according to Morrison-Schiff and Martin-Glauber theory. To derive the former, Eq. (73) was used while the latter was obtained from results published by the authors themselves, (249).

Figure 72

"Fermi-Kurie" Type Plot of Continuous Spectrum from Fe^{55}.

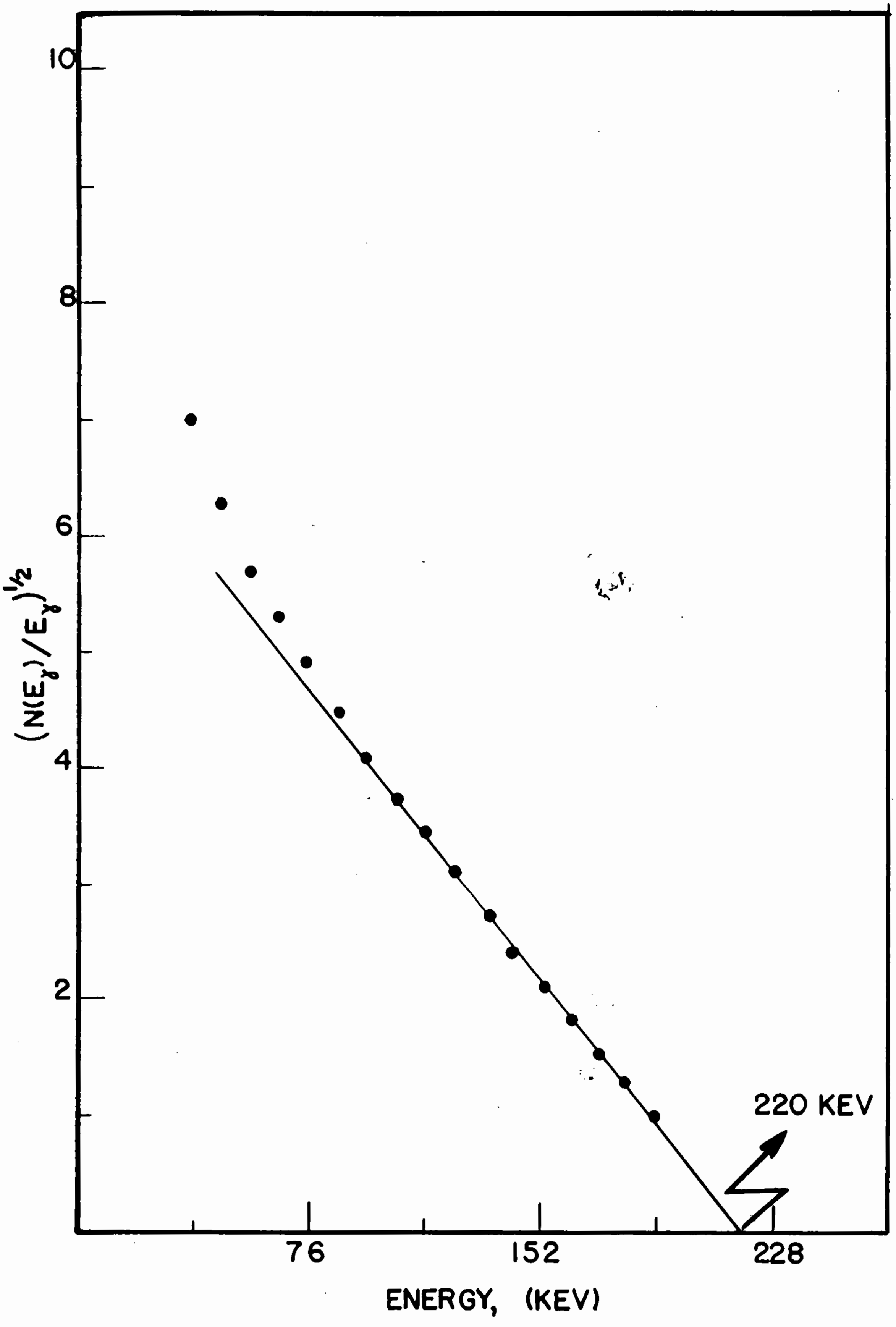
10
8
6
4
2
$(N(E_\gamma)/E_\gamma)^{1/2}$
76
152
228
ENERGY, (KEV)
220 KEV

The results which were obtained are shown in Fig. 73. Good agreement is particularly observed when the experimental spectrum is compared to Martin-Glauber theory.

(c) Discussion

When the experimental spectrum was corrected, contributions for Compton electrons and backscattered photons (coherent and incoherent scattering) were neglected. In this case, this is probably safe since the energy of the photons is relatively low. Also, the experimental spectrum was not corrected for instrumental resolution.

From the transition energy that was experimentally found, we have attempted to derive the ratio of the capture probabilities, P_L/P_K. This could be calculated according to the formulae given by Marshak (41) in the case of allowed transitions:

$$\frac{P_L}{P_K} = \left(\frac{g_{L_1}(R)}{g_K(R)}\right)^2 \cdot \left(\frac{E_o - E_L}{E_o - E_K}\right)^2 \cdot \left(1 + \frac{f^2_{L_{11}}(R)}{g^2_{L_1}(R)}\right) \qquad \ldots\ldots\ldots (74)$$

where E_L and E_K are the L- and the K-shell electron binding energies:

$\left(\frac{g_{L_1}(R)}{g_K(R)}\right)^2$ and $\left(\frac{f_{L_{11}}(R)}{g_{L_1}(R)}\right)^2$ are the ratios between L_1- and K-shell (see Fig. 1) and between L_{11}- and L_1-shell electron densities (54) at the nuclear radius (R).

Figure 73

Comparison between Experimental and Theoretical Distribution of the Internal Bremsstrahlung Photons from Fe^{55}.

(a) Uncorrected Spectrum

(b) Corrected for iodine escape effect

● spectrum corrected for escape and efficiency.

○ Morrison-Schiff Theory Eq. (73)

◒ Martin-Glauber Theory (226).

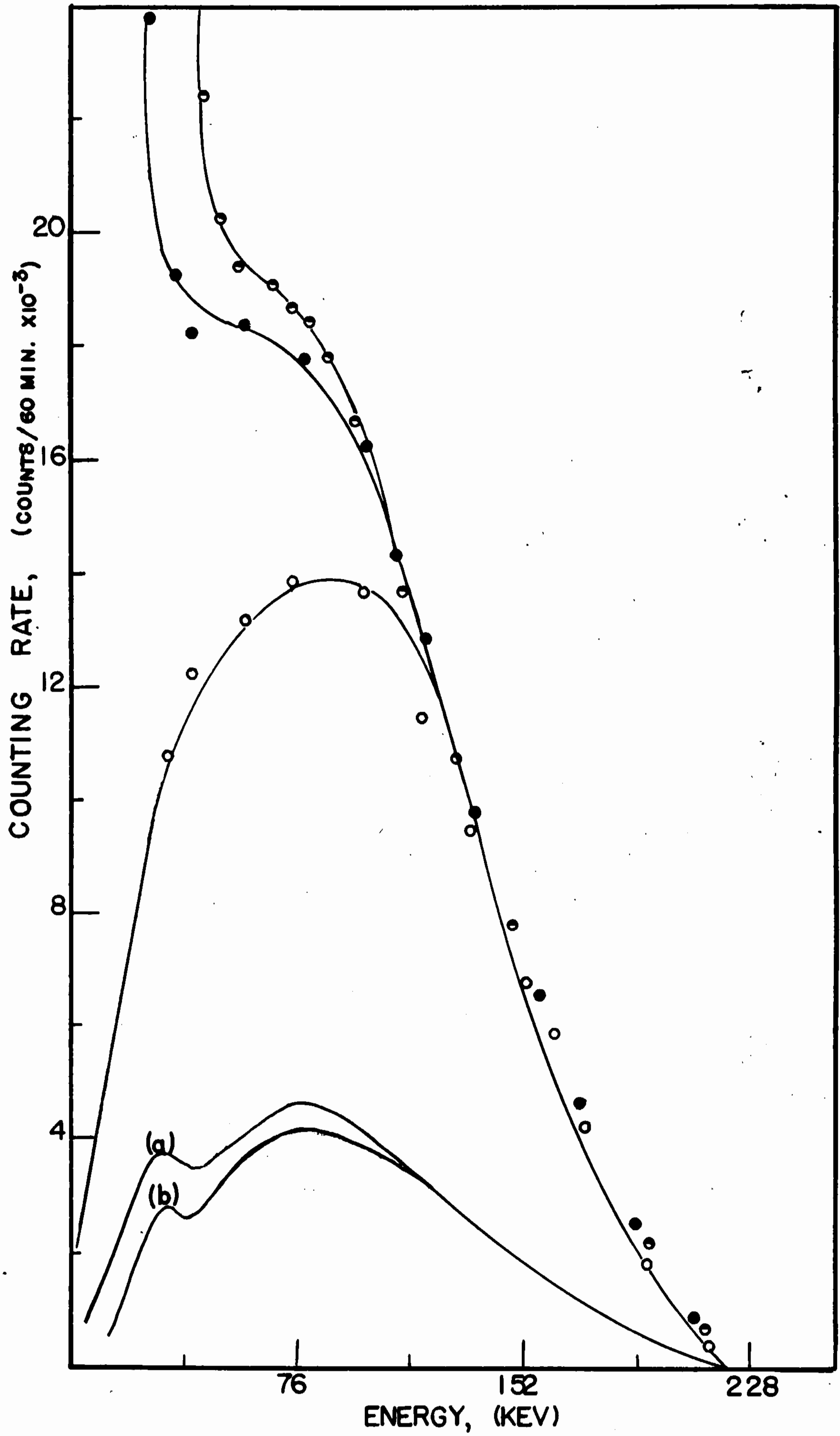
COUNTING RATE, (COUNTS/60 MIN. X10⁻³)
20
16
12
8
4
(a)
(b)
76
152
228
ENERGY, (KEV)

From

$$\left(\frac{g_{L_1}(R)}{g_K(R)}\right)^2 = 0.092$$

and

$$\left(\frac{f_{L_{11}}}{g_{L_1}}\right)^2 = \frac{3}{16} \cdot \left(\frac{Z - 4.15}{137.3}\right)^2 \qquad \text{.........} \ (75)$$

and with the known values for E_L and E_K, we obtain for the capture probabilities:

$$\frac{P_L}{P_K} = 0.096$$

This ratio is in good agreement with theoretical results (0.097) derived from Brysk and Rose (51) and recent experimental results (0.108) obtained for the first time by Scobie, Moler and Fink (218).

With the simple Morrison-Schiff theoretical equation Eq. (73), we have derived the number of photons per K-capture events and compare the result of the calculations with the experimental number of internal bremsstrahlung photons. In the former case, we obtained 3.58×10^{-5} photon per disintegration while in the latter, a value greater than 4.6×10^{-6} photon per disintegration was experimentally derived.

The series of nomographs which were published by Moszkowski (203) enabled us to derive the logarithm of the "comparative half-life" log (ft). When a half-life of 2.69 years, (158) and an energy transition of 226 kev were used, the log (ft) was found to be 6.3. From the selection rules for beta decay, this transition $Fe^{55} \xrightarrow{K} Mn^{55}$ can be classified as allowed. According to the currently accepted ideas of the nuclear shell model, this transition should be $(2p_{3/2} \rightarrow f_{5/2})$, that is, with a change of angular momentum of one unit and with no parity change, (-,-).

Recently, Lee and Mooring (227) have published an accurate measurement of the ground-state Q-value for **the** Mn^{55} (p,n)Fe^{55} **reaction.** From their reported value of -1.011 ± 0.005 mev, the energy transition, $(E_{\nu} + E_K)$, of $Fe^{55} \xrightarrow{K} Mn^{55}$ could be derived through calculations employing the energy balance of the reaction Mn^{55} (p,n)Fe^{55}. The value obtained was 223 kev which is also in good agreement with our experimental result.

2) K-FLUORESCENCE YIELD MEASUREMENTS OF ARGON AND IRON

(a) Introduction

In the experimental determination of K-fluorescence yield values, the inner shell ionization has most commonly been produced by X-ray excitations (61), (194). However, when a radioactive nuclide undergoes an orbital capture of an electron, in the K-state for instance, a vacancy is created in the K-shell. Similarly, if a nuclear photon is internally coverted in the K-shell, the same vacancy occurs. Subsequently, a characteristic X-ray or Auger electron will be emitted. The K-fluorescence yield, W_K of the K-shell will be defined as the number of K X-rays emitted per K-shell vacancy. It can be derived if the number of K X-rays or K Auger electrons per K-shell vacancies can be measured. The same phenomenon can occur in the L-shell and the same treatment can be adopted. However, with nuclides decaying by orbital capture, K-shell vacancies have a preponderance over L-shell vacancies.

The development of proportional counter techniques for electron and X-ray detection has provided another method with considerable merit for the determination of fluorescence yields (75), (127), and (228). Two different methods employing a proportional counter were used to determine the fluorescence yield of argon and iron. These two elements lie in the low region of the W_K versus Z curve and in that portion of the curve ($Z < 26$), the uncertainty in the interpretation of the experimental results, published during the past years, represents a scattering of at least 10 per cent (60).

(b) Experimental Technique and Results

I. K-fluorescence Yield From Argon

The probability that a K X-ray escapes from the counter following a photoelectric absorption in the K-shell depends mainly on the value of the K-fluorescence yield for the individual gases and the value of the pressure.

We have studied this escape probability when K X-rays from a source of Fe^{55} (5.9 kev) and Mn^{54} (5.4 kev) were alternatively interacting with a mixture of $A-CH_4$ (9:1) at various pressures. The two peaks (escape and K-photopeak) were observed in the pulse-size distribution and the K-fluorescence yield of argon could be determined from their relative intensities. Due to its small photoelectric absorption coefficient, the contribution of CH_4 was neglected.

Assuming I_1 and I_2 as respectively the intensity of the radiations contributing to the escape peak and the main photopeak, the following relation could be written (171),

$$\frac{I_1}{I_1 + I_2} = W'_K \bullet \left[1 - \frac{\int_0^V \pi . A . dV}{\int_0^V \pi . dV} \right]$$

where

V = sensitive volume of the counter.

$\eta . dV$ = probability that an impinging X-ray will be absorbed in the element of volume dV.

A = probability that a characteristic X-ray of argon generated in the same element of volume dV will be absorbed in the counter.

W'_K = "K-fluorescence yield" assuming the X-rays are absorbed in the K-shell only. This value will be treated later.

Hence, the term

$$\frac{\int_0^V \eta . A . dV}{\int_0^V A . dV} \qquad \ldots\ldots\ldots\ldots (77)$$

will take care of the re-absorption of the characteristic X-ray of argon. As the pressure is decreased, this term will vary linearly with the pressure, and at pressures approaching zero, its value will be negligible. On this assumption, $\frac{I_1}{I_1 + I_2}$ was plotted for various pressures and according to Fig. 74, the extrapolation to a pressure equal to zero gave a value of 0.081 for W'_K.

Now, W'_K must be corrected for the contribution of the photoelectric effect occuring in the L-shell of argon. The photoelectric coefficient of argon, τ_K, τ_L, and τ_M for this range of energy was obtained from Bethe (256). Obviously, τ_M will be neglected on account of its small value. Integrating the values of τ_K, and τ_L in the following equation,

$$W_K = \left(1 + \frac{\tau_L}{\tau_K}\right)\left(\frac{W'_K}{1+\frac{\tau_L}{\tau_K} . W'_K}\right) \qquad \ldots\ldots\ldots (78)$$

Figure 74

"W_k" as a function of pressure.

● Mn^{54} (5.4 kev)

○ Fe^{55} (5.9 kev)

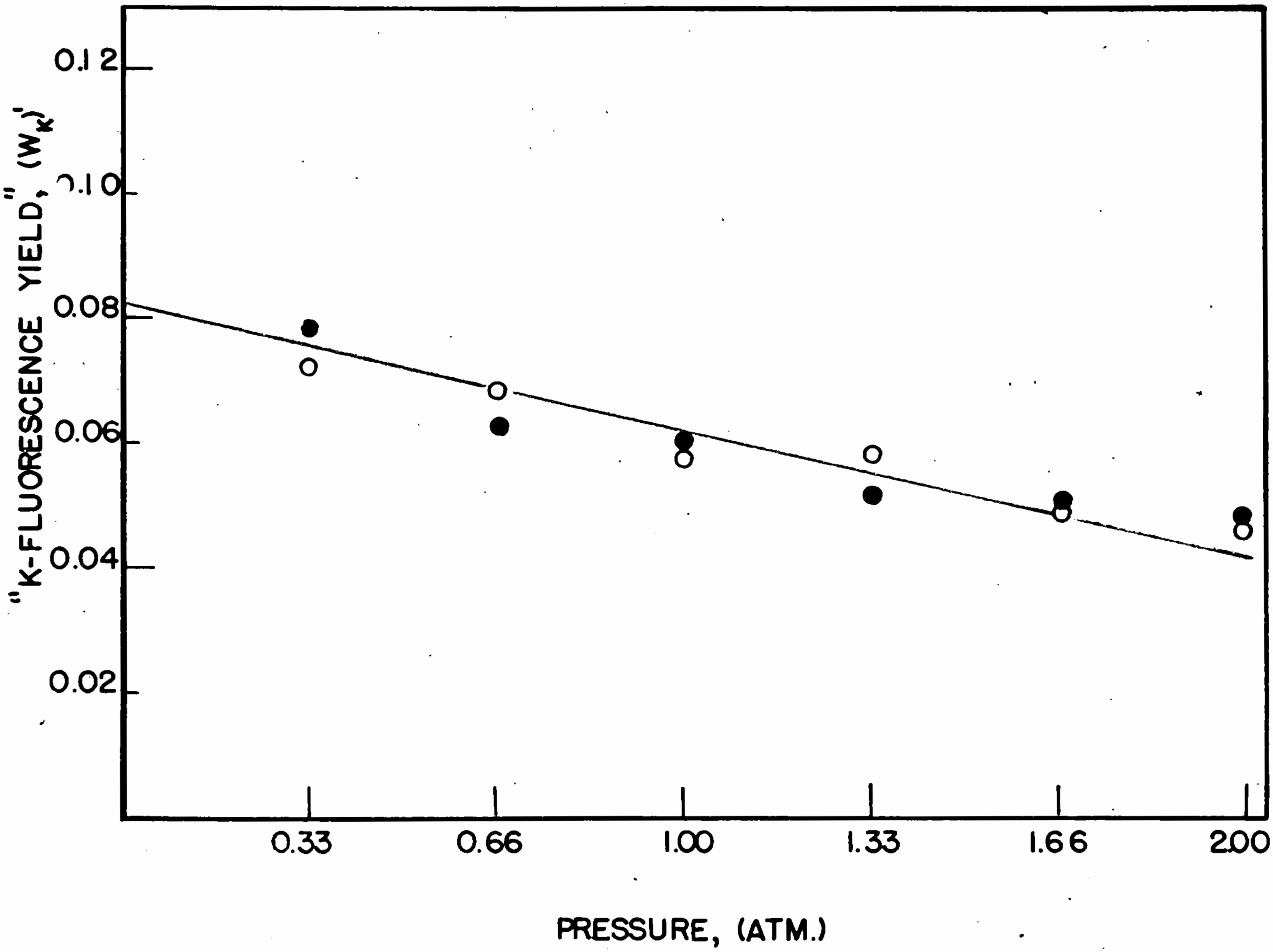
0.12
0.10
0.08
0.06
0.04
0.02
"K-FLUORESCENCE YIELD", (W_K)'
0.33
0.66
1.00
1.33
1.66
2.00
PRESSURE, (ATM.)

where, $\frac{\tau_L}{\tau_K}$ = 0.071, W_K was found to be 0.086.

According to the literature (31), experimental values of the K-fluorescence yield of argon are scattered between 0.06 and 0.149. Nevertheless, two values which were reported in 1955 deserve to be mentioned. Both experiments utilized proportional counter techniques. The first value, 0.081, was reported by Heintze (230) while the second one, 0.129, was reported by Harrison, et al. (231). At the present days, the adopted value is 0.100 ± 0.020 (205).

II. K-fluorescence Yield of Iron

Some dried $Fe^{55}Cl_3$ was dissolved in absolute ethanol. Then, 20 microliters containing about 2 x 10^5 dis./min. were mounted on an aluminum foil. The activity was measured in the upper part of a calibrated 4π proportional counter which can be used at elevated pressures for the measurement of soft X-rays, (27). Aluminum absorbers having a thickness of 0.8 micron were integrally added over the source and corresponding counting rates were measured. The results are shown in Fig. 75.

To obtain the number of K-capture events, two corrections were applied, namely a correction for the dead time of the counter and a correction for the total absorption of the counter. The former correction was of the order of one per cent. This

Figure 75

Transmission of Radiations from Fe^{55} through Various Aluminum Absorbers.

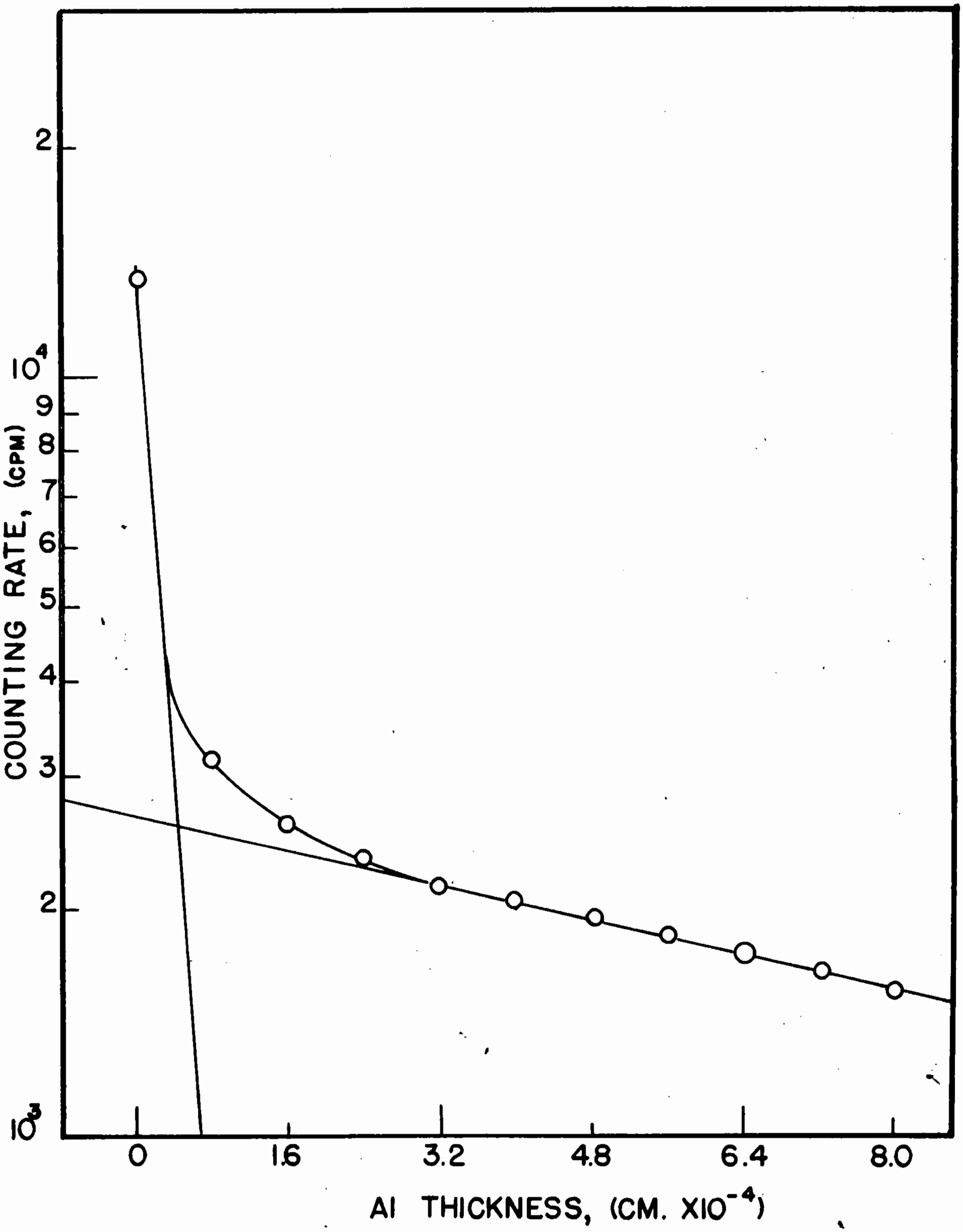
COUNTING RATE, (CPM)
2
10^4
9
8
7
6
5
4
3
2
10^3
0
1.6
3.2
4.8
6.4
8.0
Al THICKNESS, (CM. X10^{-4})

assumption is fair since according to Fig. 38 a coincidence loss of about one per cent was experimentally obtained at counting rates of the order of 10^5 counts per minute. This, of course, is a reliable assumption since the counter was connected to the same auxiliary electronic equipment used previously and the gas multiplication is roughly the same. To correct for the second factor, namely the total absorption of the X-rays inside the sensitive volume, data shown in Fig. 63 were applied. The results of the corrections are shown in Table XIII. From these experimental data, and calculations, the K-fluorescence yield of iron was derived and gave 0.28. For the same nuclide, Roos (195) has reported an experimental value of 0.308.

(c) Discussion

As expressed in Table XIV the experimental results are not inconsistent with those derived from the semi-empirical formulae of Burhop (61) Hagedoorn and Wapstra (205), and Laberrique-Frolow (232). In particular, the formula of Hagedoorn and Wapstra which is effectively Burhop's semi-empirical equation having the constant slightly modified seemed to be the most compatible with our results.

However, for $26 < Z < 50$, recent data from Roos (195) are quoted by Robinson and Fink (116) to be the most accurate, (±2 to 3 per cent), and Hagedoorn and Wapstra have written that

TABLE XIII

Determination of K-events

Counting Rate:	103.4×10^3 cpm.
Corrected for Dead Time:	104.4×10^3 cpm.
Corrected for X-ray Transmission:	106.2×10^3 cpm.
Number of K events:	106.2×10^3 cpm.
Number of K X-rays:	29.8×10^3 cpm.

TABLE XIV

Element	W_K Exp'l	W_K (a)	W_K (b)	W_K (c)
Argon	0.086 ± 0.004	0.081	0.095	0.095
Iron	0.28 ± 0.01	0.29	0.31	0.33

(a) Semi-empirical from Hagedoorn and Wapstra.

(b) Semi-empirical from Laberrique-Frolow.

(c) Semi-empirical from Burhop.

for this region, the Laberrique-Frolow equation would be the most suitable to reconcile the experimental results obtained by Roos.

Our values for the K-fluorescence for argon and iron are shown in Fig. 76 and within the deviation of the values of various investigators which were reported by Broyles et al. (31), they agreed well.

3) CAPTURE PROBABILITIES OF Fe^{55}

(a) Introduction

In general, three fundamental techniques are available for the determination of the probabilities of orbital capture ratios. These are briefly described.

(i) External source spectrometry. The radioactive material is placed outside the sensitive volume, and the relative intensity of K and L X-rays is measured. The application of this method would involve absorption and self scattering, if present, and in some cases self-excitation of fluorescent X-rays (233) for differential air and window absorption and for K and L-fluorescence yields. One must also consider that a K-shell vacancy may be filled by an L-electron either by a radiative transition (X-ray) or by a radiationless (Auger electron) transition. In cases where electron capture is followed by gamma-ray emission, the conversion of the gamma ray in one of the

Figure 76

K-fluorescence Yield vers. Atomic Number

Our measurements

Other investigators reported by Broyles, C.D., Thomas, D.A., Haynes, S.K. Phys. Rev. 89, 715, (1953).

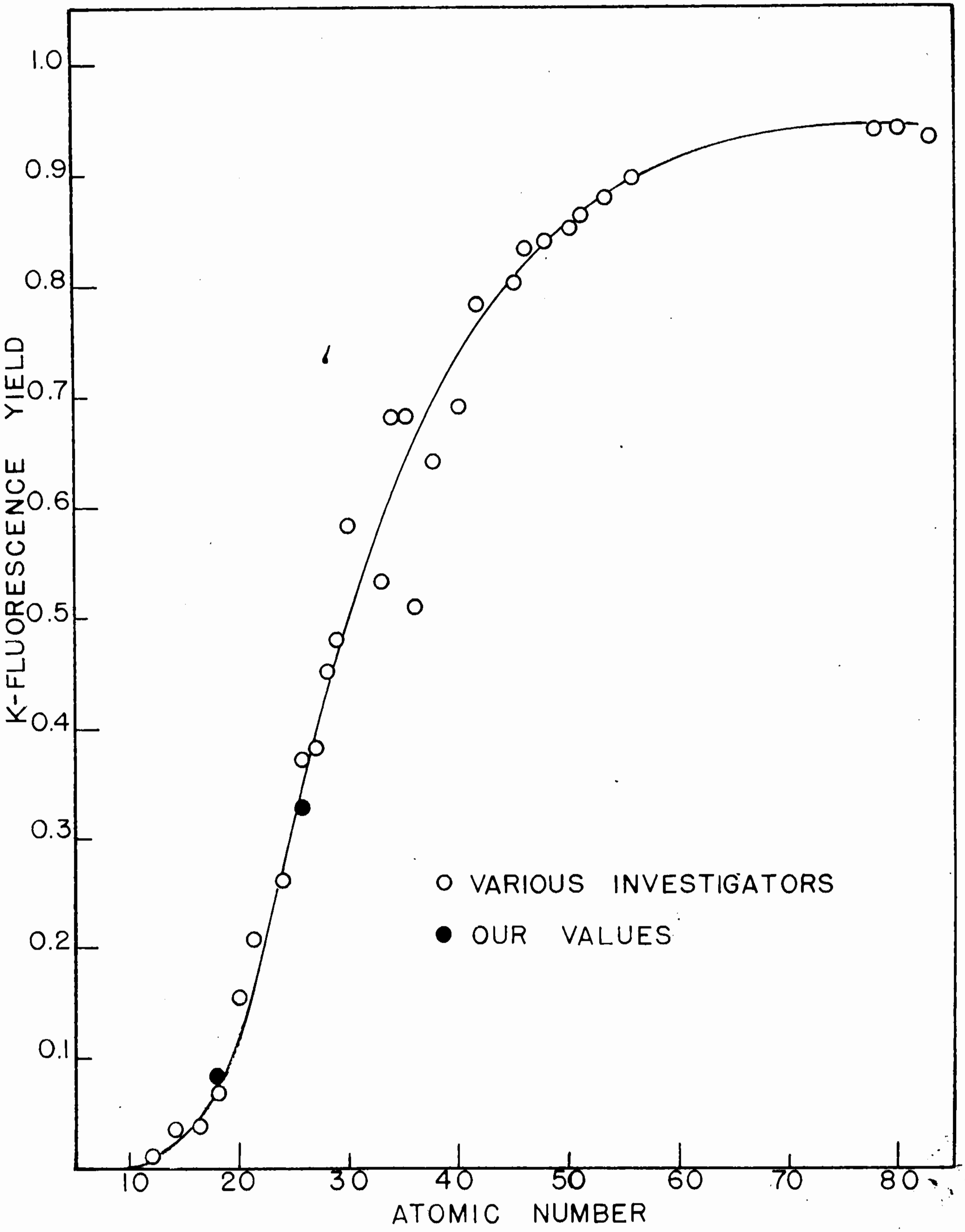
1.0
0.9
0.8
0.7
0.6
0.5
0.4
0.3
0.2
0.1
K-FLUORESCENCE YIELD
10
20
30
40
50
60
70
80
ATOMIC NUMBER
○ VARIOUS INVESTIGATORS
● OUR VALUES

shells must be taken into account.

The X-ray intensity ratio I_L/I_K will be related to the ratio of capture probabilities P_L/P_K by the following expression (174),

$$\frac{I_L}{I_K} = \left(\frac{P_L}{P_K} + n_{K,L}\right) \cdot \left(\frac{W_L}{W_K}\right) \qquad \ldots\ldots\ (79)$$

where,

$n_{K,L}$ = number of L-shell vacancies produced in the filling of a K-shell vacancy. This value was computed for various atomic numbers, (234).

W_K and W_L = K-fluorescence yield and mean L-fluorescence yield.

For the heaviest elements, in particular, this technique has been applied to many nuclides (235), (236). The intensities of the X-rays have been measured carefully by the use of proportional counters and a bent X-ray spectrometer. However, most of these nuclides had low-energy gamma transitions which were highly converted in the L-shell so that the interpretation of X-ray intensities was tenuous.

(ii) Internal source spectrometry. The radioactive material (in gaseous or vapor form) is contained within the sensitive volume of the detector. The detector can either be a proportional counter or a solid or a liquid scintillator. The technique employing a proportional counter was pioneered by Kirkwood et al. (75).

It is the most widely used method since it has the advantage of determining the L/K capture ratio without requiring the knowledge of the L-fluorescence yield. The ratio of the intensity, of the K and L peaks I_L/I_K, arises from K-Auger electrons and K X-rays following a K-capture and from L-Auger electrons and L X-rays following directly in a gas proportional counter. The L/K capture ratio is given by (174)

$$\frac{P_L}{P_K} = \left(\frac{I_L}{I_K}\right) \cdot \left(1 - P.W_K\right) - \left(P.k.W_K\right) \qquad \ldots\ldots (80)$$

P = probability that an impinging X-ray will escape from the counter without being detected.

k = fraction of K_α in the K series.

Usually, one chooses P so it approaches either unity or zero. In the former case, low pressures and low atomic number counter gases are required and the results are critically dependent on W_K (237), (238). In the latter case, this can be easily realized with the use of proper counter gas conditions, (nature of the gas and pressure) and proper geometrical arrangement. In this case the results are independent of W_K. Another elegant approach to the problem was suggested by der Mateosian and Smith, in 1952 (239). Traces of radioactive elements were grown into scintillation crystals. In the opinion of the author, no attempt has yet been made to obtain P_L/P_K through homogeneous dissolution of some radioactive material into a liquid scintillator.

(iii) Coincidence spectrometry. This technique is particularly useful for relatively complicated decay schemes, provided that there is a high energy gamma-ray transition directly to the ground state or to a low-lying state. It was developed by Gupta and Jha in 1957 (240) and it consists in the absolute measurement of the characteristic K X-rays in coincidence with the de-excitation photon, $I_{K-\gamma}$, and the absolute measurement of the K X-rays, I_K. Then, the following relation will hold,

$$\frac{I_{K-\gamma}}{I_K} = \left(\frac{N_K}{N}\right) \cdot \left(W_K . S . \varepsilon_K . e^{-\mu t}\right) \qquad \text{........ (81)}$$

$$\frac{I_{K-\gamma}}{I_K} = \left[\frac{1}{1 + \left(\frac{P_L}{P_K}\right)}\right] \cdot \left(W_K . S . \varepsilon_K . e^{-\mu t}\right) \qquad \text{........ (82)}$$

where,

N_K = number of K electron capture leading to excited state.

N = total number of capture event.

S = solid angle subtended by the source at the crystal.

ε_K = K X-ray efficiency of the crystal.

$e^{-\mu t}$ = absorption of the K X-rays in the cover of the crystal.

Once the factors are ascertained, capture probabilities can be derived directly from the measurements.

Another method which deserves to be mentioned utilizes the absorption technique. This involves some absorption measurement of L and K X-rays intensities and it has been reported by Wilkinson and Hicks (241) and Chu (242).

In our determination of the capture probabilities of Fe^{55}, a technique similar to the first one was applied. This particular method was chosen because in our experimental conditions I_L and I_K could be measured directly. At that time (July 8, 1958) Fe^{55} offered some interest since no one had yet attempted this measurement.

(b) Experimental Technique and Results.

The source of Fe^{55}, was mounted in the same manner as the source used for the determination of the K-fluorescence yield of iron. The Auger electrons were screened off with sufficient thickness of aluminum absorber, that is, with 0.8 micron, (about 0.4 micron is enough to screen off all Auger electrons). Then, the source was placed in the proportional counter and the relative intensities of L and K X-rays were spectrometrically measured.

The results of the analysis are shown in Fig. 77. Applying the correction factors, f_e, f_a, which were already experimentally evaluated and f_t from the Campion-Merritt equation,

Figure 77

Spectrum of Fe^{55}.

Counter gas: A-CH_4 (9:1).

Pressure: 1 atmosphere.

(a) L X-ray Intensity.

(b) Escape Intensity (multiplied by 10).

(c) K X-ray Intensity (multiplied by 10).

262a

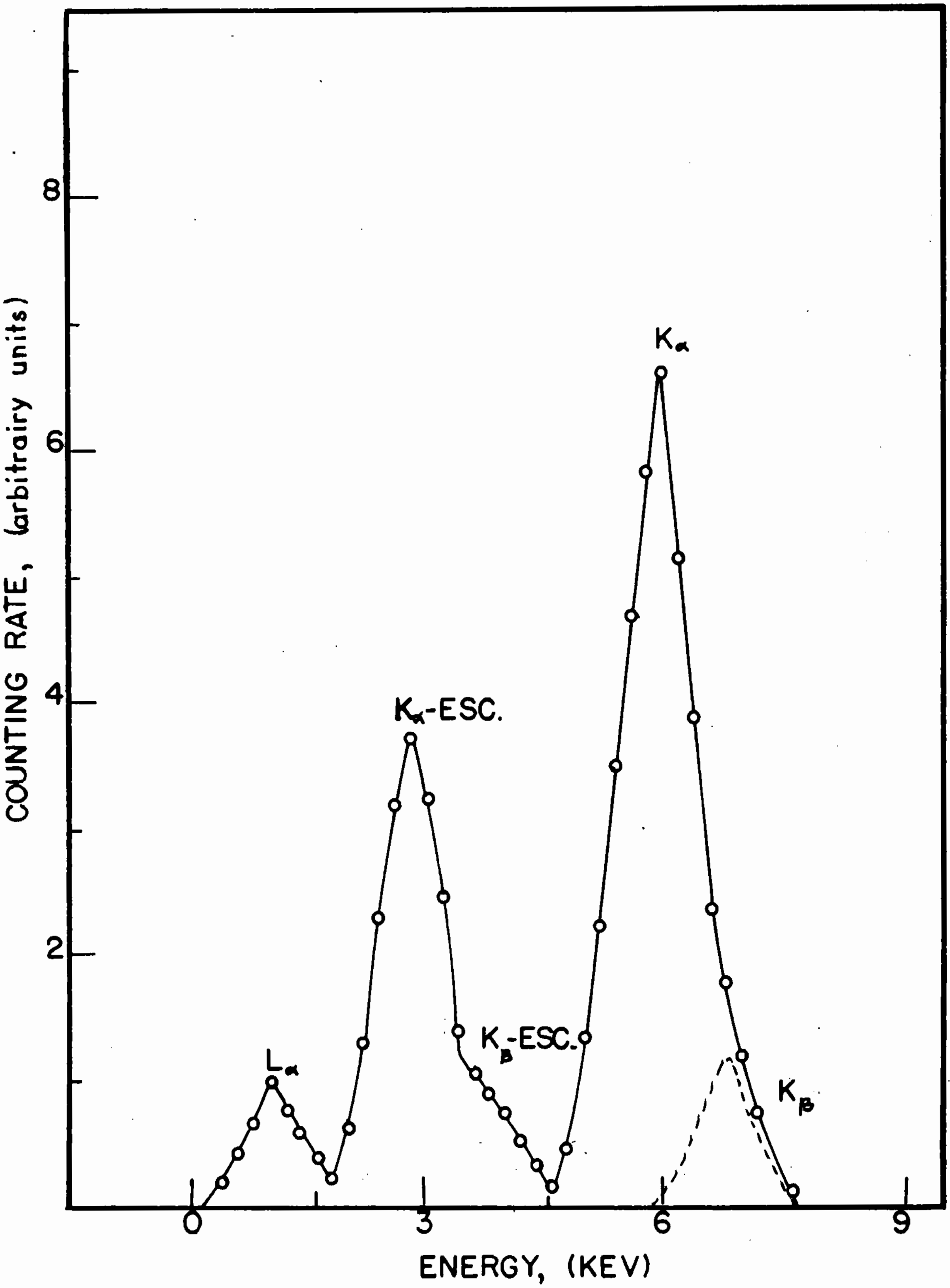
COUNTING RATE, (arbitrairy units)
8
6
4
2
ENERGY, (KEV)
0
3
6
9
L_α
K_α-ESC.
K_β-ESC.
K_α
K_β

(see Appendix VII) for the mass absorption coefficient of aluminum for various energies the disintegration rates for K capture events, N_K, and L capture events, N_L, were respectively determined. Then the capture probabilities could be derived through the following relation,

$$\frac{N_L}{N_L + N_K} = \frac{1}{1 + \left(\frac{P_L}{P_K}\right)} \qquad \ldots\ldots\ldots (83)$$

By integrating the experimental values for N_L and N_K, the ratio P_L/P_K was found to be 0.011.

(c) Discussion

The experimental result obtained for the determination of P_L/P_K for Fe^{55} does not correspond to the theoretical value of 0.096 which was already derived from Marshak's general formulae for an allowed transition. Moreover, the theoretical curves of Brysk and Rose (51) gave a ratio of 0.097. The incompatibility between experimental and theoretical results must be due to unobserved source of errors in the application of the method. Some of them could be due to the self-absorption of the soft radiation component within the source and the lack of accuracy of the Campion-Merritt equation for such low energy X-rays. Also, the L X-rays (about 650 kev) would have a short range inside the sensitive volume of the counter and sometimes the electric field might not be high enough to produce the first Townsend avalanche. A way to correct for this would be the positioning of the source close to the anode.

Recently, Scobie, Moler and Fink (218) have successfully determined the L/K capture ratio of the same radionuclide. They have utilized vaporous ferrocene containing Fe^{55}. Their experimental result which was 0.108 agreed very well with the theoretical predictions.

I. BIBLIOGRAPHY

1. Curtis, M.L., Heyd, J.W., and Eickelberger, J.F., Nucleonics, 13, No. 5, 38, (1955).
2. Robinson, H.P. Nuclear Science Series, Report 24. N.R.C. of U.S.A., Publication 573, (1958).
3. Mann, W.B. Int. J. of App. Rad. and Isotopes, 1, 1, (1956). Nuclear Science Series, Report 24. N.R.C. of U.S.A., Publication 573, (1958).
4. Simpson, J.A. Rev. Sc. Inst., 15, 119, (1944).
5. Haxel, O., and Houtermans, F.G., Z. fur Phys., 124, 705, (1948).
6. Pate, B.D., and Yaffe, L. Can. J. Chem., 33, 15, (1955).
7. Pate, B.D., and Yaffe, L. Can. J. Chem., 33, 929, (1955).
8. Pate, B.D., and Yaffe, L. Can. J. Chem., 33, 610, (1955).
9. Pate, B.D., and Yaffe, L. Can. J. Chem., 33, 1656, (1955).
10. Pate, B.D., and Yaffe, L. Can. J. Chem., 34, 265, (1956).
11. Engekemeir, A.G., and Libby, W.F. Rev. Sc. Inst., 21, 550, (1950).
12. Mann, W.B., and Parkinson, G.B. Rev. Sc. Inst., 20, 41, (1949).
13. Gunnick, R., Colby, L.J., and Cobble, J.W. Anal. Chem., 31, 796, (1959).
14. Campion, P.J. Int. J. of App. Rad. and Isotopes, 4, 232, (1959).
15. Campion, P.J., and Merritt, J.S., Can. J. Phys., 36, 983, (1958).
16. Littler, D.J. Atomics, 1, 189, (1950).
17. Manov, G.C., and Curtiss, L.F., J. Res. Natl. Bur. Stds., 46, 328, (1951).
18. Borkowski, C.J., Anal. Chem., 21, 348, (1949).
19. Cobble, J.W., Oak Ridge National Laboratory. ORNL, Memo, C.F., 50-6-114, (1950).

20. Colby, L.J., and Cobble, J.W., Anal. Chem., 31, 798, (1959).

21. Friedlander, G., Perlman, M.L., Alburger, D., and Sunyar, A.W. Phys. Rev., 80, 30, (1950).

22. Bisi, A., and Zappa, L. Il Nuovo Cimento, 12, 211, (1954).

23. Putman, J.L., and Allen, R.A. A Circular to National Physical Laboratory, England. Advisory Committee on Radioactive Standards, AERE, (1954).

24. Rasmussen, N.C. Circular to National Research Council, (U.S.A.). Subcommittee on Beta and Gamma-ray Measurements and Standards, (1955).

25. Allen, R.A. Int. J. of App. Rad. and Isotopes, 1, 289, (1957).

26. Lyon, W.S., and Reynolds, S.A., Int. J. of Applied Rad. and Isotopes, 2, 84, (1957).

27. Campion, P.J., and Merritt, W.P., Atomic Energy of Canada Limited, AECL, Report 532, CRP - 745, (1957).

28. Auger, P. J. Phys. Rad., 6, 205, (1925).

29. Broyles, C.D., Thomas, D.A., and Haynes, S.K., Phys. Rev., 89, 715, (1953).

30. Curie, I., and Joliot, F., C.R., 198, 254, (1934). J. Phys. Rad., 5, 153, (1934).

31. Chadwick, J., Nature, 129, 312, (1932). Proc. Roy. Soc., 136, 692, (1932).

32. Heisenberg, W., Zeit. f. Phys., 77, 1, (1932), 78, 156, (1932), 80, 587, (1933).

33. Fermi, E., Zeit. f. Phys., 88, 161, (1934).

34. Tamm, I., Nature, 133, 981, (1934).

35. Iwanenko, D., Nature, 133, 981, (1934).

36. Yukawa, H., Proc. Phys. Math. Soc. Japan, 17, 48, (1935).

37. Yukawa, H., and Sakata, S., Proc. Phys. Math. Soc. Japan, 17, 467, (1935).

38. Yukawa, H., and Sakata, S., Proc. Phys. Math, Soc. Japan, 18, 128, (1936).

39. Møller, C., Phys. Rev., 51, 84, (1937). Phys. Z. Sowjet Union, 11, 9, (1937).

40. Bethe, H.A., and Backer, R.F., Rev. Mod. Phys., 8, 82, (1936).

41. Marshak, R.E., Phys. Rev. 61, 431, (1942).

42. Mercier, A., C.R., 204, 1117, (1937).

43. Hoyle, F., Nature, 140, 235, (1937). Proc. Phil. Soc., 33, 286 (1937).

44. Konopinski, E.J., Rev. Mod. Phys., 15, 209, (1943).

45. Benoist, P., and Bouchez, R., Revue d'optique theorique et instrumentale, Paris, (1949).

46. Bouchez, R., de Groot, S.R., Nataf, R., and Tolhoek, H.A., J. Phys. Rad., 11, 105, (1950).

47. Bouchez, R., de Groot, S.R., Nataf, R., and Tolhoek, H.A., Physica, 15, 863, (1949).

48. Nataf, R. and Bouchez, R., J. Phys. Rad. 13, 190, (1952).

49. Bouchez, R., Physica, 18, 1171, (1952).

50. Benoist-Geutal, P., Annales de Phys., 8, 593, (1953).

51. Brysk, H., and Rose, M.E., Rev. Mod. Phys. 30, 1169, (1958).

52. Hartree, D.R., and W., Proc. Roy. Soc., 166, 450, (1938).

53. Reitz, J., Phys. Rev., 77, 10, (1950).

54. Rose, M.E., and Jackson, J.L., Phys. Rev., 76, 1540, (1949).

55. Fine, S., and Hendee, C.F., Nucleonics, 13, 36, (1955).

56. Hughes, A.L., Am. J. Phys., 16, 415, (1948).

57. Fermi, E., "Nuclear Physics", at the University Press, University of Chicago, (1950).

58. Barkla, C.G., and Saddler, C.A., Phil. Mag., 16, 550, (1908).

59. Moseley, H.G.J., Phil. Mag., 26, 1024, (1913), Phil. Mag., 27, 703, (1914).

60. Meyer, see Avignon, P., Annales de Phys., 1, 10, (1956).

61. Burhop, E.H.S., Proc. Roy. Soc., 148, 272, (1935). "The Auger Effect", Cambridge University Press, England, (1952).

62. Avignon, P., Ann. Phys., 1, 10, (1956).

63. Coster, D., and Krönig, R de L., Physica, 2, 13, (1935).

64. Pincherle, L., Il Nuovo Cimento, 12, 81, (1935).

65. Massey, H.S.W., and Burhop, E.H.S., Proc. Roy, Soc., 153, 661, (1935).

66. Robinson, B.L., and Fink, R.W., Rev. Mod. Phys., 32, 117, (1960).

67. Morrison, P., and Schiff, L.I., Phys. Rev., 58, 24, (1940).

68. Glauber, R.J., and Martin, P.C., Phys. Rev., 95, 572, (1954).

69. Glauber, R.J., and Martin, P.C., J. Phys. Rad. 16, 573, (1955).

70. Glauber, R.J., and Martin, P.C., Phys. Rev., 104, 158, (1956).

71. Glauber, R.J., and Martin, P.C., Phys. Rev., 109, 1307, (1958).

72. Madansky, L., and Rasetti, F., Phys. Rev., 94, 407, (1954).

73. Jacobsen, J.C., Nature, 139, 879, (1937).

74. Alvarez, L., Phys. Rev., 52, 134, (1937).

75. Kirkwood, D.H.W., Pontecorvo, B., and Hanna, G.C., Phys. Rev. 74, 497, (1948).

76. Hayward, R.W., Circular to National Research Council, (U.S.A.). Subcommittee on Beta and Gamma-ray Measurements and Standards. Publication, No. 573, (1958).

77. Heitler, W., "The Quantum Theory of Radiations". Oxford University Press. (1944).

78. Hulme, H.R., McDougall, J., Buckingham, R.A., and Fowler, R.H., Proc. Roy. Soc., 149A, 131, (1935).

79. Hall, H., Rev. Mod. Phys., 8, 358, (1936).

80. Klein, O., and Nishina, Y., Z. Phys., 52, 853, (1929).

81. Anderson, C.D., Phys. Rev., 43, 491, (1933).

82. White, G.W., Natl. Bur. Standards. Circular, 583, (1957).

83. Bethe, H.A., Ann. Physik, 5, 325, (1930).

84. Pate, B.D., Ph.D. Thesis, McGill University, (1955).

85. Nachod, F.C., "Ion Exchange: Theory and Applications". New York Academic Press Inc. (1949).

86. Blanchard, J.A., Kahn, B., and Birkhoff, R.D., Health Physics, 3, 246, (1960), also, Oak Ridge National Laboratory, ORNL - Report 2419, (1957).

87. West, H.I., Meyerhoff, W.E., and Hofstadter, R., Phys. Rev., 81, 141, (1951).

88. Seliger, H.H., and Mann, W.B., National Bur. Standards Circular 594, (1958).

89. Seliger, H.H., Nuclear Science Series Report, No. 24. Publication 573, (1958) N.R.C. (U.S.A.).

90. Eggler, C., and Huddleston, C.M., Nucleonics, 14, 34, (1956).

91. Korff, S.A., "Electron and Nuclear Counters". D. Van Nostrand Co. (1957).

92. Segre, E., "Experiment in Nuclear Physics". Vol. I. John Wiley and Sons, (1953).

93. Curran, S.C., and Craggs, J.D., "Counting Tubes". Academic Press, Inc. New York, (1949).

94. Wilkinson, D.H., "Ionization Chambers and Counters". Cambridge University Press, England, (1950).

95. Price, W.J., "Nuclear Radiation Detection". McGraw-Hill Books, Co. (1958).

96. Rossi, B., and Staub, H.H., "Ionization Chambers and Counters". McGraw-Hill Books, Co. (1949).

97. Rutherford, E., and Geiger, H., Proc. Roy. Soc. 81A, 141, (1908).

98. Geiger, H., and Müller, W., Phys. Z., 29, 839, (1928).

99. Neher, H.V., and Harper, W.W., Phys. Rev. 49, 940, (1936).

100. Rossi, B.B., Z. Phys., 68, 64, (1931).

101. Trost, A., Z. tech. Phys., 16, 407, (1935).

102. Trost, A., Phys. Z., 36, 801, (1935).

103. Trost, A., Z. fur Phys. 105, 399, (1937).

104. Rose, M.E., and Ramsay, W.E., Phys. Rev., 61, 504, (1942).

105. Rose, M.E., and Korff, S.A., Phys. Rev., 59, 850, (1941).

106. Dunworth, J.V., Rev. Sc. Inst. 11, 167, (1940).

107. Putman, J.L., Brit. J. Radiol., 23, 46, (1950).

108. Brysk, H., and Rose, M.E., Oak Ridge National Laboratory ORNL, Report 1862, (1955).

109. Fink, R.W., Atomic Energy Commission, (U.S.A.). Report, ORO-173, (1958).

110. Bernstein, W., and Ballentine, R., Rev. Sc. Inst. 21, 158, (1950).

111. Hawkings, R.C., Hunter, R.F., and Mann, W.B., Can. J. Res., 27B, 555, (1949).

112. Hawkings, R.C., Hunter, R.F., Mann, W.B., and Stevens, W.H., Can. J. Res., 27B, 545, (1949).

113. Burtt, B.P., Conference on Absolute Beta Counting, Nuclear Science Series Report, No. 6. N.R.C. (U.S.A.), (1955).

114. Zumwalt, L.K., Atomic Energy Commission of U.S.A., Report MDDC-1346, (1949).

115. Curran, S.C., Augus, J., and Cockroft, A.L., Nature, 162, 302, (1948).

116. Curran, S.C., Angus, J., and Cockroft, A.L., Phil. Mag., 40, 36, (1949).

117. Insch, G.M., Phil. Mag. 41, 857, (1950).

118. Joliot, F., and Curie, I., C.R., 190, 1292, (1930).

119. Rothwell, P., and West, D., Proc. Phys. Soc. London, 63A, 541, (1950).

120. Edwards, J.E., and Pool, M.L., Phys. Rev. 69, 549, (1946).

121. Siegbahn, K., and Slätis, H., Ark. Mat. Astr. Fys. 34A, 12, (1947).

122. Reiffel, L., Nucleonics, 13, 22, (1955).

123. Starfelt, N., Cederlund, J., and Liden, K., Int. J. of App. Rad. and Isotopes, 2, 265, (1957).

124. Cameron, J.F., and Rhodes, J.R., Int. J. of Applied Rad. and Isotopes, 7, 244, (1960).

125. Martin, W.M., and Brekson, S.W., Can. J. Phys., 30, 643, (1952).

126. Meinke, W.W., University of California Radiation Laboratory. UCRL, Report 432, (1949).

127. "Collected Radiochemical Procedures". Los Alomos Scientific Laboratory of the University of California. Report 1721 (1954).

128. Bailey, R.A., and Yaffe, L., Can. J. Chem., 37, 1527, (1959).

129. Morrison, G.H., and Freiser, H., "Solvent Extraction in Analytical Chemistry". McGraw-Hill Co. New York (1957).

130. Morrison, G.H., Anal. Chem., 20, 632, (1958).

131. Holland, L., "Vacuum Deposition of Thin Films". John Wiley and Sons, Inc. New York (1956).

132. Friedlander, G., and Kennedy, J.W., Nuclear and Radiochemistry, John Wiley and Sons, Inc. New York (1949).

133. Krauss, K.A., and Nelson, F., Peaceful Uses of Atomic Energy, 12, 113, (1953).

134. Moeller, T., "Inorganic Chemistry". John Wiley and Sons, Inc. New York (1953).

135. Faris, J.P., Anal. Chem., 32, 520, (1960).

136. Walter, R.I., J. Inorg. Nucl. Chem., 6, 58, (1958).

137. Berman, S.S., and McBryde, W.A.E., Can. J. Chem., 36, 835, (1958).

138. Gruverman, I.S., and Kruger, P., Int. J. of App. Rad. and Isotopes, 5, 21, (1959).

139. Kraushaar, J.J., Wilson, E.D., and Bainbridge, K.T., Phys. Rev., 90, 610, (1953).

140. Segre, E., and Wiegand, C., Phys. Rev., 75, 39, (1949).

141. Bouchez, R., Tobailem, J., Robert, J., Muxart, R., Millet, R., and Daudel P. and R., J. Phys. Rad., 17, 363, (1956).

142. Kafalas, P., and Irvine, J.W., Phys. Rev., 104, 703, (1956).

143. Meyer, P., and Schlieder, S., Z. Phys., 135, 119, (1953).

144. van Nooijen, B., Konijn, J., Heyligers, A., van der Brugger, J.F., and Wapstra, A.H., Physica, 23, 753, (1957).

145. Schuman, R.P., Jones, M.E., and Newherter, A.C., J. Inorg. Nucl. Chem., 3, 160, (1956).

146. Lyon, W.S., Phys. Rev., 87, 1126, (1952).

147. Wright, H.W., Wyatt, E.I., Reynolds, S.A., Lyon, W.S., and Handley, T.H., Nucl. Sc. Eng., 2, 427, (1957).

148. Ter-Pogassian, M., and Porter, F.T., Phys. Rev., 81, 1057, (1951).

149. Herrmann, G., and Strassman, F., Z. Naturforsch., 11a, 946, (1956).

150. Brosi, A.R., Oak Ridge National Laboratory, ORNL, Report 150, (1946).

151. Meinke, W.W., Phys. Rev., 90, 410, (1953).

152. Delasso, L.A., White, M.G., Barkas, W., and Creutz, E.C., Phys. Rev., 55, 113, (1939).

153. Bradt, H., Gugelot, A.C., Huber, O., Medicus, H., Preiswork, P., and Schesser, P., Helv. Phys. Acta, 18, 351, (1945).

154. The Matheson Co. Inc., Rutherford, New Jersey.

155. Jentschke, W., and Prankl, F., Phys. Zeits., 40, 706, (1939).

156. Radvanyi, P., Colloques Internationaux du Centre National de la Recherche Scientifique, C.N.R.S., Paris, (1955).

157. Bertolini, G., Bisi, A., and Zappa, L., Il Nuovo Comento, 10, 1424, (1953).

158. Hendee, C.F., Fine, S., and Brown, W.B., Rev. Sc. Inst., 27, 531, (1956).

159. Preiss, I.L., Atomic Energy Commission of U.S.A., A.E.C., Report ORO-164 (1957).

160. Dolby, R.M., Brit. J. of App. Phys., 11, 64, (1959).

161. Holloway, J.T., Lu, D.C., and Zaffarano, D.J., Rev. Sc. Inst. 31, 91, (1960).

162. White, E.L.C., U.S. Patent No. 2,358,428. Sept. 19 (1944).

163. Brown, M., Rev. Sc. Inst., 31, 403, (1960).

164. Read, P., Rev. Sc. Inst., 31, 979, (1960).

165. Locher, G.L., Phys. Rev. 55, 675A, (1939), Phys. Rev. 42, 525, (1932).

166. Bearden, J.A., Rev. Sc. Inst., 4, 271, (1933).

167. Wakefield, E.H., Rad. C. Lab., 1, No. 1, (1954).

168. Hershey, A.V., Phys. Rev., 56, 908, (1939).

169. Curran, S.C., and Rae, E.R., Rev. Sc. Inst., 18, 871, (1948).

170. Gray, L.H., Proc. Phil. Soc. Cambridge, 40, 72, (1944).

171. Pontecorvo, B., Helv. Phys. Acta, 23, 97, (1950).

172. Valentine, J.M., and Curran, S.C., Phil. Mag., 43, 964, (1952).

173. Valentine, J.M., Proc. Roy. Soc. 211A, 75, (1952).

174. Cranshaw, T.E., and Harvey, J.A., Can. J. Res., 26A, 243, (1948).

175. Tunnicliffe, P.R., and Ward, A.G., Proc. Phys. Soc. 65A, 233, (1952).

176. Hanna, G.C., Phys. Rev., 80, 530, (1940).

177. Compton, A.H., and Allison, S.K., "X-ray in Theory and Experiment". D. Van Nostrand, Co., Inc., (1936).

178. Nelms, A.T., Natl. Bur. Standards, Circular 542, (1953).

179. Bethe, H.A., and Ashkin, J., "Experimental Nuclear Physics". Edited by E. Segre, Vol. 1. John Wiley and Sons, Inc. (1953).

180. Geiger, H., and Klemperer, O., Z. Phys., 49, 753, (1928).

181. Korff, S.A., Rev. Mod. Phys., 11, 211, (1939).

182. Korff, S.A., Rev. Sc. Inst., 12, 94, (1941).

183. Brudbaker, G., and Pollard, E., Rev. Sc. Inst., 8, 255, (1937).

184. Montgomery, C.G., and Montgomery, D.D., Rev. Sc. Inst., 11, 237, (1940).

185. Tozer, B.A., and Craggs, J.D., J. Electronics and Control, 8, 103, (1960).

186. Loeb, L.B., "Fundamental Processes of Electrical Discharge in Gases". John Wiley and Sons, Inc. (1939).

187. Bouissieres, G., Bull. Soc. Chim., France 19, 536, (1952).

188. Hanna, G.C., Kirkwood, D.H.W., and Pontecorvo, B., Phys. Rev., 75, 985, (1949).

189. Frisch, O., Prog. Nucl. Phys., 3, 18, (1953).

190. Snyder, H.S., Phys. Rev., 72, 181, (1947).

191. Whitehouse, W.J., and Putman, J.L., "Radioactive Isotopes". Clarendon Press, Oxford. (1953).

192. Fano, U., Phys. Rev. 70, 44, (1946), Phys. Rev. 72, 26, (1947).

193. Curran, S.C., Cockcroft, A.L., and Insch, G.M., Phil. Mag., 41, 517, (1950).

194. Husain, S.A., and Jaffe, A.A., Nucl. Inst. and Methods, 6, 50, (1960).

195. Roos, C.E., Phys. Rev., 105, 931, (1957).

196. Hollback, N., Ph.D. Thesis, McGill University, (1957).

197. Scobie, J., Moler, R.B., and Fink, R.W., Phys. Rev., 116, 657, (1960).

198. Drever, R.W.P., Moljk, A., and Curran, S.C., Nucl. Inst., 1, 41, (1957).

199. Mayer, M.G., and Jensen, J.H., "Elementary Theory of Nuclear Shell Structure". John Wiley and Sons, Inc. New York, (1955).

200. Richards, H.T., Smith, R.V., and Browne, C.P., Phys. Rev., 80, 524, (1950).

201. Way, K., et al., see reference 94W55 in Strominger, D., Hollander, J.M., and Seaborg, G.T. Rev. Mod. Phys., 585, (1958).

202. Brown, F., Hanna, G.C., and Yaffe, L., Proc. Roy. Soc., 220A, 203, (1953).

203. Moszkowski, S.A., Phys. Rev., 82, 35, (1951).

204. Welcher, F.J., "The Analytical Uses of EDTA". D. Van Nostrand, Co., Inc. Toronto (1957).

205. Hagedoorn, H.L., and Wapstra, A.H., Nuclear Physics, 15, 146, (1960).

206. Pomerance, H., Phys. Rev., 88, 412, (1952).

207. Preiss, I.L., Fink, R.W., and Robinson, B.L., J. Inorg. Nucl. Chem. 4, 233, (1957).

208. Wiles, D.R., Nucleonics, 11, 32, (1953).

209. Blatt, J.M., and Weisskopf, V.F., "Theoretical Nuclear Physics". John Wiley and Sons, Co. New York, (1954).

210. Rose, M.E., "Beta and Gamma-ray Spectroscopy". Edited by K. Siegbhan. Interscience Publishers Inc. New York (1955).

211. Pauli, W., "Rapport du 7e Conseil de Physique de Bruxel" Gauthier-Villars et Cie Paris (1934).

212. Reines, F., and Cowan, C.L., Phys. Rev., 92, 830, (1953).

213. Tables for the Analysis of Beta Spectra. Natl. Bur. Standards. App. Math. Series 13, (1952).

214. Curran, S.C., Angues, J., and Cockroft, A.L., Phys. Rev., 76, 853, (1949).

215. Owen, G.E., and Primakoff, H., Phys. Rev., 74, 1406, (1948).

216. Fulbright, H., "Beta and Gamma-ray Spectroscopy". Edited by K. Siegbahn. Interscience Publishers, Inc., New York (1955).

217. Schonland, B.F.J., Proc. Roy. Soc. 108A, 187, (1925).

218. Knipp, J.K., and Uhlenbeck, G.E., Physica, 3, 425, (1936).

219. Wu, C.S., Phys. Rev. 59, 481, (1941).

220. Jaunch, J.M., see, Bell, P.R., Jaunch, J.M., and Cassidy, J.M., Science, 115, 12, (1952).

221. Saraf, B., Phys. Rev., 94, 642, (1954).

222. Saraf, B., Phys. Rev., 95, 97, (1954).

223. McGowan, F.K., "Beta and Gamma-ray Spectroscopy". Interscience Publishers Inc., New York, (1955).

224. Axel, P., Rev. Sc. Inst., 25, 391, (1954).

225. Kurie, F.N.D., Richardson, J.R., and Paxton, H.C., Phys. Rev. 49, 368, (1936).

226. Glauber, R.J., Martin, P.C., Colloques Internationaux. "Rôle du Cortège Electronique dans les Phénomènes Radioactifs". Centre National de la Recherche Scientifique, C.N.R.S., Paris, (1955).

227. Lee, L.L., and Mooring, F.P., Phys. Rev., 115, 969, (1959).

228. West, D., and Rothwell, P., Phil. Mag., 41, 873, (1950).

229. Bethe, H.A., Hand. d. Phys. 24, 479, (1933).

230. Heinzte, J., Z. Phys. 143, 153, (1955).

231. Harrison, G.R., Crawford, R.C., and Hopkins, J.I., Phys. Rev., 100, 841, (1955).

232. Laberrique-Frowlow, J., and Radvanyi, P., J. Phys. Rad., 17, 944, (1956).

233. Fink, R.W., Phys. Rev., 106, 266, (1957).

234. Robinson, B.L., and Fink, R.W., Rev. Mod. Phys., 27, 424, (1955)

235. Hoff, R.W., University of California Radiation Laboratory, UCRL, Report-2325, (1953).

236. Jaffe, H., University of California Radiation Laboratory, UCRL, Report-2537, (1954).

237. Langevin, M., and Radvanyi, P., C.R., 241, 33, (1955).

238. Langevin, M., J. Phys. Rad. 16, 509, (1955), Ann. Phys., 10, 584, (1955).

239. der Mateosian, E., and Smith, A., Phys. Rev., 88, 1186, (1952).

240. Gupta, R.K., and Jha, S., Il Nuovo Cimento, 5, 1524, (1957).

241. Wilkinson, G., and Hicks, H.G., Phys. Rev., 75, 696, (1949).

242. Chu, T.C., Phys. Rev., 79, 582, (1950).

J. APPENDICES

Appendix I

K-Fluorescence Yield versus Atomic Number.

From Broyles, C.D., Thomas, D.A., and Haynes, S.K.
Phys. Rev., 89, 715, (1953).

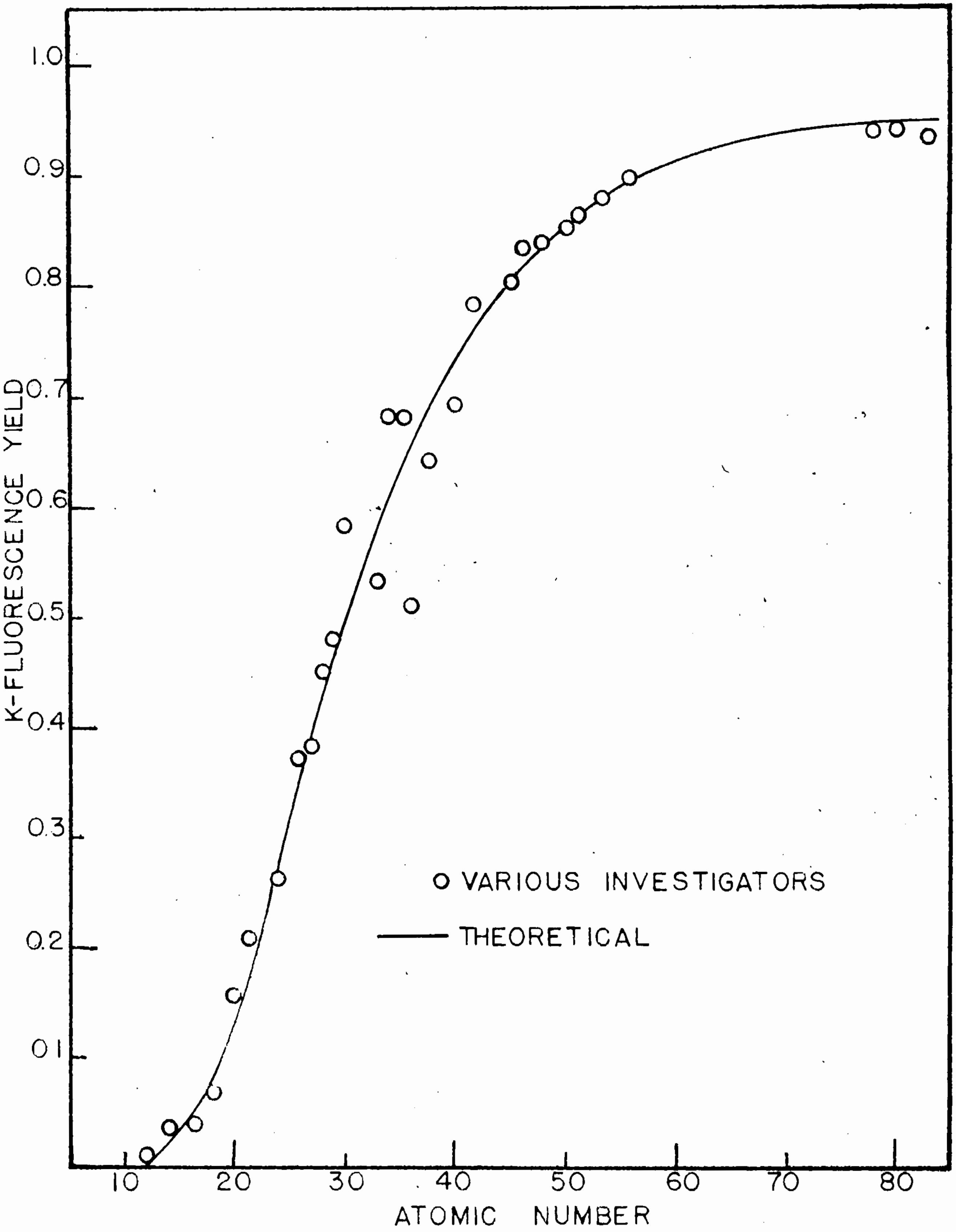
1.0
0.9
0.8
0.7
0.6
0.5
0.4
0.3
0.2
0.1
K-FLUORESCENCE YIELD
10
20
30
40
50
60
70
80
ATOMIC NUMBER
○ VARIOUS INVESTIGATORS
THEORETICAL

Appendix II

Absorption Coefficient for Argon versus Photon Energy (partial absorption coefficients included).

From White, G.R., Natl. Bur. Standards (U.S.) Circ. 583,(1957).

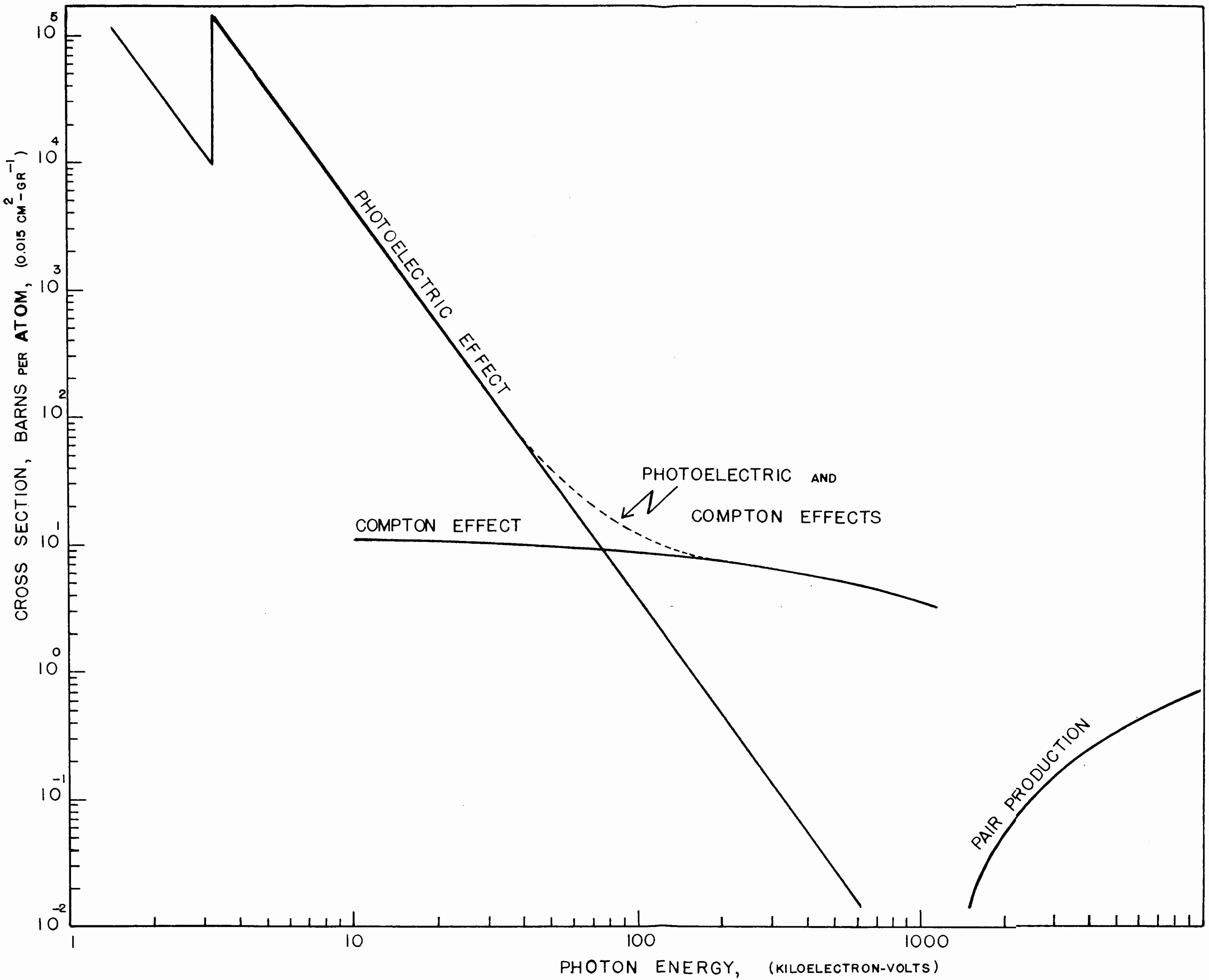
CROSS SECTION, BARNS PER ATOM, (0.015 CM^2-GR^{-1})
10^5
10^4
10^3
10^2
10^1
10^0
10^{-1}
10^{-2}
PHOTOELECTRIC EFFECT
PHOTOELECTRIC AND COMPTON EFFECTS
COMPTON EFFECT
PAIR PRODUCTION
1
10
100
1000
PHOTON ENERGY, (KILOELECTRON-VOLTS)

Appendix III

Range of Electrons in Metallic Beryllium and Aluminum.
From Nelms, A.T., Natl. Bur. Standards, U.S. Circ. 577, (1958).

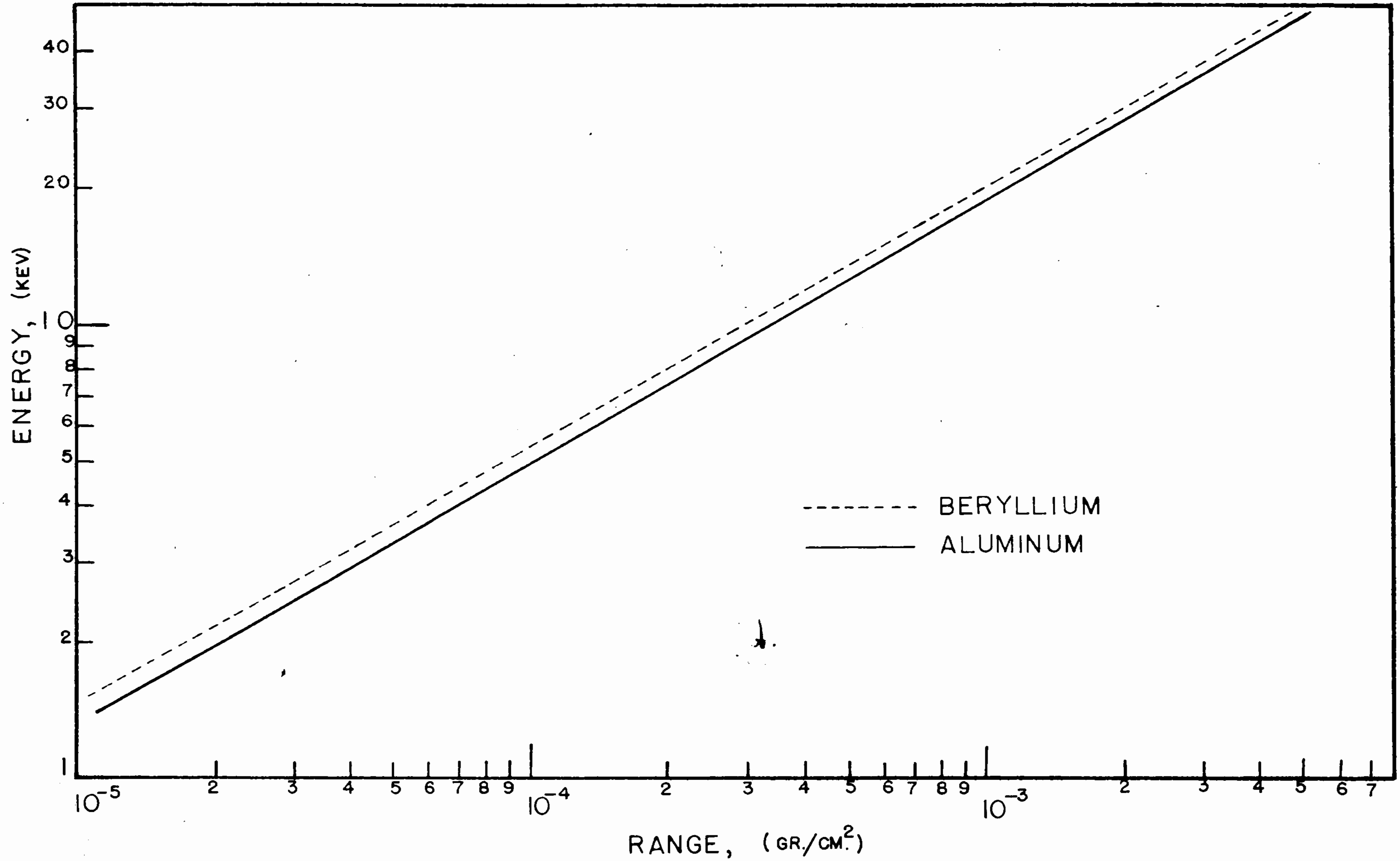
ENERGY, (KEV)
40
30
20
10
9
8
7
6
5
4
3
2
1
10^-5
2
3
4
5
6
7
8
9
10^-4
2
3
4
5
6
7
8
9
10^-3
2
3
4
5
6
7
RANGE, (GR./CM.^2)
BERYLLIUM
ALUMINUM

Appendix IV

(a) Decay Curve of Be^7

(b) Decay Curves of V^{48}

(c) Decay Curves of Cr^{51}

(d) Decay Curves of Pd^{103}

(e) Decay Curves of Cd^{107}

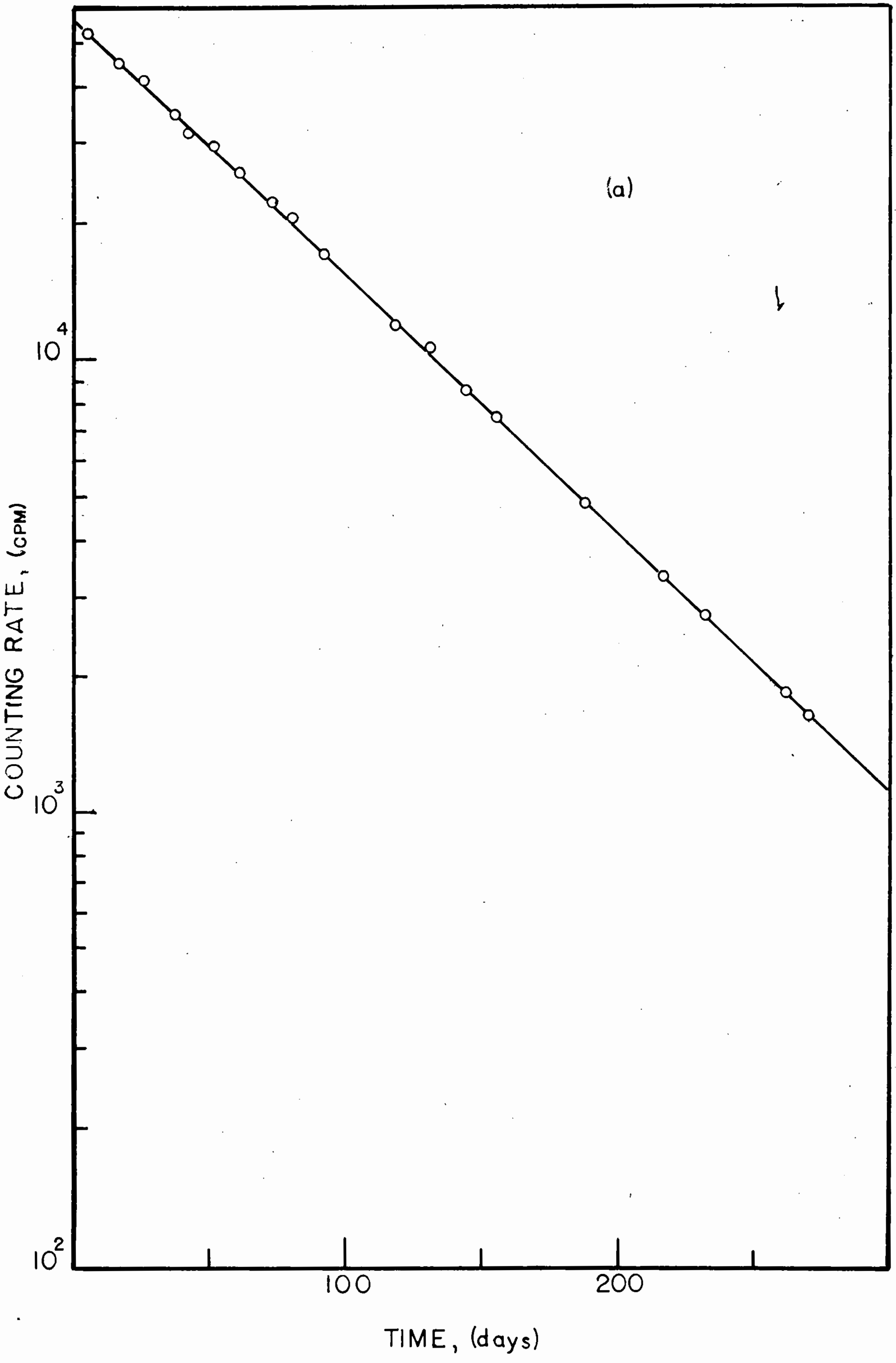
(a)
COUNTING RATE, (CPM)
10^4
10^3
10^2
100
200
TIME, (days)

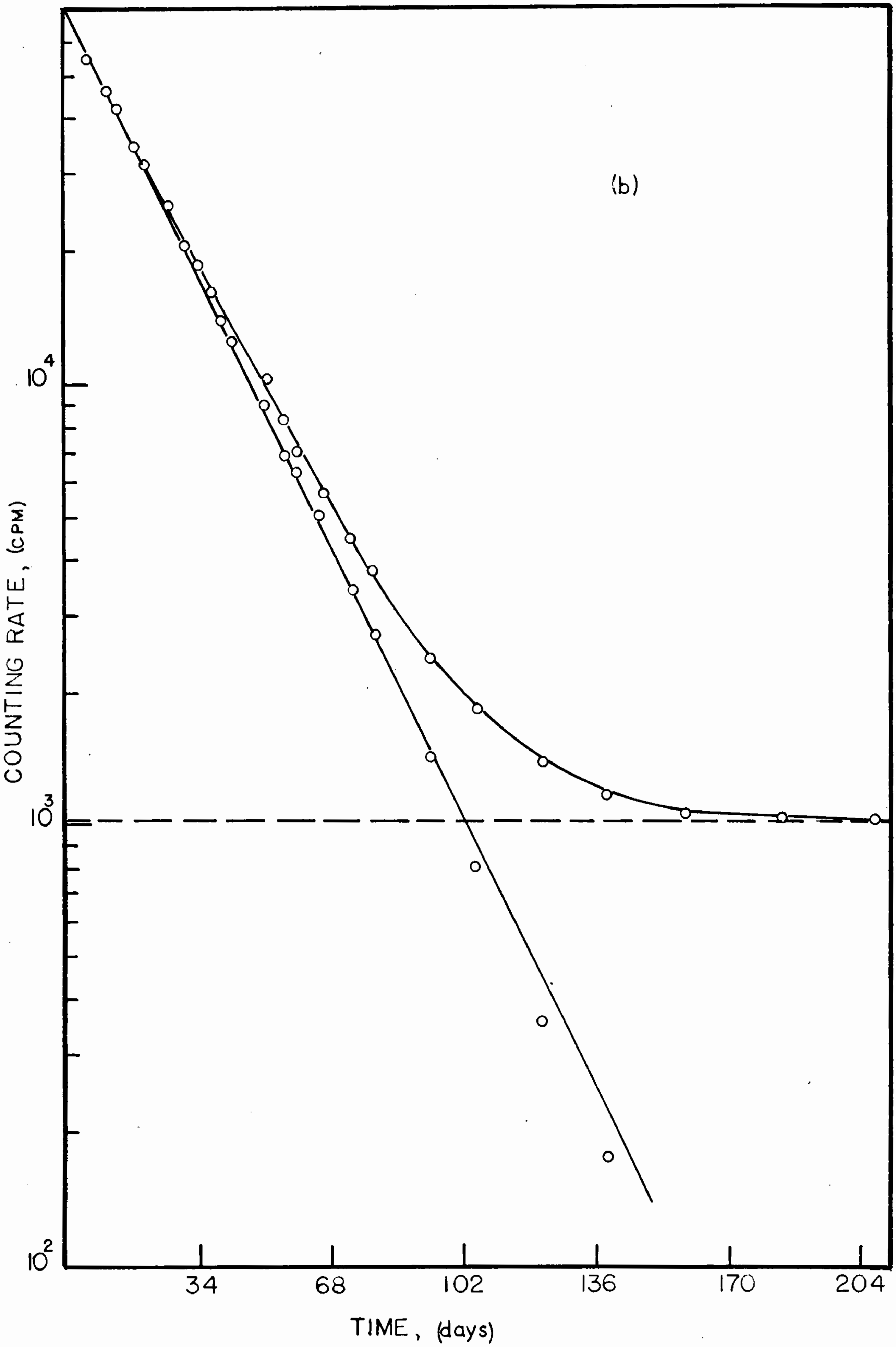
(b)
COUNTING RATE, (CPM)
10^4
10^3
10^2
34
68
102
136
170
204
TIME, (days)

282c

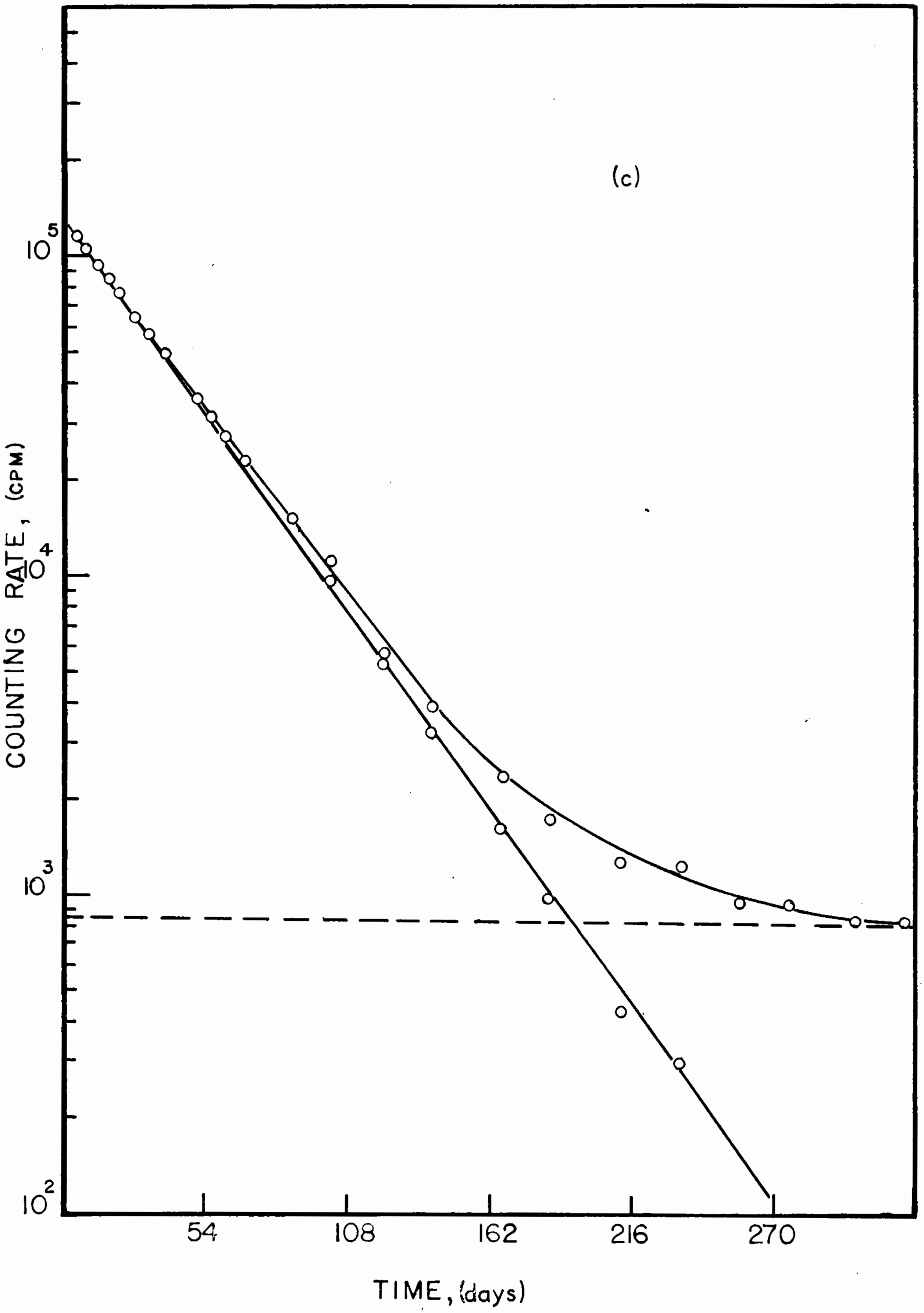
(c)
10^5
10^4
10^3
10^2
COUNTING RATE, (CPM)
54
108
162
216
270
TIME, (days)

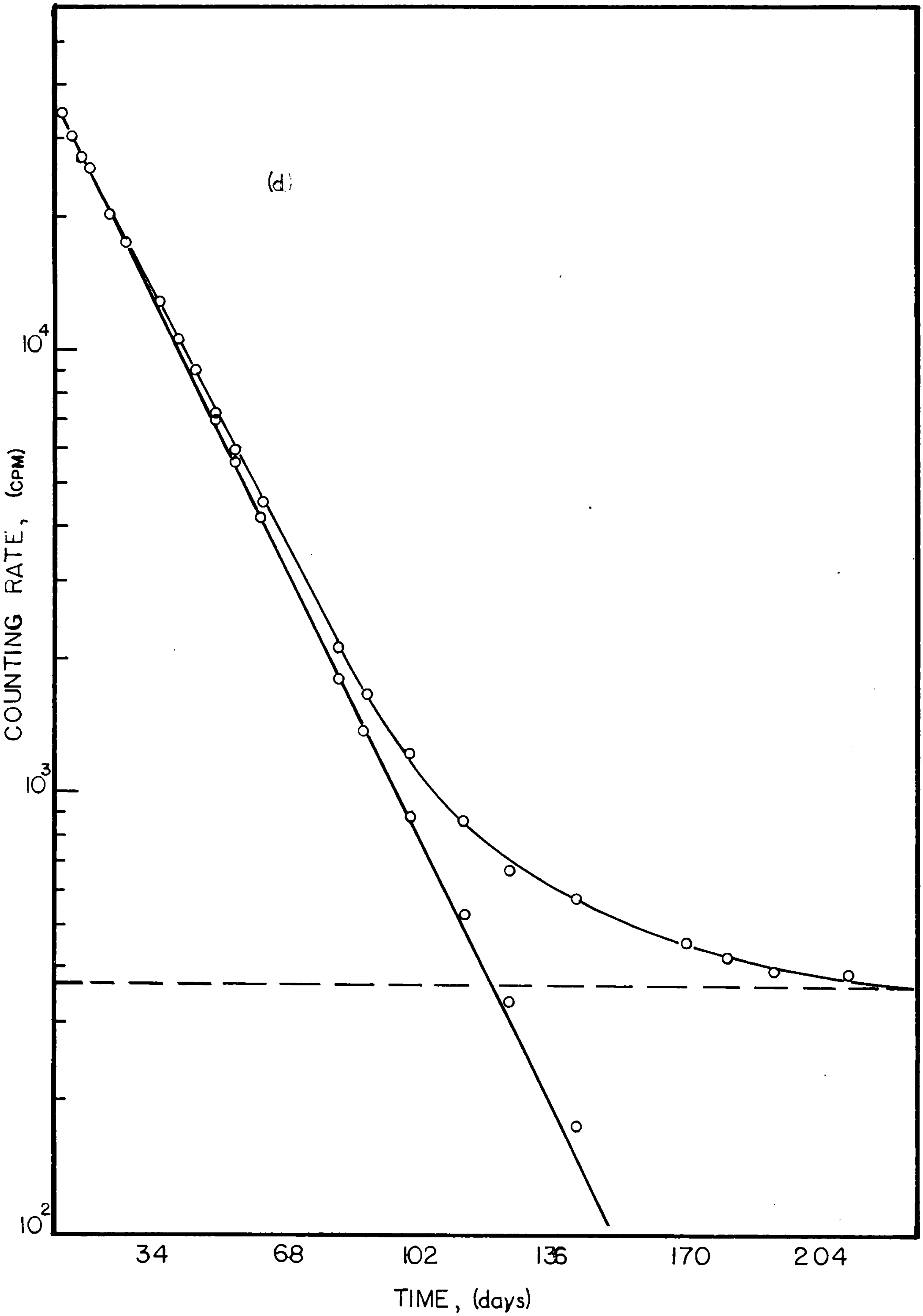
(d)
COUNTING RATE, (CPM)
10^4
10^3
10^2
34
68
102
136
170
204
TIME, (days)

282e

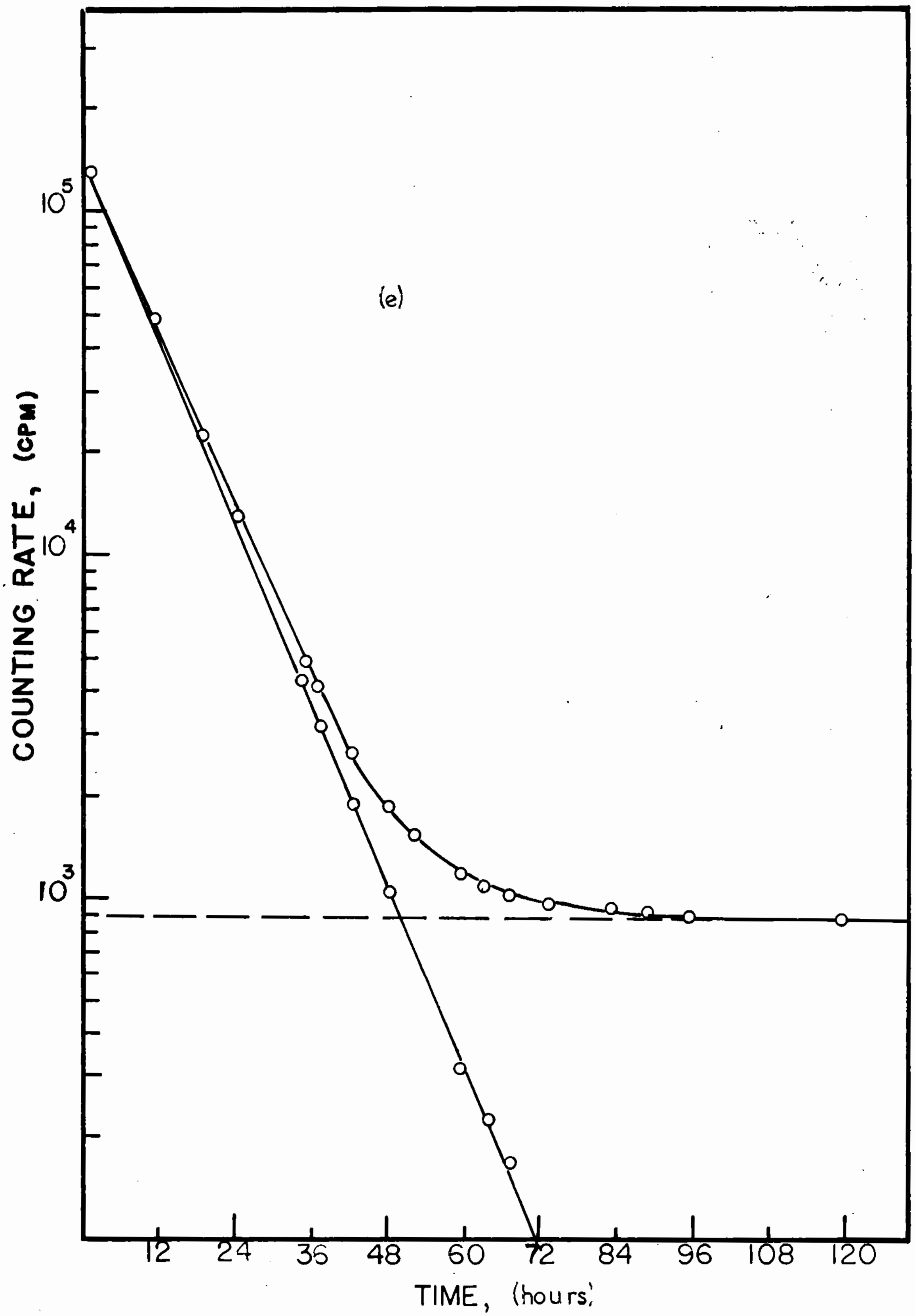

(e)
COUNTING RATE, (CPM)
10^5
10^4
10^3
TIME, (hours)
12
24
36
48
60
72
84
96
108
120

Appendix V

Energy Dissipation per Ion-Pair,

Data taken from Valentine, J.A., Proc. Roy. Soc. 211A, 75, (1952).

Appendix V

Energy Dissipation, W, per Ion Pair.

Gas	Electrons		Alpha rays from Polonium		Protons 340 Mev.
	W in ev	W gas/W$_A$	W in ev	W gas/W$_A$	W gas/W$_A$
A	27.0	1.00	25.9	1.00	1.00
He	32.5	1.20	31.7	1.22	1.17
H_2	38.0	1.41	37.0	1.43	1.38
N_2	35.8	1.32	36.0	1.39	1.31
Air	35.0	1.29	35.2	1.36	1.30
O	32.2	1.19	32.2	1.24	1.23
CH_4	30.2	1.11	29.0	1.12	-

Appendix VI

Mass Absorption Coefficient versus Photon Energy.

For Xenon, Krypton, and Argon:

from Hagedoorn, H.L., and Wapstra, A.H., Nuclear Physics, 15, 146, (1960).

For Neon and Helium:

from Handbook of Chemistry and Physics, Edition (1957-1958).

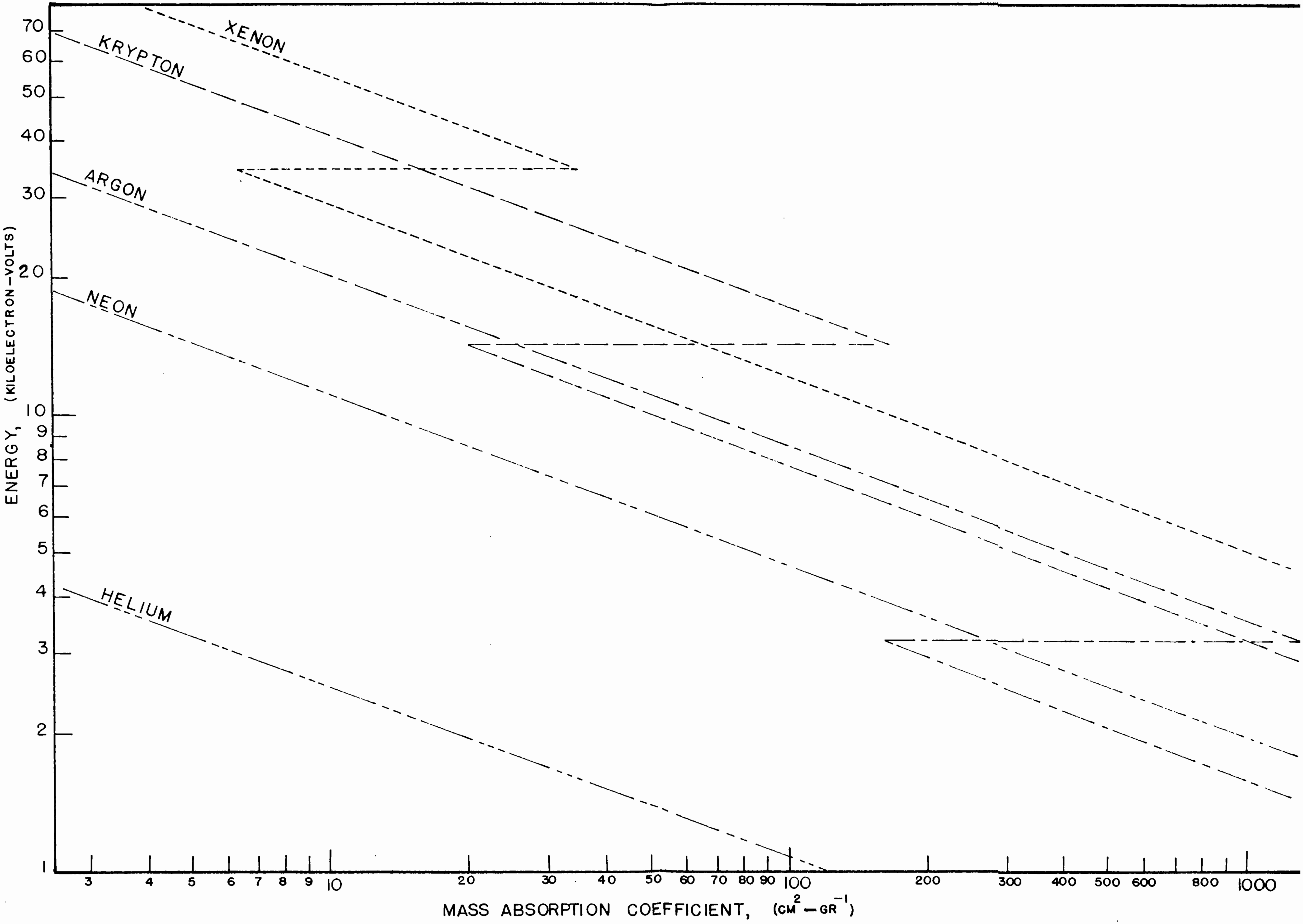
XENON
KRYPTON
ARGON
NEON
HELIUM
ENERGY, (KILOELECTRON-VOLTS)
70
60
50
40
30
20
10
9
8
7
6
5
4
3
2
1
3
4
5
6
7
8
9
10
20
30
40
50
60
70
80
90
100
200
300
400
500
600
800
1000
MASS ABSORPTION COEFFICIENT, (CM^2—GR^{-1})

Appendix VII

Mass Absorption Coefficient for Aluminum versus Photon Energy.

Taken from Handbook of Chemistry and Physics, Edition (1957-1958).

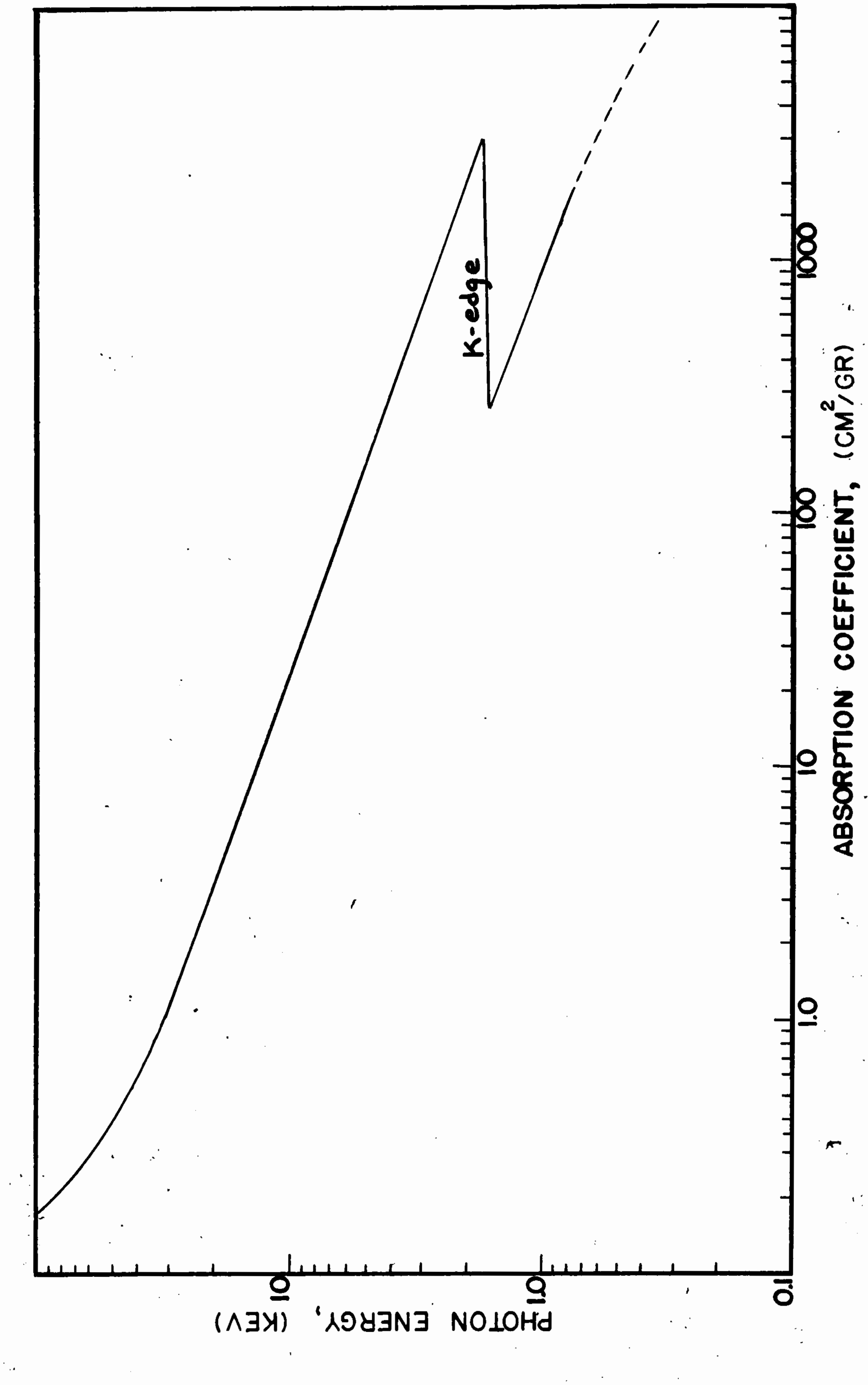
K-edge
ABSORPTION COEFFICIENT, (CM^2/GR)
1.0
10
100
1000
PHOTON ENERGY, (KEV)
0.1
1.0
10

Appendix VIII

3 in. by 3 in. NaI(Tl) Photopeak Efficiency. (sample resting on the crystal).

Data obtained from G.R. Grant, M. May and G.V.S. Rayudu from this laboratory.

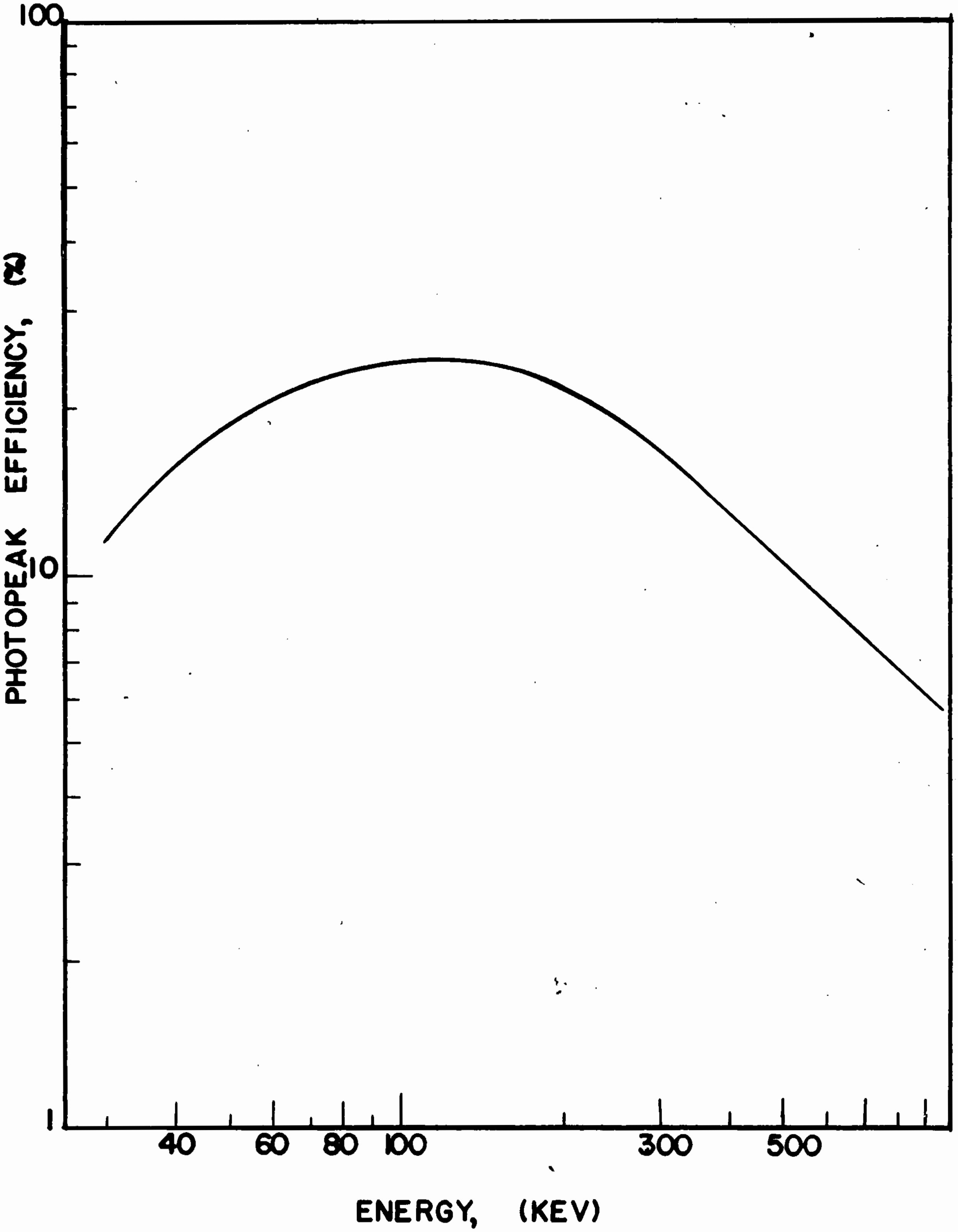

100
10
1
PHOTOPEAK EFFICIENCY, (%)
40
60
80
100
300
500
ENERGY, (KEV)

K. SUMMARY AND CONTRIBUTION TO KNOWLEDGE

1. A survey of the literature on the most recent methods available for the absolute measurement of nuclear and atomic radiations (alphas, betas, gammas, and soft X-rays) was made. The application of each individual method to the problem of standardization of radio-nuclides ($Z < 50$) which decay by orbital capture was analyzed. The method that was adopted employs an ionization chamber which is operated in the proportional region and the radio-nuclides are standardized by spectrometric analysis of the characteristic X-rays.

2. Some fourteen radio-nuclides which covered an energy range between 0.7 kev to 24 kev were studied. Among the radio-nuclides that were prepared in an almost "carrier-free" fashion three of them employed a method which was developed in this laboratory. When possible, the decay was followed and the experimentally determined half-life was compared with values in the recent literature. This enabled us to verify the purity of the chemical separation.

3. An evacuation and filling system, two cathode followers, and two windowless 2π-proportional counter were constructed and calibrated. Fundamental properties and characteristics such as energy and gas multiplication factor "A", linearity, dead time, and background corrections, gas-flow system, air tolerance, nature

and pressure of counter gases, variation of the anode wire diameter, escape radiation of the counter gas, and counter wall effects were investigated.

4. The linearity of the gas multiplication factor "A" was studied for values $10^3 < A < 10^6$. The anode diameters which were used were: 0.001", 0.002", 0.003", 0.004", and 0.005". The counter gases were a mixture of A-CH_4 (9:1) and Kr-CH_4 (9:1) at pressures between 0.3 atm. and 2.0 atm. Rose and Korff's theoretical equation was compatible with our experimental results if an additional variable f(o) was used in the exponential factor. For krypton, the rate of increase of ionization cross-section with impinging energy was published recently and these data were used for the first time to compare the experimental factors "A" to the calculated ones.

5. The statistical fluctuation in the pulse formation and in the primary ionizing event were investigated for energies between 3 kev and 20 kev. In both cases, the experimental results were compared with theory and good agreement was observed.

6. The application of the calibrated proportional counter as a spectrometer enabled the determination of disintegration rates of radio-nuclides decaying by orbital capture. The investigation covered atomic numbers smaller than 50. The X-ray efficiency was found for any pressures smaller than 2.0 atmospheres and for

different gases such as $A\text{-}CH_4$ (9:1) and $Kr\text{-}CH_4$ (9:1). For a 2π-steradian geometrical efficiency and with a mixture of $A\text{-}CH_4$ (9:1) as counter gas, the ratio of the escape radiation to K-photopeak was found for energies between 3.2 kev and 20.2 kev.

7. The absolute disintegration rate of a source of Ca^{41} was measured and the half-life of Ca^{41} was re-determined to be $(7.5 \pm 1.1) \times 10^4$ years.

8. For the first time, the beta spectrum of tritium was obtained when the solid radioactive source was made of tritiated benzidine. A Fermi-Kurie plot was derived and linearity down to an energy of 3 kev was obtained. The end-point energy was found to be 18.2 ± 0.4 kev.

9. Experimental results on the distribution of the internal bremsstrahlung photons from Fe^{55} were compared with the Morrison-Schiff and Glauber-Martin theories and good agreement was obtained when compared with the latter.

10. The K-fluorescence yield for argon and iron were experimentally determined and the results agreed very well with a semi-empirical formulae derived by Hagedoorn and Wapstra.

L. SUGGESTIONS FOR FURTHER WORK

Regarding the continuation of this work, the following suggestions are made.

1. Further studies on the capture probabilities, (P_K to P_L to P_M...) and Auger yields of nuclides decaying by electron capture.

2. In the field of beta spectroscopy, further applications to other beta emitters. In particular, this would enable possible investigations on sources self-absorption and backscattering phenomena.

3. Since most of the radio-nuclides which decay by orbital capture are accompanied by positron emission, studies on branching ratios would be particularly interesting when comparisons are made between the calibrated 2π-proportional counter for soft X-rays and a calibrated detector for positrons.

4. The investigation of the low energy end of the distribution of the internal bremsstrahlung photons of nuclides decaying by orbital capture would be possible with the detector which was described in this thesis. Particularly, in the low energy region, this would enable a better comparison of the Glauber-Martin theory with experimental results. Up to now, these spectra were studied to an energy down to about 25 kev.

5. Search for the possibilities of using gaseous and vaporous radioactive sources internally mixed with the counter gas.